

# **Elucidating the role of Mitoferrin (Mfrn), Iron Regulatory Proteins (IRP1 and IRP2) and Hephaestin (Heph) in Iron Metabolism by tagSNP and Protein-Protein Interaction (PPI) analysis**

**Velaga M Ravindranath**

**A thesis submitted for the degree of**

**Doctor of Philosophy to**

**London Metropolitan University**

**First supervisor: Dr. Kenneth White**

**Second supervisor: Dr. Una Fairbrother**

# ABSTRACT

Precisely how Hephaestin (Heph) facilitate iron release from cells is poorly understood. The work in this thesis tried to establish the role of different iron metabolic proteins, Mitoferrin (Mfrn), IRPs and Heph in iron homeostasis. Analysis of 18 tagSNPs in the Mfrn gene was carried out in an Asian-Caucasian population to establish any correlation between the Mfrn tagSNPs, haemoglobin levels and birth weight in the presence of covariates such as sex of the fetus, gestational age and mother's booking weight. Two-way ANCOVA analysis was carried out to check if the covariates have any influence on the dependent variable in the presence of fixed factors. From the ANCOVA analysis of Mfrn tagSNPs it can be concluded that neither the haemoglobin levels nor the birth weight are dependent on the genotype, fetal sex, nor on their interaction.

Owing to the significance in identifying the interacting partners of IRPs and Heph to understand more about their role in iron metabolism, protein-protein interaction studies were also carried out. IRPs and Heph genes were successfully cloned with One-Strep tag. Full length clones were sequence confirmed for any variation after PCR. Before carrying out immunoprecipitation to identify the interacting partners, transfection efficiency, viability and the role of magnetic particles on K562 cells was performed by using IRPs and Heph cloned with One-Strep tag. Lipofectamine-LTX plus transfection had more viable cells and higher efficiency compared with magnetic-assisted transfection. Also, this study confirms that magnetic nanoparticles do not have any adverse or significant effect on IRPs during the transfection. An unsuccessful attempt was made to identify the interacting partners of IRPs and Heph by immunoprecipitation. The current thesis work also involved identification of a potential ferroxidase. Ceruloplasmin (Cp) was used as a positive control. Non-denaturing gel electrophoresis of the K562, MDA-MB-231 and PNT2-C2 cell fractions confirmed the presence of the extra band establishing the ubiquitous nature of the band. Mass spectrometry analysis identified the excised band as Calreticulin (CALR). This is the first report of calreticulin having ferroxidase activity.

# DEDICATION

This thesis is dedicated to **“TIME”**

# ACKNOWLEDGEMENTS

If I hadn't met Dr. Kenneth White, I wonder how and where I would have ended up. Meeting you has been a very fortunate time of the journey. I have learned from you so much in terms of research, personality development and how calmly one can take things when going gets tougher. Thank you for all the opportunities you gave me whenever I wanted to learn or explore. Without your support I would not have met Dr. Wolfgang. I would like to thank you from the bottom of my heart for all your time and for being there when ever I needed as a guiding figure. Thank you Dr. White.

Dr. Wolfgang, you inspired me, taught me and been there every time I knocked your door for the support. Even with all your busy schedules in US you replied at the first possible opportunity as you know I will be waiting for you feedback across the Atlantic. I sometimes wonder and feel so fortunate to have that one conversation in front of the Medical centre which you let me have, though when you were busy going to see someone else. Thank you Dr. Wolfgang.

I would like to thank Prof. Rob Evans for his kind collaboration during CALR work in Imperial College, UK, for exchange of ideas and literature help.

My best mates, Syam Kommana, Kasyap Bhogaraju, Subhakar Suryadevara, Amit Thotakura, Venkat Pappula, JJ Sivala, Bhavani Kommineni and Hamid Reza Khalatbari without whom, it would not have been possible to see this day. Because of you, I realised how important friendships for life are. Thank you very much for being there in every possible way guys.

Thank you Ephraim, Muy, Ed, Samireh, Sharad, Katia, Amara and Laura. Without you being around in the lab, we would not have those technical and personal (stress busters) discussions which sometimes lasted for hours. But never felt hours have passed by and I am confident you are and will have great times ahead. Without the help of Brigitte Awamaria, John Morgan, Arun, Ruth, Pam, Sophie, and Suresh it would not have been easy at all to get hands on lab resources. You always walked an extra mile to help me. Thank you guys.

Thank you to Dr. Una for being a second supervisor and for your support. Special thanks to Prof. Chris Palmer for all the energy and radiant smile whenever I came across you. Prof. Jameel, thank you for your encouraging words in the summer of 2007.

My heartfelt thank you to Simon Williams from exams office who has been very kind in considering me towards the semester end exam invigilation duties.

Thank you Mom and Dad. I know this is late to say a thank you. No thanks will count for what you have been in my life. I do not think I can repay your patience, but surely can try to be a good human being. Thank you. My dear brothers, Dattu and Venu, I know you have thought, suggested, guided and motivated a lot for my own good. Sure we had our own hard times and thanks for the emotional kicks you gave me all the while. I surely can understand why you guys were tough. No hard feelings. I am sure; I do not even need to mention that without your presence in my life I would have lost long time ago. Thank you for your support and patience which again can never be paid back like Dad's and Mom's.

## Table of Contents

ABSTRACT .....	2
DEDICATION.....	3
ACKNOWLEDGEMENTS.....	4
LIST OF FIGURES .....	11
LIST OF TABLES .....	14
CHAPTER 1 .....	15
INTRODUCTION .....	15
1.01 Significance of Iron .....	16
1.02 Availability of Iron.....	16
1.03 Body Iron Requirements.....	17
1.04 Bioavailability of iron .....	18
1.04.001 Non-haem iron .....	19
1.04.002 Haem iron .....	19
1.05 Intestinal Iron absorption.....	20
1.05.001 Intestinal iron absorption.....	21
1.05.002 Export of iron into plasma.....	23
1.05.003 Iron transport to Mitochondria .....	26
1.05.004 Mitochondrial iron storage and export.....	29
1.06 Cellular iron regulation .....	31
1.06.001 Regulation of iron in stores .....	32
1.06.001.1 Molecules involved in the regulation of cellular iron.....	35
1.06.001.2 Regulation by Inflammatory and Stress Signals .....	38
1.06.001.3 Regulation of iron absorption by erythropoiesis.....	40
1.07 Current study .....	41
1.07.001.1 Mitoferrin, a solute carrier in SLC25 super family.....	42
1.07.001.2 Phylogenetic analysis of SLC25 carriers.....	44
1.07.001.3 SLC25 solute carrier structure .....	45
1.07.001.4 SLC25A37 and its physiological role .....	47
Figure 16: Blast output of human SLC25A37. Figure B shows the sequence identity of human Mfrn and yeast MRS3 and MRS4 genes. ....	48
1.07.001.5 tagSNPs in Mitoferrin .....	48
1.07.001.6 Mfrn as a candidate.....	50
1.08 Protein-Protein Interactions (PPIs).....	51

1.08.001.1 Iron Regulatory Proteins (IRPs) .....	52
1.08.001.2 The IRP-IRE system .....	53
1.08.001.3 Iron regulatory protein 1 (IRP1) and IRP2 .....	55
1.09 Hephaestin (Heph).....	59
1.09.001 Heph and Blast analysis.....	59
1.09.002 Heph and sla mice .....	60
1.09.003 Heph and Cp .....	60
1.09.004 Heph and IREG1.....	62
Aims and Objectives of the research study .....	66
MATERIALS AND METHODS.....	67
CHAPTER 2 .....	68
2.01 UK/Irish and South Asian Cohort for Mfrn tagSNP analyses .....	68
2.01.001 Mfrn tagSNP selection.....	68
2.01.002 Primer design for Mfrn tagSNP genotyping.....	69
2.01.003 Initial PCR reaction .....	70
2.01.004 Single base extension reaction .....	71
2.01.005 MALDI-TOF Mass Spectrometry .....	71
2.02 Cell culture.....	71
2.03 RNA extraction from K562 cells.....	72
2.04 Amplification of cDNA (complementary DNA) using RNA extracted from K562 cells by Reverse Transcription.....	72
2.04.001 RT reaction mix.....	72
2.04.002 cDNA primers.....	72
Gene .....	73
Heph .....	73
2.05 Polymerase Chain Reaction (PCR) .....	73
2.06 Agarose gel electrophoresis .....	74
2.07 Low melting gel electrophoresis.....	74
2.08 RNA and DNA quantification .....	74
2.09 Real-Time quantitative Polymerase Chain Reaction (qRT-PCR) .....	74
2.09.001 qPCR Data analysis .....	74
2.1 Molecular Cloning of Heph, IRP1 & IRP2 .....	75
Step 1: Donor Vector generation.....	75
2.1.01 Workflow of Donor Vector Generation .....	75

2.1.01.001 Donor Vector with GOI .....	77
2.1.01.002 Donor Vector Plasmid DNA extraction .....	78
2.1.01.003 Donor Vector identification .....	78
Step 2: Destination Vector generation .....	79
2.2 Destination Vector generation .....	79
2.2.01 Destination Vector Generation work flow .....	79
2.3 GOI transfer reaction into destination vector .....	81
2.3.01 Destination Vector Plasmid DNA extraction.....	81
2.3.02 Destination Vector Identification .....	81
2.4 GOI transfection and expression .....	81
2.4.01 Chemical based Transfection.....	82
2.4.02 Particle based transfection.....	84
2.5 Protein expression analyses by Western Blotting .....	85
2.5.001 Western blotting solutions and buffers.....	85
2.5.001 Sample preparation for SDS-Polyacrylamide Gel Electrophoresis (SDS-PAGE).....	88
2.5.002 SDS-Polyacrylamide Gel Electrophoresis.....	88
2.5.003 Analysis of SDS-PAGE.....	89
2.5.004 Immunochemical protein detection using the ECL System.....	89
2.6 Protein expression analyses by Flow Cytometry .....	89
2.6.001 Sample preparation for Flow Cytometry analyses .....	90
2.6.002 Intracellular Antigen Staining for Flow Cytometry.....	90
2.7 Protein-protein interactions.....	90
2.7.001 One-STrEP tag background.....	90
2.7.002 One-STrEP tag suitability for PPI studies .....	91
2.7.003 Preparation of cell lysates for PPI studies .....	92
2.7.004 Buffers used to perform purification of protein complex .....	92
2.7.004 Purification of One-Strep-tag fusion proteins .....	93
2.7.005 Protein Identification on Coomassie stained gels .....	93
2.8 Ferroxidase assay.....	94
2.8.001 Preparation of K562, MDA-MB-231 and PNT2-C2 cell fractions for Ferroxidase assay .....	94
2.8.002 Non-denaturing gel electrophoresis.....	94
2.8.003 Non-denaturing gel analysis .....	94
2.8.04 SDS-PAGE electrophoresis to analyse the ferroxidase bands .....	95
2.8.04.001Gel piece of interest excision & preparation.....	95

2.8.04.002 Preparation of Samples/gel piece of interest.....	95
2.8.04.003 Analysis of the M1 band by MS.....	95
RESULTS AND DISCUSSION .....	96
CHAPTER 3 .....	97
Mfrn tagSNP result and discussion.....	97
3.02 Normalisation of the data .....	102
3.03 ANCOVA analysis using SPSS software .....	103
3.04 Mfrn tagSNPs in correlation with Hb levels and birth weight .....	104
3.04.001 ANCOVA results and analysis.....	104
3.04.002 Mfrn tagSNPs discussion .....	107
CHAPTER 4 .....	109
Protein-Protein Interaction results and discussion .....	109
4.01 Introduction.....	109
4.02 qRT-PCR data of Heph, IRP1, IRP2 and Mfrn .....	110
4.03 Relative gene quantification of Heph, IRP1, IRP2 and Mfrn by the Livak method.....	112
4.04 Detection of Heph, IRP1 and IRP2 by western blotting.....	112
4.05 Cloning and sequence confirmation of Heph and IRPs from K562 cells.....	115
4.05.001 Cloning of Heph, IRP1 and IRP2 using K562 cells .....	115
4.05.002 Sequencing results confirming PCR amplicon identity.....	115
4.06 Construction and confirmation of Donor Vectors .....	119
4.06.001 Donor Vector generation and restriction digestion analysis.....	119
4.06.002 Donor Vector sequence confirmation analysis .....	120
4.07 Cloning and confirmation of Destination Vector.....	124
4.07.001 Destination Vector generation and restriction digestion analyses .....	124
4.07.002 Destination Vector sequence confirmation analysis.....	128
4.08 Protein expression analyses of One-Strep tagged Heph, IRP1 and IRP2 using Flow Cytometry...	130
4.09 Discussion of Heph and IRPs Molecular cloning, expression and protein protein interaction studies .....	132
Chapter 5 .....	136
After repeated failures to carry out successful pull-downs to identify the interacting partners of IRPs and Heph, Dr. Kenneth White suggested to continue the work initiated by Philip Goff under his supervision in identifying an extra band which appeared in the membrane fraction of K562 cells.....	136
5.01 Calreticulin (CALR) .....	136
5.01.001 Introduction of CALR .....	136
5.01.002 Structure of CALR .....	137

5.01.003 Role of CALR in and out of the ER.....	139
5.01.004 CALR and Heph .....	140
M1 Results and discussion.....	141
5.02 Identification of M1 band in K562 cells .....	141
5.02.001 Identification of M1 band as CALR in K562, MDA MB231 and PNT2-C2 cell fractions .....	142
5.03 Bioinformatics analysis of CALR.....	147
5.04 Metal-binding nature of CALR .....	148
5.05 CALR and diseases .....	149
5.06 Significance in identifying iron binding sites of CALR for its ferroxidase activity.....	150
CONCLUSIONS .....	152
CHAPTER 6 .....	153
FUTURE WORK.....	155
CHAPTER 7 .....	156
REFERENCES.....	157

## LIST OF FIGURES

Figure 01	Availability of Iron in humans	Pg 17
Figure 02	An individual cell showing roles of molecules in intestinal iron export and import	Pg 23
Figure 03	Iron regulation in enterocyte, macrophages and hepatocytes	Pg 25
Figure 04	Iron trafficking within the mitochondria	Pg 29
Figure 05	Interaction between Mfrn1 and Abc10 in erythroid cells	Pg 30
Figure 06	Molecules involved in mitochondrial iron transport	Pg 31
Figure 07	Cellular iron metabolism	Pg 33
Figure 08	Systemic iron regulation in iron overload and deficient conditions	Pg 35
Figure 09	Schematic representation of iron regulation	Pg 37
Figure 10	Regulation of HAMP expression	Pg 38
Figure 11	HAMP regulation by inflammatory stimuli	Pg 41
Figure 12	Iron regulation by HAMP using erythropoietic signals	Pg 42
Figure 13	Metabolic roles of different mitochondrial carriers	Pg 44
Figure 14	Phylogenetic tree of human mitochondrial carriers	Pg 46
Figure 15	SLC25 carrier protein structure	Pg 47
Figure 16	Blast output of human SLC25A37	Pg 49
Figure 17	Schematic representation of SNPs and tagSNPs	Pg 51
Figure 18	IRP-IRE system	Pg 56
Figure 19	IRP1 and IRP2 in iron replete and deficient cells	Pg 59
Figure 20	Blast output of human, mouse and rat Heph	Pg 61

Figure 21	Efflux of iron across the basolateral membrane	Pg 65
Figure 22	Haplotype block of Mfrn tagSNPs	Pg 70
Figure 23	Workflow for donor vector generation	Pg 77
Figure 24	Donor vector generation and StarCombinase Recognition site	Pg 78
Figure 25	Work flow of Destination vector generation	Pg 80
Figure 26	LB agar plates with X-gal and ampicillin	Pg 81
Figure 27	Transfection process involving Lipofectamine-LTX plus reagent	Pg 84
Figure 28	MATra principle	Pg 85
Figure 29	Work flow in protein complex purification and analysis	Pg 92
Figure 30	Normalisation of the data using SPSS	Pg 102-03
Figure 31	Gene expression of Heph, IRP1, IRP2 and Beta-actin in K562 cells	Pg 111
Figure 32	Gene expression of Heph, IRP1 and IRP2 after normalisation	Pg 112
Figure 33	Protein expression analysis of Heph, IRP1 and IRP2 by western blotting and Image J	Pg 114
Figure 34	PCR amplicons of Heph, IRP1 and IRP2	Pg 116
Figure 35	Sequence confirmation of Heph obtained after PCR	Pg 117
Figure 36	Sequence confirmation of IRP1 forward sequence obtained after PCR	Pg 118
Figure 37	Sequence confirmation of IRP1 reverse sequence obtained after PCR	Pg 118
Figure 38	Sequence confirmation of IRP2 forward sequence obtained after PCR	Pg 119
Figure 39	Sequence confirmation of IRP2 reverse sequence obtained after PCR	Pg 119
Figure 40	0.7% gel electrophoresis picture of Heph, IRP1 and IRP2 restriction digestion	Pg 121
Figure 41	Forward sequence confirmation of donor vector generated using Heph	Pg 122
Figure 42	Reverse sequence confirmation of donor vector generated using Heph	Pg 123
Figure 43	Forward sequence confirmation of donor vector generated using IRP1	Pg 123
Figure 44	Reverse sequence confirmation of donor vector generated using IRP1	Pg 124

Figure 45	Forward sequence confirmation of donor vector generated using IRP2	Pg 124
Figure 46	Reverse sequence confirmation of donor vector generated using IRP2	Pg 125
Figure 47	0.7% gel electrophoresis of donor vectors Heph and IRP1	Pg 127
Figure 48	0.7% gel electrophoresis of donor vectors Heph and IRP2	Pg 128
Figure 49	Forward sequence of Heph tagged with One-Strep tag destination vector	Pg 129
Figure 50	Forward sequence of IRP1 tagged with One-Strep tag destination vector	Pg 13
Figure 51	Forward sequence of IRP2 tagged with One-Strep tag destination vector	Pg 130
Figure 52	Viability analysis of K562 cells transfected with Heph by Lipofectamine LTX-plus and MATra	Pg 132
Figure 53	Percentage of K562 cells transfected by Lipofectamine-LTX plus and MATra reagents	Pg 133
Figure 54	CALR structure	Pg 139
Figure 55	Physiological and pathological roles of CALR	Pg 141
Figure 56	8% non-denaturing ferroxidase and coomassie stained gel	Pg 144
Figure 57	8% SDS coomassie stained gel showing the M1 band in K562 and MDA-MB-231 membrane fraction	Pg 145
Figure 58	8% SDS coomassie stained gel showing the M1 band in K562 and PNT2-C2 membrane fraction	Pg 146
Figure 59	10% SDS-PAGE gel used to run the excised M1 band for proteomic analysis	Pg 147
Figure 60	Blast analysis of CALR, Cp and Heph protein sequence	Pg 149
Figure 61	Blastp results of CALR, Cp and Heph showing the e-value	Pg 149

## LIST OF TABLES

Table 01	PCR primers for Heph, IRP1 and IRP2	Pg 74
Table 02	Percentage SNP success and HWE p values for tagSNP analysis	Pg 99 – 102
Table 03	Leven's test of equality of error variance and p values	Pg 106
Table 04	Effect size on the independent variable interaction	Pg 107
Table 05	Fold increase and decrease of Heph, IRP1 and IRP2 in treated and untreated K562 cells	Pg 113
Table 06	Quantification of Heph, IRP1 and IRP2 in treated and untreated K562 cells using ImageJ	Pg 115
Table 07A	Restriction analysis of Donor vectors	Pg 120
Table 07B	Restriction analysis of Destination vectors	Pg 126
Table 08	p and Sf vaues for CALR obtained after MS-MS	Pg 147
Table 09	Putative iron ligands in Cp and Heph	Pg 152

# CHAPTER 1

## INTRODUCTION

All living organisms require iron for metabolic functions. The ability of iron to react with oxygen to form hydroxyl radicals may cause oxidative damage to proteins and nucleic acids that will lead to cell death. Thus maintaining iron homeostasis is necessary to achieve an optimal balance of iron import and export in the body. This ensures release of the required amounts of iron to maintain all the biochemical activities while preventing the harmful effects of low or high iron uptake. Iron homeostasis is maintained in the cells through the coordinated regulation of uptake, storage and secretion. These processes in the cells are regulated by the proteins that respond to changes in iron availability by transcriptional and post-transcriptional mechanisms.

Iron is an essential nutrient. Iron is required in all living organisms, from the most primitive to the most complex living organisms for metabolic functions (Testa, 2002). Different organisms adopted different mechanisms to control iron metabolism as they evolved. Mammals have developed an intricate iron withholding defence mechanism against microbial infections. Biochemical steps in the metabolism virtually left no free iron in the cells. The situation is more complex in advanced species like *Homo sapiens* who require more genes to accomplish iron metabolism from absorption to transport.

## 1.01 Significance of Iron

Iron is essential for many biological processes like oxygen transport and storage, DNA synthesis, mitochondrial electron transfer, enzymatic and redox reactions (Andrews, 2000). Iron forms the central atom in the haem moiety of haemoglobin, that provides the capacity to bind and carry oxygen. Binding of iron to oxygen depends on oxygen tension, in that oxygen is bound by haemoglobin at high oxygen levels and is delivered to tissues that have low oxygen levels. Iron forms a part of ribonucleotide reductase, the enzyme that is involved in the synthesis of deoxy-ribonucleotides from ribonucleotides. Iron also plays an important role in the activity of the cytochromes of the respiratory chain in its capacity to accept and loose electrons.

## 1.02 Availability of Iron

Though iron is more readily absorbed in the ferrous state ( $\text{Fe}^{2+}$ ) the majority of dietary iron exists in the ferric state ( $\text{Fe}^{3+}$ ). The ferric form ( $\text{Fe}^{3+}$ ) is completely insoluble in water at neutral pH. The redox reaction ability of iron is due to the unfilled atomic orbitals and therefore is able to undergo changes in oxidative state ( $\text{Fe}^{2+}$  and  $\text{Fe}^{3+}$ ) involving one electron. As a transition metal, iron readily engages in one-step oxidation-reduction reactions between its  $\text{Fe}^{3+}$  and  $\text{Fe}^{2+}$  states. The redox property of iron in excess can be toxic as free iron can participate in 'Fenton chemistry', in which donating electrons to hydrogen peroxide ( $\text{H}_2\text{O}_2$ ) or lipid peroxides generates highly reactive hydroxyl and lipid radicals  $\text{OH}\cdot$  or  $\text{LO}\cdot$  or  $\text{LOO}\cdot$  respectively. The resulting oxygen metabolites can readily react and damage proteins, lipids and DNA. During the evolutionary process to allow absorption and metabolism of iron all living organisms developed complex iron oxidative-reductive and transport mechanisms. The acidic gastric secretions in the stomach play an important role in iron absorption in that they facilitate the solubilisation of non-haem iron from the food.

The approximate total iron content of the body is about 4.5 grams in healthy adult males (Andrews, 1999). In men the loss of iron from the gastro-intestinal tract, skin and urinary tract is estimated to be about 1mg/day and 2mg/day in a menstruating female (Green et al., 1968). Iron losses in post-menopausal women are assumed to be similar to those observed in men. National survey data shows that in Britain, on an average, adult men consume 13.2 mg iron/day and women 10.0 mg/day from food sources (Henderson et al., 2003). Due to the absence of an active excretion pathway for absorbed iron, under most conditions, absorption of dietary iron is the critical determinant of iron status. Loss of iron in the human

body is unregulated and the total body iron stores depend on the changes in the rate of intestinal iron absorption.

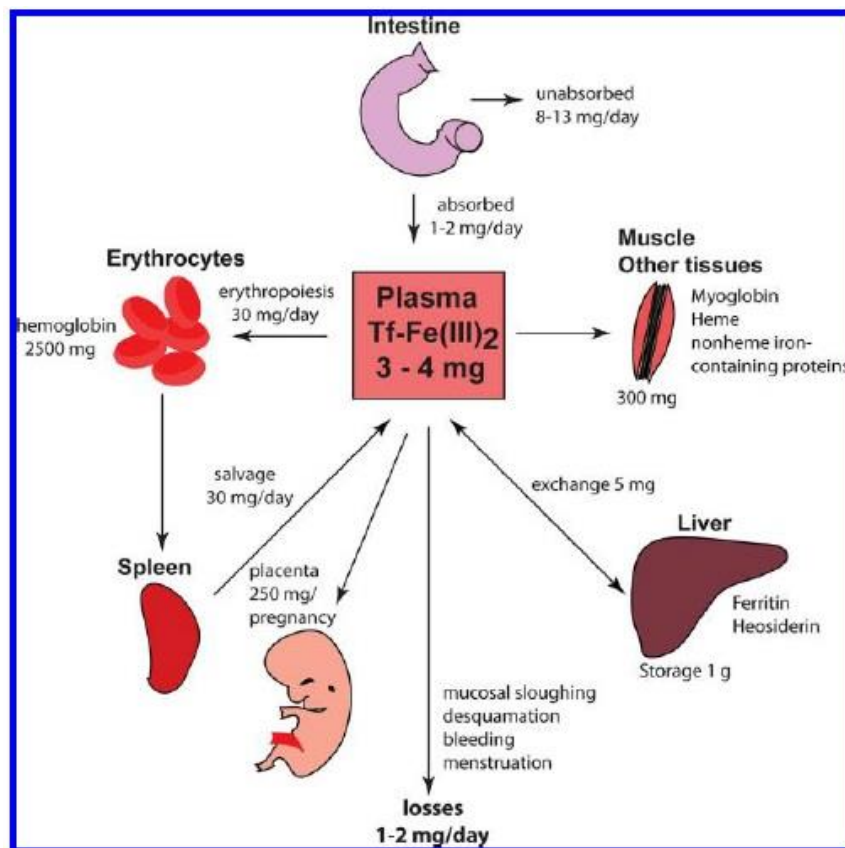


**Figure 1: Availability of Iron in humans.** A high percentage of body iron is incorporated in haemoglobin of circulating erythrocytes (60-70%). Approximately 20-30% of iron in the body is in the form of ferritin and hemosiderin in hepatocytes and reticulo-endothelial system (RES) macrophages as an excess iron. The amount of iron bound to transferrin is about 3-4 mg but the plasma transferrin compartment functions as a transit compartment through which approximately 20 mg of iron flows each day. Under circumstances of iron overload non-transferrin bound iron (NTBI) can appear in the plasma. The bone marrow is the main consumer of circulating iron. 18-20 mg of iron, mostly recycled, is used for haemoglobin synthesis in 200 billion new erythrocytes every day. Healthy people absorb 1-2 mg of iron per day, which compensates for a corresponding iron loss. **Figure taken from Pantopoulos et al., 2012.**

### 1.03 Body Iron Requirements

Approximately 30-40 mg of iron is required daily for internal utilisation by the body, largely to re-synthesise the haemoglobin destroyed along with old red blood cells (RBCs). A normal adult man has 40 – 50 mg/kg body weight of total body iron (Andrews 1999, Wessling-

Resnick 2000). Of the total body iron, approximately 60 – 65% is present in the circulating erythrocytes in the form of haemoglobin, 10% is present in the skeletal muscle as myoglobin and about 30 – 35% is present in the liver, spleen and bone marrow as storage iron in the form of ferritin and hemosiderin. Approximately between 80 – 85% of the absorbed iron is transported to the developing RBCs by transferrin in the bone marrow for incorporation into haemoglobin and the remainder is transported to liver or muscle via transferrin for either storage or utilisation for haem synthesis (Tavill and Bacon 1986, Conrad and Barton 1981, Conrad et al., 1999). Iron is not excreted from the body in the urine or through the intestines, but is lost only with cells from the exteriors or interior surfaces of the body through the exfoliation of gastro-intestinal mucosal cells, dead cells from the skin or urinary tract. Adult women experience an additional loss of iron due to menstruation. Menstrual loss of iron varies among women but losses for an individual woman usually remain constant from menarche and throughout her fertile life (Hallberg et al., 1966). To ensure that the required amounts of iron are absorbed from an average western type diet without any reduction in iron supply to the tissues, the diet must contain about 19mg of dietary iron (estimating that at most 15% of the available iron can be expected to be absorbed from this type of diet) (Hallberg and Rossander-Hulten., 1991).

During pregnancy, the requirement of iron increases as additional iron is needed to replace basal losses to allow for expression of maternal red cell mass and to serve as a nutrient for the needs of the fetus and placenta (International Nutritional Anaemia Consultive Group, 1981). It has been suggested that the iron requirements are 1mg/day in the first trimester, 4mg/day in the second trimester and 6mg/day in the third trimester (Bothwell et al., 1989). A series of studies using different techniques to measure iron absorption have provided clear evidence that iron absorption increases during pregnancy (Hahn et al., 1951, Svenberg, 1975, Whittaker et al., 1991). After four months of infancy, 0.9mg of iron is required daily of which 0.7mg is required to sustain body growth and 0.2mg is required to replace iron losses (Dollman, 1980).

#### **1.04 Bioavailability of iron**

Since dietary iron does not exist in a readily usable form ( $\text{Fe}^{2+}$ ) available iron is bound to other components that must be digested before iron can be absorbed. Thus, the process of iron absorption can be sub-divided into three phases (Carpenter & Mahoney, 1992): iron digestion, iron intestinal absorption and iron utilisation.

#### **1.04.001 Non-haem iron**

Dietary iron is present in two different forms and they are non-haem iron and haem iron. Non-haem iron is not present in readily soluble form and hence the digestion process first releases the non-haem iron in a soluble form that can be absorbed by the small intestine. The low pH present in the gastric juice facilitates iron solubility as suggested by the striking correlation observed between the gastric juice pH and dietary iron absorption (Bezwoda et al., 1978). Due to the gastric digestion process, non-haem iron is solubilised from its ordinary dietary forms into a common pool that reaches equilibrium with all dietary constituents to which iron can bind. The existence of a common pool for all dietary non-haem iron was validated by a large number of studies (Hallberg, 1981, Charlton & Bothwell, 1983). It was also shown that non-haem iron remaining outside of this pool is not available for iron absorption (Hallberg, 1981, Charlton and Bothwell, 1983). Gastric and duodenal mucin binds to iron at acidic pH and keeps the iron soluble at neutral pH (Conrad et al., 1991). Some studies suggest that an iron-binding component present in gastric juice called gastroferrin, may act as an inhibitor of iron absorption (Davis et al., 1967, Multani et al., 1970). This observation was made due to the low levels of gastroferrin in gastric juices of patients with haemochromatosis and could be to some extent responsible for the increased iron absorption observed in this condition (Davis et al., 1966). However, this hypothesis was repudiated in several studies showing that gastroferrin was present in the gastric secretions of haemochromatosis (Winter et al., 1968).

#### **1.04.002 Haem iron**

Haem iron is derived from haemoglobin, myoglobin and other haem proteins. During the process of digestion, haem iron forms an important pool in the gastro-intestinal tract. Before its absorption, haem must be detached from globin and then be absorbed as free haem. Exposure to the acidic pH and proteases of the gastric juice induces the release of haem from globin and haem is then converted to hemin through oxidation of iron contained in haem (Hazell et al., 1978). The release of haem from globin continues in the duodenum as a consequence of the activity of proteolytic duodenal enzymes such as trypsin (Wheby et al., 1970).

## 1.05 Intestinal Iron absorption

Movement of iron from the intestinal lumen to the circulation through epithelial cells of the digestive tract, known as iron absorption occurs largely from the proximal small intestine. Iron absorption in the intestine is dependent on the intraluminal factors such as the quantity of iron ingested, pH of the gut, chemical form of the available iron and also on the mucosal factors such as the absorptive surface of the microvilli (Conrad and Umbreit, 2002). Mammals absorb dietary iron through the duodenal epithelium of the small intestine (Gitlin and Cruchoad, 1962) which is organised in villus structures to maximise its absorption surface area (Donovan *et al.*, 2006). Iron that accumulates within the mature enterocytes is lost from the body when they become old and are shed into the gut lumen. Absorption of iron involves two steps, uptake of iron from the intestinal lumen into the mucosa and the transfer across the mucosal cells and serosal membrane into the circulation

The majority of iron entering the mucosal cells is not transferred to the plasma but remains trapped within the cells and is excreted into the lumen when cells are shed. Iron absorption depends on the amount of the body iron content. When the iron content in the body decreases a high proportion of the available iron is absorbed and as the body iron content raises the rate of iron absorption falls. However, when compared to the iron absorption during iron homeostasis, the relative enhancement of absorption during iron deficiency is greater than the inhibition observed during iron overload. Uptake of iron is also controlled by the rate at which red blood cells are produced (erythropoiesis). Iron absorption increases when there is an increased rate of erythropoiesis as extra iron is required to sustain new haemoglobin synthesis. Changes in iron absorption levels are received from the body via the intestinal crypt cells.

Studies carried out in rats showed that absorption of iron was uniform throughout the length of the small intestine, while it showed a steep decrease from the duodenum to the ileum (Johnson *et al.*, 1983). Iron in physiological amounts is absorbed by an active transport mechanism consisting of an initial mucosal uptake followed by intracellular transfer to the basolateral membrane and finally entering into the portal venous blood (Manis *et al.*, 1962). A study carried out in Caco-2 cells showed that iron must first be reduced by reductases present in the brush border membrane before being absorbed (Han *et al.*, 1995). The kinetics of iron absorption was carefully investigated in human upper small intestine microvillus membrane vesicles (Teichmann and Stremmel, 1990). The initial phase of iron

absorption was reported to be fast and begin within seconds after iron reaches the mucosal surface.

#### **1.05.001 Intestinal iron absorption**

In the past decade much progress has been made to understand the cell biology of iron absorption. Most of the non-haem iron in the diet is present as the  $\text{Fe}^{3+}$  form. Non-haem iron is first reduced by Dcyt *b* (cytochrome *b*-like ferrireductase) an iron regulated di-haem protein, and then it is transported into the enterocyte via a transmembrane DMT-1 (Syed et al., 2006). Dcyt *b* is a 6-transmembrane domain, ferric reductase protein. Dcyt *b* which has approximately 45% sequence similarity with the sheep cytochrome *b* 561 reductase, which increases the availability of  $\text{Fe}^{2+}$  from the dietary iron pool. B-type cytochromes are the di-haem proteins involved in the transfer of electrons across membranes. Dcyt *b* is expressed on the brush border membrane of enterocytes along the villi. Iron-deficient mice showed high levels of Dcyt *b*. Evidence supporting the function of Dcyt *b* as a ferric reductase comes from *Xenopus Oocytes* and cultured cells, where expression of exogenous Dcyt *b* resulted in induction of ferric reductase activity, which was partially blocked with antibodies directed against Dcyt *b* (Chen et al., 2003, Philpott 2002, Mckie et al., 2001).

The major transporter involved in cellular non-haem iron uptake (import) is divalent metal transporter 1 (DMT1; also known as Nramp2, DCT1 and SLC11A2) (Gruenheid et al., 1995, Fleming et al., 1997, Gunshin et al., 1997), which is a principal mammalian proton-coupled metal iron transporter. DMT1 is a member of the NRAMP family and has 65% homology with the phagocyte specific homolog Nramp1 and is highly conserved in prokaryotes and eukaryotes. The pattern of expression of Dcyt *b* and DMT1 is very similar; the expression decreases from duodenum to ileum. The region of high Dcyt *b* expression correlates with that of high ferrireductase activity (Raja et al., 1992). In iron-deficient mice, mRNA is predominantly found in the upper villus of mature enterocytes and is absent in the crypts (McKie et al., 2001, Latunde-Dada et al., 2002). In the iron deficient mice it was also shown that the region of high Dcyt *b* expression overlaps with the major site of iron absorption, where the DMT1-mediated  $\text{Fe}^{2+}$  transport occurs. Experiments on knock-out (KO) mice, *Dmt1<sup>int/int</sup>* generated by Gunshin et al, have demonstrated that Dmt1 is essential for intestinal inorganic iron absorption, where anaemia was noted after depletion of parenteral iron stores (Gunshin et al., 2005). Studies have shown that unlike in the intestine and bone marrow, Dmt1 is dispensable in placenta and liver (Gunshin et al., 2005).

Besides  $\text{Fe}^{2+}$ , DMT1 has a wide range of substrate specificity, including  $\text{Zn}^{2+}$ ,  $\text{Mn}^{2+}$ ,  $\text{Co}^{2+}$ ,  $\text{Cd}^{2+}$ ,  $\text{Cu}^{2+}$ ,  $\text{Ni}^{2+}$  (Gunshin et al., 1997). DMT1 was first discovered from the cDNA library of iron-deficient rat intestine as a 4409 bp DMT1 mRNA, which stimulated iron uptake (Gunshin et al., 1997). DMT1 is a 561 amino acid protein with 12 putative transmembrane domains, which accounts for its high hydrophobicity (Cellier et al., 1996). DMT1 is synthesised from its 60 kDa precursor via extensive N-linked glycosylation, and the glycosylation sites have been predicted in the fourth extracellular loop where a consensus metal transport motif is located (Gruenheid et al., 1995). The presence of glycosylation sites may help DMT1 to localise at the apical membrane rather than in the endosomes (Tabuchi, 2002). The apical transporter/iron importer at the apical membrane was identified simultaneously by two different laboratories using two different approaches. Gunshin et al (1997) undertook expression cloning of the iron transporter by injecting messenger RNA (mRNA) into *Xenopus Oocytes* and looked for stimulation of iron accumulation. mRNA, encoded by Nramp2 gene was abundant in iron-deficient rat intestine and it significantly stimulated iron uptake (Gunshin et al., 1997).

Nramp2 was reported in a microcytic anemic mouse through a positional cloning/candidate gene approach (Fleming et al., 1997). DMT1 is active in a low-pH environment, as found in the duodenum, because it requires proton cotransport (Gunshin et al., 1997). DMT1, expressed in the brush border of duodenal enterocytes, appears to be responsible for the transport of ferrous iron from the duodenal lumen into the enterocytes (Syed et al., 2006; Chen et al., 2004). Free iron from both haem and non-haem sources ends up in the same iron pool inside the enterocyte (Chen et al., 2003). It was reported that disruption of the murine duodenal cytochrome b (Dcytb) gene did not significantly impair intestinal iron absorption under normal conditions (Gunshin et al., 2005), suggesting that other intestinal reductases may substitute or that mice have an efficient mechanism for non-enzymatic iron reduction (Donovan et al., 2006). The enterocyte haem importer protein, haem carrier protein (HCP1) was found (Shayeghi et al., 2005; McKie et al., 2006; Qiu et al., 2006) to mediate dietary haem along with folate across the apical membrane. Once dietary haem enters the intestinal epithelial cells, it is likely to be cleaved by intracellular haem oxygenase 1 to release iron (Raffin et al., 1974). From figure 2 it can be seen that two independent transmembrane iron transporters are necessary to bring dietary iron into the cells and to transfer the iron within the cell into the plasma.

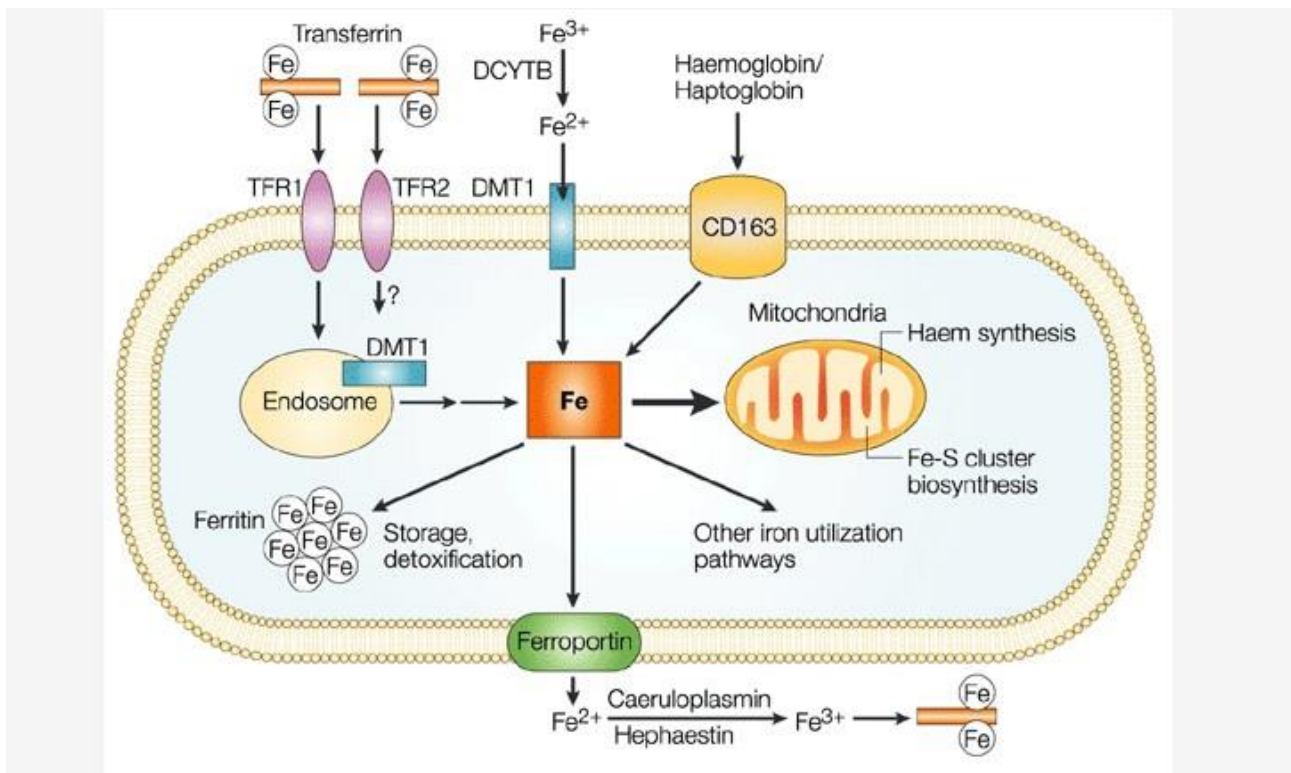


**Figure 2: An individual cell showing the role of molecules involved in intestinal iron import and export.** Readily available iron is picked by transferrin (Tf) and binds to the transferrin receptor (TfR), which is expressed on the surface of the cell. Some of the iron that enters the cells is transferred to the early endosome, where it is exported into the cytoplasm, probably through DMT1. In the intestinal lumen, ferric iron ( $\text{Fe}^{3+}$ ) is reduced to ferrous iron ( $\text{Fe}^{2+}$ ) by the cytochrome-b-like reductase DCYTB. DMT1 then facilitates the absorption of  $\text{Fe}^{3+}$  from the lumen into the cytoplasm. In the cytoplasm, excess iron is stored in the form of ferritin. In macrophages, haem-bound iron in the form of haemoglobin or haptoglobin is taken up by the cell through the haemoglobin scavenger receptor (CD163). Iron is exported from the enterocyte by a permease known as ferroportin IREG-1/FPN-1). For circulation in the body,  $\text{Fe}^{2+}$  is oxidized to  $\text{Fe}^{3+}$  by either the intestinal membrane-associated oxidase, hephaestin, or the plasma-located oxidase, caeruloplasmin the role of which in iron efflux still needs to be established. In the cell, the synthesis of haem and Fe-S clusters takes place in the mitochondria. **Figure taken from Ulrich and Stefan, 2004.**

### 1.05.002 Export of iron into plasma

Intracellular iron can either be stored in ferritin (Torti and Torti, 2002) or transported across the basolateral membrane of the enterocyte and subsequently into the circulation (Figure 2). Degradation of ferritin and iron release helps to mobilise iron for cellular utilisation (Hentze et al., 2004). The iron regulatory proteins (IRPs – IRP1 and IRP2) are the key proteins in

this complex interaction, as they represent the sensors of cytoplasmic iron and the controllers of ferritin and the transferrin receptor (TfR) expression. Ferroportin (also known as IREG1, MTP1 or SLC40A1) was identified as a candidate for the basolateral iron exporter (Abboud and Haile DJ 2000; Donovan et al., 2000, McKie et al., 2001). Localisation studies in polarised epithelial cell lines confirmed the expression on the basolateral membrane and iron efflux was demonstrated in *Xenopus Oocytes*. Apart from the duodenum, tissue-screening studies indicated expression of IREG1 in the kidney, liver (Kupffer cells), testis and the placenta (McKie et al., 2000). Selective inactivation of the murine IREG1 gene in intestinal cells established that IREG1 is the major intestinal iron exporter (Donovan A et al., 2005). Binding of IRP to a conserved 5' UTR Iron Responsive Element (IRE) was demonstrated *in vitro* suggesting genetic iron regulation (Hentze et al., 1987; McKie et al., 2000). *In vitro* functionality of the 5' IRE by means of a reporter assay as well as further tissue distribution and iron regulation of IREG1 *in vivo* were demonstrated by Abboud and colleagues (Abboud and Haile, 2000). It was also shown that mutations in IREG1 in humans, leads to iron retention in the macrophages and liver abnormalities (Pietrangelo, 2007).

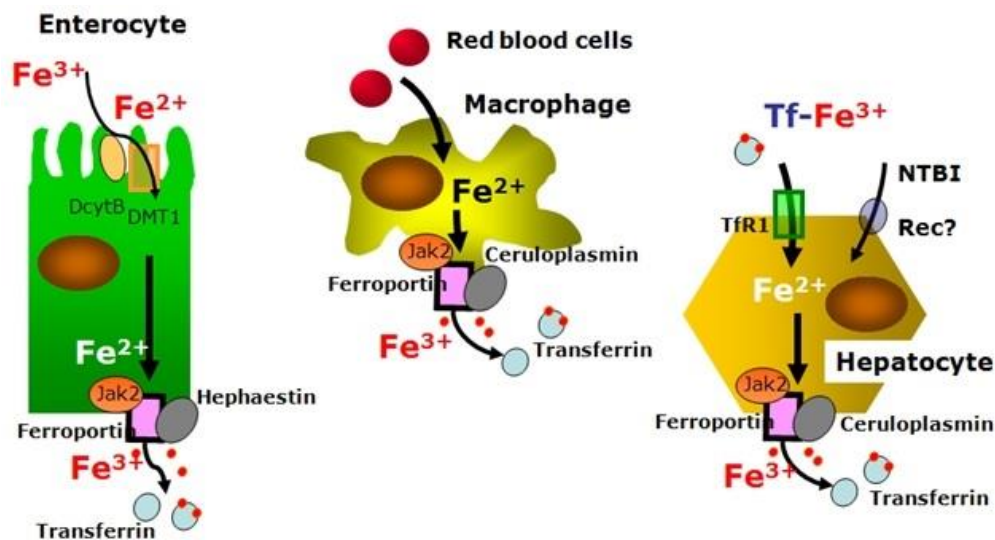


**Figure 3: Iron regulation in enterocytes, macrophages and hepatocytes.** Enterocytes, macrophages and hepatocytes acquire iron to maintain iron homeostasis and deliver the excess iron to the rest of the body through the iron exporter IREG-1, which needs copper-ferroxidases (either Cp or Heph the role of which still need to be established) to release iron

to the plasma transferrin (Tf). Heph is expressed predominantly in enterocytes rather than in macrophages or hepatocytes. **Figure taken from Mariani et al., 2009.**

Iron transported by IREG1 is ferrous as there appears to be a close relationship between IREG1 and multicopper oxidases: membrane bound hephaestin (HEPH) expressed on the basolateral membrane of the enterocytes, and plasma soluble homologue ceruloplasmin (CP) (Chen et al., 2006; McKie et al., 2001). A positional cloning/candidate gene approach was also used to gain the insights into basolateral iron transport. Mice with sex-linked anaemia (sla mice) were identified after radiation mutagenesis (Grewal., 1962). Sla mice have a partial defect in intestinal iron absorption that was shown to be associated with a problem in basolateral iron transfer (Edwards & Bannerman., 1970). Vulpe et al., found that sla is associated with a deletion mutation in a gene encoding a membrane-bound homolog of the multicopper ferroxidase, ceruloplasmin (Cp) (Vulpe et al., 1999). Since Cp was previously thought to play a role in cellular iron export they postulated that this new protein, designated as Hephhaestin (Heph) was the sla gene product. The link with the iron efflux had been demonstrated as early as 1968 when Cartwright and colleagues showed impaired iron export in copper-deficient pigs (Leet et al., 1968).

Iron deficiency increases the expression of IREG1 in the duodenum and decreases in the liver. Harris et al, created a Cp<sup>-/-</sup> mouse as a model for aceruloplasminemia, which presented with iron overload in macrophages and hepatocytes as a result of impaired iron efflux through IREG1 (Harris et al., 1999) which have normal copper metabolism (Meyer et al., 2001). Studies have demonstrated the requirement of glycosylphosphatidylinositol (GPI) anchored CP for the stability of cell surface IREG1 in brain and macrophages (De Domenico et al., 2007a). As in copper deficient animals, serum iron concentrations of Cp<sup>-/-</sup> mice do not change significantly after the administration of damaged red cells, but do increase after the administration of Cp and not aceruloplasmin (Harris et al., 1999). The current model shows that Heph expresses in the basolateral membrane of placental transport cells and duodenal enterocytes. Heph like Cp is categorised as a ferroxidase which helps in changing the oxidative state of iron released by IREG1, facilitating the incorporation into transferrin, the major serum iron carrier protein (Donovan et al., 2006). The anaemia of sla mice resolves after the neonatal period, suggesting that Heph is primarily needed for iron transfer during the accumulation of initial stores and that serum Cp may substitute later (Donovan et

*al.*, 2006). Though it is widely hypothesised that Heph may play its role in basolateral iron transfer its exact function needs to be established.

The released iron is sequestered by the apo form of transferrin (Tf). It is currently unclear whether the iron is passed to Tf directly or indirectly (Syed et al., 2006). Once bound to Tf, Fe<sup>3+</sup> is transported to tissues where it is taken up by receptor mediated endocytosis of the transferrin receptor (TfR). TfRs are present on the basolateral surface of the intestinal epithelium and undergo recycling as in other cells (Buys et al., 1991; Anderson et al., 1990; Hughson and Hopkins 1990). TfR assists iron uptake into the mammalian cells through a cycle of endocytosis and exocytosis of the iron transport protein Tf (Richardson and Ponka, 1997). Iron release in the endosomes may also be facilitated by membrane-bound oxidoreductases (Nunez et al., 1990). Fe<sup>3+</sup> is transferred from the endosomal compartments to the cytoplasm and other cellular organelles, through a process mediated by DMT1 (Fleming *et al.*, 1998). The cellular iron trafficking, following its release from the endosome, has still not been well characterised, except that in non-erythrocytes excess iron is taken up and stored in ferritin. It is hypothesised that a number of proteins must be involved in cellular iron trafficking. The reduced transport of iron from the mucosal cell to the circulation in *sla* mice provides the evidence that Heph plays a role in iron transport. On the basis of its homology with Cp, it has been proposed that Heph is a ferroxidase necessary for iron release from the intestinal epithelial cells (Vulpe et al., 1999).

### **1.05.003 Iron transport to Mitochondria**

Mitochondria are mostly appreciated for their role in energy transduction and other metabolic pathways (Richardson et al., 2010). Reversible oxidation states of iron enables the mitochondrion to catalyse the electron transport via haem- and iron-sulfur cluster (ISC)-containing proteins used in the process of energy transduction. However, it is less well known that mitochondrion can be considered a focal point when it comes to the metabolism of the most common transition metal in cells, namely iron (Napier et al., 2005). Iron in mitochondrion may be stored as mitochondrial ferritin (Richardson et al., 2010). Mitochondria are the sole site of haem synthesis and a major generator of ISCs both which are present in mitochondria and cytosol (Lill and Muhlenhoff, 2008). Haem is exported from the mitochondrion for use in the cytosol (Napier et al., 2005). Haem synthesis begins and ends in the mitochondria, with several intermediate steps taking place in the cytoplasm, which requires transport of biochemical precursors across the mitochondrial membrane (Andrews, 2009).

Iron is taken up by mitochondria by one or more mechanisms including direct uptake of iron (II) from the cytosol, driven by mitochondrial membrane potential (Lange et al., 1999), uptake of a chelator-inaccessible low-Mr iron pool from the cytosol (Shvartsman et al., 2007) and by a kiss-and-run mechanism, at least in haemoglobin-synthesising cells such as reticulocytes, in which Tf-laden endosomes make brief contact with the outer mitochondrial membrane (Sheftal et al., 2007, Richardson et al., 2010). Once iron is transported out of endosomes via DMT1, it enters the labile iron pool. The only strong evidence that a mitochondrial iron pool exists comes from studies with chelators that mobilise iron from cells (Ponka et al., 1979, Richardson et al., 1997). Since Tf-bound iron is efficiently used for haem synthesis (Richardson et al., 1996, Ponka et al., 1997) an intimate direct transfer of iron from Tf to the mitochondrion was proposed to occur (Ponka et al., 1976, Isobe et al., 1997). The idea of a direct transfer of iron to mitochondrion has developed and led to the kiss and run hypothesis (Ponka 1997). The kiss and run model suggests that a direct transfer of iron from the Tf-containing endosome to the mitochondrion occurs, bypassing the cytosol (Richardson et al., 1996, Ponka 1997, Richardson et al., 1997, Zhang et al., 2005). The precise molecular details and a possible contact between the endosome and the mitochondrion remain unknown.

The labile iron pool (LIP) serves as a bridge for metal transit between cell components and between the cell and the medium (Breuer and Cabantchik, 2000). LIP also mediates oxidative damage in iron overload conditions leading to iron-dependent tissue damage and in hereditary and transfusional haemochromatosis, neurodegenerative disorders and anaemia of the reticuloendothelial system. In such diseases, a better understanding of how precisely iron homeostasis is disrupted and how LIP is regulated will benefit for therapeutic interventions. Fluorescent metal sensors are used as tools to trace LIP in disease models, which share iron de-compartmentalisation as a common causative factor (hereditary haemochromatosis, genetic ataxias, sideroblastic anaemia and neurodegeneration) (Espósito et al., 2002). To find different therapeutic approaches for iron-dependent diseases it is important to understand the regulatory mechanisms that enable LIP to reconstitute iron-requiring enzymes without exposing cells to the damaging effects of metal-triggered formation of reactive free radicals. The targeted delivery of probes to organelles such as mitochondria and lysosomes may open different avenues to explore the relationship between the cytosolic LIP and organellar iron loops, which are the key components of iron homeostasis in the cells. In order to design probes targeting mitochondria, designing cellular

models of gene expression and assessing the molecular and cellular functions of the expressed genes, along with developing analytical tools that define the iron status in the same cells, and its movement across distinct organelles will help understand the role of Mitoferrin (Mfn1) in iron metabolism. Also assessing and correlating the cell's ability to adjust to different LIP levels in response to varying amounts of iron with the known regulatory activities of IRPs and ferritin may also help in understanding the role of LIP in iron homeostasis. Using novel oral iron chelators as therapeutic agents for conditions of iron overload (Thalasaemia and haemochromatosis) to understand the mechanisms whereby LIP permeates into cardiac cells and raises labile cell iron pools (LCIP) in different cell organelles of the heart were studied (Glickstein et. 2005; Cabantchik et al. 2004).

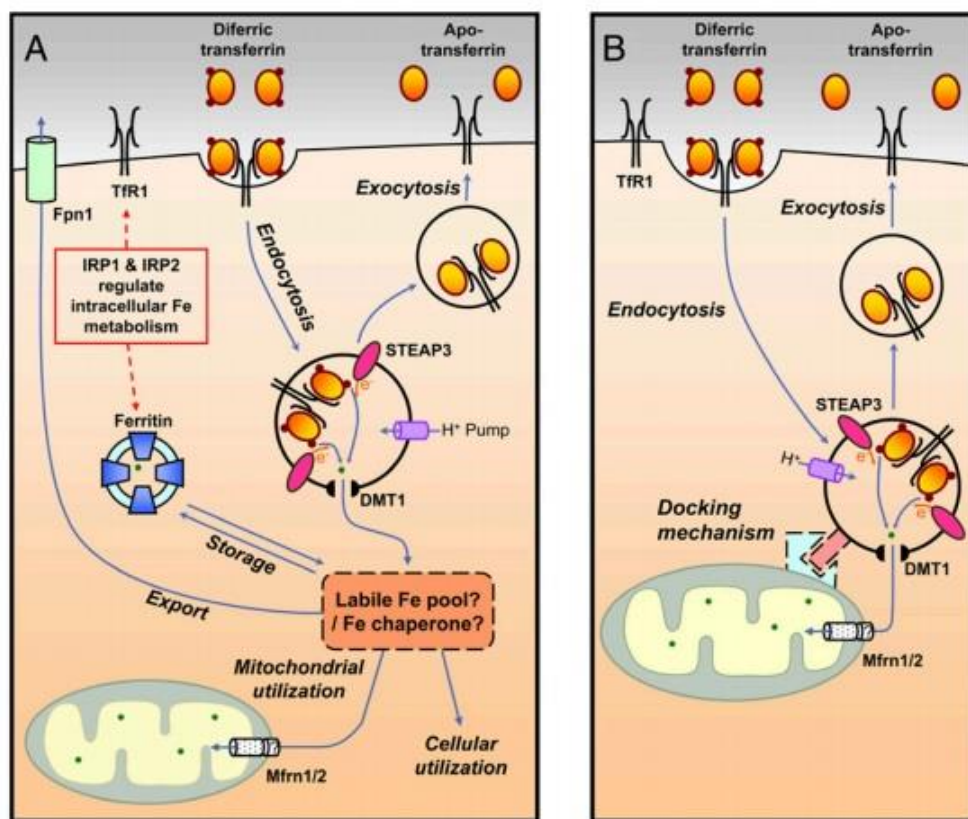


**Figure 4: Iron trafficking within the mitochondria.** A schematic representation of iron trafficking within the mitochondria. (A) Iron uptake and utilisation. (B) The kiss and run hypothesis suggests that a direct transfer of iron from the Tf-containing endosome to the mitochondrion occurs, by-passing the cytosol. **Figure taken from Richardson et al., 2010.**

Foury and Roganti suggested a role for the eukaryotic mitochondrial solute carriers, Mrs3 and Mrs4, in mediating mitochondrial iron metabolism in yeast (Foury and Roganti, 2002). Although the precise biochemistry of Mitoferrin1 (Mfn1 also known as SLC25A37) and

Mitoferrin2 (SLC25A28), which are homologous to Mrs3 and Mrs4 in yeast-mediated iron import by mitochondrion, is an unknown gene mutation in anaemic frascati zebrafish showed that Mfrn1 transports iron across the mitochondrial membrane (Shaw et al., 2006). Mfrn1 stabilisation is accomplished through interaction with Abc10 (also known as Abc-me) which is restricted to erythroid mitochondria (Chen et al., 2009). An interaction between Mfrn1, Abc10 and ferrochelatase was discovered by Chen's group in 2010. The interaction between Mfrn1 and Abc10 probably promotes efficient haem synthesis by funnelling iron directly to ferrochelatase, the enzyme that inserts iron into protoporphyrin IX to form haem (Lawen and Lane, 2013). It is still unknown how iron is transported across the outer mitochondrial membrane and clearly other transporters may yet be identified.

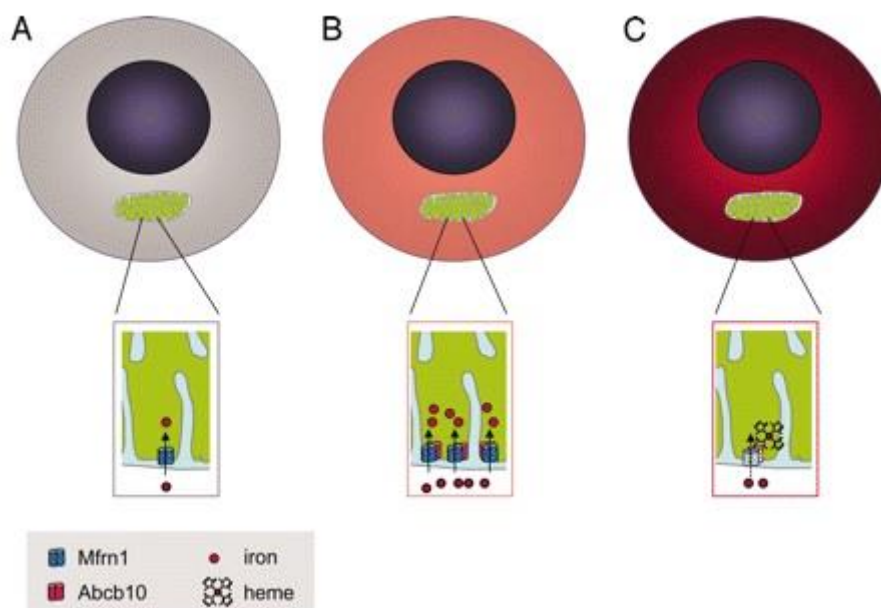


**Figure 5:** Figure showing the interaction between Mfrn1 and Abcb10 in erythroid cells. (A) In the absence of Abcd10, Mfrn1 is relatively unstable in erythroid progenitor cells limiting mitochondrial iron transfer. (B) During erythroid differentiation, Mfrn1 is stabilized by Abcd10 in the inner mitochondrial membrane to increase iron transfer. (C) After haem production is complete, haem acts to decrease Abcd10 protein levels, leading to turnover of Mfrn1. **Figure taken from Andrews, 2009.**

#### 1.05.004 Mitochondrial iron storage and export

Some mammalian tissues express a mitochondrial-specific ferritin (FTMT/MTF) that has a high level of sequence identity with a typical H-ferritin. Similar to cytosolic H-ferritin, FTMT also shows ferroxidase activity and binds iron (Levi et al., 2001). FTMT expression levels appear to be in correlation with the number of mitochondria rather than cellular iron content

(Drysedale *et al.*, 2002).FTMT has been found be highly expressed in testes and the erythroblasts of sideroblastic anaemia patients (Cazzola *et al.*, 2003, Santambrogio *et al.*, 2007). FTMT has also been detected in the heart, brain, spinal cord, kidney and pancreas (Santambrogio *et al.*, 2007). However, in contrary to H-ferritin, FTMT does not express in liver and spleen, suggesting a distinct role of FTMT. FTMT is encoded by an intron-less gene and hence fTMT expression is not post-transcriptionally regulated by intracellular iron levels (Drysedale *et al.*, 2002). The role of FTMT in iron metabolism was examined in a stably-transfected cell line that over-expressed FTMT (Nie *et al.*, 2005). FTMT over-expression leads to partitioning of iron between haem and ISC synthesis in the mitochondrion (Nie *et al.*, 2005). This effect not only alters mitochondrial iron metabolism, but also intracellular iron metabolism (Nie *et al.*, 2005).

Excess iron in the mitochondrion needs to be transported out into the cytosol. A candidate iron exporter mammalian mitochondrial ABC protein 3 (MTABC3; also known as ABCB6) was identified (Mitsuhashi *et al.*, 2000). MTABC3 had been shown to rescue mitochondrial iron loading, respiratory dysfunction and mitochondrial DNA damage in *atm1* (human ortholog of ABCB7) deficient yeast cells (Mitsuhashi *et al.*, 2000). It is still unclear how haem is exported from the mitochondrion. Given the low solubility and highly toxic nature of haem, haem-binding protein 1 has been identified as a haem carrier candidate (Taketani *et al.*, 1998). Although haem-binding protein 1 could be a candidate for haem transport, direct evidence for the carrier nature has been lacking.

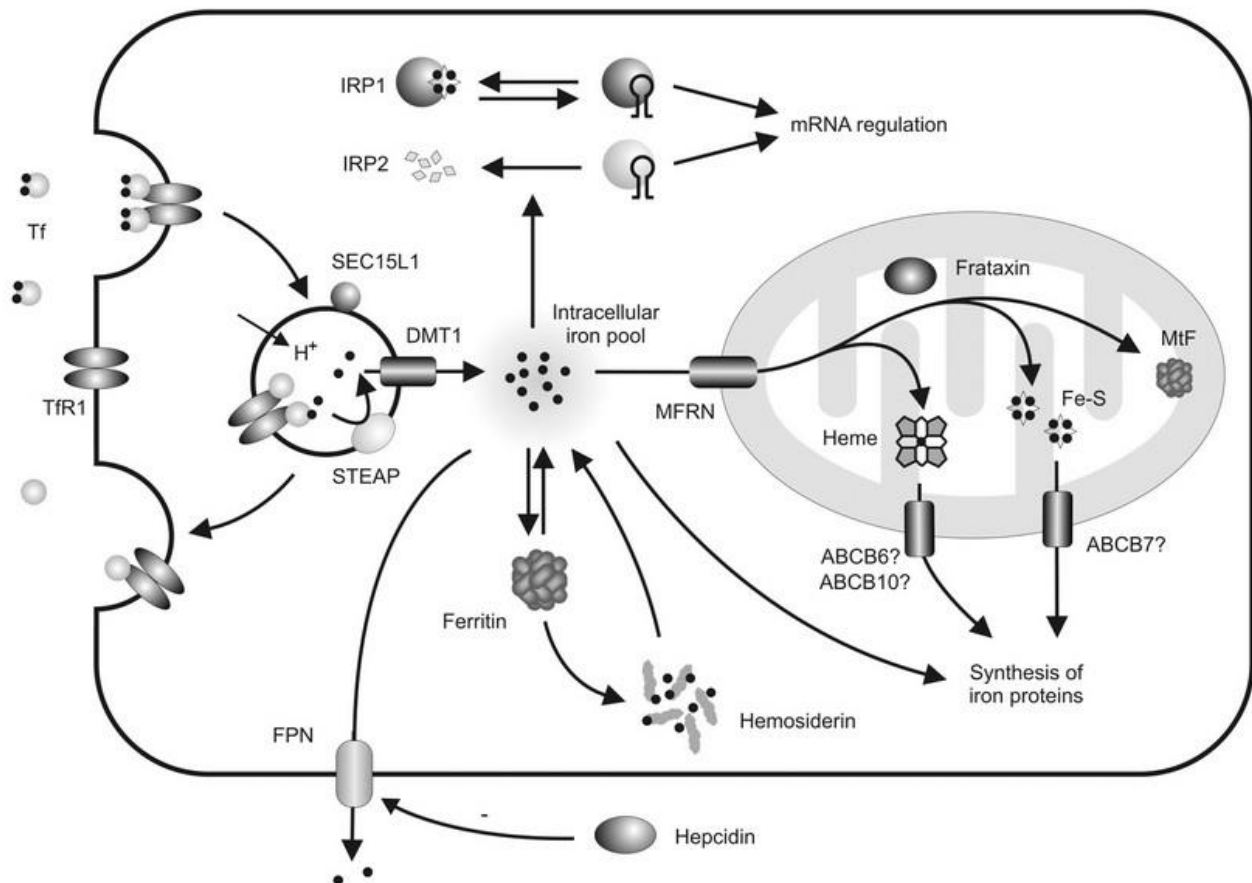


**Figure 6: Molecules involved in mitochondrial iron transport.** Iron is taken up by most body cells as Tf-bound iron, which binds to TfR1 on the cell surface. The iron can also enter the mitochondria via the transporter mitoferrin (MFRN) after which it is be incorporated into haem or iron-sulfur clusters for use in protein synthesis. Although the role of Frataxin is unknown it is also involved in iron-sulfur cluster formation. The ABC transporters are thought to play a role in the export of haem and iron-sulfur clusters from mitochondria, although the precise molecules involved are still unclear. Excess mitochondrial iron is stored in mitochondrial ferritin (MtF). **Figure taken from Reid et al., 2009.**

### 1.06 Cellular iron regulation

Regulation of cellular iron uptake, storage and absorption must be controlled at a cellular level. Intestinal iron absorption is partially regulated in response to a signal that communicates information about the amount of iron in “the stores” (Hentze et al., 2004; Finch 1994). Erythroid cells consume most of the available dietary iron. Iron regulation is achieved at transcription, mRNA processing and decay, initiation of translation and post-translational levels. The adaptation of the body to iron deficiency or iron overload depends on the extent of iron absorption by the intestinal mucosa. Regulation of iron absorption is important to maintain iron balance within the body. Since both apical iron uptake and

basolateral iron transfer are required in iron absorption, regulation of iron absorption can involve the expression or function of proteins on either surfaces of the enterocyte. The two factors that play an important role in regulating the rate of intestinal iron absorption are the level of iron stores in the body and the level of erythroid cell production in bone marrow.

### 1.06.001 Regulation of iron in stores

The cellular and molecular mechanisms through which the above factors determine the control of intestinal absorption are poorly defined. Regulation of iron absorption may be achieved by changes in the 'number of mucosal cells' adapted to absorb iron or changes in the individual mucosal cells ability to absorb iron or both. Several theories were proposed to explain the biochemical mechanisms undergoing the control of iron absorption by mucosal intestinal cells (Cook, 1990; Flanagan, 1989). According to the Mucosal Block Theory (MBT) proposed by Hahn (Hahn, 1941) the number of iron acceptor molecules present in the intestinal mucosa is limited. As a consequence, if these acceptors are blocked either by exogenous or endogenous iron a block of dietary iron absorption takes place. Granick (Granick, 1954) revised the mucosal block theory and suggested that the ferritin-apotransferrin system in mucosal intestinal cells directly controls the amount of iron absorbed.

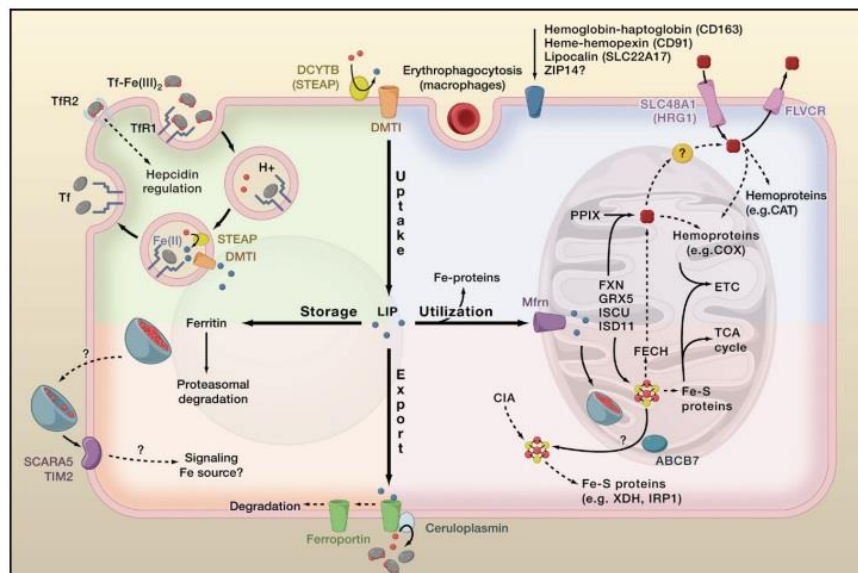


**Figure 7: Cellular iron metabolism.** Most cells acquire plasma iron via TfR1-mediated endocytosis of Tf-bound iron. Iron uptake systems feed the so-called labile iron pool (LIP). The LIP is utilized for direct incorporation into iron proteins or iron transport to mitochondria via Mfrn, where the metal is inserted into haem and Fe/S cluster prosthetic groups. The fraction of the LIP that is not utilized for metalation reactions can be exported via IREG1,

which works together with ferroxidases for iron loading onto Tf, or stored in a nontoxic form in ferritin shells. Ferritin can be released into the extracellular milieu by unknown mechanisms and interact with specific receptors on the cell surface. Some cells also express a mitochondrial form of ferritin to protect the organelle against iron-induced toxicity. The size of the LIP is determined by the rate of iron uptake, utilization, storage, and export and these processes should be efficiently regulated to avoid any iron excess or deficiency. **Figure taken out from Hentze et al., 2010.**

Granick's theory lost the support since no apoferritin or ferritin was observed on brush border intestinal membranes. In contrast to the MBT, several studies have shown that iron continues to be absorbed even when tissues are loaded with iron. The observation that iron is localised in the epithelial cells of intestinal mucosa was made from the dietary and body iron stores (Conrad et al., 1964, Chisari et al., 1966) led to the hypothesis that the quantity within the absorptive cells regulates iron absorption in the intestinal mucosa. Experiments using isolated duodenal epithelial mucosal cells challenged this hypothesis (Balcerzak and Greenberger, 1968).

The existence of an iron-dependent control mechanism of intestinal iron uptake was demonstrated by Goddard et al in 1997 in human enterocytes. The metal cation transporter DMT1 may play a relevant role in the intestinal iron absorption (Goddard et al., 1997). Another theory suggests that iron absorption is regulated by a balance mechanism. This theory is based on the probability of exchanges that may occur between the plasma and various cellular iron pools (Cavill, 1975). Ultra-structural methods using Prussian blue staining proved that low levels of stainable iron within the small intestinal mucosal cells of iron-deficient animals is found in comparison with specimens from normal fasting rats (Parmeley et al., 1979). Observations made by Parmeley et al in 1979 showed that the quantity of iron within small intestinal mucosal cells varies directly with the degree of iron repletion and suggests that this phenomenon may play a role in the regulation of iron absorption. With free ionic iron being a toxic oxidant it is difficult to accept that the ionic iron directly inhibited iron uptake by the intestinal mucosal cells. Hence it was postulated (Conrad et al., 1987) that this iron might make iron-binding receptors of some molecules within the mucosal cells act as regulators of iron absorption. The transcriptional mechanisms of iron regulation involving Heparin (HAMP) has been well characterised as most of the iron

sensing is thought to be mediated posttranscriptionally (IRP-IRE loop) or through HAMP on a systemic level. Direct effects of levels of iron, hypoxia or localised inflammation are difficult to distinguish from liver HAMP mediated effects as HAMP responds to all the conditions. Iron homeostasis is also altered in response to hypoxia, through a proposed humoral “hypoxia regulator” (Hentze et al., 2004). Liver-specific stabilization of the hypoxia-inducible factor 1 (HIF1) and HIF2 decreases HAMP expression and chemical HIF stabilizers can suppress HAMP mRNA expression in hepatoma cells (Peyssonnaud et al., 2007). From these findings it can be hypothesised that iron-dependent prolyl hydroxylases involved in HIF degradation may act as hepatic iron sensors but their interaction with HAMP promoter is currently controversial.

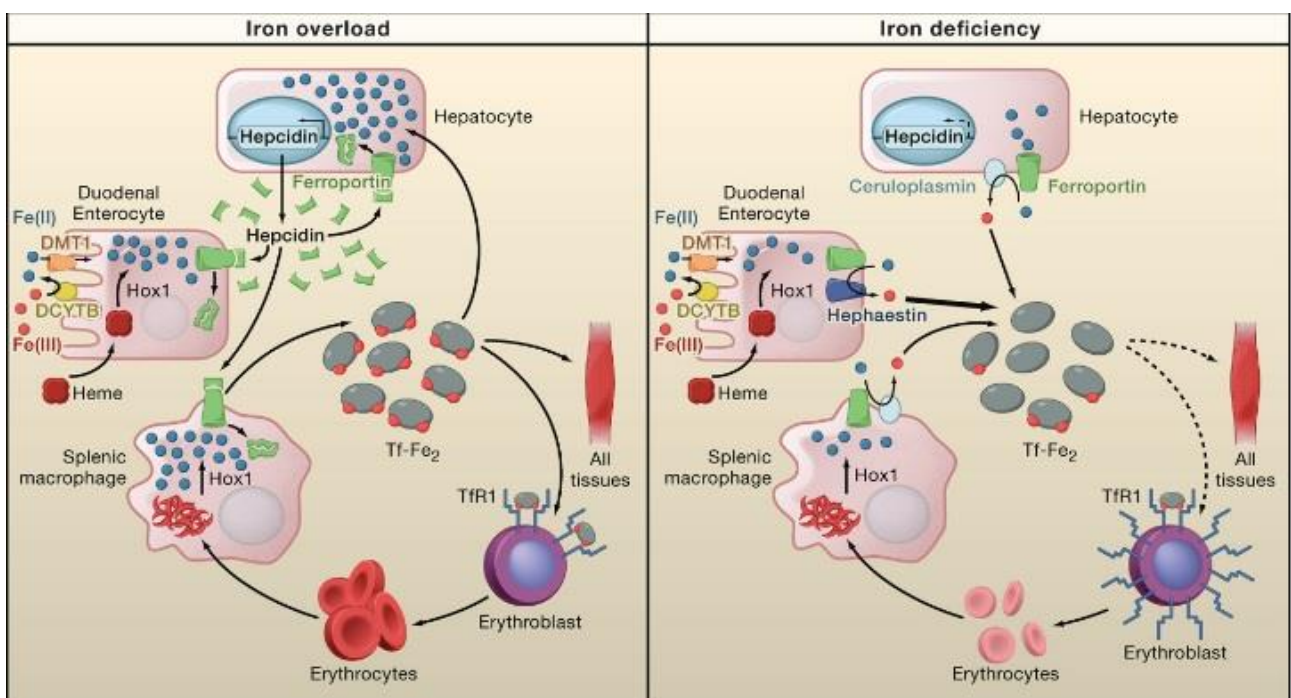


**Figure 8: Systemic iron regulation in iron overload and deficient conditions.** Figure depicts the systemic iron regulation in both iron overload and iron deficiency conditions are shown. Iron-loaded (diferric) transferrin (Tf-Fe<sub>2</sub>), indicated by red dots, supplies iron to all cells by binding to the TfR1 and subsequent endocytosis. TfR1 is highly expressed on haemoglobin-synthesizing erythroblasts. Hepatocytes sense Tf saturation/iron stores and release HAMP accordingly. Red cell iron is recycled by macrophages via IREG1 and the ferroxidase Cp. In iron overload (left), high HAMP levels inhibit IREG1-mediated iron export by triggering internalization and degradation of the complex to reduce Tf saturation. HAMP expression is also high. In iron deficiency (right), iron is released by IREG1 into the circulation. Haemoglobin-derived haem is catabolized in macrophages by haemoxygenase-

1 (HOX1). Hepcidin expression is low in case of iron deficiency. **Figure taken from Hentze et al., 2010.**

#### **1.06.001.1 Molecules involved in the regulation of cellular iron**

Communication between the sites of uptake, utilisation and storage in an organism controls the cellular iron balance. The trafficking of iron into plasma is largely controlled by the iron regulatory hormone hepcidin (HAMP). HAMP, is a 25 residue peptide which was purified from serum with antimicrobial activity LEAP1 (liver expressed antimicrobial peptide) (Krause et al., 2000; Pantopoulos et al., 2012). Later HAMP was isolated from human urine, by Park and colleagues, in which additional peptides of 20 and 22 residues were detected in which HAMP was truncated at the N terminus (Park et al., 2001). The authors showed the homology with small cystine rich peptides –  $\beta$  defensins, reported to be involved in innate immunity and with broad spectrum antimicrobial activity (Park et al., 2001). The mature, active form of HAMP is the 25 amino acid peptide. The 25 amino acid form is rich in  $\beta$  sheets and contains four disulphide bonds integrated within the conserved cysteines. Hepcidin is a circulating peptide secreted by hepatocytes (Krause et al., 2000, Park et al., 2001, Pigeon et al., 2001) that binds to ferroportin at the cell surface to initiate ferroportin internalisation and degradation (Nemeth et al., 2004) thus reducing the dietary iron absorption. Ferroportin is the only exporter of inorganic iron in mammalian cells (Pantopoulos et al., 2012). Therefore, inactivation of ferroportin causes intracellular iron retention (Weiss 2009, Brasse-Lagnel et al., 2011). Hepcidin has also been shown to promote proteasomal degradation of DMT1 (Brasse-Lagnel et al., 2011). Loss of hepcidin protein results in severe iron overload in mice (Nicolas et al., 2001) and human patients (Roetto et al., 2003, Papanikolaou et al., 2004), confirming the role of HAMP in regulating iron balance in the body. Expression of HAMP, which is known as a negative regulator of iron absorption, decreases in response to anaemia and hypoxia (Nicolas et al., 2002). The negative regulatory effect of hepcidin turns out to be advantageous as it makes more iron available for erythropoiesis. However, expression of HAMP increased during inflammation (Nemeth et al., 2004) and non-genetic iron overload (Pigeon et al., 2001). Increased expression of HAMP during inflammation and non-genetic iron overload minimises the availability of iron, inhibiting the growth of pathogens and limiting iron availability (Donovan et al., 2006).

Genetic experiments have suggested that HAMP helps iron release from enterocytes and macrophages. It was reported that injection of synthetic HAMP into mice inhibited iron uptake in isolated duodenal segments (Laftah et al., 2004). IREG1 has shown to be the

HAMP receptor (Nemeth et al., 2004). HAMP causes the internalisation and degradation of IREG1 and in doing so switches off the iron export (Robson and Drakesmith, 2005). Studies confirmed that the iron exporting tissues and cells have no significant alternative to the IREG1 efflux pathway and provide further support for the fundamental role of the HAMP-IREG1 interaction in systemic iron homeostasis (Donovan et al., 2005).

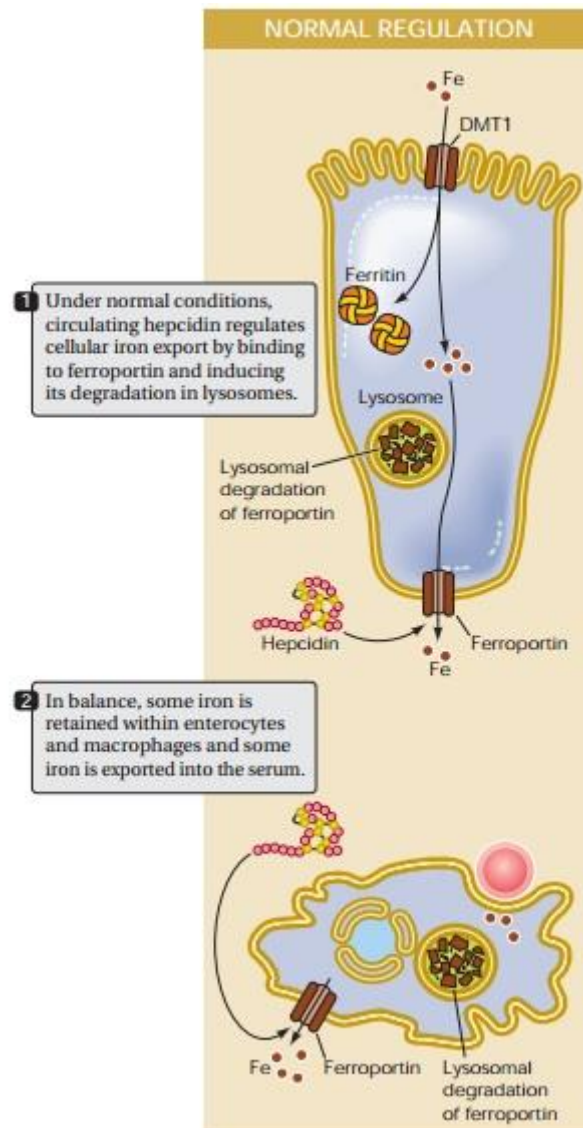


**Figure 9: Schematic representation of normal iron regulation.** Figure taken from Donovan et al., 2006.

Though the discovery of HAMP and the conditions that regulate HAMP expression is known, the question of how HAMP expression is altered in response to body iron requirements is not well known. Membrane proteins like transferrin receptors (TfR1 and TfR2), hemojuvelin (HJV/HFE2) and HFE (major histocompatibility complex MHC-1 class protein) have been associated with modulating hepcidin expression *in vivo* (Anderson and Frazer, 2006) and

iron-dependent induction. Mice and humans deficient in HFE have been reported to have reduced hepcidin expression despite iron overload (Ahmad et al., 2002, Muckenthaler et al., 2003, Bridle et al., 2003). The fact that HFE forms a protein complex with the transferrin receptor (TfR) has led to a hypothesis that a soluble factor such as diferric Tf (which competes with HFE for TfR binding) might modulate HFE activity and regulate a potential pathway signalling to the hepcidin promoter. HFE is strongly expressed in hepatocytes, like HAMP, suggesting that it is in hepatocytes that HFE is exerting its effect on HAMP expression (Zhang et al., 2004). Evidence suggests that hepatic iron and circulating iron induce HAMP expression by distinct pathways (Corradini et al., 2011, Ramos et al., 2011).

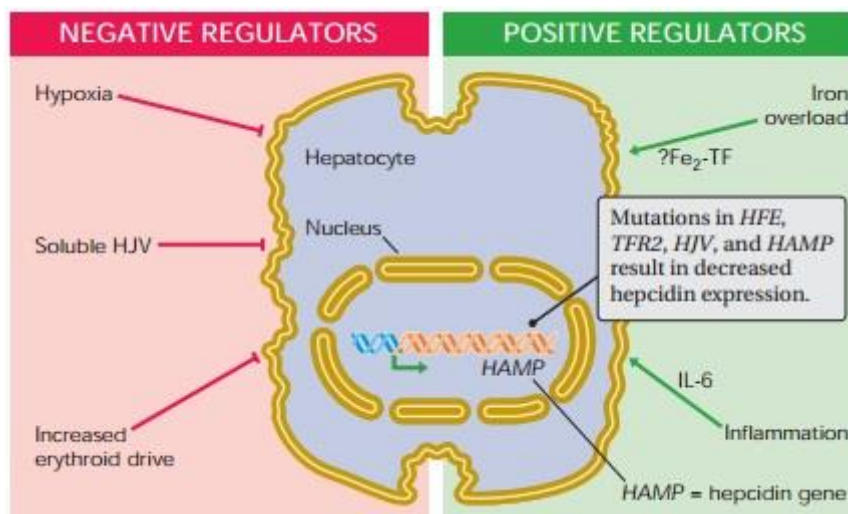


**Figure 10: Regulation of HAMP expression.** Figure shows the negative and positive regulators in HAMP regulation. **Figure taken from Donovan et al., 2006.**

HJV is expressed in different tissues like liver, heart, skeletal muscle and also found in plasma in a soluble form. Cell-associated HJV is required for normal HAMP expression in hepatocytes and soluble HJV negatively regulates HAMP expression in hepatocytes (Lin et al., 2005). Disruption of HAMP regulation is associated with disturbances of iron metabolism by at least two independent mechanisms which both converge their effects on to the bone morphogenic proteins (BMP) signalling pathway. The membrane-associated protease, TMPRSS6 physically interacts with HJV and cleaves HJV when both proteins are expressed on the cell surface, suggesting that HJV is the major TMPRSS6 target for iron regulation (Silvestri et al., 2008a). Genetically, the deficiency of both HJV and TMPRSS6 causes iron overload, suggesting that TMPRSS6 acts upstream of HJV (Truksa et al., 2009, Finberg et al., 2010). Increased HJV surface expression has however yet to be confirmed in TMPRSS6-deficient mice or IRIDA patients. However, it needs to be investigated, how

TMPRSS6 expression and activity are regulated, and the relative contributions of TMPRSS6 to the regulation of HJV and systemic iron homeostasis.

High HJV expression in skeletal muscle leads to speculation that, soluble HJV (sHJV) is released as a muscle signal in iron deficiency. The release of sHJV mainly from the muscle into the blood can act to antagonise BMP signalling because of the competition for the hepatocyte BMP receptors. Release of sHJV not only depends on the amount of serum holotransferrin but also on the iron status of the muscle. Release of sHJV from the muscles is mediated by furin cleavage which is regulated by iron (Silvestri et al., 2007). In the iron-depleted condition sHJV downregulates HAMP by interfering with BMP signalling and this negatively regulates HAMP expression. Whereas increased levels of serum holotransferrin reduces the release of sHJV thus augmenting BMP signalling and increased HAMP expression.

Membrane proteins like HFE, TfR1 and TfR2 have also been implicated in hepatocyte HAMP regulation by iron (Schmidt et al., 2008; Robb and Wessling-Resnick, 2004). Like HFE, deficiency of TfR2 attenuates HAMP expression in mice (Kawabata et al., 2005) and humans (Nemeth et al., 2005) and results in moderate iron overload. TfR2 is expressed in both hepatocytes and erythroblasts. Since no erythropoietic abnormalities have been reported in mice or humans, it suggests that TfR2 requirement for HAMP regulation is intrinsic to hepatocytes and not the result of feedback through the anaemia/hypoxia regulatory pathway. HJV-deficiency in mice (Huang et al., 2004, Papanikolaou et al 2004) and in humans (Huang et al., 2005, Niederkofler et al., 2005) has been shown to reduce the HAMP levels further than HFE and TfR2, resulting in severe iron over-loading. TfR1 when bound to HFE keeps it in an inactive state and the competition between holotransferrin and HFE for TfR1 forms the key component of iron sensing. An increase in serum holotransferrin will result in release of HFE from TfR1 thus allowing it to bind to TfR2 which in return begins the signal for HAMP induction. An *in vivo* study in mice has suggested that BMP stimulation may be independent of HFE, TfR2 and IL-6 (Truksa et al., 2006). Hence, through an unknown pathway the HFE/TfR2 complex could directly regulate HAMP transcription.

#### **1.06.001.2 Regulation by Inflammatory and Stress Signals**

The inflammatory cytokines IL1 and IL6 are both potent inducers of hepcidin expression. IL6 activates the Janus kinase (JAK)/signal transducer and activator of transcription (STAT)

signalling pathway, which activates the hepcidin promoter via a STAT-binding motif close to the transcription start site (Fleming 2007). The BMP signalling pathway also contributes to the inflammatory response via SMAD4 (Casanovas et al., 2009; Wang et al., 2005). Hepcidin transcription was severely impaired in mice with targeted deletion of IL-6 in the liver (Pietrangelo et al., 2007). Mice injected with lipopolysaccharide (LPS) increases the hepcidin transcription even in the context of iron overload. LPS counteracts the diminished hepcidin expression in response to iron deficiency, suggesting that the two signals are integrated at the hepcidin promoter and that inflammatory and iron store regulators operate independently rather than following a strict hierarchy (Huang, et al., 2009a). Stress in the endoplasmic reticulum (ER) also increases HAMP expression. This stress response can be controlled by the transcription factor cyclic AMP response element-binding protein H (CREBH) (Vecchi et al., 2009) or by the stress-inducible transcription factors CHOP and C/EBPalpha (Oliveira et al., 2009). It has also been suggested that increased hepcidin transcription and iron deprivation may represent defense mechanisms against excessive cell proliferation and cancer, possibly by binding of the p53 tumor suppressor protein to a response element in the hepcidin promoter (Weizer-Stern et al., 2007).

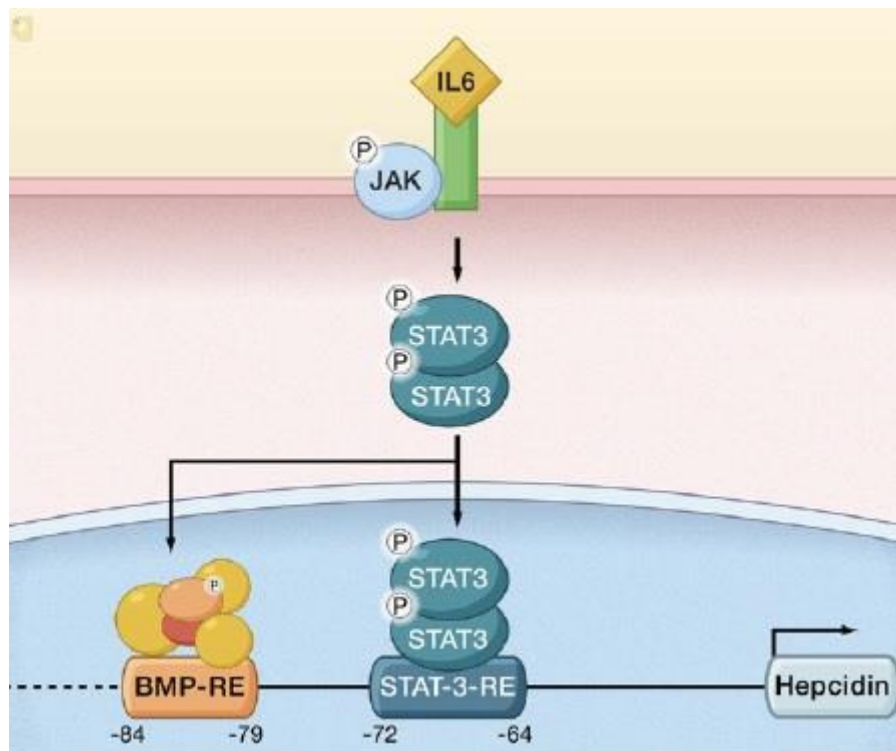


**Figure 11: HAMP regulation by inflammatory stimuli.** Figure depicts Hepcidin regulation by inflammatory stimuli. Interleukin 6 (IL6) activates the Janus kinase (JAK)/ signal transducer and activator of transcription (STAT) signaling pathway and stimulates the hepcidin promoter via a STAT binding motif close to the transcription start site. The BMP signalling pathway also contributes to the inflammatory response via SMAD4. **Figure taken from Hentze *et al.*, 2010.**

### 1.06.001.3 Regulation of iron absorption by erythropoiesis

The effect of erythropoietic rate on iron absorption can be dependent on the basis of its effect on plasma iron turn over. The theory proposed by Carpenter and Mahoney (1992) is based on the idea that iron absorption is controlled through mechanisms similar to those responsible for iron-dependent control of the synthesis of ferritin, transferrin and transferrin receptor. It must be pointed out that a close parallel exists between iron absorption and rate of erythropoiesis (Finch, 1982). HAMP expression in hepatocytes is regulated by multiple paths, mainly by systemic iron availability (such as diferric transferrin, Tf-Fe<sub>2</sub>), iron stores in hepatocytes, erythropoietic activity, hypoxia, and inflammatory/infectious states. Erythropoiesis requires considerable quantities of iron, and the inhibition of HAMP expression by erythropoietic signals. HAMP suppression in response to phlebotomy or hemolysis depends on intact erythropoietic activity in mouse models: irradiation and

cytotoxic inhibition of erythropoiesis prevent HAMP suppression (Pak *et al.*, 2006). GDF15 and TWSG1 are both released by erythroid precursors. High doses of GDF15 are detectable in the serum of patients with ineffective erythropoiesis such as  $\beta$ -thalassemia (Tanno *et al.*, 2007). Lower GDF15 concentrations fail to suppress hepcidin in cellular models and are apparently ineffective in patients with sickle cell anaemia, myelodysplastic syndrome, and ACD. In cellular models, the BMP-binding protein TWSG1 inhibits BMP-dependent activation of Smad-mediated signal transduction that leads to hepcidin activation (Tanno *et al.*, 2009). However, the molecular mechanisms and factors responsible for erythropoiesis are still poorly understood.

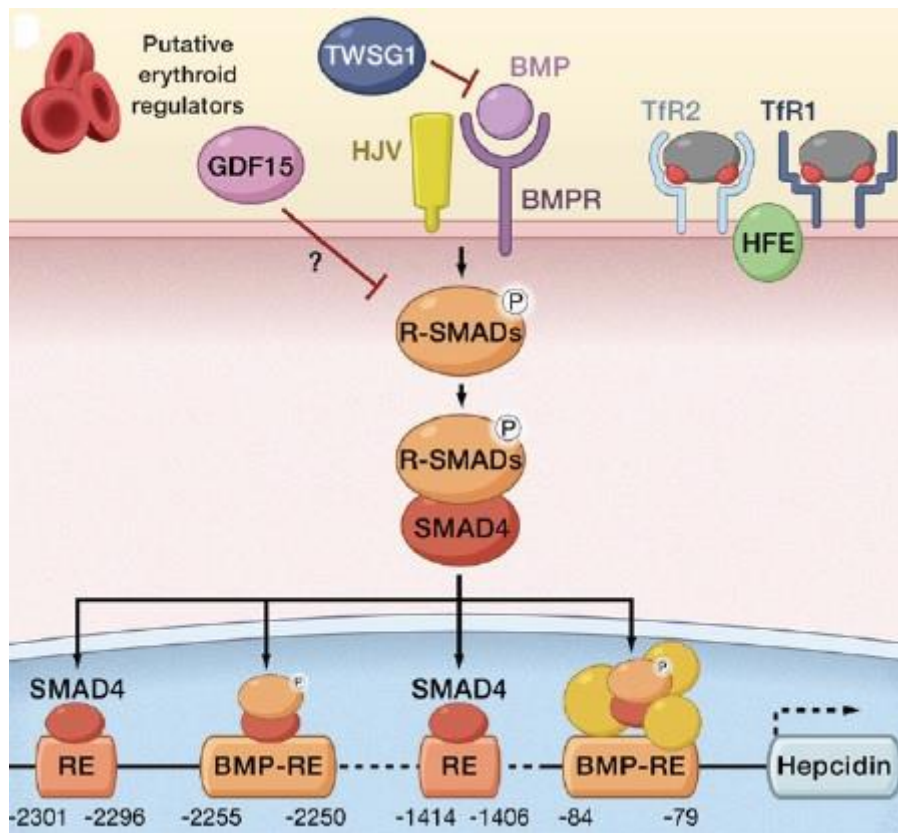


**Figure 12: Iron regulation by HAMP using erythropoietic signals.** Growth differentiation factor 15 (GDF15) and twisted gastrulation BMP signalling modulator 1 (TWSG 1) are released by erythroid precursors to inhibit BMP/SMAD activation of HAMP in iron-loading anaemia. **Figure taken from Hentze et al., 2010.**

### 1.07 Current study

Although the molecular mechanisms regulating iron absorption remain to be determined it is clear that the entire process of iron absorption, storage and transport is a highly regulated process. Though the mechanism and regulation of iron absorption has been well

documented, establishing the role of few candidate proteins would advocate possible roles for all of them in iron metabolism. Though Heph is known to be expressed on the basolateral membrane of the cell, its role in efflux of excess iron along with Cp has not been established yet. Since protein:protein interaction studies reflect on the interacting partners of protein of interest, the current study seeks to establish any interactions between Heph, Cp and other molecules expressed on the basolateral membrane of the cells to confirm the role of Heph in iron efflux. By carrying out a protein:protein interaction approach the current study was also focussed on establishing the role of IRPs (IRP1 and IRP2) in the regulation of systemic iron metabolism. Along with Heph and IRPs in this study tagSNP analysis of Mfrn gene was also carried out to establish any correlation between the tagSNPs of the Mfrn gene and DNA samples of Asian and Caucasian DNA samples for which different covariates, like gestational age, mother's booking weight and birth weight were considered.

#### **1.07.001.1 Mitoferrin, a solute carrier in SLC25 super family**

SLC25A37 belongs to the SLC25 family of nuclear-encoded transporters embedded in the inner mitochondrial membrane and in a few cases other organelle membranes. The members of SLC25 family are widespread in eukaryotes. SLC25 mitochondrial carriers can be easily recognized by their striking sequence features, i.e., a tripartite structure, six transmembrane  $\alpha$ -helices and a 3-fold repeated signature motifs. Although the molecular mechanism of substrate translocation may be basically the same among the SLC25 members, they vary greatly in the nature (most of the transported substrates are negatively charged, but some are positively charged or zwitterions at physiological pH values) and size of their transported substrates and modes of transport (i.e., uniport, symport or antiport). Based on substrate specificity, 24 subfamilies have been functionally characterized mainly by transport assays upon heterologous gene expression, purification and reconstitution into liposomes.  $\text{Fe}^{2+}$  acts as a major substrate for SLC25A37. Mutations in the SLC25 genes have been shown to be responsible for 11 diseases, highlighting the important role of SLC25 in metabolism. Mitochondria and cytosol share and participate mutually in a large number of metabolic cellular processes. Due to the enzyme compartmentalization, a continuous and highly diversified flux of solutes into and out of mitochondria takes place across the inner membrane. Mitochondrial carriers (MCs) are involved in many important metabolic pathways, such as oxidative phosphorylation, the citric acid cycle, fatty acid (FA) oxidation, amino acid degradation, gluconeogenesis, lipogenesis, transfer of reducing equivalents, synthesis and breakdown of mtDNA, mtRNA and mitochondrial proteins, urea synthesis, haem

biosynthesis, ketone body production and utilization, modulation of the nucleotide and deoxynucleotide pools in the mitochondrial matrix, heat production,  $\text{Ca}^{2+}$  cell signaling, and necrotic and apoptotic cell death.

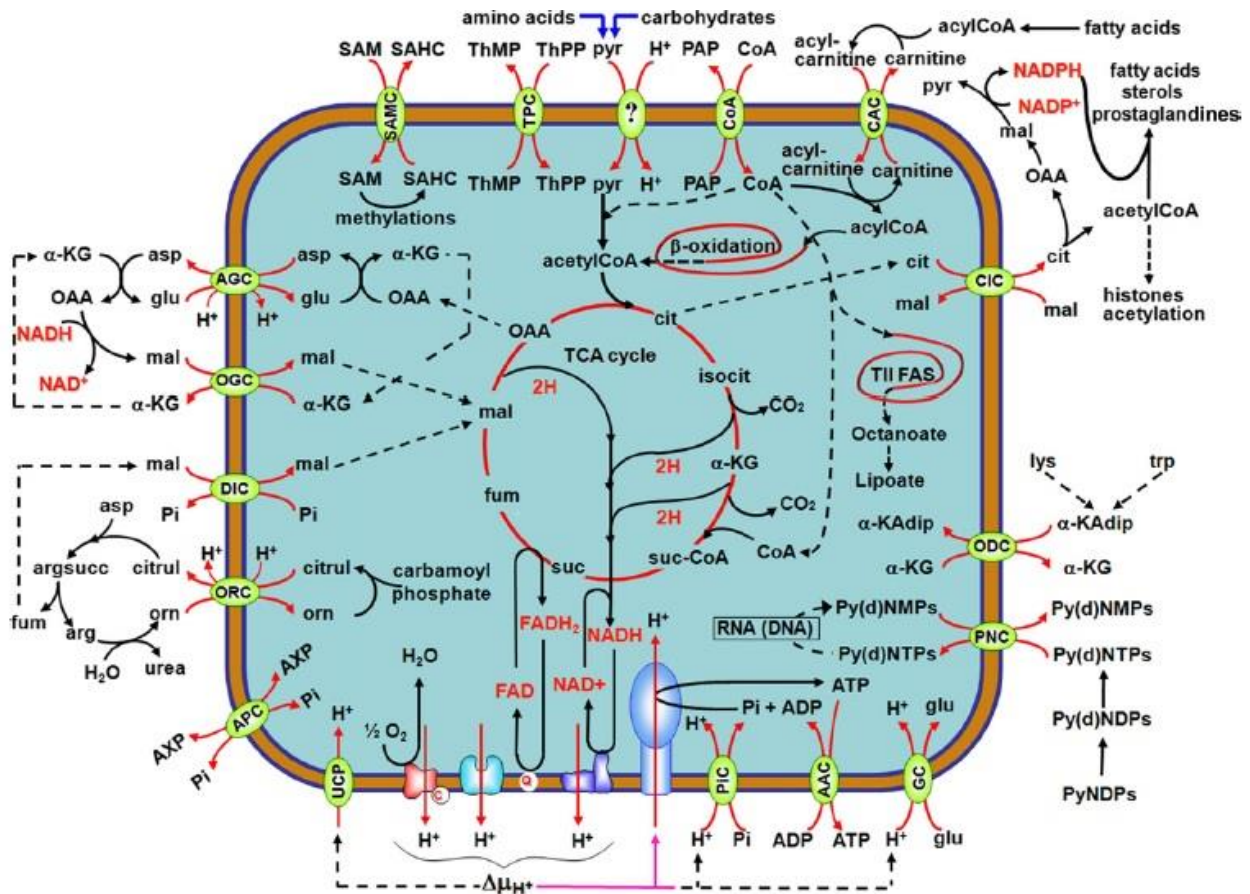


**Figure 13: Metabolic roles of different mitochondrial carriers (MCs).** The schematic representation of the above figure shows 16 functionally identified MCs catalyzing metabolite, nucleotide or coenzyme transport through the inner mitochondrial membrane. These carriers are involved, with partial overlap, in: oxidative phosphorylation (AAC, PiC, UCP); oxidation/reduction pathways (AGC, OGC, DIC, CIC, CAC); synthesis and breakdown of mitochondrial DNA and RNA (PNC); homeostasis of the intramitochondrial adenine nucleotide pool (APC); methylation of mtDNA, mtRNA and some intramitochondrial proteins (SAMC); import of thiamine pyrophosphate (ThPP) required for pyruvate- and oxoglutarate-dehydrogenase complex activities (TPC); import of coenzyme A (CoA) required for fatty acid (FA)  $\beta$ -oxidation, Krebs cycle, biosynthesis of haem, branched-chain amino acid catabolism, urea cycle and mitochondrial type II FA synthase (CoA carrier); and amino acid metabolism (AGC, ORC, GC, ODC). **Figure taken from Palmieri, 2013.**

### **1.07.001.2 Phylogenetic analysis of SLC25 carriers**

A phylogenetic tree of all human MCs is revealed in figure 13. Based on sequence similarity, human MCs cluster into many different clades suggesting a large variety of specialized functions. Given that the MCs of *H. sapiens*, *S. cerevisiae* and *A. thaliana* cluster into the same clades, with very few exceptions, one can deduce that a common ancestor for all eukaryotes had already possessed many MC functions that have been retained in fungi, plants and animals (Palmieri *et al.*, 2011). Low-grade sequence similarity detected in the two helices of each repeat, has aided in hypothesising that the primordial repeat may itself have evolved by the duplication of a DNA sequence encoding a single transmembrane segment (Fiermonte *et al.*, 1999).

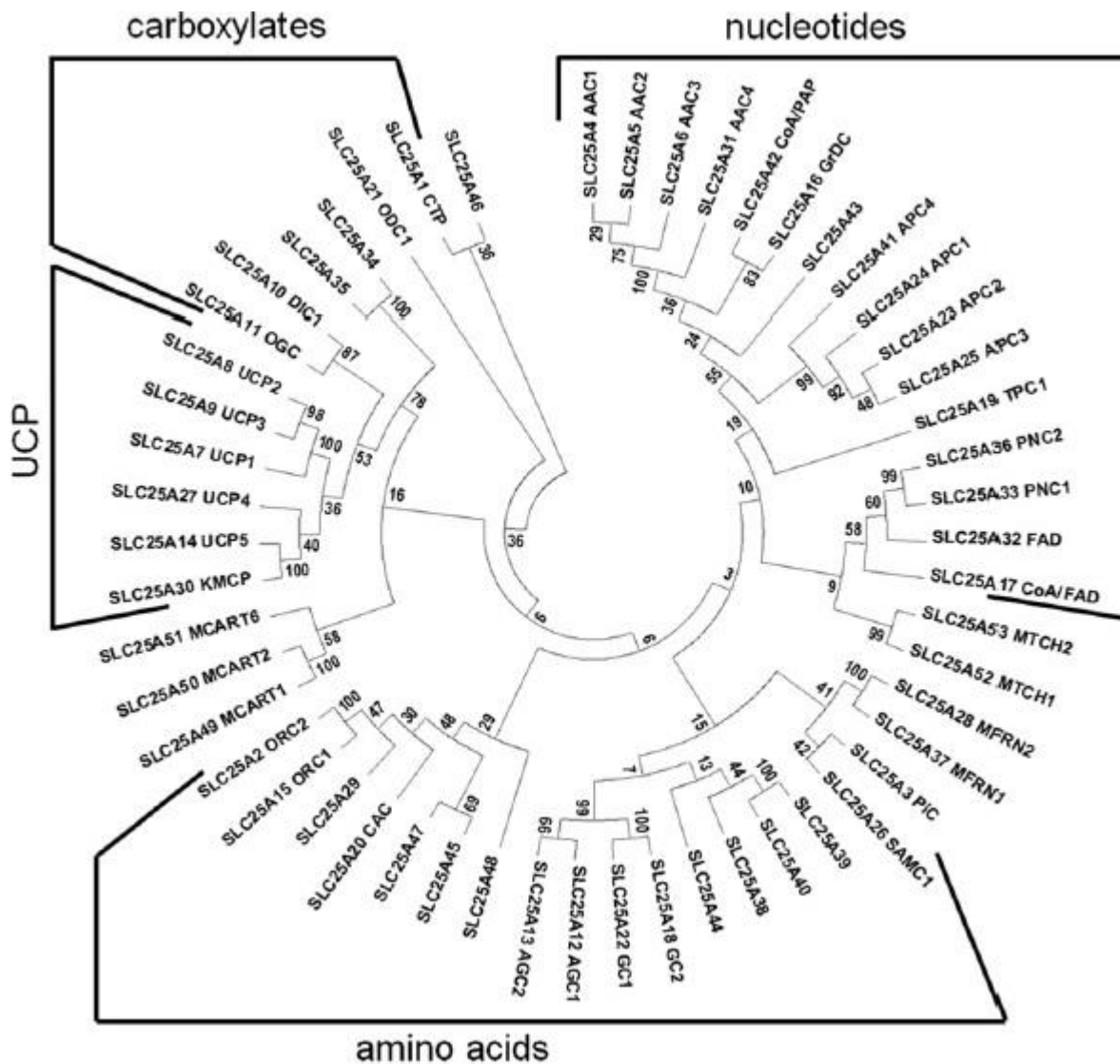


**Figure 14: Phylogenetic tree of human mitochondrial carriers.** Phylogenetic tree of human MCs was result of ClustalW multiple-sequence alignments by using the neighbor-joining method implemented in MEGA5. All 53 human mitochondrial carriers are shown. Bootstrap values for 1000 replicates are reported on each node (Palmeieri, 2013). Based on the substrate specificity, MCs can be divided into carriers for carboxylates, keto acids, amino acids, nucleotides, dinucleotides and other substrates. The carriers categorised under uncoupling proteins (UCP) and carriers transporting nucleotides, carboxylates and amino acids are boxed. **Figure taken from Palmeieri, 2013.**

### 1.07.001.3 SLC25 solute carrier structure

All mitochondrial carrier family members, including SLC25A37 have a tripartite structure, i.e., consist of three tandemly repeated homologous domains of about 100 amino acids in length;

each repeat contains two hydrophobic stretches, that span the membrane as  $\alpha$ -helices, and a signature sequence motif  $PX[D/E]XX[K/R]X[K/R]$  (20–30 residues)  $[D/E]GXXXX[W/Y/F][K/R]G$ , which may not be completely conserved (Palmieri, 2013). Based on their hydropathy profile and accessibility to impermeable reagents, proteolytic enzymes and peptide-specific antibodies, MCs possess six helices traversing the membrane, N- and C-termini on the cytosolic side of the membrane, three repeats linked by two loops on the cytosolic side and the two transmembrane  $\alpha$ -helices in each repeat connected by three loops on the matrix side (figure 14). The 3D crystallographic structure of the ADP/ATP carrier in complex with its inhibitor, carboxyatractyloside, was solved to 2.2 Å (Pebay-Peyroula *et al.*, 2003). The structure of uncoupling protein 2 (UCP2), in complex with GDP was determined by nuclear magnetic resonance (Berardi *et al.*, 2011). The atomic structure of MCs consists of a six-transmembrane  $\alpha$ -helix bundle (H1–H6) and three short  $\alpha$ -helices (h12, h34, h56) parallel to the membrane plane on the matrix side.

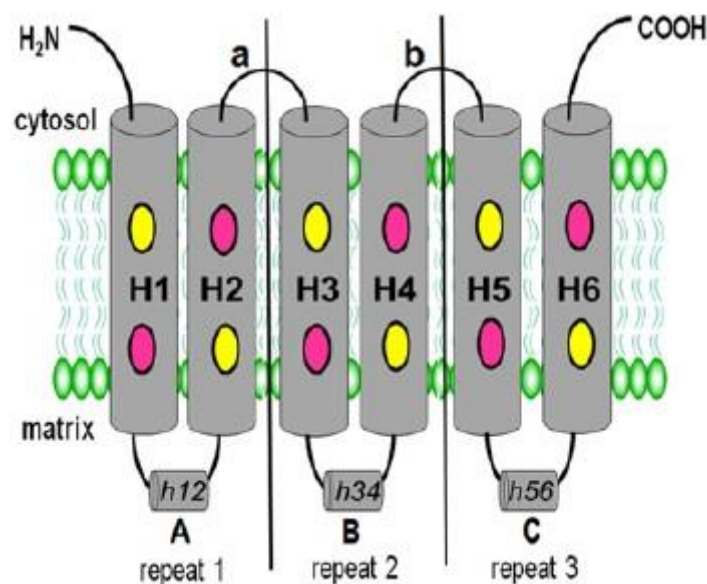


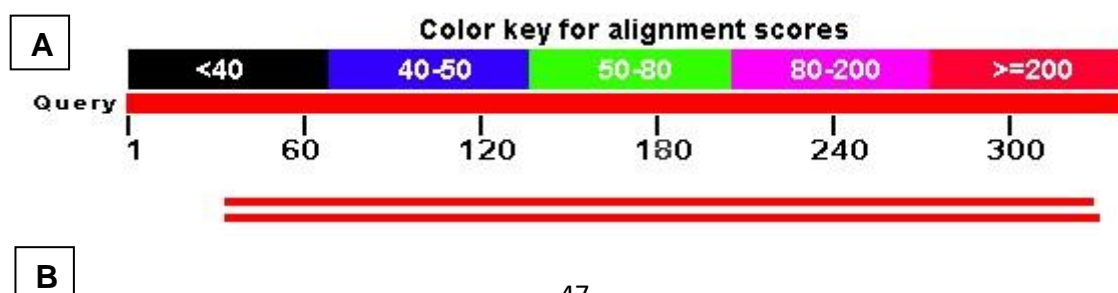
**Figure 15: SLC25 carrier protein structure.** In the figure above the SLC25 carrier protein sequence was divided into three similar domains, each with two transmembrane  $\alpha$ -helices. Within each domain the two helices are connected by long matrix loops, whereas the domains are connected by shorter cytosolic loops. **Figure taken from Palmieri, 2013.**

MCs have only one binding site which is alternately exposed on the two opposite sides of the membrane, namely, the cytosol in the c-conformation or towards the mitochondrial matrix in the m-conformation. When the substrate enters the carrier from the cytosolic side (in the c-state) or from the matrix side (in the m-state) the protein rearranges until the

transition state is reached. The substrate-induced conformational changes occurring during the transition from the c- to the m-state, and *vice-versa*, are largely due to “flexible hinged helix movements” of the even and odd transmembrane  $\alpha$ -helices, which consist of a tilt of the helical segments and a kink/swivel of their termini at the level of the conservative prolines and glycines (Palmieri *et al.*, 2011). In brief, viewing the carrier from the cytosol, the even and odd helices would be seen rotating clockwise during the c- to m-state transition, counter-clockwise during the m- to c-state transition, and *vice-versa*, viewing the carrier from the matrix side (Palmieri, 2013).

#### 1.07.001.4 SLC25A37 and its physiological role

SLC25A37 shares 40–41% identical amino acids with yeast MRS3 and MRS4, which have been proposed to transport Fe into mitochondria. SLC25A37, as well as zebrafish *slc25a37*, has been shown to efficiently complement the growth defect of MRS3–4D yeast mutant in iron-depleted conditions (Shaw *et al.*, 2006), indicating that *slc25a37* is also a mitochondrial iron transporter. A zebrafish null mutant for *slc25a37* manifests hypochromic anaemia and erythroid maturation arrest (Shaw *et al.*, 2006). This phenotype was rescued by microinjecting mouse SLC25A37 cDNA into defective embryos. Studies on mitochondrial DNA showed that European haplogroups with presumed functional differences were associated with AIDS progression (Hendrickson *et al.*, 2008). During tumor progression healthy cells acquire an altered metabolism to become cancer cells, either as a cause or as a consequence of an increased need of energy and nutrients. Carbohydrates, proteins, lipids and nucleic acids, the four major classes of macromolecules are affected during the transformation of a normal cell to a cancer cell. As a result, solute carriers (SLCs) which are the major transporters of these molecules are differently expressed thus making them important targets in the treatment of cancer. It has been suggested that SLC2A13 (HMIT) might be a potential CSC marker in oral squamous cell carcinoma based on microarray studies (Lee *et al.*, 2011). Microarray data revealed that members of the SLC25 (mitochondrial carrier family) and SLC39 (metal ion transporter family) families were more common in noncancer stem cells (CSCs) (El-Gebali *et al.*, 2013).



	Description	Max score	Total score	Query cover	E value	Ident	Accession
<input type="checkbox"/>	<a href="#">sp P10566 MRS3_YEAST Mitochondrial RNA-splicing protein MRS3 OS=Saccharomyces cerevisiae (strain ATCC 204508 / S288c) GN=MRS3 PE=1 SV=4</a>	228	228	86%	5e-76	41%	1374
<input type="checkbox"/>	<a href="#">sp P23500 MRS4_YEAST Mitochondrial RNA-splicing protein MRS4 OS=Saccharomyces cerevisiae (strain ATCC 204508 / S288c) GN=MRS4 PE=1 SV=1</a>	229	229	87%	7e-77	40%	1375

**Figure 16: Blast output of human SLC25A37.** Figure B shows the sequence identity of human Mfrn and yeast MRS3 and MRS4 genes.

### 1.07.001.5 tagSNPs in Mitoferrin

Mitoferrin (Mfrn/SLC25A37) is located on chromosome 8. The human genome encodes the blueprint of life, but the function of the vast majority of its nearly three billion bases is unknown (The ENCODE Project Consortium, 2012). Despite intensive study, especially in identifying protein coding genes, our understanding of the genome is far from complete, particularly with regard to noncoding RNAs, alternatively spliced transcripts, and regulatory sequences (The ENCODE Project Consortium, 2012). There are about three million single nucleotide polymorphisms (SNPs) in the human genome, two thirds of which are in non-coding DNA (Fairweather et al., 2007). Mutations in the proteins involved in iron metabolism may have an impact on iron metabolism and subsequently on human health. Rare genetic mutations and knock-out animal models have been invaluable tools in understanding the molecular events controlling iron metabolism (Donovan and Andrews, 2004).

Most SNPs do not occur in the coding region of genes or even in genes (Venter et al., 2001). Few SNPs that are present in the coding region, changes an amino acid (which are termed as non-synonymous SNPs) within a protein (Cargill et al., 1999). Based on the presumption that amino acid change will lead to a change in protein function, non-synonymous SNPs generally become the primary targets for SNP analysis. However, non-synonymous SNPs, though obvious suspects in causing a proportion of human disease, do not account for all SNPs that can cause disease or susceptibility to disease. SNPs implicated in human disease or susceptibility to disease include SNPs in the promoter region (Klerkx et al., 2003), introns (Tokuhiro et al., 2003), splice sites (Betticher et al., 1995) and intragenic regions (Helms et al., 2003). Even synonymous SNPs (which do not cause change of amino acid when there is a change of base in coding sequence) have been reported as having a functional implication via unknown mechanisms (Duan et al., 2003).

SNPs constitute 90% of the variation in the population (Kruglyak and Nickerson, 2001). Since a mutation is a very rare event, each new allele is associated with another allele that happened to be present on the same chromosome. The specific set of alleles observed on a single chromosome, or part of a chromosome, is called a haplotype. The coinheritance

of SNP allele on these haplotypes leads to associations between these alleles in the population (known as linkage disequilibrium, LD) (HapMap consortium 2003). The further the SNPs are from each other the less are the chances of association and coinheritance. Previous studies (Reich et al., 2001, Sklar et al., 2002) have shown that highly significant levels of LD, and often strong associations occur between nearby SNPs. These strong associations between the nearby SNPs results only in a few haplotypes, and these associations account for most of the variation among people in those specific chromosomal regions (Gabriel et al., 2002). SNPs with a strong association in a chromosomal region have a practical advantage. Genotyping only a few chosen SNPs in the region will provide enough information to predict much of the information about the remainder of the common SNPs in that region (The International HapMap Consortium 2003). By which, only a few of these 'tag' SNPs (also known as htSNPs) are required to identify each of the common haplotypes in a region (Johnson et al., 2001).



Along with understanding the role of Mfrn tagSNPs in iron metabolism, realising how protein-protein interactions play a major role in cellular processes, the current study also tried to elucidate the role of Iron regulatory proteins (IRPs) and Heph in iron metabolism. It is now becoming clear that protein-protein interactions determine the outcome of most cellular processes (Giot et al., 2003).

### **1.08 Protein-Protein Interactions (PPIs)**

Vital processes of life in an organism, such as adaptation to a given environment, reproduction and differentiation are dependent on an efficient communication between cells and cell compartments. Virtually every cellular function requires physical protein-protein interactions (PPIs) between cellular proteins (Westermarck et al., 2013). Commonly PPIs are understood as physical contacts with molecular docking between proteins that occur in a cell or in a living organism *in vivo* (Rivas and Fontanillo, 2010). Cellular signals (e.g. hormones) or environmental conditions (e.g. extracellular matrix composition) are recognised by a variety of specific cell surface receptors which in turn are transmitted to the nucleus via signalling cascades that eventually activate specific subsets of genes in the nucleus. In order for the cell to integrate different but connected signals into one expressional output, many signalling pathways cross talk with each other resulting in a complex signalling network. Further, these signalling processes are controlled by PPIs, which are further regulated by protein modifications. Identifying different interaction partners of a given gene product thus facilitates the identification of the function of the gene of interest in the organism.

Protein-protein interactions can be classified into different types depending on their strength (permanent and transient), specificity (specific or non-specific), the location of interacting partners within one or on two polypeptide chains, and the similarity between the interacting sub-units (homo and hetero oligomers) (Shoemaker and Panchenko, 2007). The issue of whether two proteins share a functional contact is quite distinct from the question of whether the same two proteins interact directly with each other (De Las Rivas and Fontanillo, 2010). Identification of PPIs is at the heart of functional genomics (Keskin et al., 2008).

PPIs can be analysed by approaches which have been categorised into biochemical (in which interactions between proteins are detected or analysed *in vitro*, for example cross-linking and co-purification), genetic (which the classical yeast two- hybrid is the most popular method to detect protein–protein interactions *in vivo*) and physical [X-Ray crystallography,

fluorescence resonance energy transfer (FRET)] (Shoemaker and Panchenko, 2007). Previously PPI studies were carried out in *in-vitro* models such as Yeast two Hybrid Systems (Y2H) and pull-down assays which were integrated with more physiological approaches to assess the complexity of PPIs in living cells. A generic procedure to co-purify proteins expressed at their natural level with a Tandem Affinity Purity (TAP) tagged bait protein under native conditions using TAP purification (Rigaut et al., 1999) was developed. However, extended washing and time consuming cleavage steps made TAP tagging process prone to artefacts and unable to detect PPIs with transient interacting partners (Glockner et al., 2007). Since it is also important to understand the PPIs with short half-lives which could be lost during the extended washing steps during the pull down Junntila et al., in 2005 proposed a 3kDa sized One-Strep tag to enable a rapid one-step pull down of the protein complex that can be analysed for interactions without losing weak interacting partners.

In the current study, to understand the role of IRPs and Heph in iron metabolism, we carried out biochemical approach by co-purification. The discovery of many molecules involved in iron uptake, storage and transport enhances the possibility to understand the roles of different proteins in iron metabolism in different cell types. Thus understanding the roles of IRPs and ferroxidases may enhance the understanding of their respective role in iron metabolism. As is well known, proteins in the cells do not act in isolation. A critical aspect in understanding and comprehending the role of an individual protein is by evaluating and elucidating the activity and function of each protein in the cell. The role of an individual protein is controlled and modified through its interactions with neighbouring polypeptides and with other molecular components of cells such as nucleic acids, phospholipids, carbohydrates and secondary messenger molecules. To understand the complexity of cellular functions, studying localised protein interactions is not only necessary but also knowledge of the connections between different protein complexes is also necessary. Hence protein-protein Interactions (PPIs) play an important role for every process in a living cell. The half-life of some PPIs may be long enough to form stable protein complexes or may be very brief which is enough to modify the interacting partners thus changing the PPI.

#### **1.08.001.1 Iron Regulatory Proteins (IRPs)**

Mammalian cells must manage the import, export and sequestration of iron to achieve the cytosolic concentrations needed to support the synthesis of iron binding proteins and prevent unfavourable iron dependent oxidation events (Rouault, 2009). Iron regulatory protein's (IRPs) recognise the iron response elements (IREs) in a sequence and structure-

specific manner (Leibold et al., 1987, Rouault et al., 1988). IREs are short conserved hair pin loops bound by iron response proteins. IREs are found in the untranslated regions (UTRs) of various mRNAs whose products, the proteins, play an important role in iron metabolism. Mutagenesis studies of the 3'-untranslated regulatory region of the transferrin receptor mRNA revealed two types of mutations. Key to iron homeostasis are the IRPs, which respond to the cytosolic iron pool by binding to target mRNA and regulating the synthesis of iron metabolic proteins (Rouault, 2006). Some mutations abrogated iron-dependent regulation of the transferrin receptor while other mutations produced an increased and unregulated expression of transferrin receptor mRNA (Casey et al., 1988, Mullner et al., 1989, Owen et al., 1987). Other studies led to the purification and preliminary characterisation of the iron regulatory protein (IRP) (Haile et al., 1989, Barton et al., 1990). IRPs are the key cytosolic sensors in mammalian cells and they are present as free cytosolic proteins or RNA-bound protein inside the cells. Sequence analysis of a cDNA clone encoding human IRP showed that IRP resembles mitochondrial aconitase, an enzyme containing a 4Fe-4S cluster (Rouault et al., 1990, Hentze et al., 1991). Two IRPs (IRP1 and IRP2) are present in mammalian cells. Transfection experiments of IRE mutants specific for either IRP1 or IRP2 showed that IREs maintain their IRP specificity *in-vivo* and are able to mediate translational control (Menotti et al., 1998). Though IRP1 and IRP2 share 64% amino acid sequence similarity, different mechanisms are thought to control the regulation of their RNA binding activity.

#### **1.08.001.2 The IRP-IRE system**

By interacting with the IREs found in the mRNAs of many genes both IRP1 and IRP2 are involved in iron sensing. According to the requirements of a cell, the IRE/IRP system responds to changes in cellular iron status and through the interaction of IRPs with IREs regulates the amount of iron taken up and/or stored by a particular cell. The IRP-IRE system is the best characterised regulatory mechanism for maintaining iron homeostasis within a single cell. The IRE canonical stem loop structure – CUGTGA – and a cytosine bulge on the stem at the 5<sup>th</sup> residue position are found to be conserved and essential for the IRP binding (Casey et al., 1988; Address et al., 1997). Stems can be of variable lengths. The IREs are found to be situated either at the 5' or 3' UTR elements of a transcript in number of different iron genes. Binding of an IRP to the 5' UTR of an IRE may repress the translation. Both H and L ferritins along with IREG1 transcripts contain a single IRE in their 5' UTR (Henze et al., 1987; McKie et al., 2000). In cellular iron deficiency, where IRP binding to IRE is

promoted, further translation of ferritin and IREG1 is inhibited at an early stage resulting in cellular iron utilisation. The opposite can be said in iron repletion condition in which IRP binding is decreased and excess iron is either stored or exported.

On the other hand, IREs located at the 3' UTR of a gene may increase the mRNA half-life. When IREs are located in the 3' UTR of TfR1 transcripts, iron deficiency promotes stabilisation and contributes to increased protein synthesis and cellular iron uptake (Hubert and Hentze, 2002; Gunshin et al., 2001). The TfR1 transcript contains five IREs in tandem in its 3' UTR (Erlitzki et al., 2002). IRP binding to these IREs protects the message from endonuclease cleavage and degradation. Although a 3' UTR IRE in DMT1 has also been identified, its role and contribution in iron regulation is still not clear (Gunshin et al., 2001). Other transcripts such as mitochondrial aconitase (Eisenstein and Ross, 2003) and hypoxia-inducible factor 2 (HIF-2) (Sanchez et al., 2007) have also been shown to possess IREs. The cellular iron pool regulates the binding of IRP1 and IRP2 to the IRE by distinct mechanisms.

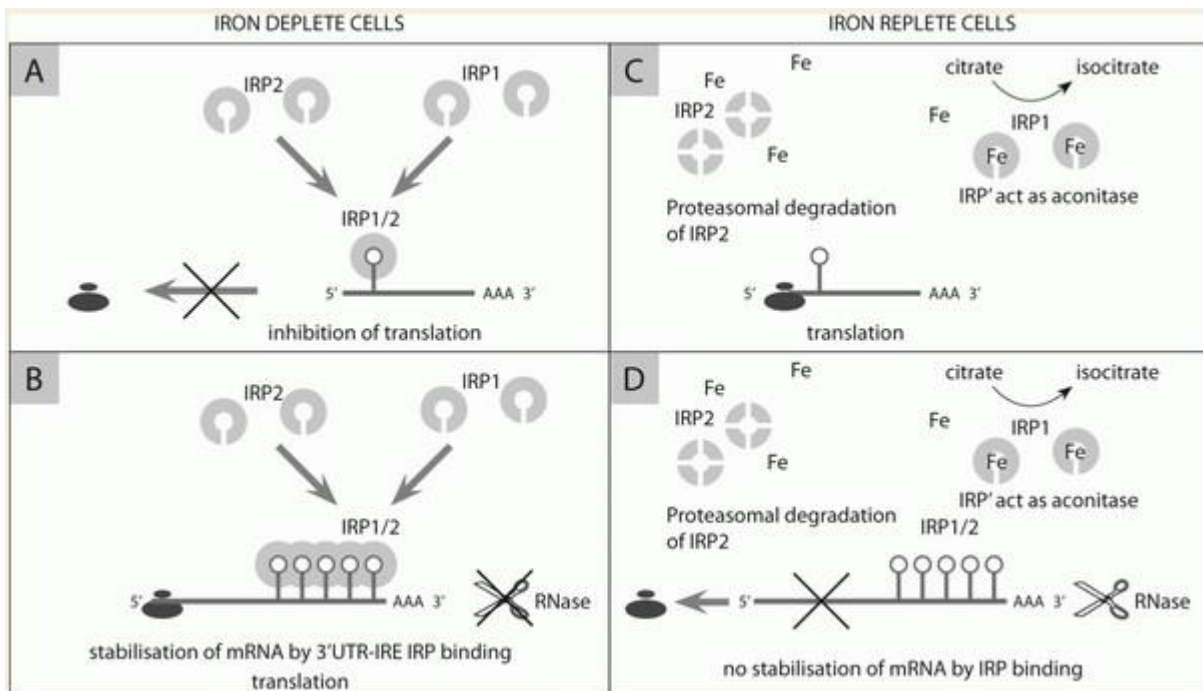


**Figure 18: IRP-IRE system.** Figure A and B show iron deplete cells in which binding of IRP1/2 at the 5'UTR IRE of ferritin and ferroportin mRNA block translation hampering its initiation and binding of IRP1/2 at the 3'UTR IRE of TfR mRNA stabilize its transcript, respectively. In iron replete cells representing C in the figure, IRP1 act as aconitase and IRP2 is degraded by proteases so translation of 5'UTR IRE mRNA of ferritin and IREG1 is carried out undisturbed and in the presence of sufficient iron there is no binding of IRP1/2 and stabilization of 3'UTR IRE transcript of TfR (D). **Figure taken from Tandara and Salamunic, 2012.**

### 1.08.001.3 Iron regulatory protein 1 (IRP1) and IRP2

IRP1 and IRP2 which are capable of binding to an IRE, though at different binding sites are also conserved across the species at 90% sequence identity (Henderson et al., 1993; Samaniego et al., 1994; Guo et al 1995; Butt et al 1996).

The IRP1 gene on 9q13-22 encodes an IRP1 (98kDa) protein which is identical in sequence to cytosolic aconitase that catalyses the conversion of citrate to isocitrate via the intermediate cis-aconitase in the Krebs cycle (Rouault et al 1991; Hentze and Argos 1991). Based on the crystal structure of the homologous mitochondrial aconitase it is thought that IRP1 is a 4 domain protein, with domain 4 linked by a hinge region to the other 3 domains, and a cleft forming between domains 1-3 and domain 4 (Dupuy et al 2005, 2006). IRP1 in complex with the ferritin IRE (Selezneva et al 2006) supports the importance of the cleft region in IRP1's mutually exclusive functions (Figure 1.4C). Increased iron levels in a cell

promotes the formation of the iron-sulphur cluster (4Fe-4S), which can occupy the cleft and determine the function of the protein, which acts either as an active cytosolic aconitase (holoprotein) or as an RNA binding protein (apoprotein) when the protein lacks this cluster (Constable et al 1992, Haile et al 1992) (Figure 1.5A). IRP1 is a dual function protein that performs two mutually exclusive activities depending on cellular iron status. Reduced cellular iron levels increases IRP1's affinity to bind to IRE and *vice-versa*. In the iron replete form, IRP1 is the cytosolic isoform of aconitase (Haile et al., 1992, Rouault et al., 1991) and promotes the disassembly of the 4Fe-4S cluster and the cleft widens enough to accommodate an RNA molecule, which is critical for the IRE/IRP interaction. In cells that are rich in iron, IRP1 ligates an iron-sulfur cluster and IRP1 functions as an aconitase that interconverts citrate to isocitrate through a cis-aconitate intermediate in the cytosol and has 30% aa sequence identity with mitochondrial matrix aconitase, which catalyses the same reaction in the mitochondrial matrix (Beinert and Kennedy, 1993). Knocking out IRP1 has little effect on iron regulation, suggesting that its primary role may be in maintaining cytosolic aconitase rather than to control iron metabolism (Rabie et al., 1995). Other than levels of iron in a cell, nitric oxide has also proved to be the first factor able to regulate the RNA binding activity of IRP1 to IREs (Drapier et al., 1993) and others like phosphorylation (Eisenstein et al 1993) and oxidative stress (Pantopoulos and Hentze 1995) emerged to influence the IRP1-IRE interaction.

A second IRE binding protein, called IRP2, has been identified and characterised in murine cells. Human IRP2 (105kDa) shares 61% sequence identity and 79% amino acid sequence similarity to human IRP1 (Samaniego *et al* 1994). IRP2 is always active in binding to IREs and unlike IRP1, IRP2 appears neither to be enzymatically active nor post-translationally reversibly convertible between active and inactive RNA binding forms. IRP2 is regulated via *de novo* synthesis and proteasome-mediated degradation (Guo et al 1995; Iwai et al 1995). Both IRPs have been found to be regulated by protein degradation in the presence of iron or haem (Goessling et al 1998, Clarke et al 2006), but this mechanism is more pronounced for IRP2. IRP2 (gene location on chromosome 15) (962 amino acids) contains a 73 amino acid region encoded by a single exon, which is not present in IRP1 (889 amino acids) targets IRP2 for iron dependent degradation. The unique "iron- dependent degradation domain" in IRP2 can bind free iron resulting in a localised oxidation site that forms or acts as the recognition signal for ubiquitination and the subsequent degradation of the protein (Iwai et al 1998). In iron-rich cells the oxidation of IRP2 has been proposed to be induced by haem,

as well as oxygen (Yamanaka et al 2003, Bourdon et al 2003). Unique degradation domain is dispensable for both iron and oxygen mediated degradation (Hanson et al 2003), while additional stimuli may be involved in creating recognition signals within and outside the boundaries of the degradation domain (Wang et al 2004). Unlike IRP1, protein levels which do not change following iron loading IRP2 protein levels decreases to the detectable levels in cells loaded with iron (Guo et al., 1994). Also IRP2 does not have aconitase activity like IRP1. The IRE-binding activity of IRPs differentially controls the translation of different mRNA involved in iron homeostasis. For example, when cells are low in iron, IRPs inhibits the translation of mRNA encoding the cytosolic iron-binding protein, ferritin. The inhibitor effects of IRPs on mRNA of ferritin results in reduction of iron storage, thus making it available for cellular iron processes. IRP binding also protects mRNA encoding the TfR1 (which transports iron into the cells) from degradation, and consequently boosts TfR1 expression when the concentration of cytosolic iron is low (Rouault, 2009). Vashisht et al and Salahudeen et al in 2009 reported that human cells gauge cellular iron and concomitantly alter the activity of IRPs through a mechanism that depends on the F-box and leucine-rich repeat protein 5 (FBXL5).

The human genome includes more than 20 proteins that contain both an F-box (Skaar et al., 2009) and a domain of leucine-rich repeats that provides the platform for protein-protein interaction studies (Bella et al., 2008). The C-terminal region of FBXL5 contains leucine rich repeats that help the binding to IRPs (Vashisht et al., 2009 and Salahudeen et al., 2009). Since, iron and oxygen stabilises FBXL5, targeting of IRPs for degradation occurs in cells that are replete in iron. As expected (Rouault, 2009) changes in FBXL5 activity affected the amounts of ferritin (Vashisht et al., 2009) and TfR1 mRNA levels in cells (Salahudeen et al., 2009). Thus, the activity of the IRE-IRP regulatory system is controlled by FBXL5, which directly reflects cellular iron status through the iron binding of its conserved haemerythrin domain [(haemerythrin is a conserved domain recognised as oxygen-carrying proteins in invertebrates and as a potential oxygen sensor in bacteria, and are absent in higher organisms (Stenkamp, 1994)] (Feig and Lippard, 1994). In the slow but never ending evolutionary process, haemerythrin was surpassed by haem as the oxygen carrier of choice (Kurtz, 1999). However, it seems that in higher organisms, the haemerythrin domain was successfully repurposed as an iron sensor to function in cellular iron homeostasis. Both Vashisht et al and Salahudeen et al (2009) reported that the binding of iron and oxygen to

the haemrythrin domain stabilises FBXL5, whereas a lack of iron (or lack of oxygen in the presence of sufficient iron) results in FBXL5 degradation.

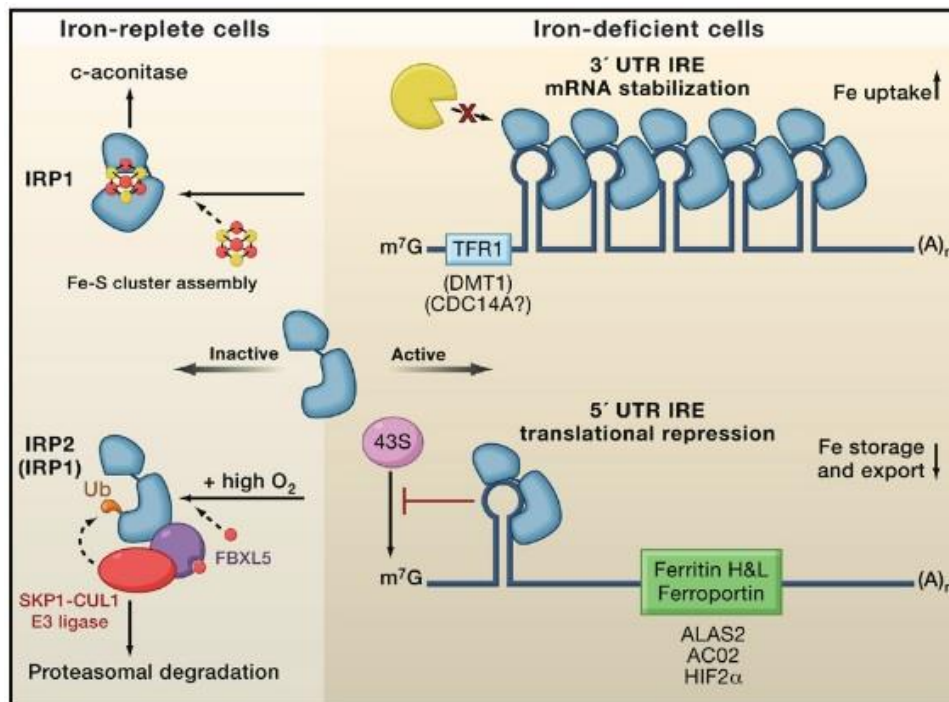


**Figure 19: IRP1 and IRP2 in iron replete and deficient cells.** In iron-deficient cells (right panel in the figure), IRP1 or IRP2 bind to cis-regulatory hairpin structures called iron-responsive elements (IREs). The binding of IRPs to single IREs in the 5' UTRs of target mRNAs inhibits their translation, whereas the interaction of the IRP with multiple 3' UTR IREs in the Tfr1 transcript increases its stability. As a consequence, Tfr1-mediated iron uptake increases whereas iron storage in ferritin and export via IREG1 decreases, thereby increasing the LIP (labile iron pool). In the iron-replete cells (left panel in the figure), the FBXL5 iron-sensing F-box protein interacts with IRP1 and IRP2 and recruits the SKP1-CUL1 E3 ligase complex that promotes IRP ubiquitination and degradation by the proteasome. IRP1 is primarily subjected to regulation via the assembly of a Fe/S cluster that triggers a conformational switch precluding IRE-binding and conferring aconitase activity to the holoprotein. IRPs also modulate the translation of the mRNAs encoding the erythroid-specific ALAS2, the mitochondrial aconitase (ACO2) and the HIF2 $\alpha$  hypoxia-inducible transcription factor. Single 3' UTR IRE motifs are present in the DMT1 and CDC14A mRNAs, but their role and mechanism of function are not yet fully defined. **Figure taken from Hentze et al., 2010.**

Based on the fact that IRP1 is more abundant than IRP2, IRP1 would be expected to be the predominant regulator but the necessity and presence of two IRPs is still not clearly understood (Hentze and Kuhn, 1996). Mis-regulation of iron homeostasis in *Ireb2*<sup>-/-</sup> mice and lack of the mouse gene encoding IRP2 exemplifies the importance of IRP2 in iron homeostasis and suggests that IRP1 alone cannot regulate iron metabolism appropriately (LaVaute et al., 2001). *Irp1*<sup>-/-</sup> mice show only compromised normal iron metabolism in tissues in which the levels of IRP1 exceed those of IRP2, suggesting that unlike IRP1, IRP2 can compensate for loss of IRP1 activity by increasing IRP2 levels (Meyron-Holtz et al., 2004a). Animals lacking both IRPs are unable to survive through gestation (Smith et al, 2006) and it is likely that IRP1 and IRP2 operate in a continuum in which the partial pressure of oxygen determines relative activity (Meyron-Holtz et al., 2004b). Though the role of IRPs in iron homeostasis is well established, understanding of the significance of multicopper ferroxidase protein, Hephaestin (Heph) is not conclusive in iron metabolism. The sex-linked anaemia (*sla*) mice develop moderate to severe microcytic hypochromic anaemia due to impaired intestinal iron absorption (Pinkerton, 1968; Bannerman, 1976). Iron uptake across the brush border membrane in *sla* mice is normal indicating there is a defect in an 'exit' step of iron absorption. Thus, Heph could possibly be the factor limiting iron transfer across the basolateral membrane of the enterocyte. It is thought Heph plays a significant role in the basolateral membrane as an iron exporter. In the current study we tried to confirm the previously established protein interactors of Heph and also tried to examine for any new interacting partners with whom Heph may be cross talking that sheds some light on iron transport at the basolateral membrane.

## **1.09 Hephaestin (Heph)**

### **1.09.001 Heph and Blast analysis**

Hephaestin (Heph) is a putative multi-copper oxidase that was identified through the study of the sex-linked anaemia (*sla*) mouse (Vulpe et al., 1999). Between humans, mouse and rat, Heph shows more than 85% homology both at protein and nucleotide levels. Heph is present on the X chromosome with 21 exons, spanning a little over 106 kb. 21 exons of Heph encode a polypeptide of 1158 amino acids (130 kDa protein) with a putative N-terminal signal peptide. Due to N-glycosylation and possibly because of post-translational modification (Nittis and Gitlin, 2004) the theoretical calculated molecular mass of the mature Heph is 150-160 kDa. Heph, in contrast to its soluble serum homologue, contains an additional 86 amino acids at the C-terminus, which includes a single predicted

transmembrane domain and a short cytosolic tail, attributing its nature to be a membrane protein with a large Cp like ectodomain (Petрак and Vyoral, 2005).

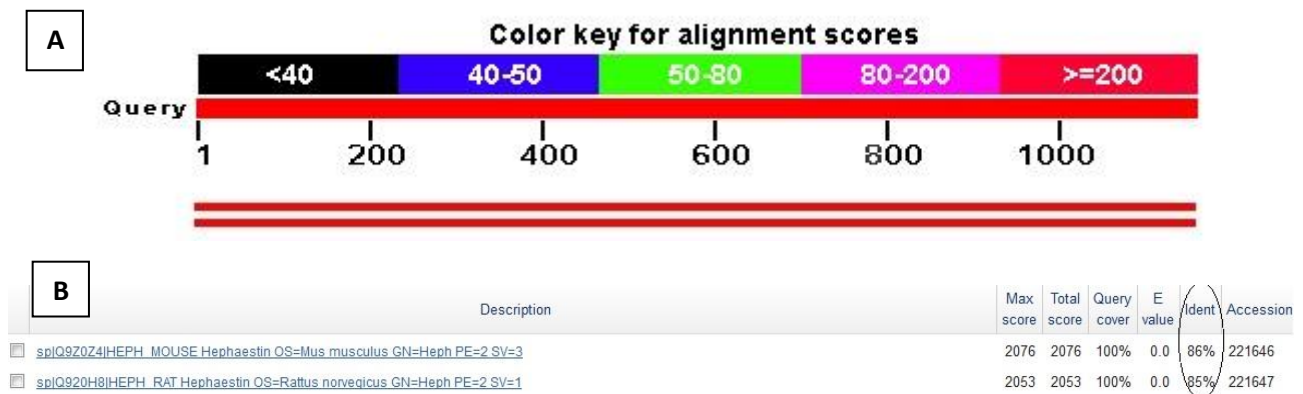


**Figure 20: Blast output of human, mouse and rat Heph.** Above parts of figure, A and B represents the blast results obtained after carrying out Protein blast with multiple alignment among human (Q9BQS7), mouse (Q9Z0Z4) and rat (Q920H8) Heph using data from UniProt database. Part A of the figure shows the alignment of mouse and rat protein sequence against human Heph. Part B of the figure shows the percentage of identity between human, mouse and rat Heph protein sequences.

### 1.09.002 Heph and sla mice

It was observed that in the sla mice the mucosal uptake of dietary iron although is normal they are unable to release it from the duodenal enterocytes into the bloodstream (Anderson et al., 1998). Although sla mice take up iron from the intestinal lumen into mature epithelial cells normally (Manis, 1970) the subsequent exit of iron into the circulation is diminished (Bannerman, 1976). As a result, iron accumulates in enterocytes and is lost during turnover of the intestinal epithelium (Edwards, et al., 1977). An in-frame mutation of Heph, which is responsible for the sla phenotype in mice, results in a truncated protein and possibly due to mislocalization of Heph, Heph was not detected on the basolateral membrane of the small intestine in sla mice (Chen et al., 2004; Kuo et al., 2004). Structural modelling shows that the mutation causes a substantial deformation of the secondary structure, partial loss of copper binding sites, reduces protein stability and implicates partial loss of ferroxidase activity of Heph in sla mice (Syed et al., 2002; Petрак and Vyoral, 2005).

### 1.09.003 Heph and Cp

Heph is homologous to Cp and is a member of the 'blue' copper oxidase family. The biochemical activity of Heph has yet to be defined. The extensive similarity between the ecto-domains of Heph and Cp (approximately 50%) suggests that they share the same fold

and further implies that Heph may function as a ferroxidase (Vulpe et al., 1999). Comparative structural modelling based on the known crystal structure of Cp revealed several important facts of the Heph's ectodomain (representing more than 92% of its sequence). Heph and Cp share a similar  $\beta$  fold and the key structural features critical for folding and function of Cp are conserved in Heph. Along with the copper-binding sites, all the cysteine residues essential for the formation of disulphide bridges are also conserved in the putative structure of Heph. The putative iron-binding site with a negatively charged aspartate-rich tract in its vicinity is also conserved in Heph (Syed et al., 2002; Petrak and Vyoral, 2005).

At the basolateral membrane,  $\text{Fe}^{2+}$  is exported into the extracellular environment via the transmembrane permease ferroportin (Mackenzie and Garrick, 2005) and is oxidised into  $\text{Fe}^{3+}$  by a ferroxidase. Outside the cell, the available  $\text{Fe}^{3+}$  loads onto serum transferrin (Tf), the iron carrier in blood. Tf specifically binds  $\text{Fe}^{3+}$ , but not  $\text{Fe}^{2+}$ , very tightly with an approximate KD of  $10^{-24}$  M at physiological pH (Richardson and Ponka, 1997). Iron-loaded Tf (holo-Tf) then travels throughout the circulation and delivers  $\text{Fe}^{3+}$  to all tissues via a binding interaction with the TfR. Because of the insoluble nature of free  $\text{Fe}^{3+}$  under physiological conditions and the potential of  $\text{Fe}^{2+}$  and  $\text{Fe}^{3+}$  to generate harmful hydroxyl-free radicals, the regulation of iron is fundamental to the prevention of cell toxicity (Aisen et al., 2001). It has been suggested that as a means of preventing the release of unbound  $\text{Fe}^{3+}$ , a direct protein–protein interaction may occur between Tf and Heph during intestinal iron export (Syed et al., 2002; Griffiths et al., 2005). This hypothesis is supported by a study that reported the formation of a stable complex between a multicopper ferroxidase and Tf in algae (Paz et al., 2007). Furthermore, the identification of an interaction between Cp and lactoferrin (a Tf analog) under physiological conditions provides additional support (Pulina et al., 2002; Sokolov et al., 2006). However, it was concluded that the human ferroxidases and Tf do not interact directly and suggest alternative mechanisms for iron-loading Tf during intestinal iron export (Hudson et al., 2008). It was established that the ferroxidases, Heph and Cp do not form a stable complex or directly interact with Tf by gel analysis and SPR in solution (Hudson et al., 2008). The localization of Heph to both the intracellular and extracellular environments presents some uncertainty concerning its function, as it is not clear how an intracellular ferroxidase would function in iron transport. However, it has been implicated that an intracellular Cp as well as Heph to play significant roles in iron absorption (Cherukuri et al., 2005). The processing of absorbed iron by Heph or Cp inside the cell could

also explain the absence of a direct interaction with Tf. It can also be explained that the lack of interaction between the ferroxidase and Tf is based on their physical locations. After being oxidised  $\text{Fe}^{3+}$  would be released into the mucosa, while Tf is typically found circulating throughout the vasculature. In such condition, an unknown iron-carrying intermediate, such as citrate, could transport iron through the interstitial fluid to the portal blood; thereby bypassing the need for a direct ferroxidase–Tf interaction. On the other hand, with Tf serum concentrations as high as 50 mM (Richardson and Ponka, 1997), Tf may act as an efficient scavenger for released  $\text{Fe}^{3+}$  without the need for intermediates or direct protein–protein interactions. Ferroportin (IREG-1/FPN-1) has been shown to export iron both in the presence of Tf but in the absence of a ferroxidase (Donovan et al., 2000) and in the presence of ferroxidase but in the absence of Tf (McKie et al., 2000).

#### **1.09.004 Heph and IREG1**

Molecular genetic studies in yeast cells (DeSilva et al., 1995; Stearman et al., 1996; Singh et al., 2006) showed that Ferroportin1 (IREG1/FPN-1) and Heph may be located on the basolateral membrane of enterocytes, and they may interact in the processes of iron export across the basolateral membrane of intestinal absorptive cells, but it remains to be explored. The transporter responsible for the export of iron across membranes was identified in three different laboratories and is variously referred to as FPN-1 (Donovan et al., 2000), Ireg1 (McKie et al., 2000), and MPT1 (Abboud and Haile, 2000). It is not clear where these proteins are exactly located, and how they are involved in the process of iron exit in intestinal enterocytes. The previous study showed that Heph protein was located on the basolateral membrane of small intestine in mice (Kuo et al., 2004). IREG-1 and Heph proteins are primarily located on the basolateral membrane of intestinal cells, which support their proposed roles in iron exit across the basolateral membrane of enterocyte. Furthermore, confocal microscopy data demonstrate that Heph is colocalized with IREG-1-GFP on the basolateral membrane in human intestinal absorptive cells. These observations support the possibility that FPN-1 and Heph may interact in the processes of iron exit across the basolateral membrane of intestinal absorptive enterocytes, as shown previously in astrocytes (Jeong and David, 2003) and yeast cells (De Silva et al., 1995; Stearman et al., 1996; Singh et al., 2006). Once ferrous ion is exported across the cell membrane, oxidation of  $\text{Fe}^{2+}$  to  $\text{Fe}^{3+}$  by Cp is required for the release of iron from the tissues into the circulation (Osaki et al., 1971). However, aceruloplasminemia in mice led to iron accumulation in many tissues but not in the intestine (Harris et al., 1999) suggesting that intestinal epithelium

utilizes another ferroxidase to convert  $\text{Fe}^{2+}$  to  $\text{Fe}^{3+}$ . Colocalisation of Heph and IREG-1 proteins on the basolateral membrane of intestinal cells suggests the possible interactions of IREG-1 with Heph in the processes of iron export across the basolateral membrane of enterocytes. Molecular genetic studies in yeast cells have shown that iron transport across cell surface requires both iron transporter (Ftr1) and an associated multi-copper oxidase (Fet3) (De Silva et al., 1995; Stearman et al., 1996; Singh et al., 2006). Ftr1 is needed for Fet3 biosynthesis and localization to the plasma membrane (Stearman et al., 1996). In yeast, the requirement that both Ftr1 and Fet3 proteins must be simultaneously synthesized for proper processing suggests that these proteins might function as a complex on the cell surface. A Cu oxidase in cultured placental cells is mainly in an intracellular membrane compartment, but not on the expected basolateral membrane (Gambling et al., 2001). In addition, whether the Cu oxidase expressed in placenta is Heph or Cp or another homologue has not been confirmed. The current evidence suggests that the expression of Heph may be regulated by Cu, Fe and Zn (Reeves et al., 2005; Kelleher et al., 2006; McArdle et al., 2008). However, there is no IRE structure in Heph mRNA, so its expression regulated by Fe may not depend on the IRE/IRP system. Iron export in mammalian cells requires the iron transporter IREG-1, and recent studies have revealed a direct association between FPN-1 and the glycosylphosphatidylinositol (GPI)-anchored multi-copper oxidase Cp during iron movement from mouse astrocytes (Jeong and David, 2003) suggesting a possibility that IREG-1 and Heph are required for the exit of iron across the intestinal basolateral membrane and express as an associated complex.

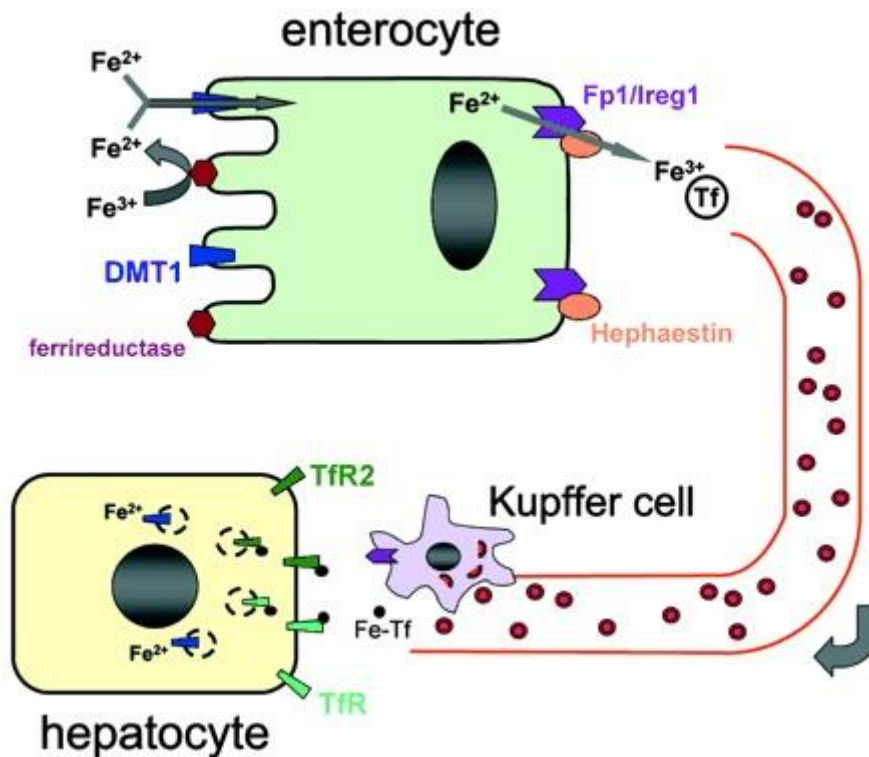


**Figure 21: Efflux of iron across the basolateral membrane.** Efflux of iron across the basolateral border is mediated by Ireg-1, in conjunction with the ferroxidase, hephaestin. **Figure taken from Griffiths and Cox, 2000.**

The role of Heph was suggested for iron egress from intestinal enterocytes into circulation and that acts as an important link between copper and iron metabolism in mammals (Vulpe et al., 1999). Contrary to the behaviour of most proteins involved in iron homeostasis, Heph expression is not regulated via iron-responsive elements and IRE-binding proteins. Known factors influencing expression levels of Heph in the intestine include iron and copper levels (Vyoral and Petrak 2004). The absence of Heph in the basolateral membrane seems to be critical and could explain the iron deposition in enterocytes of sla mice (Kuo et al., 2004). Direct evidence of Heph ferroxidase activity comes from experiments in yeast (Li et al., 2003). *In vitro* enzymatic assays confirmed Heph ferroxidase activity and showed that a residual Heph ferroxidase function is retained even in the severely truncated Heph in the sla-mice (Chen et al., 2004). Heph could be in direct contact with a membrane-bound iron exporter (possibly Ireg1) transporting ferrous iron through the membrane, and Heph may oxidise the ferrous ion to enable its subsequent binding by transferrin (Vyoral and Petrak 2004). It has been shown that Glycophosphatidylinositol (GPI)-anchored Cp physically associates with Ireg1 in astrocytes (Jeong and David, 2003). Localisation studies have suggested that Heph

co-localises with Ireg1 to the basolateral membrane in association with transferrin receptor (TfR) (Han and Kim, 2007) in differentiated Caco2 cells. It is an absolute requirement for membrane-bound Heph and basolateral localisation for proper IREG1 expression and localisation to achieve the mode of iron exit from intestinal cells (Chen et al., 2009) which is similar to that of brain (De Domenico et al., 2007b). Heph was shown to be translocated to the basolateral membrane when rats were fed an iron-replete diet (Yeh et al., 2009). In addition, the basolateral targeting of Heph results in an interaction with Ireg1 (Yeh et al., 2009) which has been reported to be reduced upon iron feeding (Yeh et al., 2011). The principle involved in the process of placental iron transport is similar to that in duodenum. IREG-1 and Heph have been identified as the important molecules involved in duodenal iron export. However, the molecular mechanism of iron efflux is still not clear.

## **Aims and Objectives of the research study**

Aim of this study was to carry out tagSNP analysis of Mitoferrin (Mfrn) SNP using an Asian and Caucasian cohort. The current research study is also aimed to establish the interacting partners of IRPs (IRP1 & IRP2) and Heph in iron metabolism using protein-protein interaction analysis in K562 cells

- To establish any correlation between Mfrn tagSNPs, birth weight and haemoglobin levels in Asian and Caucasian DNA samples.
- Identification of interacting partners of IRPs (IRP1 and IRP2) and Heph

Objectives to achieve the above mentioned aims in the current research include

- Selecting tagSNPs in Mfrn gene using HapMap and haploview
- Statistical analyses of the tagSNPs genotyping data using SPSS
- To perform relative gene expression analysis of iron metabolic genes (Heph and IRPs) in K562 cell lines using TaqMan Gene expression probes
- Molecular cloning of the Heph, IRP1 and IRP2 cDNA using One-Strep tag approach
- Pull down analysis of the Heph, IRP1 or IRP2 protein complex using Mass Spectrometry to identify the protein protein interactions

# **MATERIALS AND METHODS**

# CHAPTER 2

## **2.01 UK/Irish and South Asian Cohort for Mfrn tagSNP analyses**

In this study, a total of 1811 DNA samples were included for the Mfrn tagSNP analyses, of which 896 were UK/Irish and 915 were of South Asian descent. The samples were collected from women while they were attending 18-week antenatal scans at Northwick Park Hospital (Northwest London Hospitals) between 1997 and 1999 for genetic analysis. Data from all the women recruits was maintained to ascertain details about family origin along with different family diseases including asthma, stroke and heart diseases. Information such as birth weight, sex and gestational age of the child was also taken during the sample collection. DNA samples of both Asian and Caucasian samples were used to find if any correlation exists between birth weight, levels of haemoglobin and Mfrn tagSNPs. Since no data for the blood serum ferritin or transferrin (percentage saturation and total iron binding concentration or TIBC) was available for the cohort used in Mfrn tagSNP analysis, Hb levels were used as a proxy for body iron levels. To carry out the correlation analysis, both the population data and the samples were kindly provided by Dr. Una Fairbrother.

### **2.01.001 Mfrn tagSNP selection**

Considering the significance of Mfrn in haem biosynthesis and as an essential iron importer for the synthesis of mitochondrial haem and iron-sulfur clusters, this study chose tagSNPs in Mfrn using Haploview (Barrett et al., 2005) between the regions 23437 and 23490 on chromosome 8 to find any correlation between levels of haemoglobin, birth weight and Mfrn tagSNPs in Asian and Caucasian DNA samples. From the 74 SNPs that were found, the settings on Haploview were changed so that the Hardy-Weinberg equilibrium (HWE) cut off was  $p < 0.05$ , minimum genotyping (genotype success rate) was 80% and minor allele frequency (MAF) was also 0.05 (5%), cutting the number of SNPs from 74 to 68. The Tagger application in Haploview was then run from SNPs 4 to 74, and identified 24 SNPs capturing 65 of the 74. Two synonymous SNPs were added that did not appear in Haploview but may be of interest (rs34146184 and rs34968988) in the context of genotyping and testing the SNPs for correlation study. Considering the significant role of hepcidin in iron metabolism, region 40466 - 40469 on chromosome 19 was also analysed for potential tagSNPs in

Haploview. Haploview returned a list of 6 SNPs which were tagged to 3. Only rs10421768 was considered as it captured the SNPs that appear in the 5'UTR region.

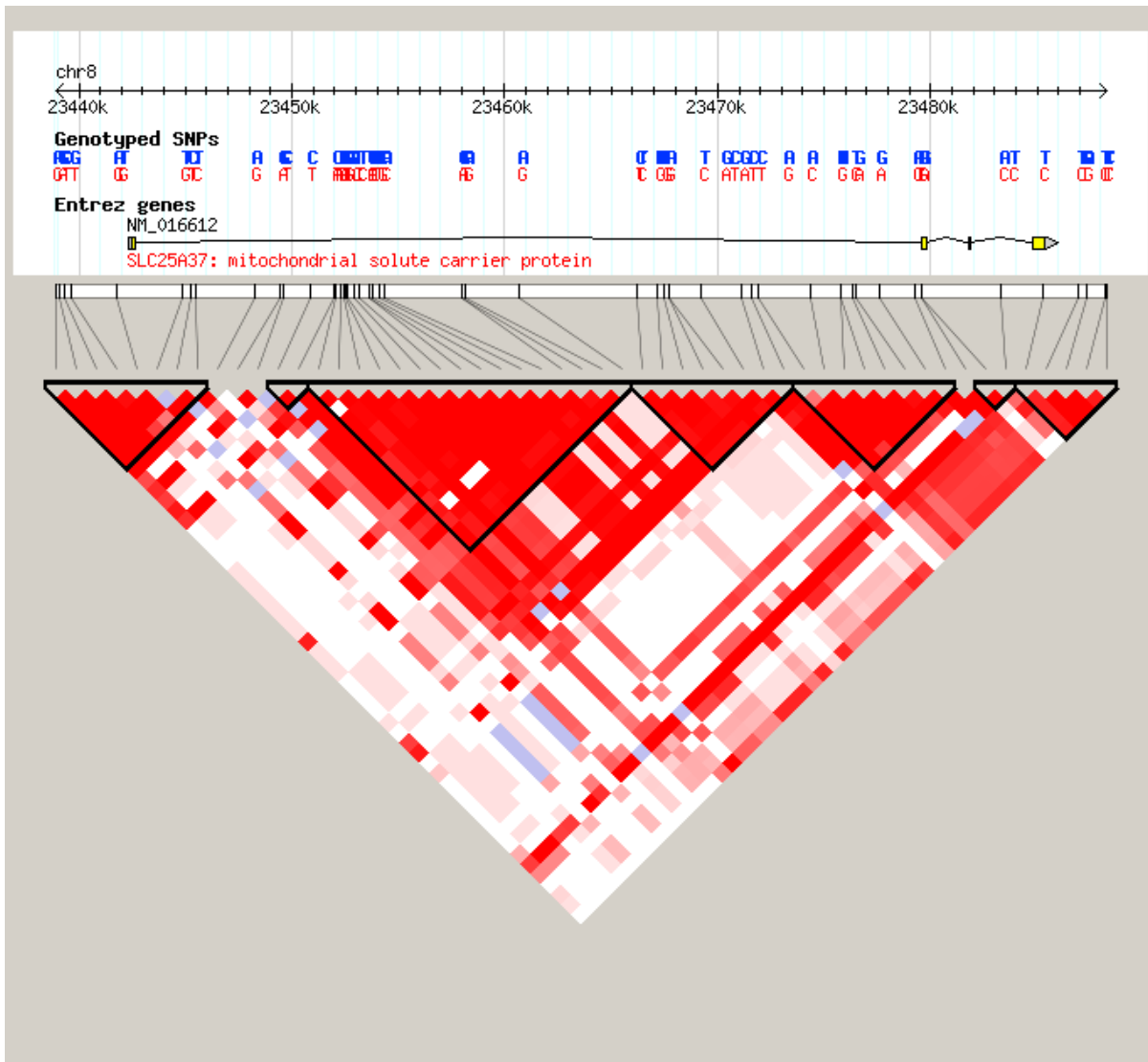


**Figure 22: Haplotype block of Mfrn tagSNPs.** Haploview 4.2 (Barrett et al., 2005) output for Mfrn tagSNPs in the region of 23437 to 23490 on chromosome 8 showing haplotype blocks.

### 2.01.002 Primer design for Mfrn tagSNP genotyping

MassARRAY software was used to design the primers for the SNPs, to accommodate the maximum number of reactions in one assay without any interference of the primer products or a reduction in performance in any of the SNPs when the Matrix-Assisted Laser Desorption/Ionisation Time-Of-Flight (MALDI-TOF) was carried out. The Ensembl database was used to obtain the 5' and 3' end sequences surrounding each SNP for uploading into the MassARRAY software. The SNP information along with the flanking 5' and 3' sequences

was copied and pasted. SNP itself was put in a square bracket with a forward slash separating the two alleles. Three sets of primers were designed for the multiplex PCR amplification with a third primer (extension primer) for the iPLEX extension reaction. The forward and reverse primers were ordered at 25 nmoles and the extension primers at 200 nmoles respectively. The extension primer anneals adjacent to the SNP, which is then extended by a single terminal base. The resulting product varies in mass depending on the base added and is easily differentiated using MALDI-TOF mass spectrometry. Maximum multiplex level was set to forty. SNP capture details were set to an amplicon length ranging between 80bp – 160bp, with the optimum being 100bp. To ensure, that the MS multiplexing remains the same, the extended primer was set so that the length of the extended primer was between 15bp and 30 bp. The lower and the upper limit mass of the extension primer was set between 4500Da and 8500Da respectively. The minimum distance between the two MassEXTEND primers was adjusted to ten and the minimum distance between the expected mass peak of the two assay analytes was kept at fifty. Once the settings were saved, the final results were displayed indicating how many assays the SNPs can be incorporated into, the full report, which was saved as an excel file. The saved file included the information regarding the assay and the primers.

### **2.01.003 Initial PCR reaction**

The primers were made up to a final concentration of 100pmoles/ $\mu$ l and the extension primers were made up to a final concentration of 500pmoles/ $\mu$ l using deionised water. 2  $\mu$ l aliquots of the South Asian DNA samples were added into each well of a 384-well plate, with water placed randomly as a blank. The PCR mix was made for a total of 500 reactions to provide sufficient quantities for all the wells of a 384-well plate. Final concentration of 25mM MgCl<sub>2</sub>, 25mM dNTP, 500nM primer mix and 5 Units/ $\mu$ l of Hot Start Taq were mixed in the final PCR reaction. 3  $\mu$ l of the PCR mix was added to the wells containing 2  $\mu$ l of DNA. PCR was carried out on a Peltier thermal cycler.

After the completion of the PCR, the obtained product was treated with shrimp alkaline phosphatase (SAP), to clean up the PCR product and also to degrade any remaining primers to prevent any non-specific carry over into the subsequent reactions. SAP was deactivated at 80°C. Once the initial PCR and clean-up step was finished, the Sequenom iPLEX extension reaction was carried out. The resulting mixture of products was run on the Sequenom MassARRAY system.

#### **2.01.004 Single base extension reaction**

The volume of the extension primer is directly proportional to the mass of the primer. A primer with a high mass was added at a higher concentration and a primer with a lower mass at a lower concentration, as the higher mass primers were hard to ionise compared with the lower mass primers. The concentration of the extension primer was determined using the regression method as recommended by Sequenom. The single base extension reaction was carried out in a thermal cycler.

#### **2.01.005 MALDI-TOF Mass Spectrometry**

Products obtained after the Sequenom single base extension reaction were treated with an anion exchange resin to remove adduct-forming ions, which can hamper the efficiency of the MALDI-TOF mass spectrum. A MassExtend clean resin treated 384-well plate is left to air dry for thirty minutes after which the adhesive film was removed. 16 µl of dH<sub>2</sub>O was added into each well. Adhesive lids were placed on the plate and the plate was constantly rotated for ten minutes which resulted in the resin being suspended within the solution. 15-25nl of the extended primer products were robotically (MassARRAY NanoDispenser) dispensed onto the SeqrtoCHIP array which contained matrix spots (3-hydroxypicolinic acid) in a 384-well format. Calibrant, which contains three standard oligonucleotides of known mass 5100, 8500 and 10,000 mass units, was also spotted and used as a standard.

Genotyping was carried out in Imperial College, UK. The design (other than choosing the candidate gene, Mfrn) involving selection of the Mfrn tagSNPs, primers, extension primers and the experimental procedure was carried out by Dr. Laura Towns. Once the genotyping data was given, I carried out the statistical analysis was carried out using SPSS (v.20) software.

#### **2.02 Cell culture**

Human carcinoma cells MCF7, chronic myelogenous leukemic cells K562 and placental choriocarcinoma BeWo cells provided by Health Protection Agency (HPA) were selected based on the expression data of IRPs and Heph as provided by the protein atlas database (Uhlen et al., 2005). MCF7 and K562 cells were cultured using RPMI1640 growth media. BeWo cells are cultured using Ham's F12 growth media. Complete media was prepared by adding 2mM of glutamine and 10% fetal bovine serum (FBS). Culture flasks were sub-cultured at 70-80% confluency for BeWo cells. Adherent cells, MCF7 and BeWo, were harvested using trypsin (Sigma, UK). Cell numbers and viability were determined using a haemocytometer and trypan blue staining, respectively. Aseptic conditions were maintained

throughout the culturing to avoid any contamination. Owing to the relatively easy handling of K562 cells, high levels of expression of both IRPs and Heph, erythroid K562 cells represent a functionally different type of cells and also there are not many studies in the literature concerning the effect of iron availability on the expression of IRPs and Heph; K562 cells were selected to carry out gene expression, gene synthesis and protein protein interaction analysis of IRPs and Heph.

### **2.03 RNA extraction from K562 cells**

Total RNA was extracted from K562 cells using the protocol provided by the E.Z.N.A total RNA kit I (Omega Biotek, VWR International Ltd, UK) for further analysis.  $1 \times 10^7$  cells were lysed using the TRK lysis buffer. Lysate was added to the HiBind RNA mini columns to bind the RNA. Columns were washed three times using RNA wash buffer I and II provided in the kit. RNA was eluted using diethylpyrocarbonate (DEPC) water, so as to inactivate any remainings of ribonuclease (RNase) enzymes which when present degrade RNA.

### **2.04 Amplification of cDNA (complementary DNA) using RNA extracted from K562 cells by Reverse Transcription**

During Reverse transcription, a single stranded DNA was synthesised from RNA using Promega's IMProm-II reverse transcription system. OligodT (0.5 $\mu$ g/reaction) and RNA (1 $\mu$ g/reaction) extracted from the K562 cells were used initially to denature the oligonucleotides.

#### **2.04.001 RT reaction mix**

The final reaction mix contained 1x IMProm-II reaction buffer, 2.0-4.0mM MgCl<sub>2</sub>, 0.5mM each dNTP and 1 $\mu$ l of Reverse Transcriptase enzyme in a 20  $\mu$ l final volume.

#### **2.04.002 cDNA primers**

Primers were designed using IBA-tagnology's (IBA, Germany) Primer D'Signer software. All primers were 3' phosphorothioate (PTO)-protected oligonucleotides which are protected against the exonuclease activity of proof-reading polymerases. The gene of interest (GOI) was extended by PCR with combinatorial sites and the StarCombinase recognition sites, introduced by the primers which are important for the oriented insertion of the PCR fragment into the entry vector during the molecular cloning. Table below shows the list of primers that were designed to synthesise Heph, HephI1, IRP1 and IRP2 cDNA.

Gene	Primer name	Sequence 5' to 3'	Scale	Length	Expected cDNA fragment
<b>Heph</b>	HuHp-F	agc ggc tct tca atg gag tca ggc cac ctc ctc	40 nmol	33	3.5kb
	HuHp-R	agc ggc tct tct ccc ctg ttt gaa aga cag aag ctt g	40 nmol	37	
<b>IRP1</b>	IRP1-F	agc ggc tct tca atg agc aac cca ttc gca cac c	40 nmol	34	2.6kb
	IRP-1R	agc ggc tct tct ccc ctt ggc cat ctt gcg gat c	40 nmol	34	
<b>IRP2</b>	IRP2-F	agc ggc tct tca atg gac gcc cca aaa gca gga t	40 nmol	34	2.9kb
	IRP2-R	agc ggc tct tct ccc tga gaa ttt tcg tgc cac aaa g	40 nmol	37	

**Table 01: PCR primers for Heph, IRP1 and IRP2.** Above table shows the Heph and IRPs primers used to synthesise the respective cDNA along with the expected PCR product size.

## 2.05 Polymerase Chain Reaction (PCR)

cDNA fragments are synthesised using the RT product by the polymerase chain reaction (PCR). PCR was performed with the final concentrations of the following reagents in a 25 µl reaction mixture containing 10 pmol of each sequence-specific primer, 5 units (U) of Phusion taq polymerase, 2-4 mM MgCl<sub>2</sub>, 10x NH<sub>4</sub> reaction buffer (160mM [NH<sub>4</sub>]<sub>2</sub>SO<sub>4</sub>, 670mM Tris-HCl pH 8.8), and 200 µM dNTPs

PCR reaction set up involved an initial denaturation step of 30 seconds at 98 °C, followed by 35 cycles of denaturation step for 30 seconds at 98 °C, an annealing step for 30 seconds at variable temperatures, followed by an extension step for another 2.30mins-3.30mins (1min/kb amplicon size) at 72 °C and finally the reaction was concluded with an extension of five minutes at 72 °C. To rule out DNA contamination a water blank was included in every experiment as a negative control.

## **2.06 Agarose gel electrophoresis**

Depending on the size of the PCR product, DNA samples were resolved on 0.7 – 3 % 1xTBE agarose gels with addition of ethidium bromide.

## **2.07 Low melting gel electrophoresis**

Since PCR resulted in non-specific amplicons in addition to the bands of the right size, 0.7% low melting gel was prepared using 1xTAE buffer to extract the respective band of Heph (3.5kb), IRP1 (2.6kb) and IRP2 (2.9kb) PCR product. Gel was placed on the UV illuminator to cut the precise band using a scalpel washed with ethanol to eliminate any contamination. The respective fragment was gel extracted using QIAquick gel extraction kit as per the provider's protocol.

## **2.08 RNA and DNA quantification**

The quality of RNA extracted from the K562 cells and gel-extracted cDNA fragments was carried out by measuring the absorbance values at 260 nm and 280 nm using a NanoDrop DNA Spectrophotometer (Thermo Scientific, UK). Only samples with 260/280 values ranging from 1.8 – 2.0 were used.

## **2.09 Real-Time quantitative Polymerase Chain Reaction (qRT-PCR)**

cDNA prepared from the K562 cells was used to analyse the differential expression of Heph, IRP1, IRP2 and Mfrn in K562 cells with and without 100  $\mu$ M FAC. Beta actin ( $\beta$ -actin) was used as a normalizing or a house-keeping gene. The TaqMan gene expression assays and the master mix were used to carry out the reaction set up. qRT-PCR analyses were carried out in triplicates in 96-well opaque plates (Bio-Rad, UK). A DNA Opticon Monitor Engine II (MJ Research) was used to carry out the quantitative real time PCR. Thermal cycling conditions of 95°C for 10 mins, 95°C for 15 sec and 60°C for 1 min for 40 cycles was used to run the samples. qRT-PCR reactions were carried out in a 20  $\mu$ l volume containing 10  $\mu$ l of master mix, 1  $\mu$ l of TaqMan gene expression assays with integrated TaqMan probes and 25-100 ng of cDNA diluted in 9  $\mu$ l of DEPC water.

### **2.09.001 qPCR Data analysis**

Calculation of relative gene expression was carried out by normalizing the target gene data to a housekeeping gene (beta actin). The advantage of using a housekeeping gene (such as GAPDH,  $\beta$ -actin, etc.) in normalizing the data is that this method overcomes the need for accurate quantification and loading of the starting material. The drawback of using relative gene quantification normalized to housekeeping gene is that this method requires that the

known reference gene ( $\beta$ -actin) has a constant expression in both treated and un-treated samples under study. Once the C(T) values [C(T) value or the threshold cycle value is the cycle number at which the fluorescence generated during the real time PCR when the fluorescence signal crosses the fluorescence threshold] are obtained, different methods like Livak method (Livak and Schmittgen, 2001),  $\Delta$ C(T) method using a reference gene (Schmittgen and Livak, 2008) or Pfaffl method (Pfaffl, 2001) can be used to determine the expression level of the target gene in the treated sample relative to the un-treated sample.

Each sample reaction was run in triplicate and expression was quantified as the C(T) of GOI minus the C(T) of the  $\beta$ -actin gene [ $\Delta$ C(T)]. The relative gene expression of the target and housekeeping gene in both treated cells to control samples was calculated with the  $2^{-\Delta\Delta C(T)}$  method [ $\Delta\Delta$ C(T)] (Livak and Schmittgen, 2001). The real time PCR statistical analysis was performed using the student t-test for two group comparisons on  $\Delta$ C(T) numbers.

## **2.1 Molecular Cloning of Heph, IRP1 & IRP2**

### **Step 1: Donor Vector generation**

#### **2.1.01 Workflow of Donor Vector Generation**

In the first step, during the cDNA synthesis by Reverse Transcription PCR (RT-PCR), the gene of interest (GOI) was extended at both the 5' and 3' ends with the combinatorial and StarCombinase sites included in the primers. The gel-extracted PCR fragment of GOI was then inserted into an Entry Vector by a one-tube reaction.

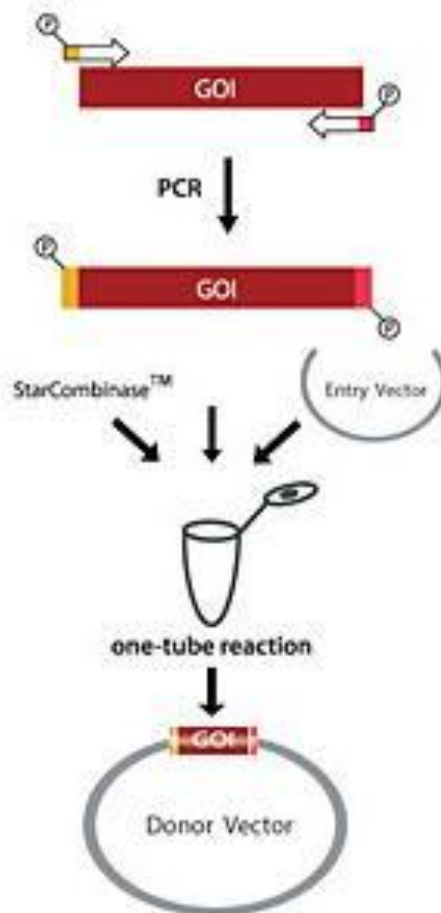


**Figure 23: Workflow for donor vector generation.** Insertion of GOI into the Entry Vector to create the Donor Vector, Figure taken from IBA, manual PR26-0022 version.

The StarCombinase recognises the recombination sites and simultaneously cleaves and ligates the DNA. This helps the PCR product and the Entry Vector to be recombined at the combinatorial sites (red and light orange regions in figure 27) leading to the Donor Vector generation and losing the StarCombinase1 recognition areas (dark orange) which results in unidirectional recombination reaction.

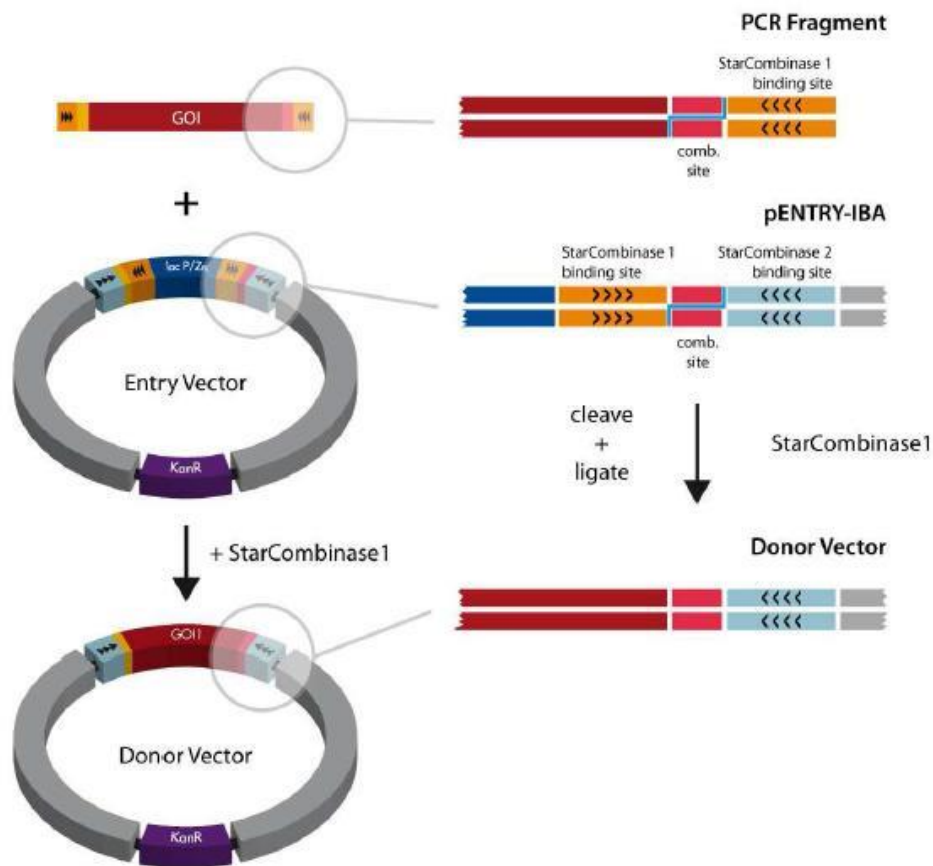


**Figure 24: Donor vector generation and StarCombinase Recognition site.** Donor Vector generation with GOI using StarCombinase Recognition sites. **Figure taken from IBA, manual PR26-0022 version.**

### 2.1.01.001 Donor Vector with GOI

The PCR product of GOI was inserted into the Entry Vector pENTRY-IBA51 to generate the Donor vectors of interest, which in this study are Heph, IRP1 & IRP2. Reaction for Donor vector generation was explained as follows: 2nM of the gel extracted PCR product was added to the 10µl of the entry vector along with the StarSolutions provided by IBA as suggested in the manual version PR26-0022. The reaction tube was mixed gently and incubated for 1hr at 30°C. A vial of competent *E.coli* cells was thawed on ice. After 1hr incubation 10 µl of the reaction mixture was added to the thawed competent *E.coli* cells. Cells were then incubated on ice for 30mins, followed by incubations at 37°C for 5mins and again on ice for 5mins. 900µl of LB medium was added to the cell mixture and the vial was incubated at 37°C for 45mins in a shaking incubator. 100µl of the cell mixture was plated on to LB agar containing 50 mg/L Kanamycin and 50mg/L X-gal. The remaining cell mixture

(900µl) was centrifuged for 30 seconds in a microfuge at 10,000 RPM. The pellet was resuspended in 100µl LB medium and the whole amount was plated. Plates were incubated overnight at 37°C for colony growth. The Entry Vector carried the LacZα gene and therefore produces blue colonies on X-gal containing plates while LacZα was replaced with GOI in the Donor Vector and hence will generate white colonies.

#### **2.1.01.002 Donor Vector Plasmid DNA extraction**

Three white colonies were cultivated in 5ml LB medium containing 50µg/L kanamycin and plasmid DNA extraction was carried out. The Donor Vector's plasmid DNA was extracted using QIAprep® Spin Miniprep kit (Qiagen, UK) using the following protocol: an overnight bacterial culture of 3ml was centrifuged at 10,000 RPM for 3mins in a table top micro centrifuge. The pellet was resuspended thoroughly in 250µl of Buffer P1. To it 250µl of Buffer P2 was added and mixed thoroughly by inverting the tube 6-7times. 350µl of Buffer N3 was added to the above centrifuge tube and mixed immediately and thoroughly by inverting the tube again for 6-7times. Then the tube was centrifuged for 10mins at 10,000 RPM in a table top micro-centrifuge. Supernatant was collected into a QIAprep spin column and was centrifuged for 1min at 10,000 RPM. The column was then washed with 500µl of Buffer PB and was centrifuged for 1min at 10,000 RPM. Again the column was washed with 750µl of Buffer PE. Additional centrifugation for 1min at 13,000 RPM was carried out to remove any residual wash buffer. 50µl of elution buffer, Buffer EB (10mM Tris-Cl, pH 8.5) was added to the centre of the column and the column was left on the table for 2mins. To elute the pDNA the column was placed in a micro-centrifuge tube and was centrifuged at 13,000RPM for 1min.

#### **2.1.01.003 Donor Vector identification**

*XbaI/HindIII* restriction enzymes were used to identify the clone with the GOI. A fragment having the length of the GOI and another fragment with 40bases long is expected as long as no *XbaI/HindIII* restriction sites are present internally in GOI. The putative clone with GOI was then selected and the sequence was confirmed via Donor Vector forward and reverse sequencing primers provided by IBA. The regions flanking the GOI should have the sequences TCTAGA (*XbaI* restriction enzyme sequence) and AAGCTT (*HindIII* restriction enzyme sequence).

## Step 2: Destination Vector generation

### 2.2 Destination Vector generation

The resulting Donor Vector after restriction enzyme and sequence confirmation was used as the basis or template for the sub-cloning of the GOI into an Acceptor Vector which has the tag, the One Strep tag in this study. The resulting Destination Vectors with the GOI are then transformed into the respective host cell such as K562 (Human Caucasian chronic myelogenous leukaemia) cells for systematic expression and purification screening.

#### 2.2.01 Destination Vector Generation work flow

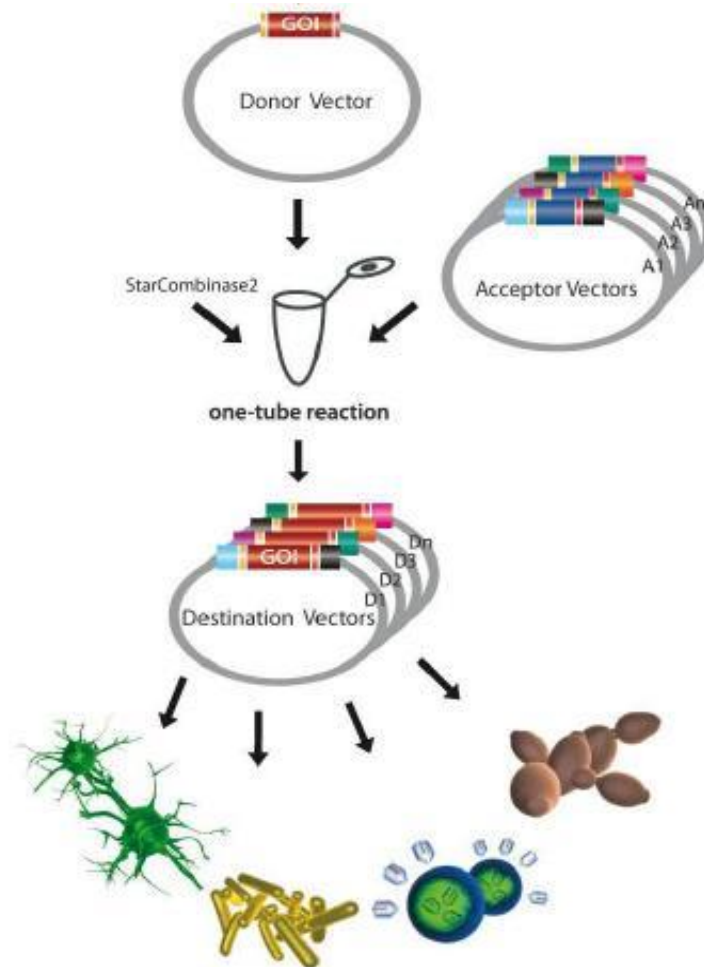


**Figure 25: Work flow of Destination vector generation.** Insertion of Donor Vector into the Acceptor Vector to create the Destination Vector. **Figure taken from IBA's manual PR26-0022 version.**

Acceptor Vectors provide the necessary genetic make up such as tag, promoter and signal sequence for the correct orientation of the GOI during the cloning process. The pESG-IBA acceptor vector was mixed with the respective Donor Vector with the GOI Heph, IPR1 and IRP2 and with StarSolutions A1-A3 to generate the desired Destination Vector after a short incubation.

The reaction mixture was then used to transform the *E.coli*. The *E.coli* transformation mix is then plated onto the LB agar plates containing ampicillin and X-gal. Desired Destination Vectors with GOI (Heph, IPR1 and IRP2) will generate white colonies while non-desired Acceptor Vectors will generate blue colonies.

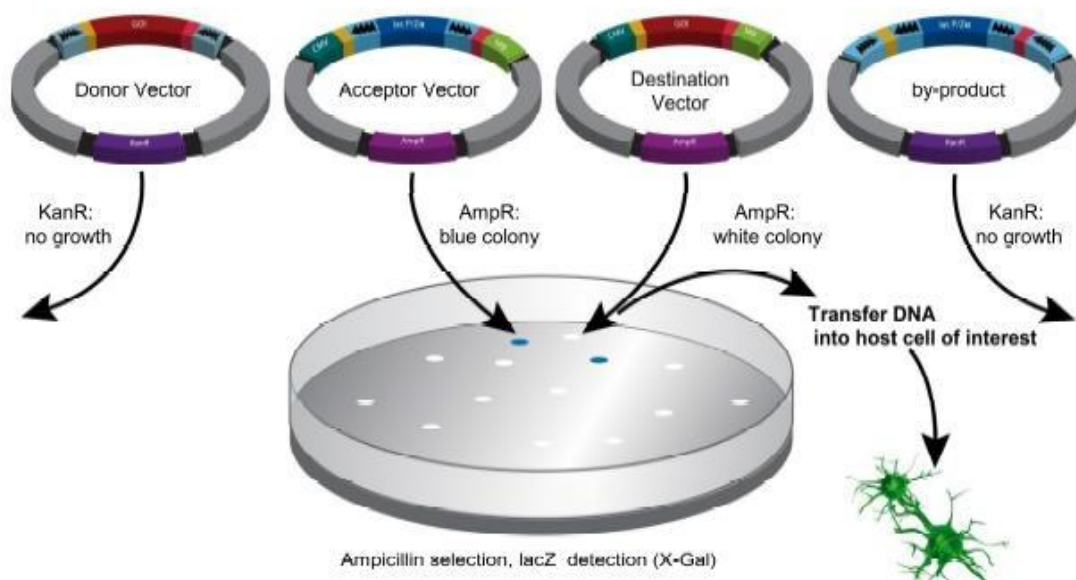


**Figure 26: LB agar plates with X-gal and ampicillin.** Selection on the LB-agar plates with X-gal and ampicillin. Due to the selection on the ampicillin plates, Donor Vector and the by-product – which provide a kanamycin resistance gene only will not be able to enable the *E.coli* growth. However, Acceptor Vector and Destination Vector's with the GOI growth is enabled due to the ampicillin resistance gene. The Acceptor Vector carries the LacZα gene and therefore produces blue colonies on X-gal-containing plates. The LacZα gene will be replaced by the GOI in the Destination Vector which therefore generates white colonies. **Figure taken from IBA's manual PR26-0022 version.**

## **2.3 GOI transfer reaction into destination vector**

Respective Donor Vector pDNA (Heph, IRP1 and IRP2) is used as a template while generating the Destination Vector during the Destination Vector generation. StarSolutions A1, A2, A3 and 2ng/μl Donor Vector were added to the Acceptor Vector. After mixing gently the tube was incubated at 30°C for 1hr. During the final minutes of the above incubation, competent *E.coli* cells were thawed on ice. After 1hr incubation of the Acceptor Vector along with the above mix, 10μl of the reaction mixture was added to the thawed competent *E.coli* cells. Then mixed gently (by pipetting) and incubated the *E.coli* cells for 30mins on ice. After 30mins of incubation the tube was mixed gently again by pipetting and was incubated on the hot plate at 37°C for subsequent 5mins. Once the incubation was finished the tube was then replaced in the ice box for 2-5mins. Then the reaction mix of 10μl was plated (mixed with 90μl LB medium) and 100μl on LB agar plates containing 100mg/L ampicillin and 50mg/L X-gal.

### **2.3.01 Destination Vector Plasmid DNA extraction**

Destination Vector plasmid DNA was extracted by following the similar method used to carry out donor vector extraction.

### **2.3.02 Destination Vector Identification**

pESGIBA an Acceptor Vector has both *XbaI* and *HindIII* restriction sites flanking the expression cassette and therefore either enzyme can be used to analyse the Destination Vector pDNA that has been extracted. Webcutter 2.0 (Maxwell, 1997) tool was used to carry out an exact calculation of the expected fragment lengths after an overnight restriction enzyme digestion of the destination vector pDNA.

## **2.4 GOI transfection and expression**

The Destination Vector pDNA with the GOI (Heph, IRP1 and IRP2) as confirmed by sequencing, was used to transfect the K562 cells. Transfection is a process in which the GOI (nucleic acids) is forcibly introduced into the expression system, in this case the eukaryotic expression system using K562 cells. The GOI cloned with One-Strep tag is introduced into the K562 cells to examine the protein expression and localisation in the cells. There are different methods of transfection and part of this study examines the chemical based (using Lipofectamine-LTX) and particle based (Magnet assisted) to establish the correct, efficient method for Iron metabolic genes (Heph, IRP1 and IRP2).

#### **2.4.01 Chemical based Transfection**

Chemical based transfection involves addition of the DNA to Lipofectamine LTX-Plus reagent (Invitrogen, UK) and subsequent release of the DNA into the cell. For eukaryotic cells, transfection efficiency is better achieved using cationic liposomes (or mixtures), because the cells are more sensitive. The Lipofectamine reagent contains the lipid subunit which forms liposomes in an aqueous environment, which then envelope the transfection material, i.e. plasmid DNA. The DNA-containing liposomes then fuse with the plasma membrane of eukaryotic cells and enter the cells, allowing nucleic acids to cross into the cytoplasm and organelle to be available to the cell for replication and expression. The process of using liposomes during transfection (i.e., Lipofection) generally uses a positively charged (cationic) lipid to form an aggregate with the negatively charged (anionic) genetic material (Felgner et al., 1987). A net positive charge has been assumed to increase the effectiveness of transfection through the negatively charged phospholipid bilayer (Felgner et al., 1987). Lipofectamine LTX-Plus reagent transfection technology performs the same tasks as other biochemical procedures utilizing polymers, DEAE dextran, calcium phosphate, and electroporation. The advantages of Lipofectamine LTX-Plus reagent are its high efficiency, its ability to transfect all types of nucleic acids in a wide range of cell types, its ease of use, reproducibility, and low toxicity.

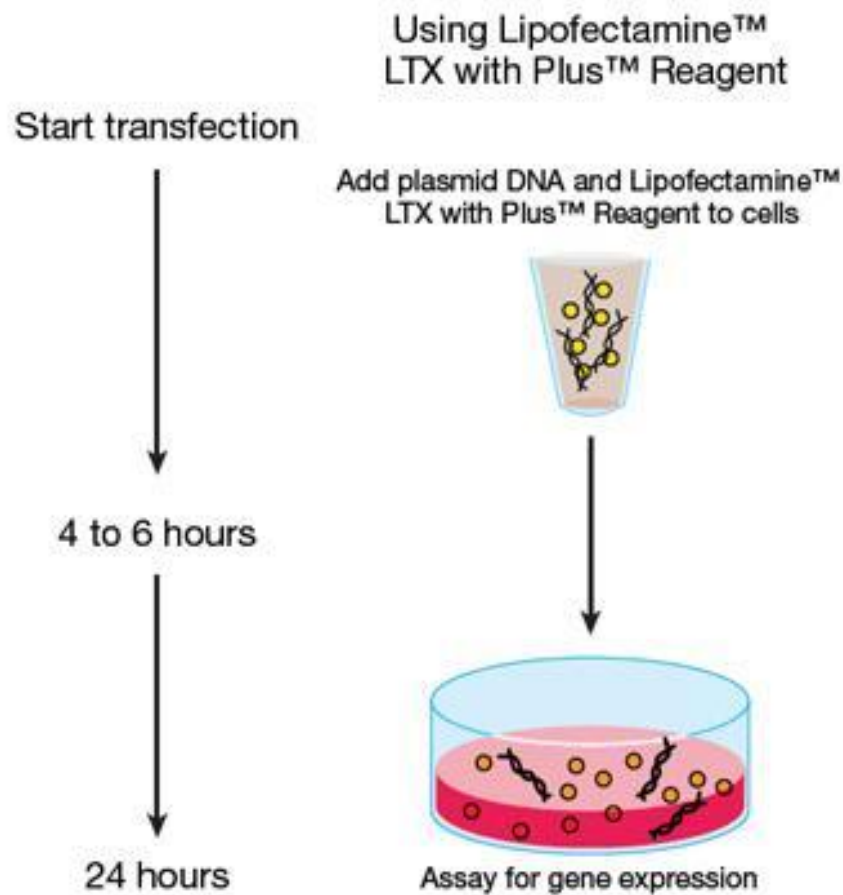


**Figure 27:** Transfection process involving Lipofectamine-LTX plus reagent. Transfection flow chart showing different steps involved in the process of transfection using Lipofectamine LTX-Plus reagent and pDNA. **Figure taken from Life technologies website.**

#### **2.4.01.001 Transfection of K562 cells using Heph, IRP1 and IRP2 by Lipofectamine LTX-Plus reagent**

On the day of transfection, K562 cell culture were counted to determine the culture density.  $3 \times 10^5$  cells per well were plated in 0.5ml of RPMI-complete growth medium. For each well of cells to be transfected, 2.0 $\mu$ g of DNA was diluted in 100 $\mu$ l of Opti-MEM® I Reduced Serum Medium (Invitrogen, UK) without serum. PLUS™ Reagent (Invitrogen, UK) was mixed gently before use and then the PLUS™ Reagent was added in a 1:1 ratio to the diluted DNA. The mix was then incubated for 5-15 minutes at room temperature. For each well of cells, 5 $\mu$ l of Lipofectamine™ LTX was diluted into the above diluted DNA solution, mixed gently and the mix was incubated for 25 minutes at room temperature to form DNA-Lipofectamine™ LTX

complexes. 100µl of the DNA-Lipofectamine™ LTX complexes was added directly to each well containing cells and mixed gently by rocking the plate back and forth. 1ml of RPMI-complete growth medium was added after 24hr incubation. Following the transfection, transfection complexes were not removed. Before assaying for transgene expression by Flow Cytometry and Western blotting, cells were incubated at 37°C in a CO<sub>2</sub> incubator for 24-48 hours post-transfection.

#### 2.4.02 Particle based transfection

Magnet-assisted transfection (MATra) is a transfection method, which uses a magnetic force to deliver DNA into the target cells. In this process nucleic acids are first associated with magnetic particles. Then, application of magnetic force drives the nucleic acid particle complexes towards and into the target cells (Bertram, 2006) leading to efficient transfection. To carry out the MATra approach cells must be adherent to the cell culture vessels. Therefore the suspended cells like K562 need pre-treatment first by incubating the cells with the magnetic reagent MATra-S Immobilizer or by using polylysine plates.

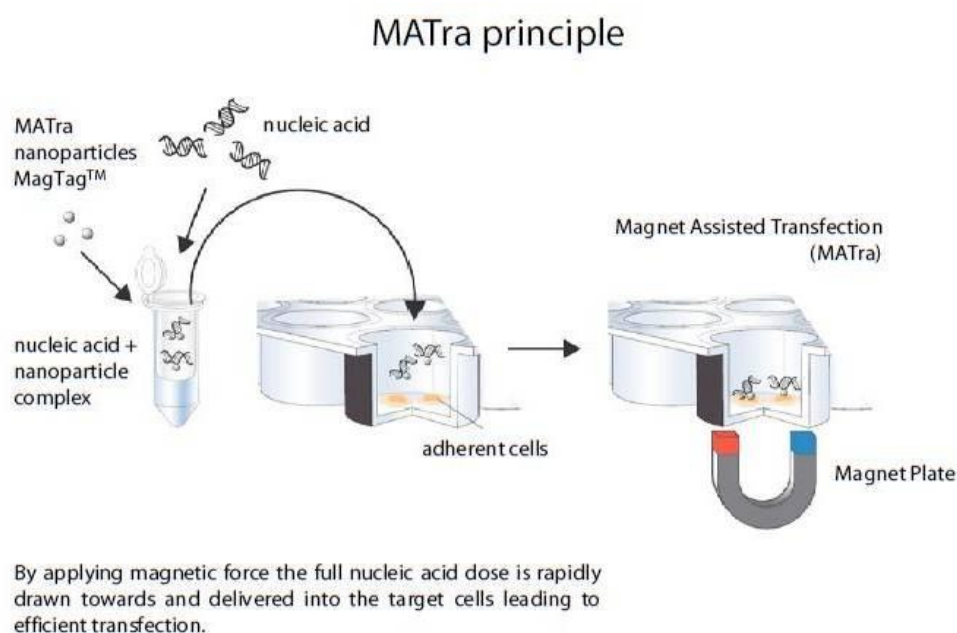


**Figure 28: MATra principle.** Flow chart showing different steps involved in carrying out magnetic-assisted transfection. **Figure taken from IBA's manual version PR09-0015.**

##### 2.4.02.001 Transfection of K562 cells using Heph, IRP1 and IRP2 by MATra

3 x 10<sup>5</sup> cells were diluted in 1ml of RPMI complete growth medium in the cell culture plate. 30ul of MATra-S Immobilizer was added to the above cell suspension and was incubated for 10mins at room temperature in the culture hood. The plate was then incubated on a magnetic plate for 15mins at 37°C. 2µg of pDNA was diluted in 50µl of serum-free RPMI cell culture medium. 2µl of MATra-A reagent was added to the above diluted pDNA mix and was mixed thoroughly. The mixture was incubated at room temperature for 20mins. After the incubation the DNA:bead mixture was added to the cells and was mixed by pipetting immediately. After mixing, the plate was placed immediately on the magnetic plate and the plate was incubated for 15mins at 37°C. Transfected cells were left in the incubator at 37°C for 48hrs prior to carrying out protein expression analysis by flow cytometry, and western blotting.

## **2.5 Protein expression analyses by Western Blotting**

### **2.5.001 Western blotting solutions and buffers**

#### **Lysis buffer- pH 7.4**

100 mM - HEPES-KOH

2 mM - CaCl<sub>2</sub>

0.2% - Triton X-100 (v/v)

10 mM - Protease inhibitor (AEBSF)

Millipore water

Made up to 50 ml and stored as 1 ml aliquots at -20°C. pH was adjusted with 4 M HCl.

#### **SDS Sample buffer- pH 6.8 (4X)**

200 mM - Tris-HCl

40% - Glycerol

2% - SDS (w/v)

0.2% - Bromophenol blue (w/v)

20 mM - DTT (added fresh on the day)

Millipore water

pH was adjusted using 4 M HCl solution

**Resolving buffer- pH 8.8 (1.5 M)**

18.17 g - Tris base

Dissolved in 100 ml deionised water and pH adjusted to 8.8

**Stacking buffer- pH 6.8 (0.5 M)**

6.06 g - Tris base

Dissolved in 100 ml deionised water and pH adjusted to 6.8

**Resolving gel solution (12%)**

2 ml - double distilled H<sub>2</sub>O

1.25 ml - 1.5 M Tris-HCl, pH 8.8

0.050 ml - 10% SDS (w/v)

1.66 ml - Acrylamide/Bis 30% (w/v)

0.025 ml - 10% APS (w/v)

0.0025 ml- TEMED

**Stacking gel solution**

1.53 ml - double distilled H<sub>2</sub>O

0.625 ml - 0.5 M Tris-HCl, pH 6.8

0.025 ml - 10% SDS (w/v)

0.335 ml - Acrylamide/Bis 30% (w/v)

0.0125 ml - 10 % APS (w/v)

0.0025 ml - TEMED

**10X Electrophoresis running buffer (1L)**

250 mM - Tris-HCl, pH 8.3

1925 mM - Glycine

50 ml - 20% SDS (w/v)

950 ml - double distilled H<sub>2</sub>O

**Coomassie Brilliant Blue G-250**

0.025% - Coomassie blue (w/v)

10% - Acetic acid (v/v)

90% - double distilled H<sub>2</sub>O (v/v)

**Destain solution (500 ml)**

35 ml - Acetic acid

25 ml - Methanol

440 ml – double distilled H<sub>2</sub>O

**Transfer buffer (10X)**

250 mM - Tris base

1925 mM - Glycine

500 ml - double distilled H<sub>2</sub>O

**Sartoblot buffer (500 ml)**

40 ml - Transfer buffer (1X)

100 ml - Methanol

360 ml – double distilled H<sub>2</sub>O

**Phosphate Buffered Saline (PBS) solution - 1L**

140 mM - NaCl

2.7 mM - KCl

10 mM - Na<sub>2</sub>HPO<sub>4</sub>

1.8 mM - KH<sub>2</sub>PO<sub>4</sub>

Double distilled H<sub>2</sub>O

**Phosphate Buffered Saline – Tween 20 (PBS-T)**

1 L - PBS

1 ml - Tween 20

**Blocking buffer**

6% - Milk powder (w/v)

100 ml - PBS-T

#### **Antibody dilution buffer (WB)**

3% - Milk powder (w/v)

100 ml - PBS-T

#### **2.5.001 Sample preparation for SDS-Polyacrylamide Gel Electrophoresis (SDS-PAGE)**

Transfected and untransfected samples were aliquoted into the 1.5ml eppendorf tubes and were washed with ice-cold PBS. PBS was replaced with cell lysis buffer and the samples were spun at 16,000g for 20mins at 4°C. Supernatant was removed and was followed by incubation at 95°C for 5 min. Before loading the samples onto the gel, a centrifugation step was performed (2,000 g, 2 min) to collect all the sample to the bottom of the reaction tube and loaded into the gel wells.

#### **2.5.002 SDS-Polyacrylamide Gel Electrophoresis**

To separate proteins according to molecular mass, the cell lysate was denatured by sodium dodecyl sulphate (SDS). SDS polyacrylamide gel electrophoresis (SDS-PAGE) was performed as described (Laemmli, 1970) using the Mini PROTEAN III Electrophoresis Unit (Bio-Rad). Gels were cast between two glass plates by pouring freshly prepared 8% resolving gel solution containing acrylamide/bisacrylamide into the gel cassette fixed in a casting frame. Unpolymerized separating gel solution was overlaid with H<sub>2</sub>O-saturated butanol to achieve an even surface. After polymerization, H<sub>2</sub>O-saturated butanol was poured off, the gel washed twice with deionised water, and the excess water was blotted using a filter paper (Whatman 3 MM, Whatman AG). Then unpolymerized stacking gel was poured into the gel cassette and a plastic comb was inserted from the top, to form the loading wells in the stacking gel.

Gels were used immediately after polymerization. Gel electrophoresis was performed by placing the gel into the electrode assembly device inside a clamping frame in the tank of the Mini PROTEAN III system. Electrophoresis running buffer was added to the inner and outer chambers of the tank and the plastic comb was carefully removed. Wells were washed with the running buffer to remove any free unpolymerized acrylamide/bisacrylamide/air bubbles so as to allow the to run sample freely. Samples were loaded into the wells of the stacking gel. Electrophoretic separation was performed at 150 V (constant voltage) until the

bromophenol blue front of the SDS sample buffer reached the end of the resolving gel. Gels were either stained with Coomassie Brilliant Blue or transferred onto nitrocellulose membrane for Western blotting analysis.

### **2.5.003 Analysis of SDS-PAGE**

Proteins separated by SDS-PAGE were transferred onto a Hybond C nitrocellulose membrane for further analysis using a semidry transfer device (Bio-Rad Sartoblot system). A Hybond C nitrocellulose membrane and two pieces of blotting paper (Whatman 3 MM, BioRad) were cut to the size of the gel. Blotting paper, nitrocellulose membrane and the sandwich-blotting cassette were equilibrated by soaking in sartoblot buffer. One piece of blotting paper was placed on the cathode plate, and the nitrocellulose membrane was placed on top of the blotting paper. The gel was removed from between the sandwich-blotting cassette which was placed in the sortoblot buffer immediately after taking out from the gel tank and placed on top of the membrane. A second blotting paper was also placed on top of the gel. Having removed air bubbles by rolling a test tube on the top blotting paper, towards the anode plate, also dampened with the sartoblot buffer was used to complete the sandwich. Electroblotting was carried at 35V (constant voltage) for 1hr.

### **2.5.004 Immunochemical protein detection using the ECL System**

The blotted membrane was incubated in blocking buffer at 4°C, overnight, in the fridge. Following blocking, the membrane was rinsed with PBS-T and incubated with the primary antibody in the desired dilution for 2 hrs at room temperature on a shaker. Three 10 min washing steps with PBS-T were performed and the membrane was incubated with goat-anti-mouse-IgG antibodies coupled to HRP in a 1:5000 dilution. After six 10 min washes with PBS-T on a shaker, protein band detection was performed using the enhanced chemiluminescence reagent system (ECL, Amersham Pharmacia). The ECL solutions (reagent A and B) were mixed at equal volumes and the membrane was incubated with the mixture for 2 mins at room temperature in the dark. Chemiluminescence was detected using a UVP ChemiDoc-It system (UVP systems, UK).

## **2.6 Protein expression analyses by Flow Cytometry**

K562 cells transfected with Heph, IRP1 and IRP2 tagged with One-Strep tag were used to carry out the protein expression analyses by flow cytometry. The Guava flow cytometer can be used to analyse various assays, however in the current study only the Guava ExpressPlus assay has been used to measure protein expression levels in transfected and untransfected samples.

### **2.6.001 Sample preparation for Flow Cytometry analyses**

Transfected samples along with Untransfected samples (controls) were washed with ice-cold PBS in a 1.5ml eppendorf tube. Cells were then centrifuged at 400g for 5 mins and the washing was carried out three times.

### **2.6.002 Intracellular Antigen Staining for Flow Cytometry**

To eliminate any potential artifacts due to dead cell contamination, fixable viability dye was performed to allow exclusion of dead cells from the analysis. After performing the fixable viability dye incubation, cells were fixed by adding 100µl of IC fixation buffer (eBioscience, UK) and mixed by vortexing. The tube was incubated for 20mins at room temperature under the cell culture hood in the dark. Without washing 1mL of 1x permeabilization buffer (eBioscience, UK) was added to each tube and was centrifuged at 400g for 5mins at room temperature. The cell pellet was resuspended in 1mL of 1x permeabilization buffer and mixed again by pipetting. The tubes were again centrifuged at 400g for 5mins at room temperature. After decanting the supernatant, the cell pellet was resuspended in 10µl of 1x permeabilization buffer and one in 500 concentration of fluorochrome-labeled antibody was added for detection of intracellular antigen and was incubated in the dark at room temperature for 20mins. Cells were then resuspended in 1mL of 1x permeabilization buffer and were centrifuged at 400g for 5mins at room temperature. Then the cells were washed with ice-cold PBS thrice and after the final wash the cells were then resuspended in 200µl of 3%PBS-BSA to carry out flow cytometry analyses.

## **2.7 Protein-protein interactions**

Protein-protein interactions (PPIs) govern almost all the important cellular processes in living organisms. Thus carrying out PPI studies and analyses only helps to establish a rapid and accurate function of the protein in question. Figure 32 shows the different steps involved in PPI studies.

### **2.7.001 One-STrEP tag background**

One-Strep tag (Strep tag) is an eight amino acid peptide (WSHPQFEK) that specifically binds to streptavidin. Since Strep-tag binds reversibly, where the natural ligand D-biotin forms the complex, it can be applied for the efficient purification of corresponding fusion proteins on affinity columns with immobilized streptavidin. The Strep-tag has a neutral amino acid composition and hence does not hamper protein folding or secretion and so does not interfere with protein function.

### 2.7.002 One-STrEP tag suitability for PPI studies

Purification of the protein complex depends on the the very low tendency of Strep-Tactin to bind with other proteins non-specifically, the highly specific Strep-tag:Strep-Tactin interaction for adsorption and the specific elution with minute amounts of biotin or desthiobiotin in the same physiological buffer. Strep tags are also ideal for the isolation of functional protein complexes to investigate *in vivo* PPIs (Rigaut et al., 1993).

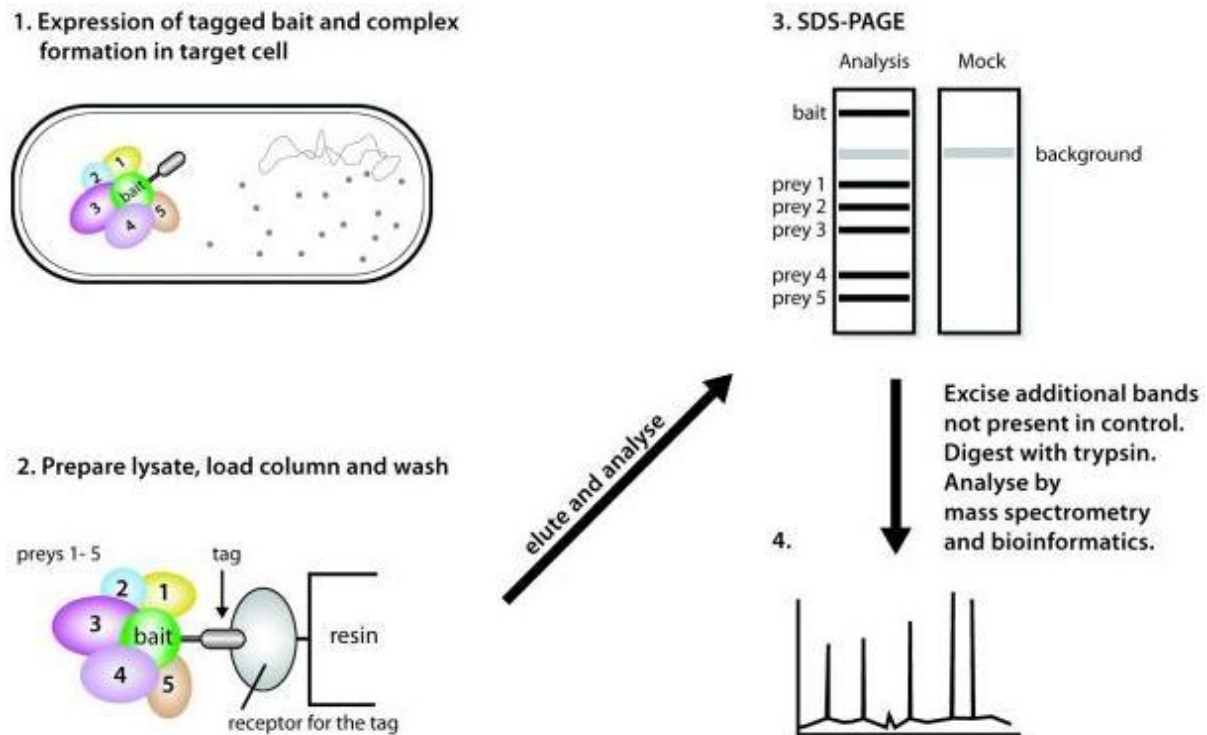


**Figure 29: Work flow in protein complex purification and analysis.** Steps 1-3 in the above figure shows the protein complex purification and Step 4 shows protein complex analysis. **Figure taken from IBA's manual PR27-0001 manual.**

Figure 29 shows the affinity tag-based protein complex isolations and protein interaction work flow. In step 1 the tagged bait (Heph-Strep, IRP1-Strep and IRP2-Strep) was expressed in K562 cells. After 24-48 hr incubation cells were lysed. The lysate containing the bait with putatively interacting preys was subjected to tag-based chromatography to perform a pull down. Isolated protein complexes were then analysed using SDS-PAGE and coomassie blue staining and compared to mocked isolates or controls. Potential preys are then identified by mass spectrometry, LC-MS-MS.

### **2.7.003 Preparation of cell lysates for PPI studies**

4mL of ice-cold lysis buffer (Buffer L) was used for every  $10^9$  K562 cells transfected and untransfected cells. Cells were homogenised on ice by using a pestle. Resulting cell mix was centrifuged at 750g for 10 mins at 4°C to pellet the cellular debris. 5µl of 5x SDS-PAGE sample buffer was added to 20µl of supernatant and the samples were stored at -20°C prior to SDS-PAGE analysis.

### **2.7.004 Buffers used to perform purification of protein complex**

#### **Lysis Buffer (Buffer L):**

50 mM Tris/HCl, pH 7.4

7.5 – 10% glycerol

1% Triton X-100

150 mM NaCl

and 2 mM MgCl<sub>2</sub> was added to Buffer L

#### **5x SDS-PAGE sample buffer:**

0.25 M Tris/HCl, pH 8.0,

25% glycerol

7.5% SDS

0.25 mg/ml bromophenol blue

12.5% v/v mercaptoethanol

Protease Inhibitors (Roche), 1 mM Na<sub>3</sub>VO<sub>4</sub>, 0.5 mM DTT; all added fresh to lysis buffer.

#### **Buffer W (washing buffer):**

100 mM Tris/HCl

150 mM NaCl

1 mM EDTA

1% Triton X-100

1% Glycerol

2 mM MgCl<sub>2</sub>, pH 8

**Buffer E (desthiobiotin elution buffer):**

100 mM Tris/HCl

150 mM NaCl

1 mM EDTA

2.5 mM desthiobiotin, pH 8

**Buffer BE (biotin elution buffer):**

100 mM Tris/HCl

150 mM NaCl

1 mM EDTA,

2 mM biotin

2 mM MgCl<sub>2</sub>, pH 8

**2.7.004 Purification of One-Strep-tag fusion proteins**

Before proceeding with protein complex purification, the cell extracts were subjected to centrifugation for 1 hr at 24,000g and 4°C to prepare the lysate (the IBA protocol suggested that the centrifugation is carried out at 100,000g but this was not possible owing to the unavailability of the centrifuge that can perform 100,000g). Storage buffer was removed from the Stre-Tactin column prior to equilibration with two column bed volumes of washing buffer (IBA, Germany). 100nmol of cell extract was added to the column. The column was washed 5 times with one volume of column wash buffer. One volume of flow through was collected in a 1.5ml eppendorf tube. 20µl of sample of each subsequent fraction was analysed by 8% SDS-PAGE.

**2.7.005 Protein Identification on Coomassie stained gels**

SDS gels were stained with Coomassie stain to identify positive bands between transfected and un-transfected samples.

## **2.8 Ferroxidase assay**

### **2.8.001 Preparation of K562, MDA-MB-231 and PNT2-C2 cell fractions for**

#### **Ferroxidase assay**

Cells from liquid nitrogen were cultured in RPMI 1640 full medium for 48 hrs or batches of cells were only used after passage three. Cells were centrifuged at 160 g, 20 °C for 5mins to remove dead cells from the supernatant. Then the cell pellet was washed twice in PBS and resuspended to  $10^7$  cells / mL in hypotonic lysis buffer (10 mM Tris, 3 mM  $MgCl_2$  pH 7.2). Cells were incubated for 2 hrs on ice. Cell lysis was checked after 45mins and an hour and half by Trypan blue exclusion. The cell lysate was then centrifuged in microfuge tubes at 25,000 g for 2 hours at 4 °C (to ensure pelleting of any PMVs that may be released by cell lysis). The supernatant was retained as cytosolic fraction. To extract the membrane fraction, the resulting cell pellet was washed once with hypotonic lysis buffer and spun 25,000 g for 5 min. The cell pellet was incubated on ice for 5mins in 150 $\mu$ l of 1.0% TX-100 / PBS. The pellet was spun at 12,000 rpm for 5 min. The supernatant was used as membrane extract. All fractions were stored in the freezer (-20 °C) for native gel analysis.

#### **2.8.002 Non-denaturing gel electrophoresis**

8% non-denaturing gel electrophoresis was carried out as described in 2.5.002, except that non-denaturing gels and buffers were prepared without the inclusion of SDS.

#### **2.8.003 Non-denaturing gel analysis**

Non-denaturing gels after electrophoresis were analysed for ferroxidase activity by performing ferroxidase staining. Gels removed from the electrophoresis tank were briefly rinsed in 0.1M acetate buffer (pH 5.8). The gel was incubated in 50ml of 5mM (0.08% w/v ferrous sulphate or ferrous ammonium sulphate) in 100mM sodium acetate with pH 5.8 for 2hrs at 37°C. After 2hrs the gel was placed in 1% (w/v) potassium ferrocyanide in 0.1M HCl. A prussian blue band was observed and the band was stable for 24hr. To confirm the Prussian blue band in ferroxidase stained gel, 8% non-denaturing gel was run for coomassie blue staining confirmation.

## **2.8.04 SDS-PAGE electrophoresis to analyse the ferroxidase bands**

### **2.8.04.001 Gel piece of interest excision & preparation**

The M1 band, a potential new ferroxidase from non-denaturing gel was transferred onto 8% SDS-PAGE by the following protocol obtained from our collaborator Dr. Rob Edwards, Imperial College, London. Gel band (M1) of interest was excised over an illuminated light box. Each gel band was placed in a labelled tube (e.g. Eppendorf microcentrifuge tube). The stained gel piece was destained in a solution of 0.2 M ammonium bicarbonate/50% acetonitrile (0.5 – 1.0 ml/tube) for 0.5 - 1 hour with shaking. The solution was discarded. In case of the M1 band the tube was incubated for 3 hrs at room temperature with frequent changes of 0.2 M ammonium bicarbonate/50% acetonitrile solution every 30mins to achieve complete decoloration. The destained gel piece was washed with 0.5 - 1 mL of water for 1 min and discarded the solution. Gel piece was dehydrated using 1 ml acetonitrile for 15 mins. After 15 mins incubation the gel pieces turned into white or dehydration step was carried out till the gel piece turned white. Gel piece was left to dry at room temperature. The preparation is now quite stable. Gel piece was rehydrated in sample treatment solution for SDS-PAGE and placed the gel piece on a standard SDS-PAGE gel to perform the electrophoresis.

### **2.8.04.002 Preparation of Samples/gel piece of interest**

2.5 µl of the sample buffer, DTT (500 mM) and Iminodiacetic acid (IDA - 250 mM) was added to the gel piece. The gel band of interest was incubated at 94°C for 2 min. Then the gel piece of interest was allowed to cool at room temperature. Then, freshly prepared IDA was added to a final concentration of 250mM. Before placing the sample on the 8% SDS-PAGE well, the eppendorf tube was incubated with the gel piece of interest at room temperature for 20 min in the dark. 8% SDS-PAGE electrophoresis was carried out as described in 2.5.002 to confirm the M1 band transfer from the non-denaturing gel to the SDS gel. The size of M1 band was approximately established against the standard protein ladder. M1 bands on SDS gel were confirmed by coomassie staining.

### **2.8.04.003 Analysis of the M1 band by MS**

The M1 band, a potential ferroxidase that appeared on the non-denaturing gel, was subjected to MS-MS by Dr. Rob Edwards, Imperial College. Data obtained from the MS-MS was analysed and the results were given to identify the potential ferroxidase.

# **RESULTS AND DISCUSSION**

# CHAPTER 3

## Mfrn tagSNP result and discussion

### 3.01 tagSNP statistical analysis

Research into identifying the proteins responsible for the absorption, transport, utilization, and storage of iron produces new insights into the pathophysiology of genetic abnormalities affecting iron metabolism. Understanding the effects of the underlying mutations or variations in a candidate gene which cause disturbances in iron metabolism that leads to clinical abnormalities helps establish the cause of the disorder. It is understood that if a variant, and hence the haplotype, is relatively common in the general population. It might be possible that studying tagSNPs could ascertain their role in disease predisposition. If, however, the disease is caused by a rare variant, the tagSNP study approach may fail to detect association. 18 tagSNPs (SNPs in the 5' UTR and Intron of Mfrn) were analysed using the Asian-Caucasian cohort for understanding the role of covariates like sex of the fetus, birth weight, haemoglobin levels, gestational age and mother's booking weight. Table 02 shows the number of samples analysed for each tagSNP (n), %SNP success before and after sorting the data and the Hardy-Weinberg Equilibrium (HWE) p value. After performing the initial PCR reaction, clean up and Sequenom single base extension reaction and finally MALDI-TOF (as in 2.01.001 – 2.01.005 sections of the thesis), data were pooled together and both %SNP success and HWE p value were calculated. To improve the % of SNP success and HWE p value data was then sorted by deleting the samples with repeated data and samples with no genotype data. SNPs with >80% SNP success and HWE p value greater than 0.05 from the below table were used to carry out ANCOVA analysis using IBM SPSS statistics 20.

**Table 02: Percentage SNP success and HWE p values for tagSNP analysis.** Percentage SNP success and HWE p value for the SNPs before and after data sorting

SNP id	n (number of samples analysed after data sorting)	Before data		After data sorting		Comments
		% SNP success	HWE p value	% SNP success	HWE p value	
rs721183	735	NA	NA	NA	NA	Only one genotype was read and hence any further analysis was carried out. Only 11 samples resulted in AA genotype
rs10104250	751	58.72%	1E-06	54.72%	0.104	Though HWE p value is significant the % SNP success is too low
rs10421768	743	81.29%	1E-06	87.75%	0.015	The difference between the observed & expected is not significant & not consistent with HWE distribution as p value is less than 0.05
rs1009840	740	80.38%	1E-06	85.94%	1E-06	The difference between the observed & expected is not significant & not consistent with HWE distribution as p value is less than 0.05

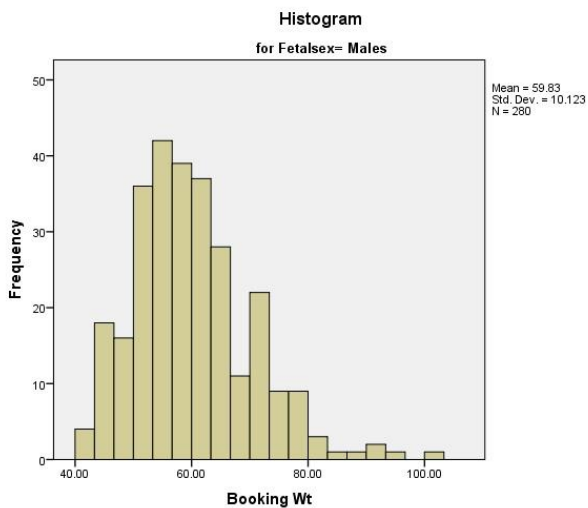
rs2928684	743	NA	NA	NA	NA	Very few samples had the genotype of which most of them were TT genotype
rs2978477	740	74.74%	1E-06	76.62%	0.008	The difference between the observed & expected is not significant & not consistent with HWE distribution as p value is less than 0.05
rs4872145	739	67.31%	1E-06	69.68%	0.03	The difference between the observed & expected is not significant & not consistent with HWE distribution as p value is less than 0.05
rs4872153	744	64.18%	1E-06	60.48%	0.0006	The difference between the observed & expected is not significant & not consistent with HWE distribution as p value is less than 0.05
rs6986233	746	81.98%	1E-06	86.59%	0.317	The difference between the observed & expected is significant & consistent with HWE distribution as p value is greater than 0.05
rs7833754	745	73.73%	1E-06	74.89%	0.609	Though the HWE p value is significant the % SNP success is low before and after data sorting

rs7834536	740	37.44%	1E-06	16.89%	0.103	Though the HWE p value is significant the % SNP success is too low before and after data sorting
rs11781222	704	85.31%	1E-06	82.95%	0.096	The difference between the observed and expected is significant & consistent with HWE distribution as p value is less than 0.05
rs13439692	741	NA	NA	NA	NA	After the data sorting only one genotype (CC) was observed in all the resulting samples. Hence no further analysis was carried out
rs17089331	745	78.87%	1E-06	82.41%	0.086	The difference between the observed & expected is significant & consistent with HWE distribution as p value is greater than 0.05
rs17089358	741	85.05%	1E-06	88.12%	0.127	The difference between the observed & expected is significant & consistent with HWE distribution as p value is greater than 0.05
rs17698981	700	75.43%	1E-06	74.28%	0.021	The HWE p value is not significant and the % SNP success is also low
rs34146184	None	NA	NA	NA	NA	No genotype data was observed from any of the nine data sheets

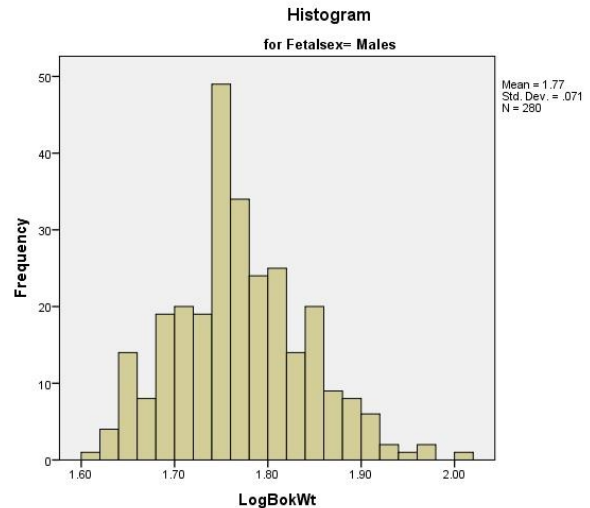
rs34968988	746	NA	NA	NA	NA	Only 37 samples resulted in a genotype which gave the least SNP success and hence did not carry out any further analysis
------------	-----	----	----	----	----	--

### 3.02 Normalisation of the data

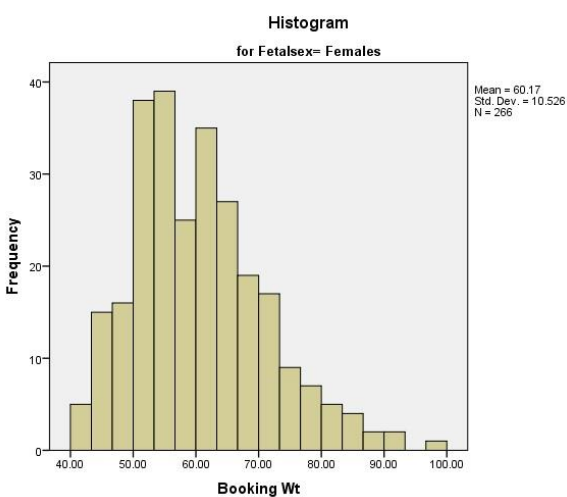
From the above resulting table, SNPs rs6986233, rs11781222, rs7089331 and rs17089358 were found to be in HWE with p values greater than 0.05. Before performing the analyses, genotype data was combined with phenotype data and the variables of fetal birth weight, maternal booking weight and gestational age were individually checked for normal distribution using the SPSS (v20) analysis software. Histograms showed maternal booking weight to be positively skewed, Gestational age to be negatively skewed and fetal birth weight showed a normal distribution. Hence the maternal booking weight and gestational age were transformed using logarithm function and reflect and square root function. Subjects with gestational age <36 weeks (as they are considered premature births) were excluded and only singleton births were considered in the analysis.



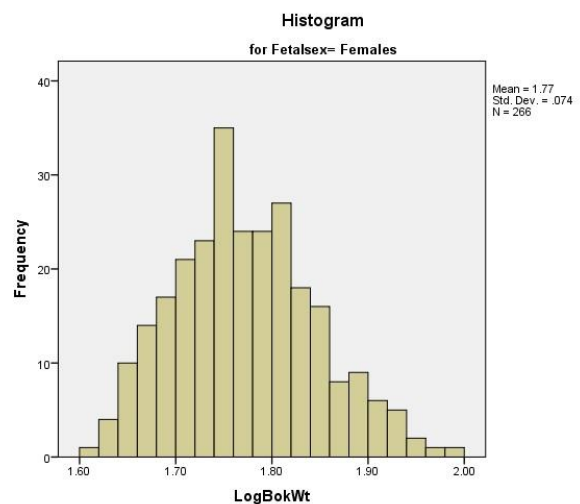
**a**



**b**



**c**



**d**

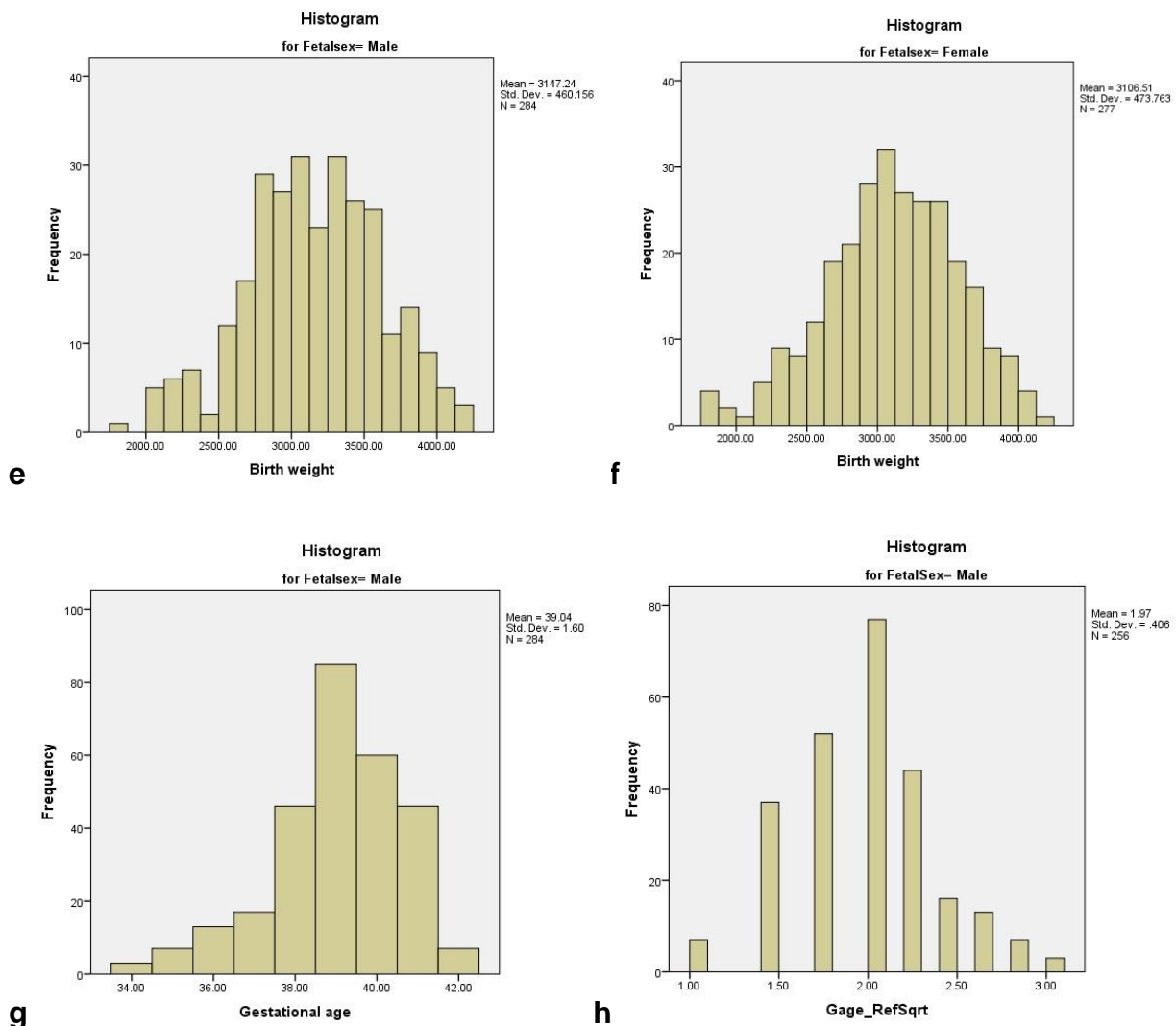


**Figure 30: Normalisation of the data using SPSS.** Above figure shows the distributions of mothers booking weight, birth weight, and gestational age before and after transforming the data. Figures a and c show positively skewed distribution of mothers booking weight. Figures b and d shows normal distribution of mother’s booking weight by transforming the data using log 10 function in SPSS. Figures e and f shows the normal distribution of birth weight in both males and females considered for tagSNP analysis. Figure g shows negatively skewed data distribution of gestational age. Figure h shows normal distribution of gestational age after transforming the data using reflect and square root function using SPSS.

### 3.03 ANCOVA analysis using SPSS software

Two-way ANCOVA analysis (two independent and two dependent variables) was carried out to check if the covariates have any influence on the dependent variable in the presence of fixed factors. Genotype and sex of the fetus are considered as independent

variables/fixed factors, birth weight and haemoglobin levels as dependent variables, gestational age and mother's booking weight as covariates. The test of between-subjects effects, tells whether there is a significant effect for any of the independent variables and whether the interaction between the two independent variables is significant or not, for which the Sig. value p value should be more than 0.05. However what the p value does not tell is the degree of association between two variables. Hence it is important to understand whether the difference has any practical or theoretical significance by observing the effect size (also known as strength of association). The most commonly used parameter to compare groups is partial eta squared effect size which can be obtained from the ANCOVA analysis output. Partial eta squared effect size statistic shows the amount of variance of the dependent variable that can be explained by the independent variable. Values can range from 0 to 1 or by multiplying the partial eta squared value by 100 to express in percentage.

### **3.04 Mfrn tagSNPs in correlation with Hb levels and birth weight**

#### **3.04.001 ANCOVA results and analysis**

Two-way ANCOVA analysis showed Leven's Test of Equality of Error Variance does not violate the assumption of equality of variance as Sig. value is greater than 0.05 for all four (SNPs rs6986233, rs11781222, rs7089331 and rs17089358) tagSNPs as shown in the below table. Significant association was considered when the p value was less than 0.05 ( $p < 0.05$ ) and trend associated when p value was  $0.05 < p < 0.1$ . From the table 03, when the dependent variable was haemoglobin no tagSNP showed any significant p value either in association with genotype and fetal sex. Also, from the below table it can be said that the effect of haemoglobin levels on either fetal sex or genotype is not statistically significant in any four (rs6986233, rs11781222, rs7089331 and rs17089358) tagSNPs as p values are greater than 0.05. Likewise when birth weight was considered as a dependent variable, birth weight did not show any significant p value in association with genotype and fetal sex in any four (rs6986233, rs11781222, rs7089331 and rs17089358) tagSNPs. Since the p value is not significant it may be said that effect of independent variable (genotype) is not dependent on the level of the other independent variable, fetal sex in the four tagSNPs analysed. Hence it can be concluded that the haemoglobin levels or the birth weight are neither dependent on genotype nor the fetal sex or in interaction. However, significant p value can be observed in rs6986233 ( $p=0.035$ ) and rs17089331 ( $p=0.019$ ) between fetal sex and birth weight and between birth weight ( $p=0.026$ ) and the genotype in rs11781222. Hence in this study we

can confirm that, in tagSNPs rs17089331 and rs6986233 birth weight is more dependent on genotype and fetal sex than on haemoglobin levels.

**Table 03: Leven's test of equality of error variance and p values.** Table shows the p values for Leven's test of equality of error variances and p values between the dependent and independent variables

SNP id	Dependent variable	Leven's test of equality of error variance p value	P value for genotype and fetal sex association	P value for	
				Genotype	Fetal sex
rs6986233	Birth weight	0.201	0.355	0.400	<b>0.035</b>
	Haemoglobin	0.195	0.984	0.101	0.618
rs11781222	Birth weight	0.206	0.228	<b>0.026</b>	0.674
	Haemoglobin	0.630	0.581	0.631	0.146
rs17089331	Birth weight	0.130	0.638	0.436	<b>0.019</b>
	Haemoglobin	0.253	0.129	0.890	0.723
rs17089358	Birth weight	0.478	0.445	0.872	0.985
	Haemoglobin	0.770	0.929	0.063	0.616

**Table 04: Effect size on the independent variable interaction.** Table shows the effect size on the independent variable interaction in the presence of dependent variables

SNP id	Dependent variable	Partial eta squared value of genotype and fetal sex interaction	Percentage eta squared (% of variance explained)	Effect size significance level
rs6986233	Birth weight	0.004	0.4	Negligible
	Haemoglobin	0.000	0	None
rs11781222	Birth weight	0.006	0.6	Negligible
	Haemoglobin	0.002	0.2	Negligible
rs17089331	Birth weight	0.002	0.2	Negligible
	Haemoglobin	0.008	0.8	Negligible
rs17089358	Birth weight	0.003	0.3	Negligible
	Haemoglobin	0.000	0	None

From the ANCOVA analysis it is observed that not haemoglobin levels but birth weight, which is also a dependent variable, has a significant association with the covariates, gestational age and squared maternal booking weight. The effect size on genotype and fetal sex interaction and also individually in the presence of either birth weight or haemoglobin levels can be analysed by considering the partial eta squared values from the ANCOVA outputs. As shown in table 04, ANCOVA analysis of all four tagSNPs rs6986233, rs11781222, rs7089331 and rs17089358 showed the partial eta squared values. Eta squared guidelines suggested by Tabachnick and Fidell, (2007) suggests that eta squared value with more than 1 % has a small, 6% has medium and anything more than 13.8% has a large effect size. ANCOVA analysis of rs6986233, rs11781222, rs7089331 and rs17089358 showed very negligible effect size with values ranging between 0 – 0.8 %. Hence it can be concluded that the significant associations in rs6986233 and rs17089331

between birth weight and fetal sex, and in rs11781222 between birth weight and genotype owing to small effect size are not practically or theoretically significant.

#### **3.04.002 Mfrn tagSNPs discussion**

Studies with *S. cerevisiae* and cells from patients have suggested that mutations in the ABC7 lead to mitochondrial iron accumulation, responsible for the cellular damage that causes the neuronal and erythroid disease and is thought to be involved in haem transport from the mitochondria (Allikmets et al., 1998). Mis-sense mutations were found in HFE in 87% of chromosomes from patients homozygous for hereditary hemochromatosis (Feder et al., 1998). Mutations in the causative gene, HFE, are responsible for most cases of hereditary hemochromatosis (Feder et al., 1996). Aceruloplasminemia is a newly recognized, rare autosomal recessive disorder of iron metabolism that results from deficiency of ceruloplasmin ferroxidase activity as a consequence of mutations in the ceruloplasmin gene (Harris et al., 1995). Molecular studies have identified multiple point mutations in the IRE of the L-ferritin mRNA affecting the highly conserved CAGUGU motif that constitutes the IRE loop and mediates the high-affinity interaction with the IRP (Beaumont et al., 1995, Girelli et al., 1995). The mutation was found to abolish the binding of IRP and result in constitutive, poorly regulated L-ferritin synthesis (Beaumont et al., 1995). Finberg et al. identified Tmprss6 mutations in individuals with iron-refractory iron deficiency anaemia (IRIDA) (Finberg et al., 2008). Normal to low urinary hepcidin levels with regards to the levels of iron stores have been found in patients with DMT1 mutations, probably accounting for the increased intestinal iron absorption (Iolascon et al., 2008).

From the above studies, it can be understood that if the correct mutation or variation when examined reveals the underlying role of the mutation/variation in causing the disease. Choosing a subset of maximally informative SNPs, or "tag" SNPs, to be genotyped in a larger sample can be reduced without losing the ability to capture most of the variation. Where available, in the case of the candidate gene approach it is preferable to compare the HapMap data with the sequence data. This has the advantage of aiding in the discovery and coverage of SNPs with frequencies in the range of 1% to 5% which are unlikely to appear in the HapMap database (Constantine et al., 2008). The discovery of new genes like DMT1 and Tmprss6 implicated in iron metabolic disorders, suggests that the molecular diagnosis of the iron metabolic disorders is within reach. However, the difficulty lies in identifying the candidate gene for analysis. Mfrn tagSNPs analysed in our study may not have resulted in showing any significant association between Hb levels and birth weight. No previous findings

or literature was available on Mfrn tagSNP association studies. However, analysing tagSNPs of other genes involved in iron metabolic disorders may reveal the role of tagSNPs in iron metabolism.

# CHAPTER 4

## Protein-Protein Interaction results and discussion

### 4.01 Introduction

The foundation for the discoveries in the field of iron homeostasis is to identify key modifiers along with the identification of mutated genes in well-characterized cohorts of patients with inherited haemochromatosis from across the globe (Roy, 2013). Mammalian iron homeostasis is maintained through the concerted action of sensory and regulatory networks that modulate the expression of proteins of iron metabolism at the transcriptional and/or post-transcriptional levels (Eisenstein, 2000). The ferroxidase activity of Heph is thought to play an important role during iron export from intestinal enterocytes and the subsequent iron loading of the blood protein Tf, which delivers iron to the tissues (Vashchenko and MacGillivray, 2012). In the absence of a regulated physiological mechanism for iron excretion, iron absorption by the proximal intestine is a critical determinant of body iron availability and loading in mammals (Hentze *et al.*, 2010; Knutson, 2010). Owing to the tight regulation of intestinal iron absorption, it is known that it increases with body iron requirements and decreases when body iron stores enlarge. Key aspects of cellular iron metabolism are controlled by both IRP 1 and 2. A recent description of a whole-transcriptome repertoire of potential novel IRP targets suggests that IRP function extends beyond iron metabolism regulation (Sanchez *et al.*, 2011). Research till today has long appreciated the importance of identifying protein interactions through different techniques such as confocal microscopy for intracellular colocalization of proteins, coimmunoprecipitation, surface plasmon resonance (SPR) and spectroscopic studies. The partners with which a protein (bait) interacts forms a key component that describes the function of any protein. In this study, using K562 cells I carried out experiments to find interacting partners of Heph and IRPs by coimmunoprecipitation using affinity-tagged proteins to understand their role in iron metabolism. Initially the expression of Heph and IRPs were checked in K562 cells by carrying out real time PCR, then the GOIs were cloned with One-Strep tag to carry out expression and coimmunoprecipitation analysis of the Heph and IRPs complexes.

#### 4.02 qRT-PCR data of Heph, IRP1, IRP2 and Mfrn

qRT-PCR was carried out using Applied Biosystems TaqMan probes for analysing the differential gene expressions of Heph (assay id: Hs00953259\_m1), IRP1 (assay id: Hs00158095\_m1) and IRP2 (assay id: Hs00386293\_m1) using  $\beta$ -Actin (assay id: Hs99999903\_m1) as a housekeeping gene. Prior to synthesising Heph, IRP1 and IRP2 for the PPI study, expression of Heph, IRP1 and IRP2 was checked in K562 cells. RNA extracted from K562 cells after 100  $\mu$ M FAC treatment for 72hrs and control cells without FAC was used as a template during qRT-PCR.

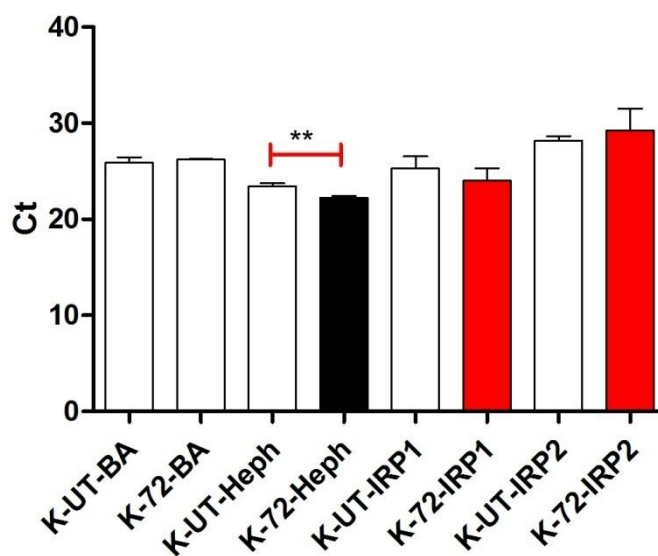


**Figure 31: Gene expression of Heph, IRP1, IRP2 and Beta-actin in K562 cells.** Figure shows the gene expression pattern of Heph, IRP1, IRP2 and beta-actin in both untreated (UT) and treated (72 hrs incubated) K562 cells (K) using the C(T) values.

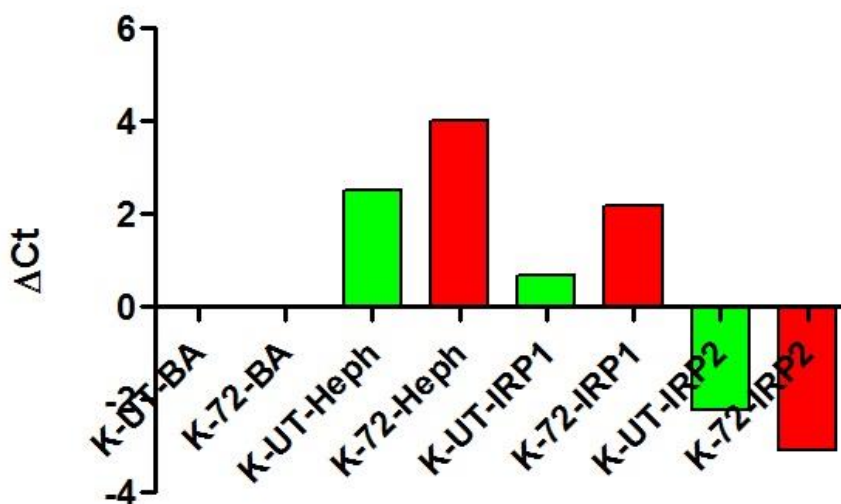


**Figure 32: Gene expression of Heph, IRP1 and IRP2 after normalisation.** Figure shows the Heph, IRP1 and IRP2 expression pattern on X-axis and the difference of Ct values between the reference gene and normalised gene on the Y-axis. K = K562 cells, UT = untreated or control sample, 72 = cells treated for 72 hrs with 100  $\mu$ M FAC.

Green bars in the figure 35 show the expression of control (K562 cells without FAC treatment) and red bars show the expression pattern of Heph, IRP1 and IRP2 in treated cells. FAC treated K562 cells showed up-regulation of Heph and IRP1 and IRP2 has been down-regulated. Statistical analysis of real time PCR data of the untreated and treated K562 cells for Heph, IRPs and beta-actin was carried out using GraphPad Prism. In all the samples  $n = 3$ , where three biological and technical replicates were used in every run. In the case of K562 cells treated with 100  $\mu$ M FAC shown more expression than normal K562 cells while K562 cells treated with 100  $\mu$ M FAC showed more down regulation of IRP2 when compared with untreated cells. Unpaired t-test was used to carry out the statistical analysis. While examining the expression of Heph using the C(T) values in the untreated and 100  $\mu$ M FAC treated K562 cells, a very significant p value of 0.005 was observed along with the Mean  $\pm$ SEM (Standard error of the mean) of  $1.213 \pm 0.217$  with the unpaired t test. Likewise when the C(T) values were considered and expression analysis was measured between the untreated K562 cells and the treated K562 cells for IRP1 and IRP2 expression, no significant p value was observed with Mean  $\pm$  SEM of  $1.267 \pm 1.037$  for IRP1 and  $-1.093 \pm 1.324$  for IRP2 gene. However, when the  $\Delta$ C(T) was measured by subtracting the C(T) of the GOI with the C(T) of the housekeeping gene there was a significant change in the fold expression in all three genes.

### 4.03 Relative gene quantification of Heph, IRP1, IRP2 and Mfrn by the Livak method

The Livak method (Livak and Schmittgen, 2001) was used to measure the fold increase or decrease of gene expression after normalizing Heph, IRP1, IRP2 and Mfrn against the housekeeping gene ( $\beta$ -actin). Table 05 shows the relative gene expression fold increase or decrease of the target gene against the reference gene.

Reference-Target gene	Fold increase or decrease of target gene expression
$\beta$ -actin – Heph	2.8 fold increase of Heph expression in 100 $\mu$ M FAC treated K562 cells
$\beta$ -actin-IRP1	2.8 fold increase of IRP1 expression in 100 $\mu$ M FAC treated K562 cells
$\beta$ -actin – IRP2	0.5 fold decrease of IRP2 expression in 100 $\mu$ M FAC treated K562 cells
$\beta$ -actin – Mfrn	0.3 fold increase of Mfrn expression in 100 $\mu$ M FAC treated K562 cells

**Table 05: Fold increase and decrease of Heph, IRP1 and IRP2 in treated and untreated K562 cells.** Table 05 shows the fold increase and decrease of Heph, IRP1 and IPR2 against the house-keeping gene,  $\beta$ -actin.

Once the gene expression of Heph, IRP1 and IRP2 was confirmed by real time PCR in K562 cells, protein expression of Heph, IRP1 and IRP2 was carried out by Western blotting to confirm the expression of the Heph, IRP1 and IRP2 proteins in K562 cells.

### 4.04 Detection of Heph, IRP1 and IRP2 by western blotting

Western blotting was carried out to analyse the expression pattern of Heph, IRP1 and IRP2 using both treated with 100 $\mu$ M FAC and untreated K562 cell lysates to examine the expression patterns between the control and sample cell lysates.

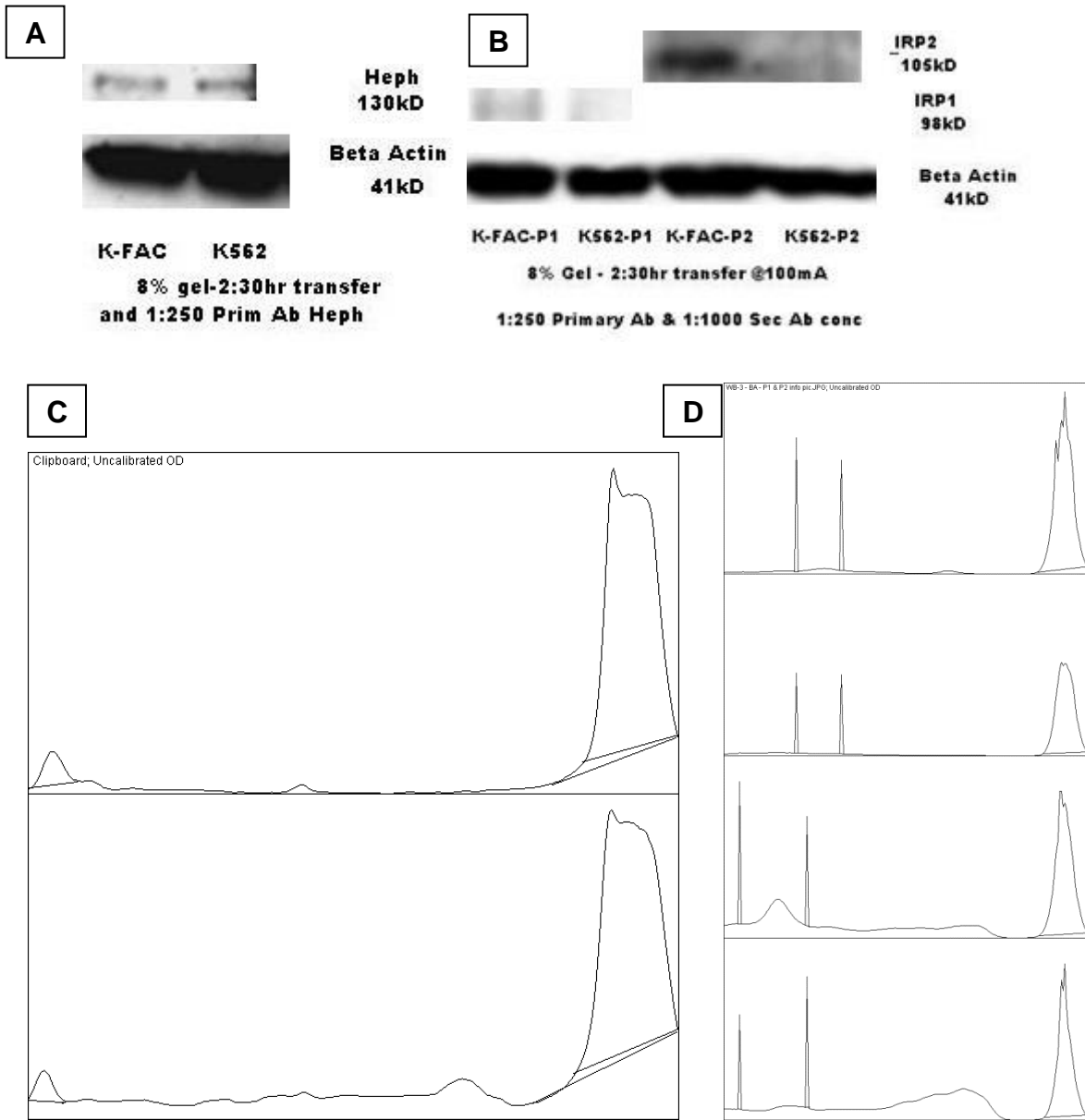


**Figure 33: Protein expression analysis of Heph, IRP1 and IRP2 by Western blotting and Image J.** Part A and B of the figure shows the Western blot membranes with bands of Heph, IRP1 and IRP2 in K562 cells treated with 100 $\mu$ M FAC and untreated cells. Part C and D of the above figure shows the peaks plotted by using Image J software (Abramoff et al., 2004). Small peaks in part C of the figure represent the Heph and large peaks represent  $\beta$ -actin. Extreme left peaks in part D of the figure represent the IRP1 and IRP2 and big peaks at the extreme right represent the  $\beta$ -actin.

Protein of interest	Area calculated by ImageJ
Heph – K562 cells control	2600.617
Heph – K562 cells treated with 100 $\mu$ M FAC	3308.902
IRP1 – K562 cells control	3691.598
IRP1 - K562 cells treated with 100 $\mu$ M FAC	2203.598
IRP2 – K562 cells control	3903.598
IRP2 - K562 cells treated with 100 $\mu$ M FAC	2593.255

**Table 06: Quantification of Heph, IRP1 and IRP2 in treated and untreated K562 cells using ImageJ.** Image J software was used to calculate the peak areas of the Heph, IRP1 and IRP2 in both K562 treated with 100  $\mu$ M FAC and normal K562 cells.

The band intensity obtained after western blot staining/detection by chemiluminiscence, in figure 36 show that Heph, IRP1 and IRP2 showed increased expression in K562 cells treated with 100 $\mu$ M FAC while K562 treated with 100 $\mu$ M FAC showed very little expression of IRP2 compared to the untreated K562 cells. Quantitative analysis of the western blots using Image J, confirmed a 1.2 and a 1.6-fold increase of Heph and IRP1 in K562 cells treated with 100  $\mu$ M FAC compared with normal K562 cells. K562 cells treated with 100  $\mu$ M FAC showed 1.5 fold less IRP2 expression compared with IRP2 expressed in normal K562 cells. In the case of Heph and IRP1 the western blotting data is in par with the gene expression data as shown previously. However, for IRP2, gene expression was more down regulated in FAC treated K562 cells compared to untreated cells, which is in contrast to the western blotting analysis. In western blotting, K562 cells treated with 100 $\mu$ M FAC expressed more IRP2 than untreated control cells. This indicates that not always gene expression and protein expression data are not always correlated owing to the different stability of mRNA and protein and different transcription and translation rates in a given cell. qPCR and western blotting studies showed that expression of Heph, IRP1 and IRP2 in K562 cells which allowed K562 cells to be used as model cells to perform protein protein interaction analysis of Heph, IRP1 and IRP2.

## 4.05 Cloning and sequence confirmation of Heph and IRPs from K562 cells

### 4.05.001 Cloning of Heph, IRP1 and IRP2 using K562 cells

The idea behind carrying out cloning of Heph and IRPs using K562 cells is to take advantage of the *in-vivo* affinity fusion-based protein purification by using a genetically fused affinity tag, which in this study is One-Strep tag. Heph (3.6kb), IRP1 (2.6kb) and IRP2 (2.9kb) genes were PCR amplified using the primers as described in 2.05.002 section. The figure below illustrates the potential PCR fragments of IRP1, IRP2 and Heph.

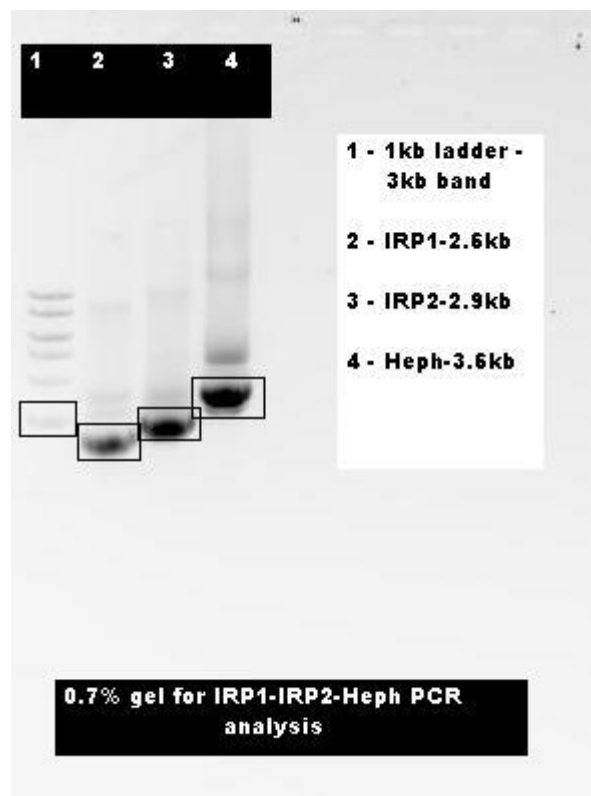


**Figure 34: PCR amplicons of Heph, IRP1 and IRP2.** Above figure shows an approximate fragment of IPR1 (2.6kb), IRP2 (2.9kb) and Heph (3.6kb) compared to the 1kb ladder in lane one. The boxed fragment in lane one is a 3kb fragment of the 1kb ladder from NEB (New England Biolabs). NEB's 1kb ladder ranges from 10kb – 0.5kb bands. The sixth band boxed in lane 1 is the 3kb band in the marker.

### 4.05.002 Sequencing results confirming PCR amplicon identity

Sequencing of the Heph, IRP1 and IRP2 PCR amplicons was carried out prior to molecular cloning to confirm their usage as templates to generate the Donor and Destination Vector's with a Strep tag for PPI studies. Sequencing of the samples was carried out at UCL's, Source

BioScience facility. Sequence data of the respective gene was compared to the raw sequence from NCBI and looked for 100% identity with no variations or base changes in the sequence. Sequencher 5.1 DNA sequencing software was used to analyse the sequencing data obtained from UCL. The below figures 35 – 39 are the forward and reverse sequences of the Heph, IRP1 and IRP2 cDNA's confirming the PCR analysis. Sequencing analysis showed no single base change which confirmed no mutation/variation was introduced during the PCR. For the subsequent PPI work, Heph, IRP1 and IRP2 PCR amplicons were used as templates.

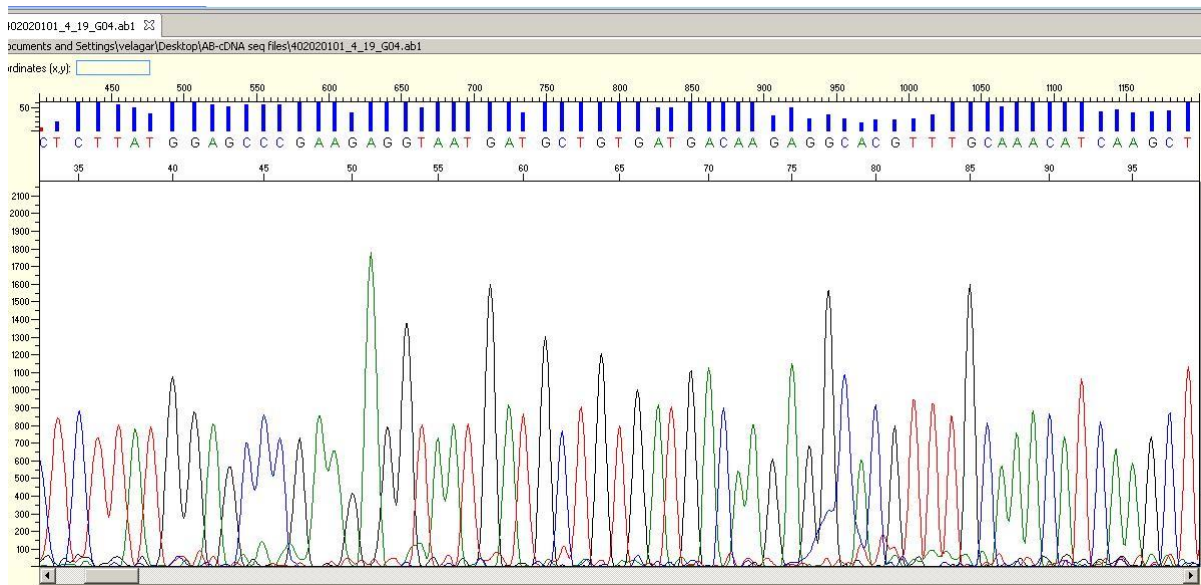


**Figure 35:** Sequence confirmation of Heph obtained after PCR. Figure represents the forward sequence of Heph cDNA analysed using Sequencher v 5.1 sequencing software.

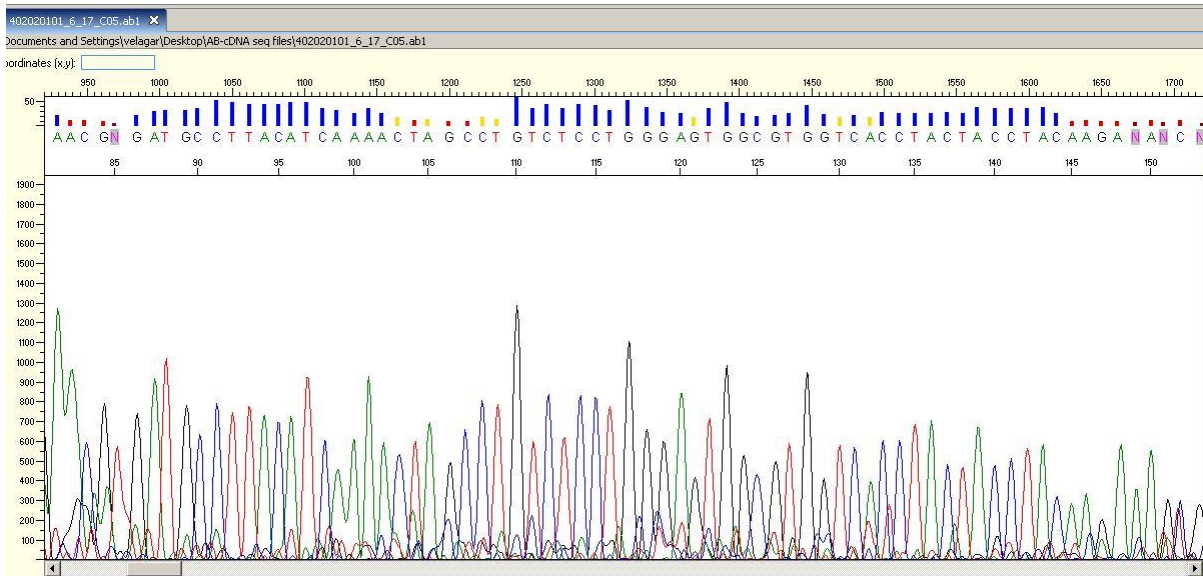


**Figure 36:** Sequence confirmation of IRP1 forward sequence obtained after PCR. Figure represents the forward sequence of IRP1 cDNA analysed using Sequencher v 5.1 sequencing software.

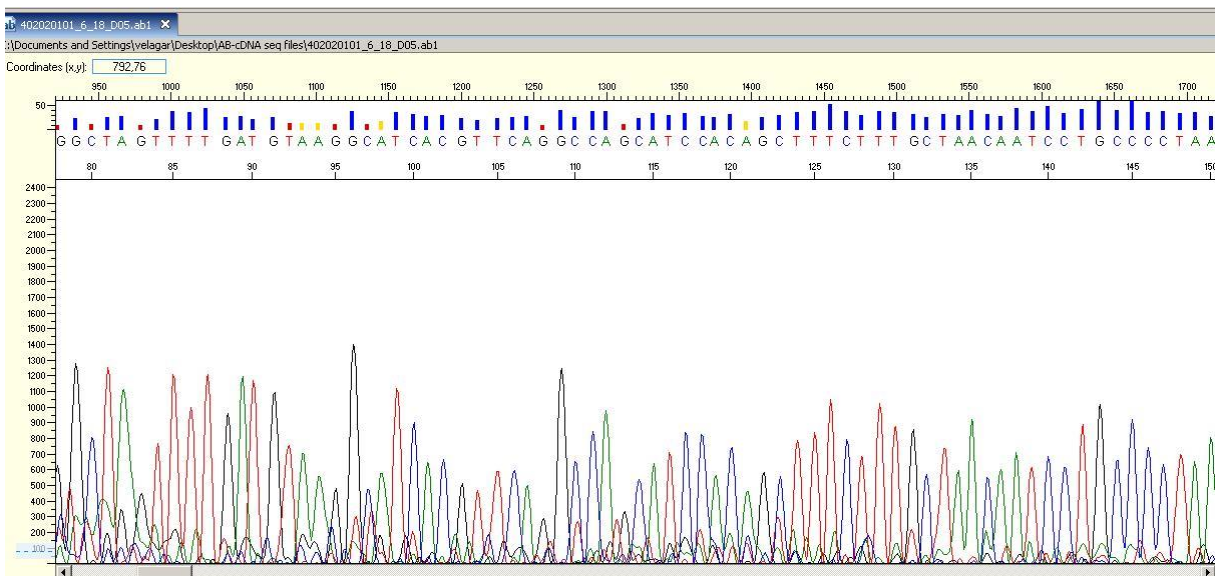


**Figure 37:** Sequence confirmation of IRP1 reverse sequence obtained after PCR. Figure represents the reverse sequence of IRP1 cDNA analysed using Sequencher v 5.1 sequencing software.

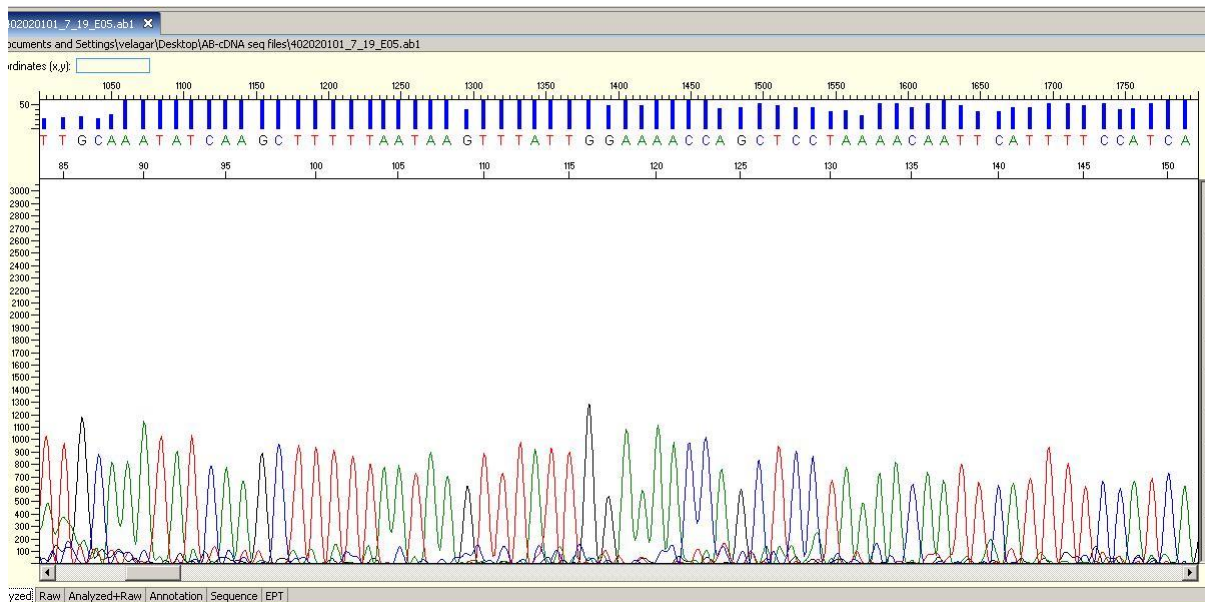


**Figure 38: Sequence confirmation of IRP2 forward sequence obtained after PCR.** Figure represents a forward sequence of IRP2 cDNA analysed using Sequencher v 5.1 sequencing software.

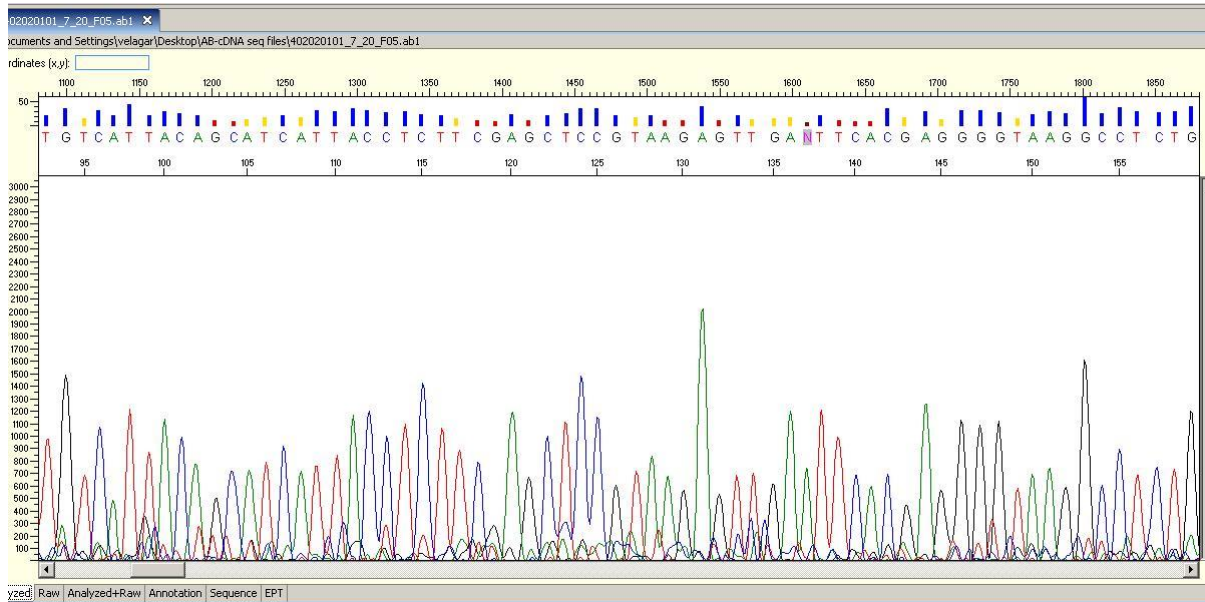


**Figure 39: Sequence confirmation of IRP2 reverse sequence obtained after PCR.** Figure represents the reverse sequence of IRP2 cDNA analysed using Sequencher v 5.1 sequencing software.

## 4.06 Construction and confirmation of Donor Vectors

### 4.06.001 Donor Vector generation and restriction digestion analysis

For the Donor Vector generation, the gene of interest (GOI) is extended at both ends with the combinatorial and StarCombinase sites by PCR. During the PCR the gene of interest (GOI) is cloned at both termini with combinatorial sites and the StarCombinase1™ recognition area which are necessary for the oriented insertion of the PCR fragment into pENTRY-IBA51, an entry vector. Recombination of the amplicon after PCR and the Entry Vector at the combinatorial sites leads to generation of the Donor Vector under loss of all StarCombinase1™ binding areas resulting in the recombination reaction unidirectional and thereby highly efficient. After the overnight incubation at 37°C of LB agar plates with 50 mg/L kanamycin and 50 mg/L X-gal DNA mini-preps were carried out by selecting the white colonies. Plasmid DNA extraction was then carried out using QIAGEN's Plasmid mini-prep kit (UK). Extracted DNA was quantified using a Nano-drop and all the DNA extractions showed purity of 1.8 – 2.0. Restriction digestion analysis of the Donor Vector's generated using the PCR product from the respective GOI was carried out using the HindIII restriction enzyme. Restriction analysis of Heph, IRP1 and IRP2 using Webcutter 2.0v revealed the information as shown in table 7A.

Donor Vector	No of times <i>HindIII</i> cuts	Fragment sizes
Heph	2	38bp & 5362bp
IRP1	1	Linearises the plasmid
IRP2	4	2200bp, 1200bp, 705bp & 500bp

**Table 7A: Restriction analysis of Donor vectors.** Above table shows the restriction fragment sizes after digestion with *HindIII* restriction enzyme.

1µg of the pDNA was incubated overnight using 10Units of *HindIII* enzyme. 0.7% agarose gel electrophoresis was used to analyse the overnight restriction enzyme digestion of Heph, IPR1 and IRP2 Donor Vector pDNA. Figure 40 the 0.7% gel image of the digested fragments along with the undigested controls.

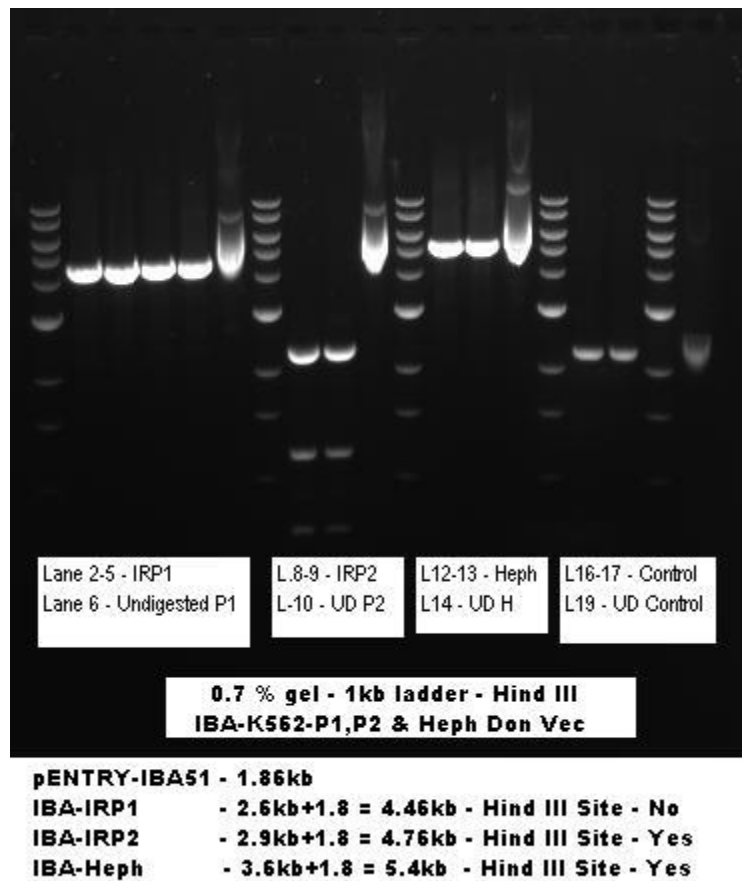


**Figure 40: 0.7% gel electrophoresis picture of Heph, IRP1 and IRP2 restriction digestion.** Figure shows the digested and undigested (controls) fragments of IRP1, IRP2 and Heph with 1kb ladder on either side of the sample.

Restriction digestion of the Donor Vector pDNA of IRP1, IRP2 and Heph with *HindIII* resulted in an expected linearised fragment of IRP1, three out of four fragments in IRP2 (the 500bp fragment ran off the gel during electrophoresis to get the clear picture of the bigger fragments) and an approximate 5.36kb fragment in Heph.

#### 4.06.002 Donor Vector sequence confirmation analysis

pDNA extracted after Donor Vector generation was also confirmed for the correct clone using Sequence analysis. Sequencing of the Donor Vector pDNA was carried out using the Source BioScience facility at UCL. 100ng/ul pf pDNA and 3.2pmol/ul of primer was submitted to the Source BioScience facility at UCL for sequencing. The sequence analysis (figures 41 – 46) with the highlighted "AATG" and "TCCTCCC" sequences flanking the GOI in all forward and reverse sequences of Heph, IRP1 and IRP2 is shown. DNA sequencing analyses was carried out using Sequencher 5.1v sequencing software. Sequencing analysis of Donor Vector extracted pDNA for the respective Heph, IRP1 and IRP2 cDNAs confirmed

the successful introduction of the required StarCombinase sites in the Donor Vector pDNA that are necessary to accept the One-Strep tag during Destination Vector Generation.

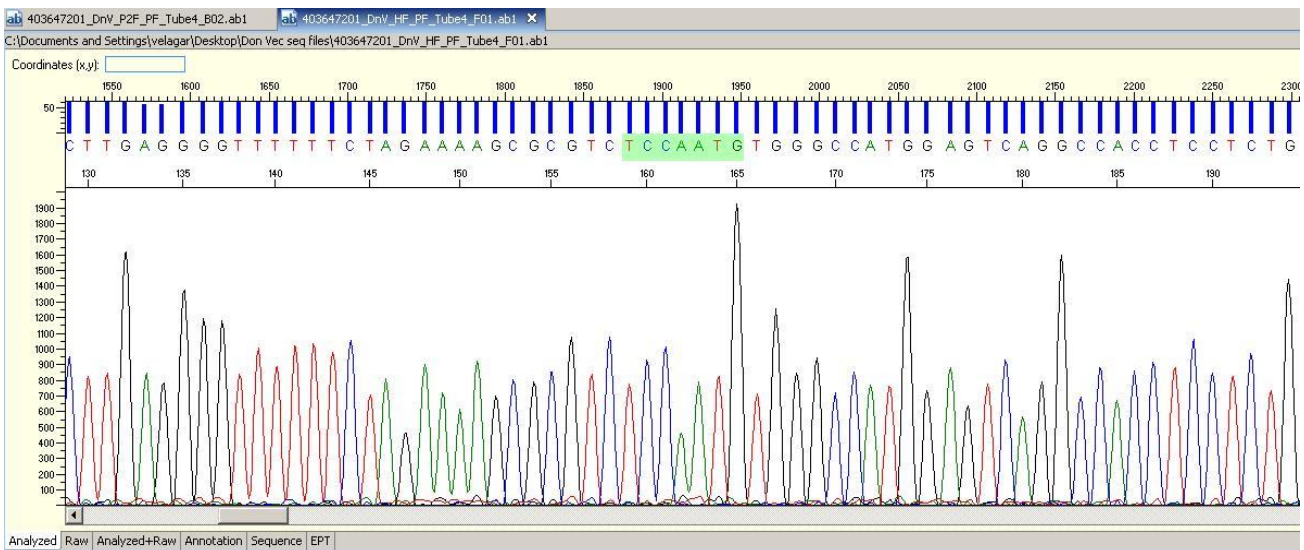


**Figure 41: Forward sequence confirmation of donor vector generated using Heph.** Forward sequence of Donor Vector with GOI-Heph showing the highlighted region “AATG” to the left of GOI which is necessary for further cloning analysis.

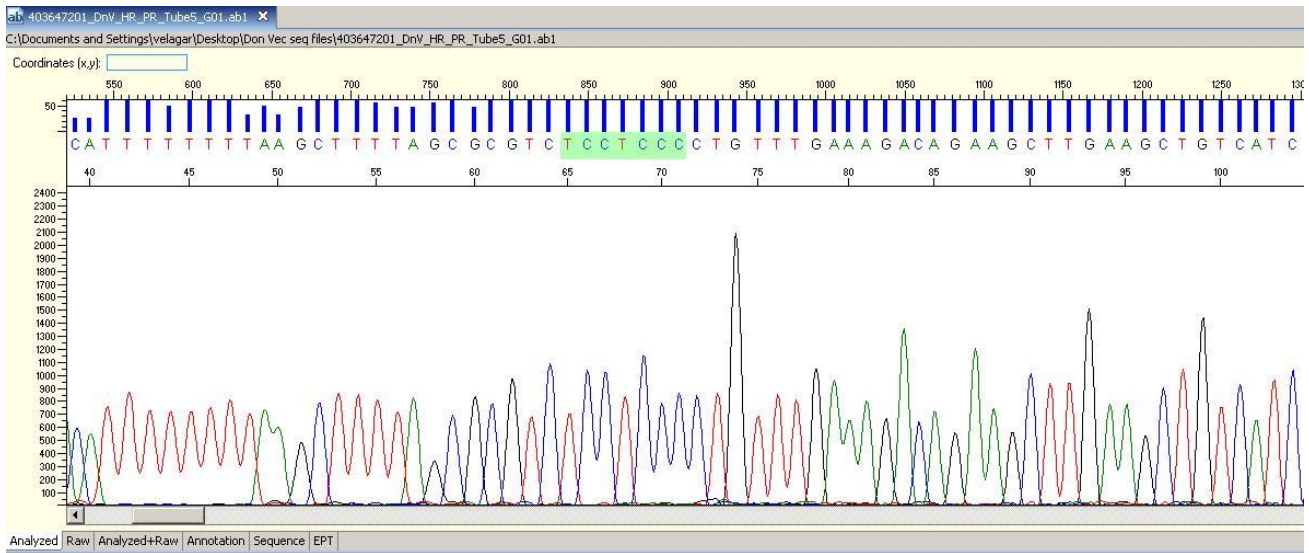


**Figure 42:** Reverse sequence confirmation of donor vector generated using Heph. Reverse sequence of Donor Vector with GOI-Heph showing the highlighted region “TCCTCCC” to the left of GOI which is necessary for further cloning analysis.

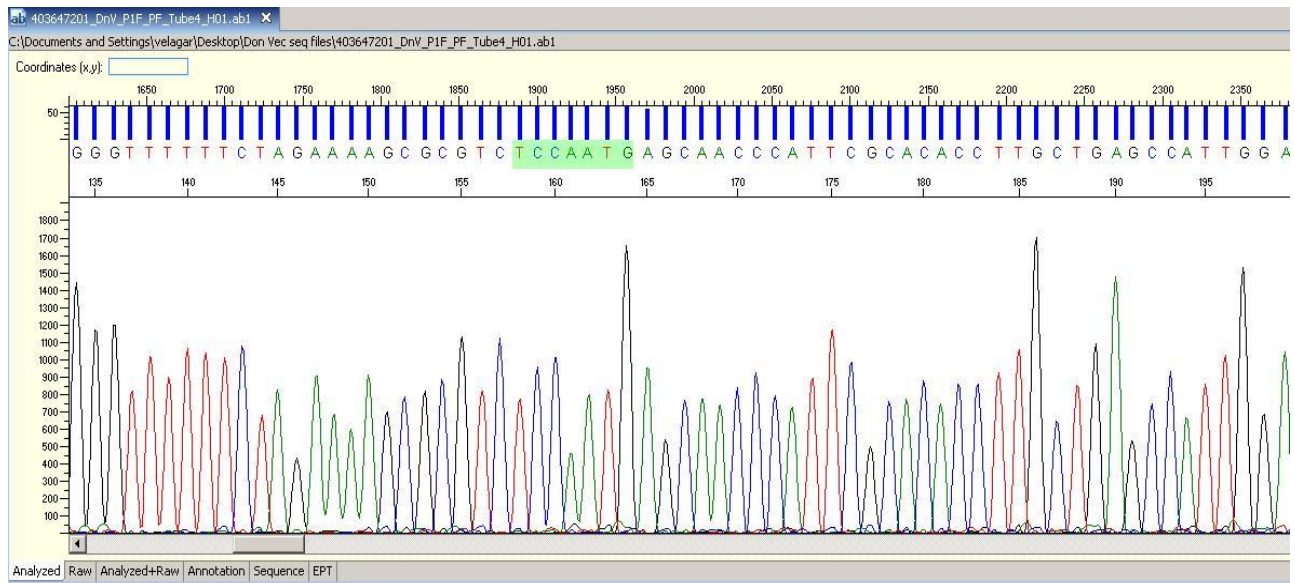


**Figure 43:** Forward sequence confirmation of donor vector generated using IRP1. Forward sequence of Donor Vector with GOI-IRP1 showing the highlighted region “AATG” to the left of GOI which is necessary for further cloning analysis.

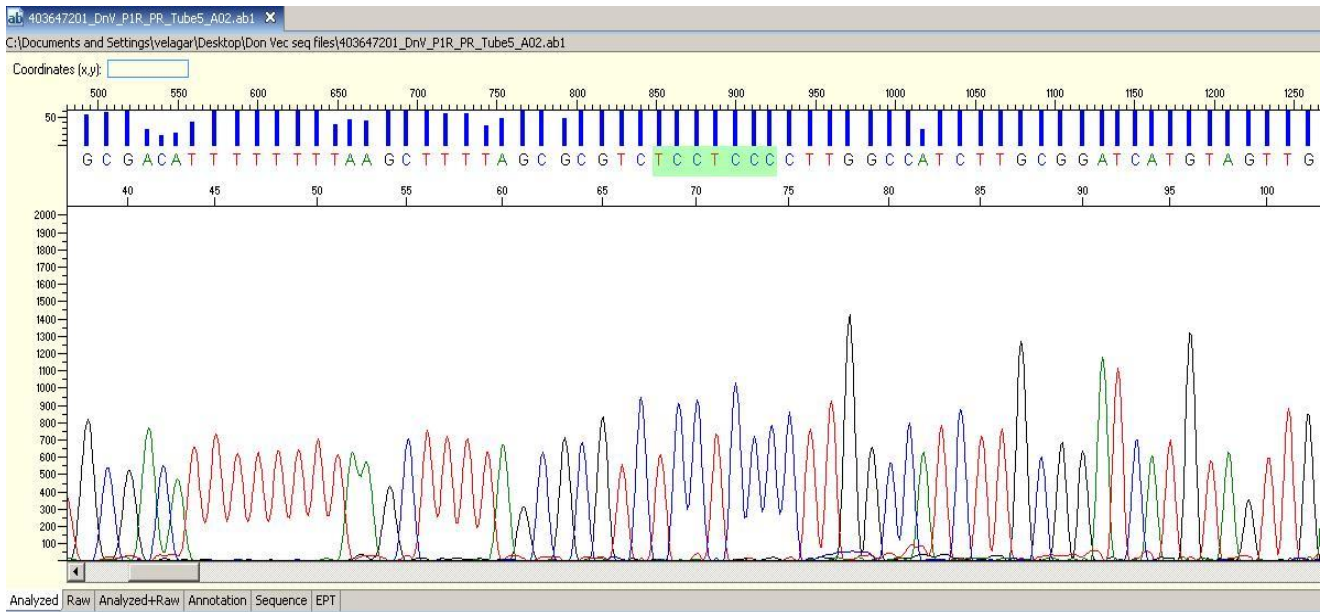


**Figure 44: Reverse sequence confirmation of donor vector generated using IRP1.** Reverse sequence of Donor Vector with GOI-IRP1 showing the highlighted region “TCCTCCC” to the left of GOI which is necessary for further cloning analysis.

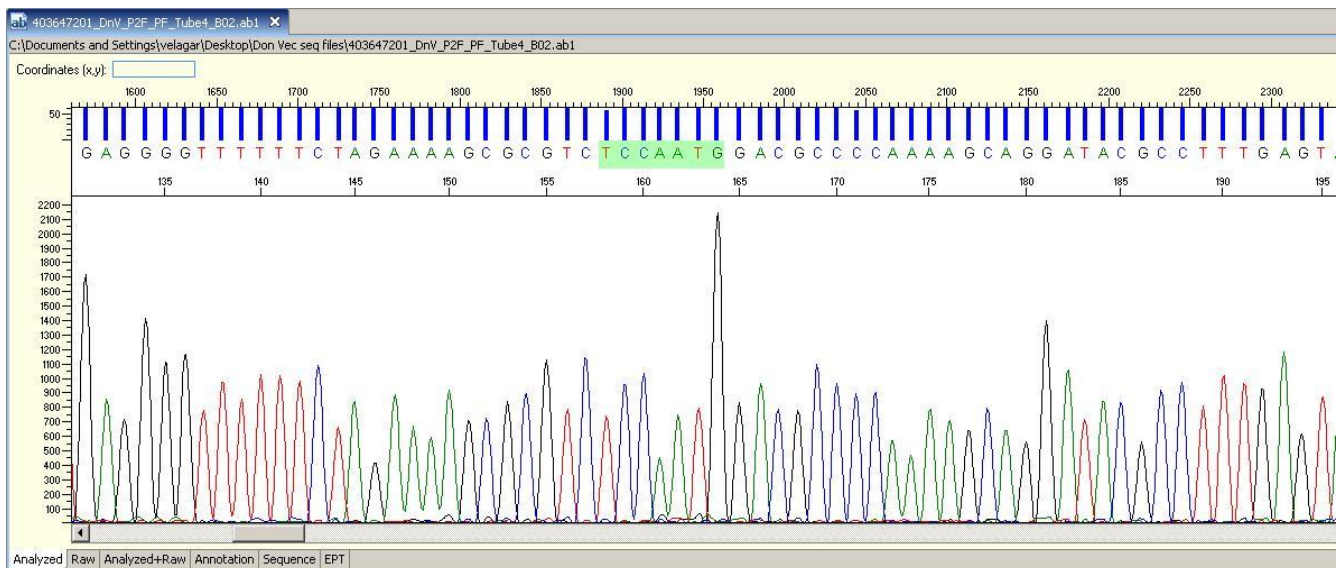


**Figure 45: Forward sequence confirmation of donor vector generated using IRP2.** Forward sequence of Donor Vector with GOI-IRP2 showing the highlighted region “AATG” to the left of GOI which is necessary for further cloning analysis.

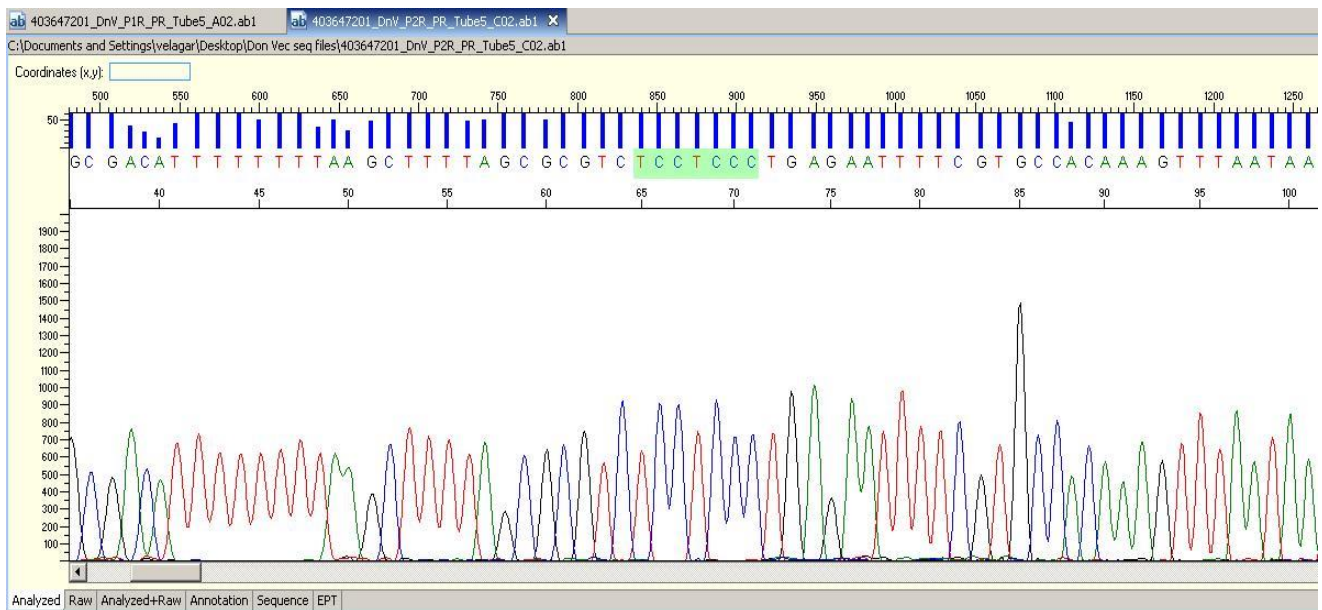


**Figure 46:** Reverse sequence confirmation of donor vector generated using IRP2. Reverse sequence of Donor Vector with GOI-IRP2 showing the highlighted region “TCCTCCC” to the left of GOI which is necessary for further cloning analysis.

## 4.07 Cloning and confirmation of Destination Vector

### 4.07.001 Destination Vector generation and restriction digestion analyses

During the destination vector generation, the GOI is transferred from the Donor Vector into an acceptor vector (pESG-IBA105 with N terminal Strep tag and pESG-IBA103 with Strep tag at the C-terminal end) which provided the desired genetic elements (i.e. tag, promoter, signal sequence etc.) by means of StarCombinase2. Since the signal peptide was present at the N terminal end of Heph, recombination was carried out such that the Strep tag is cloned at C terminal end of Heph by using the IBA-103 acceptor vector and in IRPs the signal peptide sequence was at C terminal and hence the tag was designed to be cloned at the N terminal end by using the IBA-105 acceptor vector. The resulting Destination Vector has the GOI under control of the selected promoter (CMV promoter) allowing GOI expression in the K562 cells. After the overnight incubation at 37°C of LB agar plates with 100 mg/L ampicillin and 50 mg/L X-gal DNA mini-preps were carried out by selecting the white colonies. Plasmid DNA extraction was then carried out using QIAGEN’s Plasmid mini-prep kit (Qiagen, UK). Extracted DNA was quantified using a Nano-drop and all the DNA extractions showed the purity value between 1.8 – 2.0 which is considered to be the pure extract. Destination Vectors generated using the Donor Vector pDNA from the respective

GOI (Heph, IRP1, IRP2) was analysed using the *HindIII* restriction enzyme. Analysis of Heph, IRP1 and IRP2 sequences carried in their respective destination vectors, using Webcutter 2.0v predicted the fragment sizes as shown in table 7B.

<b>Destination Vector</b>	<b>Fragment sizes</b>
<b>Heph</b>	<b>10.67kb, 0.1kb &amp; 0.03kb</b>
<b>IRP1</b>	<b>9.9kb, 0.1kb</b>
<b>IRP2</b>	<b>7.7kb, 1.2kb, 0.7kb &amp; 0.5kb</b>

**Table 7B: Restriction analysis of Destination vectors.** Above table shows the restriction fragment sizes after digestion with *HindIII* restriction enzyme.

1µg of the pDNA was incubated overnight using 10 Units of *HindIII* enzyme. A 0.7% agarose gel was used to analyse the overnight restriction enzyme digestion of Heph, IPR1 and IRP2 Destination Vector pDNA. Figure 50 shows the 0.7% gel image of the digested fragments along with the undigested controls.

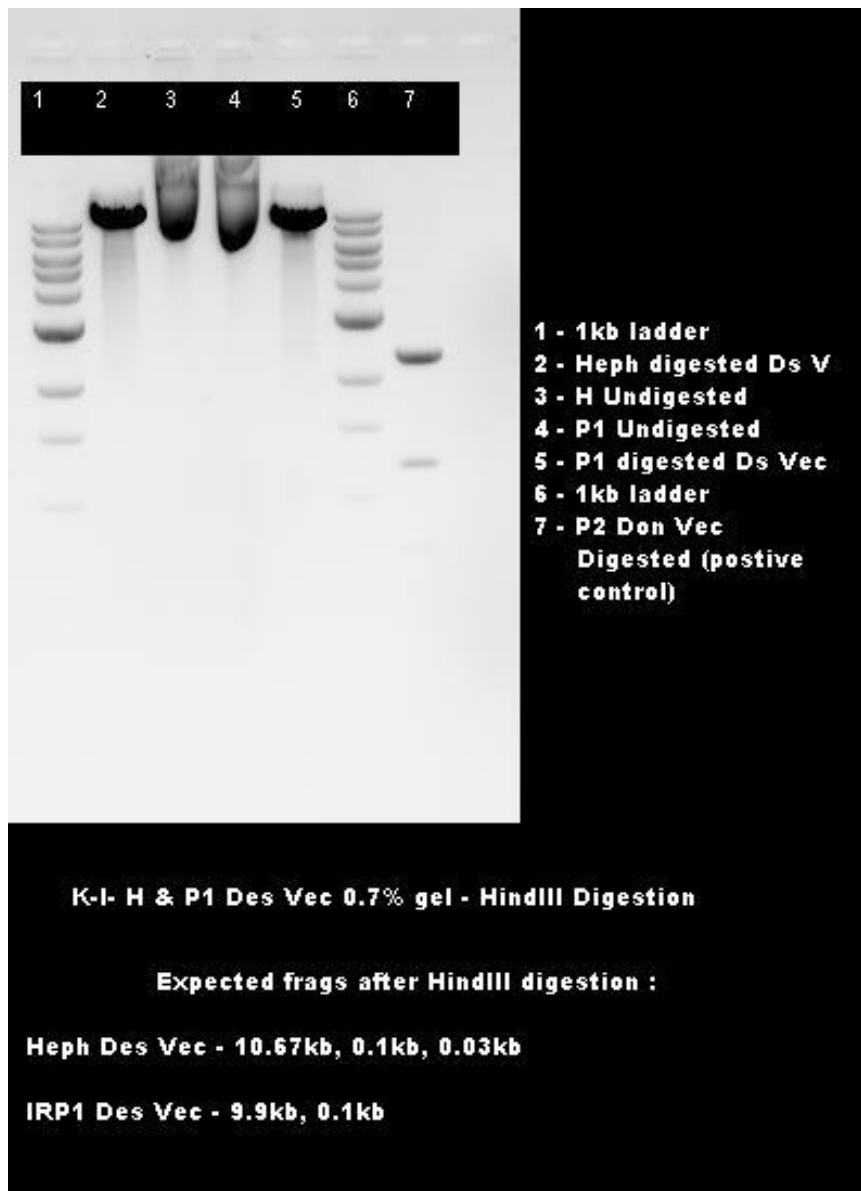


**Figure 47:** 0.7% gel electrophoresis of donor vectors Heph and IRP1. Restriction analysis of the digested and undigested (controls) fragments of IRP1 and Heph with 1kb ladder.



Expected Bands in lane 2 after Digestion

1 - 7.7kb, 2 - 1.2kb, 3 - 705bp, 4 - 500bp,  
 5 - 109bp (not expected to be seen on a 0.7% gel)

**Figure 48: 0.7% gel electrophoresis of donor vectors Heph and IRP2.** Restriction analysis of the digested and undigested (controls) fragments of IRP2 with 1kb ladder.

Restriction digestion of the Destination Vector pDNA of IRP2 with *HindIII* resulted in expected fragments of 7.7kb, 1.2kb, 0.7kb and 0.5kb. Since the gel was a concentration of 0.7% the 0.5kb band could not be seen clearly. However, the Destination vector pDNA construction has also been confirmed by sequencing analyses.

#### 4.07.002 Destination Vector sequence confirmation analysis

pDNA extracted after Destination Vector generation was also confirmed for the correct clone using Sequence analysis. Sequencing of the Destination Vector pDNA was carried out using Source BioScience facility in UCL. 100ng/μl pDNA and 3.2pmol/μl of both forward and reverse primer was submitted to the Source BioScience facility in UCL for sequencing. Sequencing analysis of the destination vector DNA with One-Strep tag were analysed for any variations in the base sequence using Sequencher software. Figures 49 – 51 confirmed the fusion of One-Strep tag with no variations observed in full length clones.



**Figure 49:** Forward sequence of Heph tagged with One-Strep tag destination vector. Forward sequence of Destination Vector with GOI-Heph showing the highlighted One-Strep tag at the C' end of clone which is necessary for further expression analysis.

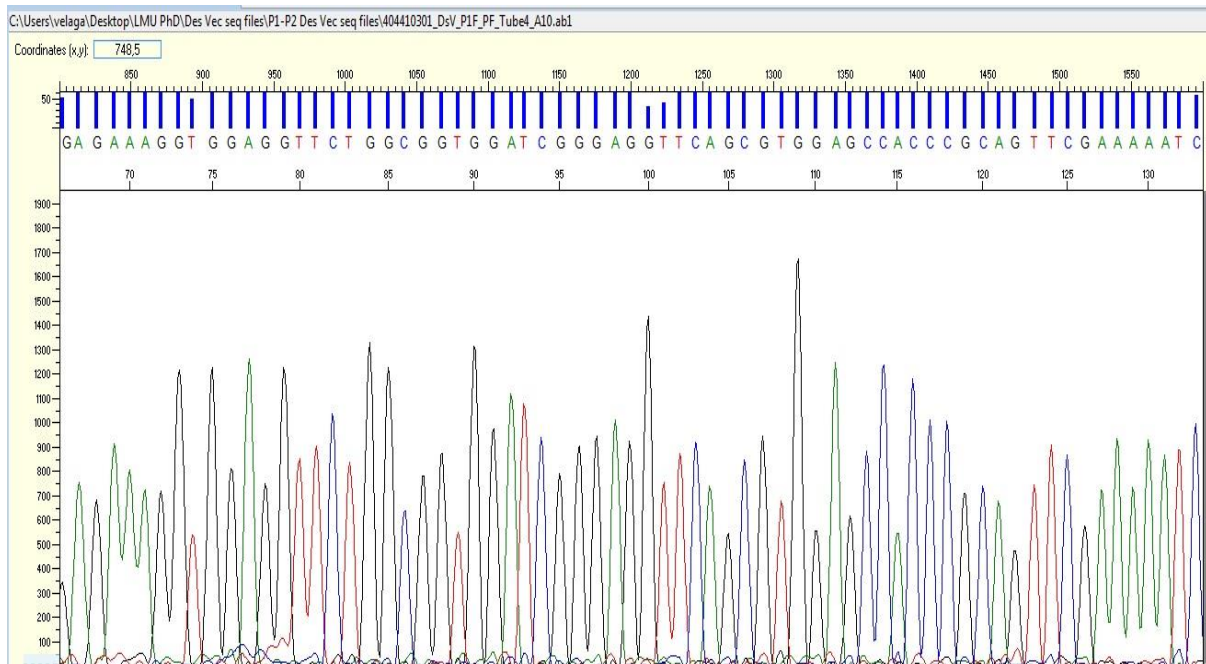


**Figure 50:** Forward sequence of IRP1 tagged with One-Strep tag destination vector. Forward sequence of Destination Vector with GOI-IRP1.

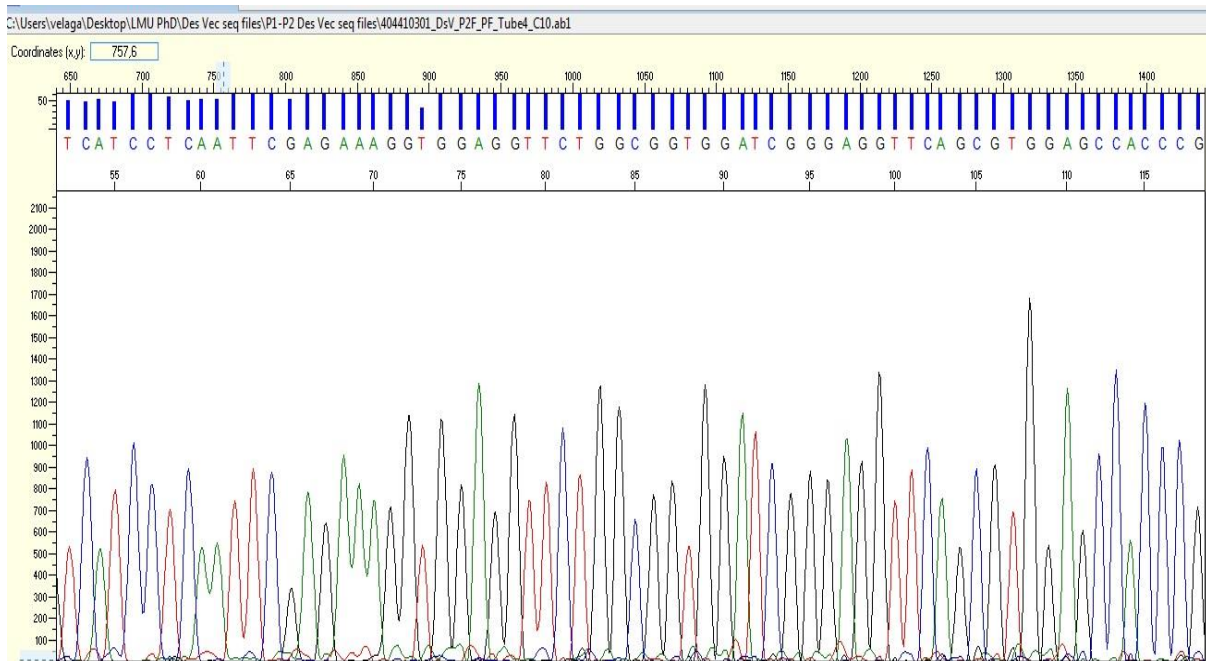


**Figure 51:** Forward sequence of IRP2 tagged with One-Strep tag destination vector. Forward sequence of Destination Vector with GOI-IRP2.

To confirm the plasmid constructs of Heph, IRP1 and IRP2 tagged with One-Strep tag, western blotting and flow cytometry techniques were used. Two batches of K562 cells were respectively transfected using Lipofectamine-LTX plus and Magnetic-assisted transfection reagents. After 48 hrs and 72 hrs of incubations, transfected cells were used to prepare cell lysates. Cell lysates were then analysed by Western blotting to analyse the expression of the respective tagged protein. To further carry out pull-downs of the respective protein in K562 cells (to find and establish different interacting partners) detection of the protein on the western blot was necessary to establish the successful transfection and over-expression of the One-Strep tagged Heph, IRP1 and IRP2. Unsuccessful attempt was made to examine the expression of One-Strep tagged Heph, IRP1 and IRP2 expressed in K562 cells on western blots. Failure in detecting the tagged protein after western blotting left a question to answer whether the transfection was successful or not. In order to assess the transfection efficiency flow cytometry was used.

#### **4.08 Protein expression analyses of One-Strep tagged Heph, IRP1 and IRP2 using Flow Cytometry**

To examine expression efficiency of One-Strep tagged Heph, IRP1 and IRP2 K562 cells were transfected with the respective tagged pDNA by both Lipofectamine LTX-Plus and MATra approaches. 2 µg of pDNA was used during both MATra and Lipofectamine-LTX transfections, so as to keep the concentration of the pDNA consistent to compare the efficiency of transfection. Having the two transfection reagents gave an opportunity to further analyse which method may be more efficient and which is more viable and also to see if the magnetic nanoparticles used in MATra have any effect on iron metabolic gene expression. Viability and expression efficiency analyses were carried out after 48hrs of transfection using via count and intra cellular staining. From the figure 52 it can be seen that K562 cells treated by MATra are more viable compared with Lipofectamine-LTX after 48hrs with significant p value of 0.014. However, when the same K562 cells are transfected with One-Strep tagged Heph using both MATra and Lipofectamine LTX, more cells were dead in the MATra transfected batch of K562 cells. There is a very significant difference between the MATra untransfected and transfected K562 cells with p value of 0.0003. A significant p value of 0.0197 was observed between Lipofectamine-LTX plus transfected and treated K562 cells. This concludes that MATra transfected cell viability is very low compared to Lipofectamine-LTX plus transfected K562 cells after 48hrs.

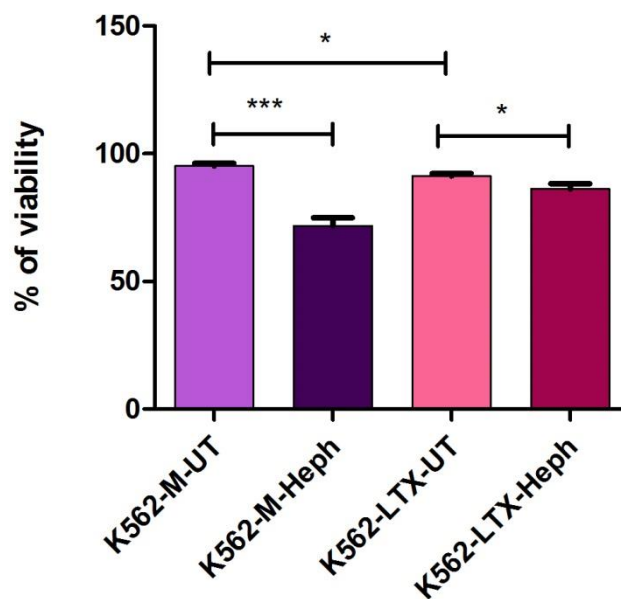


**Figure 52: Viability analysis of K562 cells transfected with Heph by Lipofectamine LTX-plus and MATra.** Comparison of % of viability between MATra and Lipofectamine-LTX plus transfected K562 cells. M – MATra, LTX – Lipofectamine-LTX plus, H = Heph.

Also, transfection efficiency and the hypothesised role of magnetic nanoparticles on IRP have also been examined by flow cytometry. Transfection of K562 cells was carried out using One-Strep tagged Heph and IRP2 by subjecting to MATra and Lipofectamine-LTX plus reagents. After 48 hrs of incubation, intracellular staining was carried out to analyse the transfection efficiency using a flow cytometer. From the Figure 56 it can be seen that Lipofectamine-LTX plus transfected K562 cells with One-Strep tagged Heph and IRP2 showed higher efficiency than MATra transfected cells. K562 transfected with Lipofectamine-LTX plus and One-Strep tagged Heph had a significant difference compared with MATra transfected K562 cells with a p value of 0.0001. Likewise, Lipofectamine-LTX plus transfected K562 cells with One-Strep tagged IRP2 showed higher transfection efficiency compared with MATra-assisted transfection with a p value of 0.0085. K562 un-transfected cells and K562 un-transfected cells but stained with antibody have been used as controls. To find if magnetic nanoparticles had any influence on the transfection efficiency of K562 cells, K562 cells transfected with One-Strep tagged Heph and One-Strep tagged IRP2 have been compared and analysed after 48 hrs. From the Figure 53 it can be concluded that there is no significant difference between the transfection efficiencies of MATra transfected K562 cells with One-Strep Heph and One-Strep IRP2 (K-M-H and K-M-

P2). Hence it can be concluded that Lipofectamine-LTX plus reagent has more transfection efficiency compared to MATra and magnetic nanoparticles do not have any adverse or significant effect on IRPs during transfection.

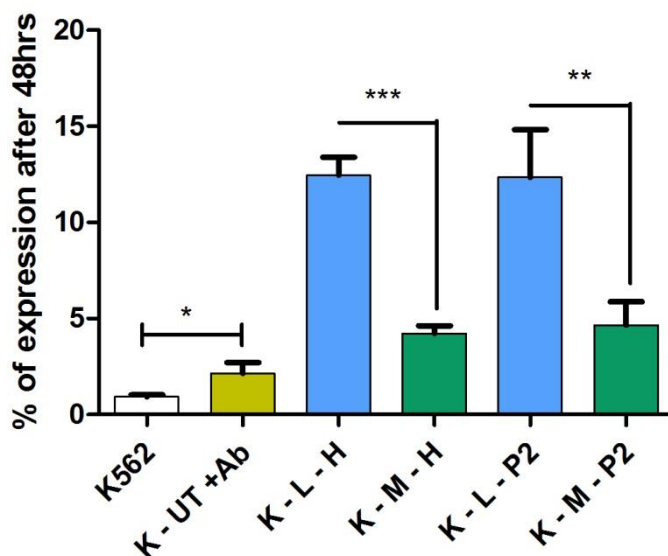


**Figure 53: Percentage of K562 cells transfected by Lipofectamine-LTX plus and MATra reagents.** Plot shows the % of K562 transfected cells using One-Strep tagged Heph and One-Strep tagged IRP2 by both Lipofectamine-LTX plus and MATra transfections. K= K562 cells, M – MATra, L – Lipofectamine-LTX plus, H = Heph and P2 = IRP2.

From the transfection efficiency studies in K562 cells it can be concluded that K562 cells have been transfected and it can be inferred that, number of transfected K562 cells with the respective One-Strep tagged protein may be significantly different to un-transfected cells but the significance achieved might not be enough to prepare a cell lysate for western blotting to identify the tagged protein on western blot. The percentage of detergent to lyse the cells may need to be optimised which might result in intact tagged protein complex during sample preparation for Western blotting. Along with the percentage of detergent, over-expression of tagged protein, that is higher transfection efficiency of K562 cells might give an opportunity to identify the protein of interest during Western blotting and also the interacting partners during the pull down studies.

#### **4.09 Discussion of Heph and IRPs Molecular cloning, expression and protein protein interaction studies**

Maintaining consistent levels of cellular protein requires a series of linked processes, spanning the transcription, processing and degradation of mRNAs to the translation,

localization, modification and of the proteins themselves. The abundance of the amount of protein reflects a balance among the cellular processes. It has long been a mystery of how this balance is achieved and to what extent each of these processes contributes to the regulation of cellular protein abundances. Approximately 40% of the variation in protein concentration can be explained by knowing mRNA abundances (de Sousa Abreu et al., 2009; Maier et al., 2009) and the remaining 60% of the variations can be attributed to a combination of posttranscriptional regulation modifications. Real time PCR studies confirmed the gene expression of Heph, IRP1 and IRP2. Preincubation with 500  $\mu$ M FAC did not result in any significant change of iron uptake by K562 cells and also did not show a significant effect on the mRNA level of Heph (Kovar et al., 2006). Caco-2 cells preincubated for 24hrs in 500  $\mu$ M FAC showed statistically significant levels of Heph mRNA along with mRNA levels of Ireg1 (40-60%) (Balusikova et al., 2009). When K562 cells were subjected to the 500  $\mu$ M FAC and incubated for 24 hrs, there was a 40% increase in Ireg1 mRNA levels, however mRNA levels of Heph though increased was not statistically significant (Balusikova et al., 2009). Since iron absorption is regulated by iron stores, before performing PPI studies, the analysis of gene expression of Heph and IRPs in K562 cells was carried out by treating K562 cells with 100  $\mu$ M FAC. Real time PCR results confirmed a 2.8 fold increase of Heph and IRP1 expression in 100  $\mu$ M FAC-treated K562 cells compared with normal K562 cells. Protein level expression was also carried out using K562 cells treated with 100  $\mu$ M FAC and K562 cells treated with normal medium by western blotting. As statistically significant increase of the mRNA levels of Heph in K562 cells treated with 100  $\mu$ M FAC, when compared with the control cells expression, correlated with an increased protein level in the case of Heph. Similar findings were reported by Balusikova et al in Caco-2 cells, where they treated Caco-2 cells with 500  $\mu$ M FAC (Balusikova et al., 2009). Iron release from non-intestinal cells was shown to require Cp ferroxidase activity (Vulpe et al., 1999; Hellman and Gitlin, 2002). It is known that membrane-bound Heph is mainly involved in the transfer of iron from intestinal enterocytes into the circulation. However, there are a few conflicting reports about the expression of Heph in iron deficient conditions. Heph expression observed in rats duodenum which were iron deficient (Frazer et al., 2001) showed a slight increase in mRNA levels. In patients with iron deficiency and haemochromatosis, a coordinated upregulation of the iron transporters DMT-1, Ireg1, Dcytb and Heph was observed (Zoller et al., 2003). Heph mRNA expression levels were not significantly different in, neither non-phlebotomized nor phlebotomized hereditary hemochromatosis (HH) patients with iron deficiency when compared with controls (Gleeson

et al., 2005). Likewise, gene expression of IPR1 and IPR2 was also carried out using K562 cells. The importance of IRPs *in vivo* was demonstrated in mice where the double knockout of IRP1 and IRP2 is embryonic lethal (Smith et al. 2006). Additionally, the double knockout of these genes in the intestine resulted in the death of intestinal epithelial cells, presumably because of iron depletion (Galy et al. 2008). Functionality of the IRP-IRE system was best exemplified in the “mucosal block”, a phenomenon by which, shortly after exposure to a large dose of iron, enterocytes become refractory to absorbing more iron (Crosby 1966). In rat enterocytes, the ingestion of high iron-containing food causes increased cellular iron content and reduced mRNA levels of DMT1 and Dcytb (Frazer et al. 2003). Cellular iron loading reduces IRE-binding activity of IRPs, which results in the susceptibility of TfR1 mRNA to degradation. It has been reported that hypertransfusional (>8 transfusions/year) iron in liver biopsies collected immediately after transfusions in beta-thalassemia and sickle cell disease correlated with increased expression (RNA) for iron regulatory proteins 1 and 2 (Jenkins et al., 2007). Gene expression analysis of IRP1 and IRP2 in K562 cells resulted in upregulation of IRP1 and IRP2 was down-regulated in K562 cells treated with 100  $\mu$ M FAC compared with normal K562 cells. The idea in this study is only to establish if Heph and IRPs (IRP1 and IRP2) expresses in K562 or not, so as to decide whether K562 cells can be used to carry out protein-protein interaction studies. Since, expression of Heph and IRPs (IRP1 and IRP2) was detected; K562 cells were used to further carry out protein-protein interactions studies. Molecular cloning of Heph, IRP1 and IRP2 with One-Strep tag was achieved and it was also shown that Lipofectamine-LTX helps achieve higher transfection efficiency in K562 cells compared with MATra approach. Though the gene expression studies, molecular cloning and transfection resulted in the desired outcomes coimmunoprecipitation work of One-Strep tagged Heph and IRPs was unsuccessful in this study.

Compared with other techniques to find interacting partners, fusion-based affinity protein purification is an excellent method to purify and identify multiprotein complexes as they aid in identifying multiple interactions. By expressing the POI directly in the cell this allows it to be directed to the right subcellular location which could help the baits interactions with its physiological targets to be restored. Since the tagged protein is expressed *in-vivo*, the protein can undergo post-translational modifications (PTMs). PTMs may have important implications during the purification of the protein complexes in the mammalian cells. In the case of regulatory proteins, its known that PTMs, such as phosphorylation, result in an

increase or decrease of the affinity towards the potential interacting partners. The affinity-based method used in finding Heph interactors may not be an optimal method in detecting the potential interacting partners, as it involved stringent rinsing procedures given its membrane-bound nature. Also, the failure to successfully carry out coimmunoprecipitation during this study can be attributed to lysis buffer concentrations. Since all interactions inside a cell occur in a concentrated mixture of molecules and the protein concentration in the cytosol may be as high as that of some proteins it is likely that the conditions were replicated in this study. The high protein concentration inside a cell influences the rate at which molecules diffuse. It can be said that the binding affinity of different proteins in a protein complex may be much higher in the crowded environment inside a cell compared to the protein complex in a buffer. Though, transient interactions with very short half lives could have existed in experiments carried out by affinity-based purification, concentration of the lysis buffer might have dissociated the interactions. In this study, the tagged Heph and IRPs were over-expressed, as compared to the expression level of endogenous counterparts to achieve transient interactions. However, over-expression of the bait might also caused disturbances in the physiological conditions. Over-expression of the bait proteins in this study might also lead to cytotoxicity that could explain non-detection of POI during western blotting.

Since the bait protein in this study was fused with an exogenous tag, One-Strep tag, this could also have caused an introduction of an artificial protein into the cell. Tag fusion with POI might also have caused the tag to become buried inside the protein complex, upon which the complex may not have been retrieved during the pull-down on the affinity column. The tag could also have caused mislocalisation of the bait protein, in which case the bait would not have interacted with its natural interactors. In this study, microscopy analysis of the tagged protein was unsuccessful. Along with the salt concentrations in the buffers used for immunoprecipitation, stringent washes could also have reduced the binding of low-affinity targets.

# Chapter 5

After repeated failures to carry out successful pull-downs to identify the interacting partners of IRPs and Heph, Dr. Kenneth White suggested to continue the work initiated by Philip Goff under his supervision in identifying an extra band which appeared in the membrane fraction of K562 cells.

## 5.01 Calreticulin (CALR)

### 5.01.001 Introduction of CALR

Calreticulin (also known as CRP55/Calregulin) was first identified as a  $\text{Ca}^{2+}$  binding protein of the muscle sarcoplasmic reticulum (Ostwald and MacLennan, 1974). Later it became clear that CALR is highly abundant in non-muscle tissues and that it is one of the major  $\text{Ca}^{2+}$  binding proteins of the endoplasmic reticulum (ER) (Michalak et al., 1992). CALR has been implicated in the regulation of a variety of cellular functions. Calreticulin is a highly conserved chaperone protein of the endoplasmic reticulum (ER) that has specificity towards glycoprotein substrates (Rutkevich and Williams, 2011). Calreticulin is important for the assembly and cell-surface expression of MHC class I molecules and hence for CD8 T cell recognition of antigens presented by MHC class I molecules (Gao et al., 2002). Calreticulin enhances the stabilities of components of the MHC class I assembly pathway (Del Cid et al., 2010; Jeffery et al., 2011) and functions in the retrieval of MHC class I molecules from post-ER compartments for their optimal assembly (Howe et al., 2009). Although calreticulin is best known for its ER chaperone functions, calreticulin also expresses on the cell surface. Induction of cell surface calreticulin in dying cells appears to be a feature of some apoptotic and preapoptotic cells (Gardai et al., 2005) and of cancer cells (Chao et al., 2010). Cell-surface calreticulin contributes to the phagocytic uptake of cancer cells and dying cells (Gardai et al., 2005; Chao et al., 2010). Preapoptotic exposure of calreticulin has been linked to enhanced immunogenicity of dying tumor cells. The prophagocytic function of cell surface calreticulin is suggested to relate to the immunogenicity of extracellular calreticulin (Zitvogel et al., 2010; Kepp et al., 2011). In mammals, CALR is a 46-kDa multifunctional calcium binding protein of the endoplasmic reticulum (first characterised in rabbit by Ostwald and MacLennan, 1974) that has many critical functions in the eukaryotic cell including regulation

of intracellular calcium homeostasis, lectin binding and chaperoning and oxidative stress responses (Liu et al., 2011).

### **5.01.002 Structure of CALR**

Calreticulin is a structural homolog of the ER chaperone calnexin. Both calreticulin and calnexin contain a globular domain arranged in a legume lectin fold (Figure 22) (Schrag et al., 2001; Kozlov et al., 2010). Each globular domain comprises a concave beta-sheet together with a convex sheet and a C-terminal alpha-helix in the globular domain. A single, conserved, high-affinity calcium-binding site in the globular domains of both calreticulin and calnexin confers structural stability to the domains (Kozlov et al., 2010; Chouquet et al., 2011). Glycan-binding sites are present on the concave beta-sheets of calnexin and calreticulin (Schrag et al., 2001; Kozlov et al., 2010), both of which have specificities for monoglucosylated glycans. A few studies also suggested that calreticulin and calnexin can interact with polypeptide substrates in a glycan-independent manner (Duus et al., 2009; Pocanschi et al., 2011). The precise locations of the polypeptide-binding sites in calreticulin and calnexin remain elusive, although recent structural studies suggest that the periphery of the glycan-binding site of calreticulin could be involved in glycan-independent interactions (Chouquet et al., 2011). It is still unclear whether this putative binding site functions as a generic polypeptide recognition site or not. Both calreticulin and calnexin contain flexible arm-like, proline-rich, P domains that interrupt and extend from the globular domain (Schrag et al., 2011). Calreticulin contains a highly acidic C-terminal region (residues 351–359) that binds multiple calcium ions with low affinity (Baksh and Michalak, 1991; Wijeyesakere et al., 2011). The counterpart of this region is absent in the luminal domains of calnexin. The acidic C-terminus of calreticulin plays a significant role in the maintenance of cellular calcium homeostasis, and cells deficient in calreticulin have reduced calcium storage capacity in the ER (Nakamura et al., 2001). The acidic C-terminus is also important for the translocation of calreticulin from the ER to the cytosol (retrotranslocation) (Afshar et al., 2005). The total absence of CALR in the embryonic stage of mice is detrimental due to alterations in cellular calcium homeostasis (Mesaeli et al., 1999, Guo et al., 2002). The acidic region of calreticulin also plays a role in ER retention of the protein, because a calreticulin construct lacking this domain is secreted despite the presence of a C-terminal KDEL sequence (Sonnichsen et al., 1994). The presence of a KDEL motif specifies binding to the KDEL receptor, which functions in the retrieval of KDEL-containing proteins from ER–Golgi intermediate compartments and the Golgi back to the ER (Dancourt and Barlowe, 2010).

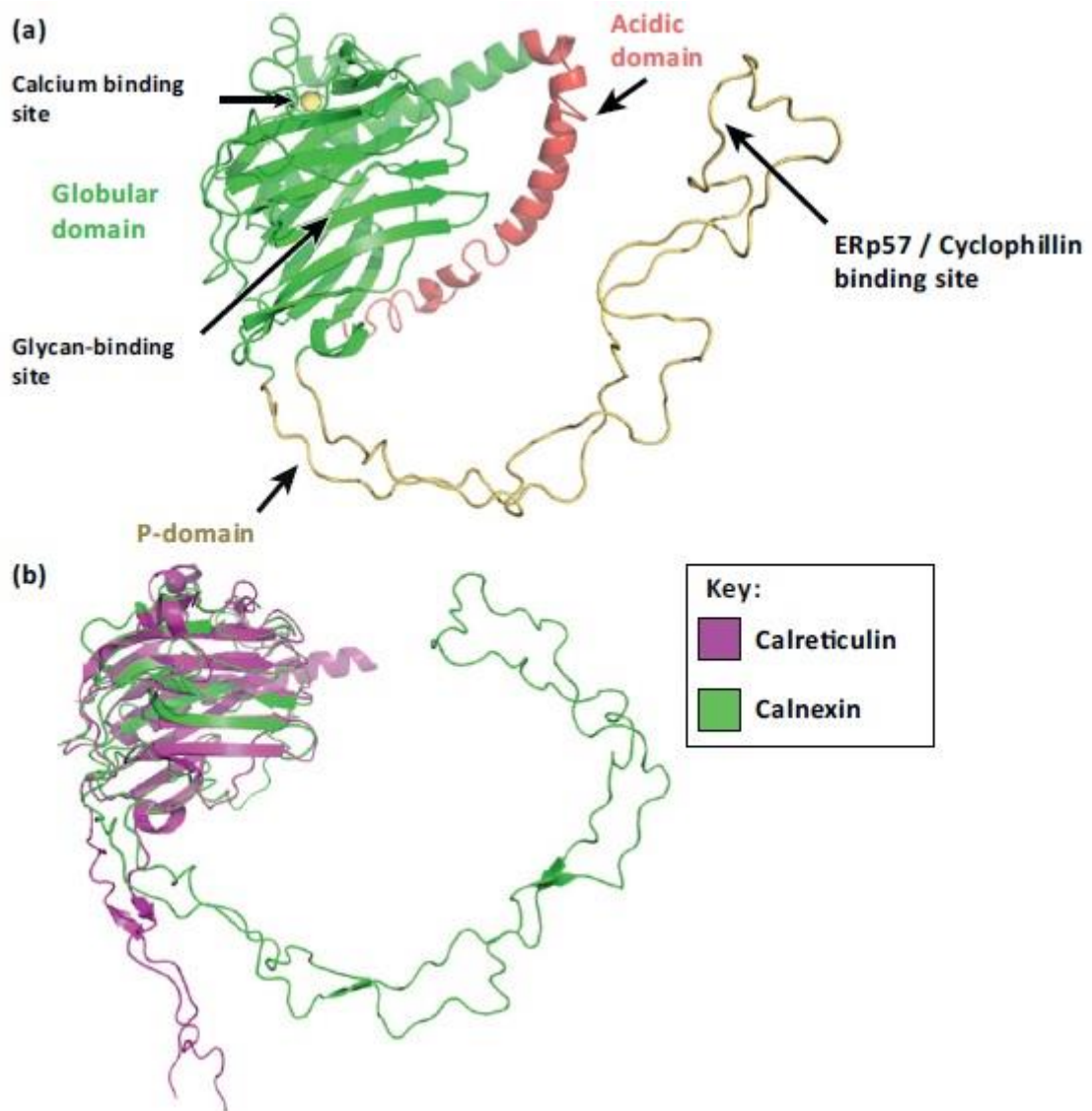


**Figure 54: CALR structure.** Figure shows the structural features of Calreticulin and Calnexin with their functional relevance. (a) The globular domain of Calreticulin is depicted in green and contains a glycan-binding site that interacts with monoglucosylated glycans of glycoproteins, including those present on major histocompatibility complex (MHC) class I heavy chains. The P domain of Calreticulin is depicted in yellow, the tip of which contains a co-chaperone binding site. The predicted structure of the C-terminal acidic region is shown in red. The acidic region contains multiple low-affinity calcium-binding sites that are important for the maintenance of endoplasmic reticulum (ER) calcium homeostasis. The model was built based on the crystal structure of the globular domain of Calreticulin (Pocanschi et al., 2011) and the NMR structure of the P domain (Ellgaard et al., 2001). The acidic domain is modeled *de novo* using the loopbuilding feature in I-TASSER (Roy et al., 2010). (b) Overlay of the structures of the luminal domain of calnexin (Schrag et al., 2001)

and the globular domain of calreticulin with a truncated P domain (Pocanschi et al., 2011) depicting the change in angle between the globular and P domains of Calreticulin compared to Calnexin. **Figure taken from Raghavan et al., 2013.**

### 5.01.003 Role of CALR in and out of the ER

Lately calreticulin is also found to have multiple functions in the cytoplasm, cell surface and extracellular matrix (Gold et al., 2010). For instance, the presence of calreticulin in the extracellular matrix is associated with the healing processes of cutaneous wounds (Nanney et al., 2008). Extracellular calreticulin addition significantly increases the rate of wound repair in pigs, wound tensile strength in rat models and moreover, in dermal cells undergoing wound repair, calreticulin expression is enhanced (Nanney et al., 2008). Specifically, the addition of calreticulin to wounds increases the expression of transforming growth factor  $\beta$ 3, a crucial wound healing factor and increases cellular proliferation and migration of keratinocytes and fibroblasts, altogether enhancing repair of dermal and epidermal damage (Nanney et al., 2008). Therefore, extracellular calreticulin plays an important role in the process of tissue repair and remodeling as shown in figure 55.

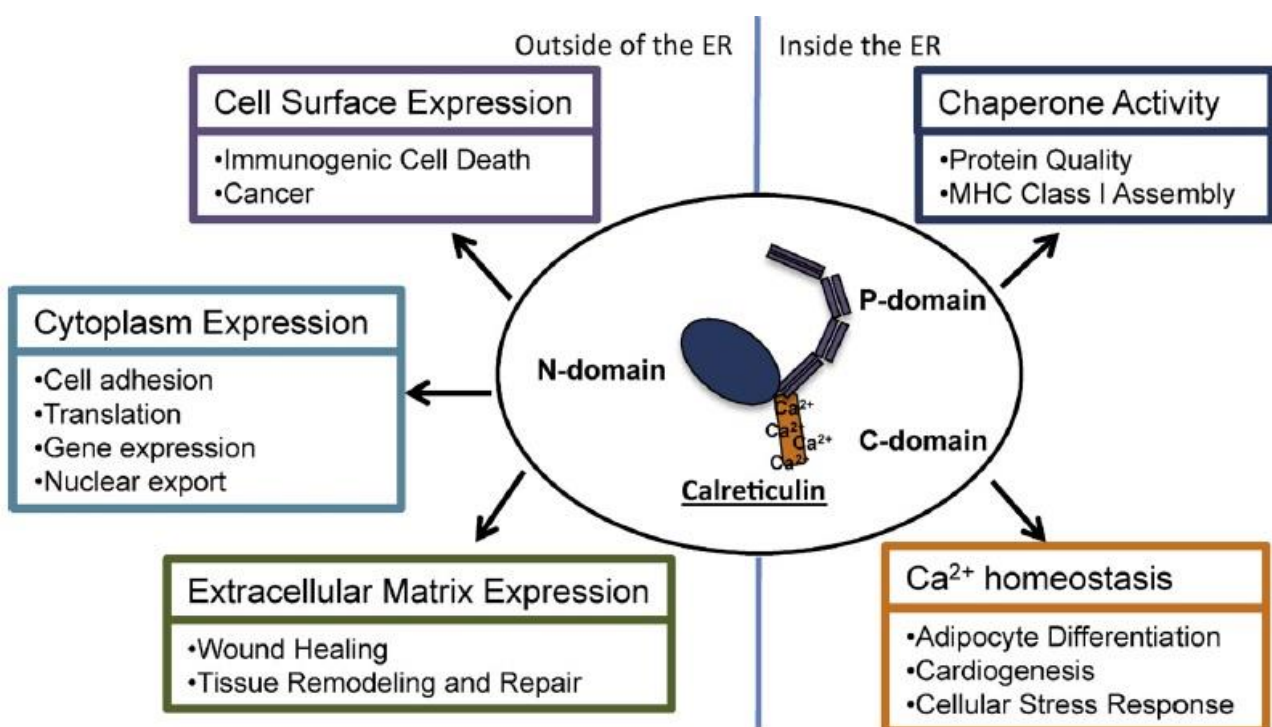


**Figure 55: Physiological and pathological roles of CALR.** Figure shows the physiological and pathological roles of calreticulin. A summary of the functions of calreticulin and their effects on health and disease related systems when present outside and inside of ER. **Figure taken from Wang et al., 2012.**

When calreticulin is present inside the endoplasmic reticulum (ER) it functions as a chaperone that regulates proper protein and glycoprotein conformation. Also it maintains the  $\text{Ca}^{2+}$  homeostasis, which can affect adipogenesis, cardiogenesis and cellular stress when present inside the ER. When calreticulin is present outside the ER it plays a role in immunity and enhances tissue repair and remodelling. calreticulin also plays a role in the cytoplasm, by regulating the cell adhesion, gene expression, translation and nuclear export.

Translocation of Calreticulin to the cell surface can be induced by anthracyclines, irradiation and diminishing ER  $\text{Ca}^{2+}$  stores, which are all involved in the triggering of ER stress (Pekárikova et al., 2009; Peters and Raghavan, 2011; Tufi et al., 2008). Very little is known about the mechanisms by which calreticulin translocates to the cell surface. However, it was reported that the surface exposure of Calreticulin is the crucial component in activating the anti-tumor response needed in chemotherapy (Chaput et al., 2007). The addition of Calreticulin or induction of cell-surface Calreticulin expression causes cancer cells to undergo immunogenic cell death via phagocytosis by dendritic cells (Chaput et al., 2007; Obeid et al., 2007). As they open up a new potential treatment avenue, studies on cell-surface exposure of Calreticulin makes them the potential candidates in cancer research. As of today, the molecular mechanisms of cell surface targeting of Calreticulin are still not well understood.

#### **5.01.004 CALR and Heph**

Owing to the ability to absorb dietary iron despite reduced expression and mislocalisation Heph in sla-mice, it could be hypothesised that Heph on its own may not be essential for oxidising ferrous ( $\text{Fe}^{2+}$ ) to ferric ( $\text{Fe}^{3+}$ ) iron. Iron is transported into mammalian cells via two different pathways. Most of the available iron is transported via transferrin. As there is no TfR in microvilli a second pathway is sought in small intestinal absorptive cells, (Parmley et al., 1985). Since microvilli do not have TfR, iron is absorbed as soluble iron chelates, such as ferric citrate with a cell-surface integrin (Conrad and Umbreit, 1993) and is subsequently transferred to a cytosolic protein named mobiliferrin (also known as Calreticulin or Calsperin) (Conrad et al., 1990). Previous studies have reported that there is an alternative pathway

for iron uptake in non-intestinal cells (Muir et al., 1984, Brissot et al., 1985 and Kaplan et al., 1991). Experiments in K562 cells suggested there might be an interrelationship between the two pathways because some iron presented to the cells bound to transferrin was isolated from the cytosol complexed to mobiliferrin (Conrad et al., 1994). Mobiliferrin is found to be associated with transferrin-containing vesicles and labelled with iron released from transferrin in the vesicles and it also releases iron to be used for the synthesis of haemoglobin (Conrad et al., 1996). The non-transferrin ferric ( $\text{Fe}^{3+}$ ) iron pathway in reticulocytes was similar to the mobiliferrin-integrin pathway originally described in intestinal cells and is independent of the transferrin-transferrin receptor pathway (Umbreit et al., 1997).

Confocal microscopy studies carried out by Simovich et al in 2002 established that mobiliferrin and hephaestin can be detected in the cytoplasmic region of cells thus suggesting intracellular roles for both CALR and Heph in addition to them serving to transit iron across the cell-surface membrane (Simovich et al., 2002). Intracellular iron accumulation leads to an oxygen radical formation (Toyokuni, 2002) and regulation of cellular iron levels is crucial in mediating an oxidative stress response (Braun, 1998). During bacterial infection, iron metabolism is particularly regulated as host and pathogen compete for control of iron stores (Ganz, 2003, Liu et al., 2010a). Iron-binding proteins and iron transport and regulatory proteins can play dual roles in both antioxidant and immunomodulatory (alteration of the immune response to a desired level) responses (Liu et al., 2011). CALR gene was also reported to play a protective role in the iron-induced oxidative stress (Nunez et al., 2001). High levels of CALR gene expression was detected in spleen and liver and the lowest expression was found in muscle (Liu et al., 2011). Considering the role of the liver in iron metabolism and storage as a part of this study, I also carried out analysis of various cytosolic/soluble and membrane extracts from different cell lines like K562 (Human Caucasian chronic myelogenous leukaemia cells), MDA-MB-231 (Human Caucasian breast adenocarcinoma cells) and PNT2-C2 (Human prostate normal, immortalised with SV40 cells) to identify if CALR has any ferroxidase activity.

## **M1 Results and discussion**

### **5.02 Identification of M1 band in K562 cells**

K562 cells express the ferroxidase hephaestin in significant amounts, compared with many other cell lines. This makes the cell line a convenient model for studying hephaestin activity. In the process of charactering the expression of hephaestin in K562 cells we used non-

denaturing electrophoresis followed by staining for ferroxidase enzyme activity in the gel *in situ*. Membrane and cytosolic fractions were prepared using hypotonic lysis by freezing and thawing. This strategy was chosen to avoid the use of detergents to make an extract of membranes and thereby avoid contamination of lysates with cytosolic proteins. Membrane and cytosolic extracts, together with 2.5 µg of pure Ceruloplasmin (Cp) from Calbiochem were subjected to non-denaturing gel electrophoresis, followed by staining for ferroxidases,. In addition to the expected ferroxidase band due to Heph an extra band appeared in the K562 membrane fraction. Even after repeated non-denaturing gel electrophoresis no bands were observed in K562 cytosolic fractions.

### **5.02.001 Identification of M1 band as CALR in K562, MDA MB231 and PNT2-C2 cell fractions**

To check if the extra band was expressed exclusively in K562 cells, MDA-MB-231 (Human breast adenocarcinoma cells) cell fractions were also analysed. Both membrane and cytosolic fractions from MDA-MB-231 and membrane fraction of K562 cells were subjected to non-denaturing gel electrophoresis (Fig. 56). A band was observed only in the membrane fractions of both the cell lines and was named M1 (M = membrane fraction, 1 = first band to be observed). To rule out any non-specificity, gel electrophoresis was repeated thrice and the M1 band was observed each time. The presence of the M1 band in both K562 and MDA-MB-231 cells confirmed its expression in cancerous cells. However, to establish whether or not the M1 band was also expressed in normal or non-cancerous cells, PNT2-C2 (Human prostate normal immortalised with SV40) cells were also fractionated and analysed (Fig. 58). The ferroxidase and coomassie stained non-denaturing gel confirmed the expression of the M1 band in K562, MDA-MB-231 and PNT2-C2 cell lines which established the ubiquitous nature of the M1 protein in both cancerous and primary cells.

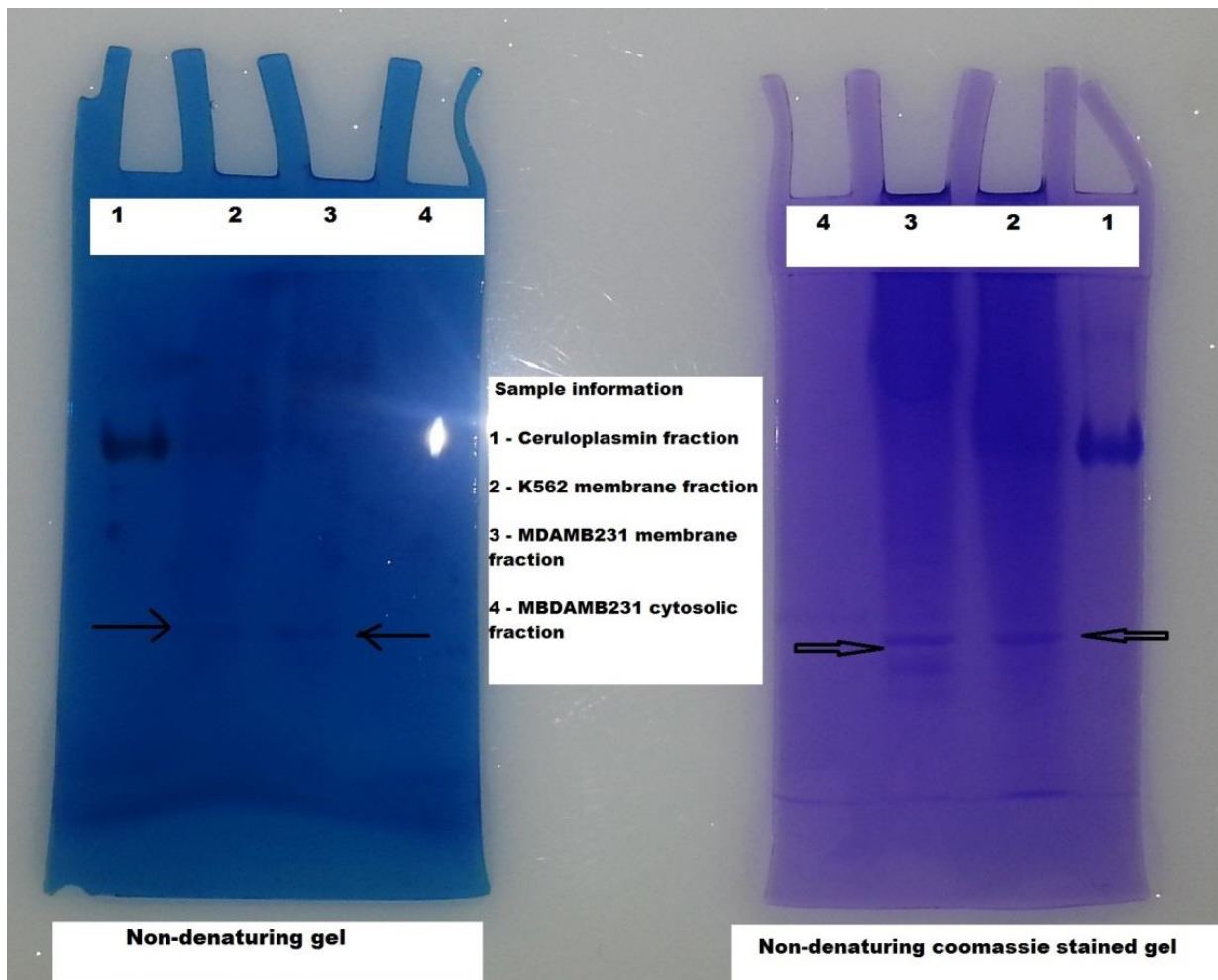


**Figure 56: 8% non-denaturing ferroxidase and coomassie stained gel.** 8% non-denaturing ferroxidase and coomassie stained gels shows the M1 band in both K562 and MDA-MB-231 membrane fractions but not in the MDA-MB-231 cytosolic fraction.

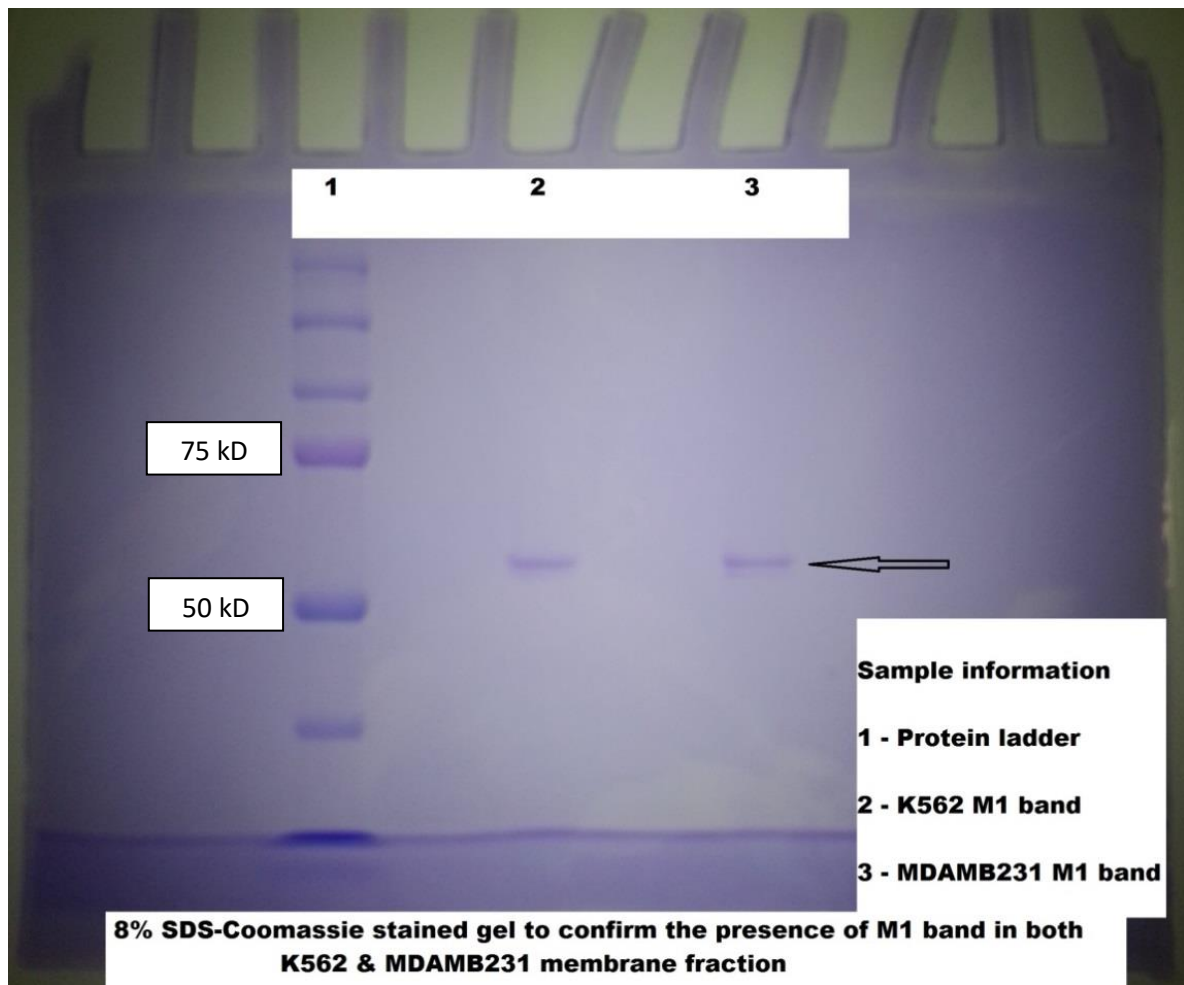


**Figure 57:** 8% SDS coomassie stained gel showing the M1 band in K562 and MDA-MB-231 membrane fraction. Figure shows the presence of the M1 band in both K562 and MDA-MB-231 membrane fractions on a 8% SDS coomassie stained gel.

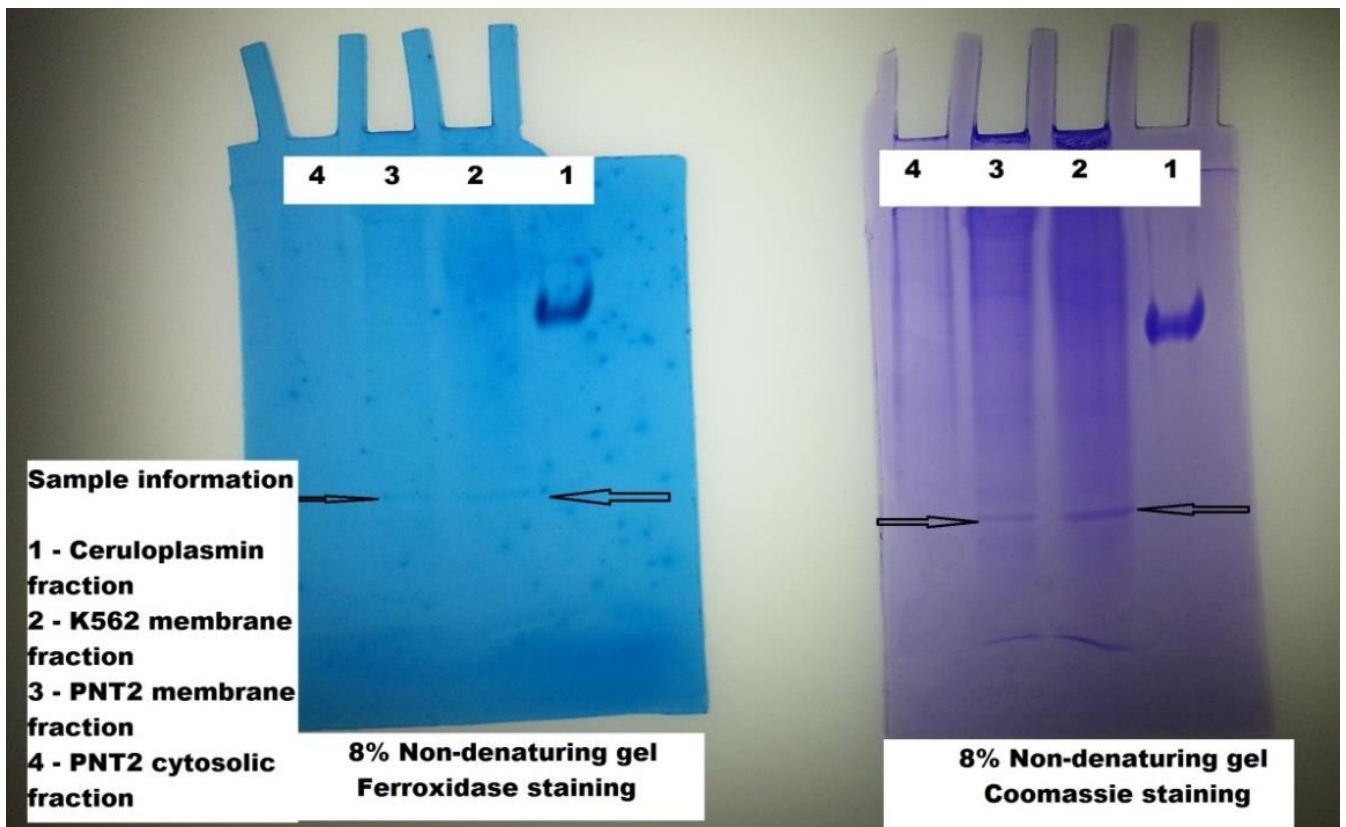


**Figure 58: 8% SDS coomassie stained gel showing the M1 band in K562 and PNT2-C2 membrane fraction.** 8% non-denaturing ferroxidase and coomassie stained gels shows the M1 band in both K562 and PNT2-C2 membrane fractions but not in cytosolic fraction.

Ceruloplasmin which is a ferroxidase (Frieden and Hsieh, 1976) was used as a positive control in all the electrophoretic runs, and gave a strong signal in both ferroxidase and protein staining (Fig. 56 and 58, lanes 1). One striking feature about M1 was that it ran as a single, separate protein band in the gel, and could be easily excised for further analysis. In all the non-denaturing gels, precision plud protein™ standard marker from Bio-rad (UK) was used as a marker. The M1 band consistently appeared between the 75 kD and 50 kD bands as represented in the protein marker lane. Since the sequence of the M1 band was not known we decided to carry out Mass spectrometry (MS-MS) to identify the M1 band. M1 band was confirmed by MS-MS in association with our collaborator in Imperial College, UK. Figure 59 shows the 10% SDS-PAGE gel picture of the M1 band run by our colleagues in Imperial College to get the sample ready for proteomic analysis. Table 08 shows the p and Sf (Sf is a statistical indicative of the certainty of the id) values of the identified band by MS-MS. MS-MS study confirmed the M1 band to be Calreticulin (CALR). It can be concluded

that CALR is only expressed only in the membrane fractions but not in cytosolic fractions of K562, MDA-MB-231 and PNT2-C2 cells.

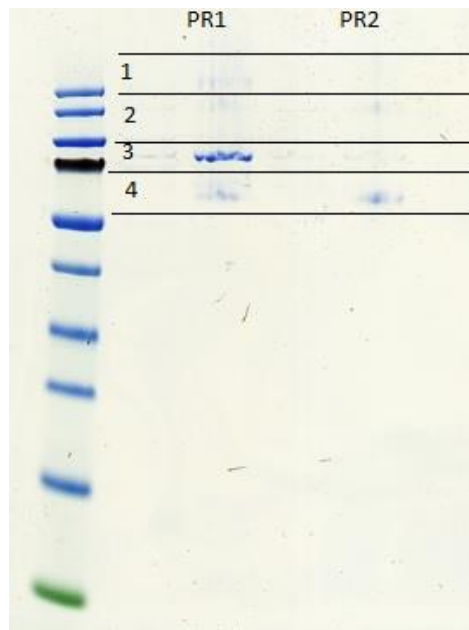


**Figure 59: 10% SDS-PAGE gel used to run the excised M1 band for proteomic analysis.**

The M1 band in a 10% SDS-PAGE gel. Four slices at and around where the staining was observed in lanes PR1 and PR2 were excised and processed for proteomic analysis.

	PR2	P	Sf
row1	calreticulin precursor [Homo sapiens]	1.00E-13	9.45
row 2	calreticulin precursor [Homo sapiens]	3.44E-15	13.67
row3	calreticulin precursor [Homo sapiens]	2.11E-15	11.19
row4	calreticulin precursor [Homo sapiens]	1.11E-16	17.22

**Table 08: p and Sf vaues for CALR obtained after MS-MS.** Table above represents the p and Sf value obtained for the M1/CALR identified after MS-MS.

However, database analysis (Uniprot) suggests the sub-cellular localisation of CALR to be attributed to the endoplasmic reticulum, cytosol, extra cellular matrix and on the cell surface. This poses the question, why was CALR not shown in cytosolic fractions of K562, MDA-MB-231 and PNT2-C2 cells used in the non-denaturing gel electrophoresis. To understand the absence of CALR in cytosolic fractions, the experimental set up was looked into and it was confirmed that membrane fractions were more concentrated than cytosolic fractions. Membrane fractions were prepared using  $10^7$  cells/ml and cytosolic fractions were prepared using  $10^6$  cells/ml. When non-denaturing gel electrophoresis was performed, the absence

of CALR band in the cytosolic fractions of the three cell lines thus can be attributed to the different concentrations of samples used.

### 5.03 Bioinformatics analysis of CALR

The identification of the M1 band as CALR by MS-MS raised further questions about any ferroxidase activity of CALR. The Protein Basic Local Alignment Search Tool (blastp) and Position-Specific Iterated Basic Local Alignment Search Tool (PSI-BLAST) analysis was carried out using the CALR protein sequence. Blastp was carried out using CALR, Heph and Cp (UniProt ids: P27797, P00450, Q9BQS7) and it was found that CALR and Cp have a 32% identity with a e-value of 3.4 and CALR-Heph showed sequence homology of 44% with a e-value of 2.3. The observed e-values 3.4 and 2.3 in figure 61 do not support the significant sequence homology between CALR, Cp and Heph. To find distant relatives and potential homologs, PSI-BLAST was performed using Cp, Heph and CALR protein sequences. While performing PSI-BLAST, reference protein database (refseq\_protein) parameter was chosen to avoid duplicate or repeated results. In the blast algorithm parameters, the threshold was changed to a generally accepted value of  $1e-4$  from the default  $5e-3$  to carry out homology analysis and also rule out any false positives. Blast was carried out in organism specific (Homo sapiens) and against all organisms in the blast database, using the CALR protein sequence (UniProt id: P27797). Any blast result with e-value less than  $1e-4$  has been considered to be homologous or related to the CALR protein. During PSI-BLAST analysis to find putative homologs which may have been missed during the first run, two iterations were carried out. Further protein sequence analysis of CALR, Cp and Heph showed metal-binding regions. In the case of CALR the metal bound was calcium and in Cp and Heph it is Cu-binding region. Both blastp and PSI-BLAST did not show any significant homology between CALR, Cp and Heph. Maybe structural analysis of CALR, Cp and Heph might reveal a specific ferroxidase signature in CALR.

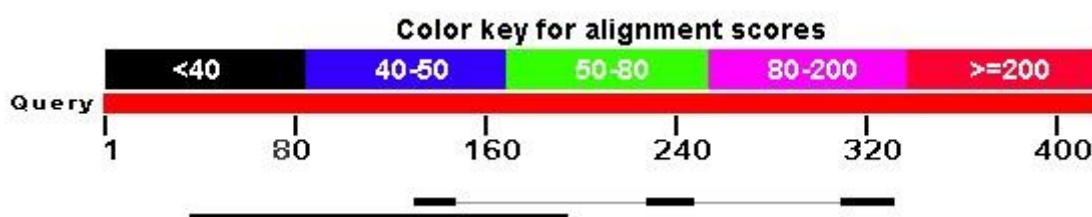


**Figure 60: Blast analysis of CALR, Cp and Heph protein sequence.** Figure shows the blastp result of CALR, Cp and Heph protein sequence alignment. Red line in the above alignment is the CALR sequence, first black spaced line is of Cp and continuous bottom black line representing Heph.

Description	Max score	Total score	Query cover	E value	Ident	Accession
<a href="#">sp P00450 CERU_HUMAN Ceruloplasmin OS=Homo sapiens GN=CP PE=1 SV=1</a>	16.9	48.1	14%	3.4	32%	54774
<a href="#">sp Q9BOS7 HEPH_HUMAN Hephaestin OS=Homo sapiens GN=HEPH PE=2 SV=3</a>	17.3	34.6	37%	2.3	44%	54775

**Figure 61: Blastp results of CALR, Cp and Heph showing the e-value.** Above figure shows the blastp result of CALR, Cp and Heph protein sequence alignment with percentage of identity and e-value.

#### 5.04 Metal-binding nature of CALR

Based on the CALR protein sequence analysis, the primary structure of CALR has been divided into four distinct domains with the signal peptide (residues 1-17), the N-domain (residues 18-197), the P-domain (residues 191-255), and the C-domain (residues 309-408). The N-domain of CALR is highly conserved among CALR species (Michalak, 1996) and contains a low-affinity, high-capacity zinc-binding site with an apparent dissociation constant (apparent  $K_d$ ) of 0.05  $\mu\text{M}$  and 14 binding sites for  $\text{Zn}^{2+}$  with apparent  $K_d(\text{Zn}^{2+})$  of 310  $\mu\text{M}$ . (Khanna et al., 1986). It has been shown that the N-domain mediates interactions between CRT and the ER folding catalysts PDI and ERp57 (Corbett et al., 1999, Baksh et al., 1995). The central P-domain contains two proline-rich repeat sequences, type 1 and type 2 motifs, which have been shown from recent NMR studies (Ellgaard et al., 2001, Ellgaard et al., 2001) to be primarily structural motifs allowing the P-domain to adopt a unique hairpin-type fold in solution. It has been established that the P-domain is likely to contain a high-affinity calcium-binding site ( $K_d$  of 0.05-10  $\mu\text{M}$  and 1 mol of calcium/mol of CRT) (Khanna et al., 1986, Ostwald et al., 1974, Ostwald et al., 1974, Baksh et al., 1991, Khanna et al., 1987, Van Nguyen et al., 1989) and the domain has been implicated in the binding of isolated oligosaccharides as well as glycoprotein ligands in *in vitro* assays (Vassilakos et al., 1998, Peterson et al., 1999). The C-domain is characterized by a high content of acidic residues (Smith et al., 1989, Fliegel et al., 1989, Baksh et al., 1991, McCauliffe et al., 1990) which is consistent with the location of a low-affinity, high-capacity calcium binding site ( $K_d$  1-2 mM and 25-50 mol of calcium/mol of CRT) (Ostwald et al.,

1974, Baksh et al., 1991, Treves et al., 1990). The N-/C- domain of CRT, but not the P-domain, responds to calcium and zinc ions through conformational rearrangements (Tan Y et al., 2006). The presence of CALR in different cellular compartments suggests CALR's role in many cellular processes both inside and outside the Endoplasmic reticulum (ER).

Along with Calnexin and ERp57, CALR plays a critical role in the folding of glycoproteins and in quality control processes of the protein secretory pathway (Ellgaard and Helenius 2003). In CALR-deficient fibroblasts, the  $\text{Ca}^{2+}$  storage capacity of the ER is reduced (Nakamura et al. 2001b), whereas in fibroblasts that over-express CALR, intracellular  $\text{Ca}^{2+}$  ion stores are increased (Arnaudeau et al. 2002). Its role in balancing the amount of  $\text{Ca}^{2+}$  is emphasized by the observation that its expression is sensitive to changes in ER  $\text{Ca}^{2+}$  concentration. For example, the emptying of ER  $\text{Ca}^{2+}$  stores results in enhanced expression of CALR (Waser et al. 1997) indicating that cells adapt to decreased ER  $\text{Ca}^{2+}$  concentrations by increasing the concentration of  $\text{Ca}^{2+}$  buffer proteins within the lumen of the ER. Changes in ER  $\text{Ca}^{2+}$  storage capacity and changes in  $\text{Ca}^{2+}$  binding to CALR impact the quality of ER protein folding because  $\text{Ca}^{2+}$  is required for formation of chaperone–substrate complexes (Lynch et al., 2006). An alteration in ER  $\text{Ca}^{2+}$  concentration disrupts normal ER dynamics, thereby impacting  $\text{Ca}^{2+}$  homeostasis and protein folding, such that these two functions are interdependent (Michalak et al., 2002). The basic CALR functions such as, regulation of  $\text{Ca}^{2+}$  homeostasis and molecular chaperoning in ER might be the key to explaining the multi-process property of CALR (Michalak et al., 2009).

## **5.05 CALR and diseases**

Though the Ensembl database shows 101 reported variations in the CALR gene none of the variation has been shown to be associated with any disease. However, Calreticulin deficiency is embryonically lethal in mice at E13.5, the lethality resulting from a lesion in cardiac development (Mesaeli et al. 1999). It appears that CALR-deficient cells have different metabolic properties which result from changes in intracellular  $\text{Ca}^{2+}$  levels. The CALR promoter is activated, and expression of the protein is high in the early stages of cardiogenesis, reaching a maximum at E14.5 (Mesaeli et al. 1999). CALR is highly expressed in the developing heart, but the expression is tightly regulated after birth, and the protein is only weakly expressed in the healthy mature heart. Close postnatal regulation of the CALR gene in the heart is vital because elevated expression of the protein in the heart after birth is fatal (Nakamura et al. 2001a). Mice that over-express CALR in cardiac cells develop bradyarrhythmia and a complete heart block, and this is followed by sudden death

(Nakamura et al., 2001a). Sensitivity of the myocardium to oxidative stress and apoptosis may also be affected by levels of CALR (Ihara et al. 2005, Ihara et al. 2006, Kageyama et al. 2002, Nakamura et al., 2000). There is evidence to confirm that CALR acts as an auto antigen in patients with systemic lupus erythematosus (SLE) by playing a supportive role in the formation of the auto antigen complex-Ro/SS-A (Eggleton et al., 1997). Synthetic linear CALR peptide analogues prepared against the N-terminal region of CALR were immunoreactive to sera from patients not only with SLE or Sjogrens syndrome (SS), but also in rheumatoid arthritis (RA) (Routsias et al., 1993). Anti-calreticulin auto antibodies are not restricted to patients with SLE, for example they have been found in patients with rheumatoid arthritis (RA) (Verreck et al., 1995, Jacob et al., 1997). CALR is targeted by auto antibodies following its release into the extracellular environment, possibly as a result of cell death, or its presence at the cell surface in response to insults such as viral infection or ultraviolet irradiation (Eggleton and Llewellyn, 1999).

### **5.06 Significance in identifying iron binding sites of CALR for its ferroxidase activity**

Uptake of non-transferrin-bound iron into enterocytes occurs either through the Integrin-Mobilferrin pathway (IMP) or the Di-valent Metal Transporter-1 pathway (DMT-1, Nramp 2). The IMP pathway is thought to transport only ferric iron (Conrad et al., 2000). Mobilferrin is a homologue of Calreticulin (Bothwell et al., 1979). It is possible that the two proteins are identical (Umbreit et al., 2002) which was reported to be identical to calreticulin for the first 20 NH<sub>2</sub>-terminal amino acids, and antibodies to both the NH<sub>2</sub>-terminal and COOH-terminal sequences of calreticulin react with mobilferrin except that mobilferrin lacks the carboxy terminal sequence of KDEL. Mobilferrin, in association with  $\beta$ 3 integrin, forms a macromolecule known as paraferitin, which has been assigned to have ferrireductase activity (Umbreit et al., 1996) resulting in the conversion of the absorbed Fe<sup>3+</sup> to Fe<sup>2+</sup>. Up-regulation of mobilferrin could be responsible for the increased absorption of iron and iron overload (Baber et al., 2000). However, the role of calreticulin as a proposed component of paraferitin still remains unanswered (Srai et al., 2007). Owing to high expression levels of CALR in liver (Khanna and Waismann, 1986) and its role as a multi-functional protein, studies on selective glycosylation sites by site-directed mutagenesis in CALR isolated from human liver cells may shed some light on CALR as a ferroxidase. Further enzymatic characterisation of the CALR obtained from the membrane fraction of K562, MDA-MB-231 and PNT2-C2 will confirm its ferroxidase properties. In Cp, the predicted high-affinity Fe(II)

binding sites are located beneath large protein loops (Lindley et al., 1997; Brown et al., 2002; Quintanar et al., 2004). The overall structure of the molecule as well as the charge distribution in Cp was predicted to be conserved in Heph (Syed et al., 2002). On the basis of the results of crystal soaking experiments (Lindley et al., 1997), Cp contains two ferrous binding sites in domains 4 and 6. Crystal soaking experiments did not reveal ferrous iron binding in domain 2 of ceruloplasmin, which contains E236, E633, N323, and Y241 in the corresponding positions (Syed et al., 2002).

Domain	Putative iron ligands	
	Ceruloplasmin	Hephaestin
2	E236,Y241,N323,E633	E264,H269,S351,E652
4	E597,H602,D684,E971	D616,H621,S703,D996
6	E935,H940,D1025,E272	E960,H965,D1050,E300

**Table 09: Putative iron ligands in Cp and Heph.** Table shows the putative ligands in Ceruloplasmin and Hepaestin. Putative iron ligand information is from Lindley et al., 1997 for Ceruloplasmin and Syed et al., 2002 for Hephaestin.

Compared with Cp, hephaestin contains conserved ligands in the Fe(II) binding site of domain 6 (E960, H965, D1050, E300), whereas in domains 2 and 4, the equivalent residues are E264, H269, S351, and E652 and D616, H621, S703, and D996, respectively. Recombinant human hephaestin (rhHp) with putative Fe(II) binding residues were constructed by site-directed mutagenesis to examine the functional role of individual amino acid residues in iron oxidation by human Heph (Vashchenko and MacGillivray, 2012). Kinetic analysis of ferroxidation rates of wild-type rhHp and mutants demonstrated the important roles of hephaestin residues E960 and H965 in the observed ferroxidase activity (Vashchenko and MacGillivray, 2012). The amino acid sequence homology between CALR, Cp and Heph may predict similar biochemical properties. However, any specific enzymatic function of CALR probably results from its structural differences from Heph and Cp and hence needs to be examined by identifying the iron binding sites in CALR.

# **CONCLUSIONS**

## CHAPTER 6

This study attempted to identify and establish the potential genetic markers and interacting partners of different iron metabolic genes Mfrn, IRPs and Heph.

Owing to the practical infeasibility of genotyping all single nucleotide polymorphisms, selecting a subset of SNPs, (that is sufficiently informative to conduct disease-gene association which information is enough to reduce the genotyping and data analysis) a process known as tag SNP selection, is a key step toward effective association studies. In the regions of low haplotype diversity, tags SNPs are sufficient to account for the majority of the haplotype diversity of the human genome. 18 tagSNPs of the Mfrn gene were analysed in an Asian-Caucasian cohort to examine the correlation between the Mfrn tagSNPs, haemoglobin levels and birth weight. Ideally serum ferritin and transferrin information (percentage saturation and total iron binding concentration or TIBC), would have been used. However due to lack of information in the data set, Hb levels were used as a proxy for body iron levels. Of the 18 tagSNPs genotyped only four tagSNPs were in Hardy-Weinberg equilibrium. The four tagSNPs (rs6986233, rs11781222, rs7089331 and rs17089358) were analysed for correlation by two-way ANCOVA using SPSS (v.20) analysis software. It can be concluded that neither of the four SNPs showed any significance correlation between the genotype, Hb levels and birth weight. This rules the Mfrn tagSNPs out as tagSNP candidates. However, investigating other solute carrier family genes could show a potential correlation between Hb levels, birth weight and the genotype.

Protein-protein interaction studies of IRPs and Heph were unsuccessful even after successful molecular cloning and expression of IRPs and Heph with One-Strep tag. Failure to carry out immunoprecipitations/pull-downs can be partly attributed to the percentage of detergent used in the lysis buffer and part to the number of transfected cells after Lipofectamine-LTX plus transfection of the K562 cells using IRPs and Heph tagged with One-Strep tag. A G418 selection process was used to isolate only transfected cells with no success. However, a couple of conclusions that came out of the protein-protein interaction study were, lipid mediated transfection by Lipofectamine-LTX plus reagent of K562 cells using IRPs and Heph tagged with One-Strep tag showed higher transfection efficiency and viability compared with magnetic assisted transfection method. By using magnetic

nanoparticles for transfection of K562 cells with IRPs tagged with One-Strep tag, it can be concluded that magnetic nanoparticles do not have any effect on iron regulator proteins.

This work identified and concluded that the M1 band appeared in the membrane fractions of K562, MDA-MB-231 and PNT2-C2 cells when analysed on an 8% non-denaturing gel. The band was identified and concluded as Calreticulin in collaboration with Prof. Rob, Imperial College by mass spectrometry. This study only found the CALR in membrane fractions of K562, MDA-MB-231 and PTN2C2 cells. However, the work carried out later by Dr. Kenneth White and Suam confirmed the presence of CALR in both membrane and cytosolic fractions of K562 cells. This study also proposes further kinetic analysis of CALR to establish CALR as a ferroxidase.

# **FUTURE WORK**

# CHAPTER 7

- Owing to the interaction of Mfrn with ABCB10, either ABCB10 or other iron metabolic genes could become the candidate gene for tagSNP analysis
- Cell line other than K562 which could achieve higher transfection efficiency could well yielded potential protein complexes after the pull down
- May be the choice of detergent used while performing the washing steps during the pull down needs to have a through look
- Comparing GOI cloned with One-Strep-tag and GFP tagged clones could tell whether using One-Strep-tag is efficient
- Identifying any potential iron binding sites in CALR will help confirm its ferroxidase nature along with kinetic studies.

## REFERENCES

1	Abboud S and Haile DJ. A novel mammalian iron-regulated protein involved in intracellular iron metabolism. <i>J Biol Chem.</i> 2000;275: 19,906–19,912.
2	Abramoff, M.D., Magalhaes, P.J., Ram, S.J. "Image Processing with ImageJ". <i>Biophotonics International</i> , volume 11, issue 7, pp. 36-42, 2004.
3	Afshar, N. et al. Retrotranslocation of the chaperone calreticulin from the endoplasmic reticulum lumen to the cytosol. <i>Mol. Cell. Biol.</i> 2005;25, 8844–8853.
4	Ahmad KA, Ahmann JR, Migas MC, Waheed A, Britton RS, Bacon BR, Sly WS, and Fleming RE. Decreased liver hepcidin expression in the Hfe knockout mouse. <i>Blood Cells Mol Dis.</i> 2002;29: 361-366.
5	Aisen P, Enns C, Wessling-Resnick M. Chemistry and biology of eukaryotic iron metabolism. <i>Int J Biochem Cell Biol.</i> 2001;33:940–959.
6	Allikmets R, Raskind WH, Hutchinson A, et al. Mutation of a putative mitochondrial iron transporter gene (ABC7) in X-linked sideroblastic anaemia and ataxia (XLSA/A). <i>Hum. Mol. Genet.</i> 1999;8:743–49.
7	Anderson GJ <sup>1</sup> , Powell LW, Halliday JW. Transferrin receptor distribution and regulation in the rat small intestine. Effect of iron stores and erythropoiesis. <i>Gastroenterology.</i> 1990 Mar;98(3):576-85.
8	Anderson,G.J., Murphy,T.L., Cowley,L., Evans,B.A., Halliday,J.W. and McLaren,G.D. <i>Genomics.</i> 1998;48, 34–39.
9	Andrews NC. Iron homeostasis: insights from genetics and animal models. <i>Nat Rev Genet.</i> 2000 Dec;1(3):208-17.
10	Andrews NC. ABCs of erythroid mitochondrial iron uptake. <i>Proc Natl Acad Sci U S A.</i> 2009;106(38):16012-3.
11	Arnaudeau S, Frieden M, Nakamura K, Michalak M, Demaurex N. Calreticulin differentially modulates calcium uptake and release in the endoplasmic reticulum and mitochondria. <i>J. Biol. Chem.</i> 2002;277(48):46696-705.

12	Arnau J, Lauritzen C, Petersen GE, Pedersen J. Current strategies for the use of affinity tags and tag removal for the purification of recombinant proteins. <i>Protein Expr Purif.</i> 2006;48(1):1-13.
13	Baksh, S. and Michalak, M. Expression of calreticulin in <i>Escherichia coli</i> and identification of its Ca <sup>2+</sup> binding domains. <i>J. Biol. Chem.</i> 1991;266, 21458–21465.
14	Baksh, S., Burns, K., Andrin, C., and Michalak, M. Interaction of calreticulin with protein disulfide isomerase. <i>J. Biol. Chem.</i> 1995;270, 31338-31344.
15	Balacerzak, S.P. and Greenberg, N.J. Iron content of isolated intestinal epithelial cells in relation to iron absorption. <i>Nature.</i> 1968;220: 270–271.
16	Balusikova K, Neubauerova J, Dostalickova-Cimburova M, Horak J, Kovar J. Differing expression of genes involved in non transferrin iron transport across plasma membrane in various cell types under iron deficiency and excess. <i>Mol Cell Biochem.</i> 2009;321(1-2):123-33.
17	Bannerman, R.M. Genetic defects of iron transport. <i>Fed. Proc.</i> 1976;35,2281–2285.
18	Barton, H.A. et al. Determinant of the interaction between the iron-responsive element-binding protein and its binding site in rat L-ferritin mRNA. <i>J. Biol. Chem.</i> 1990;265:7000–7008.
19	Barrett JC, Fry B, Maller J, Daly MJ. Haploview: analysis and visualization of LD and haplotype maps. <i>Bioinformatics.</i> 2005 Jan 15;21(2):263-5.
20	Beaumont C, Leneuve P, Devaux I, et al. Mutation in the iron responsive element of the L ferritin mRNA in a family with dominant hyperferritinaemia and cataract. <i>Nat. Genet.</i> 1995;11:444–46.
21	Beinert H, Kennedy MC. Aconitase, a two-faced protein: enzyme and iron regulatory factor. <i>FASEB J.</i> 1993;7(15):1442-9.
22	Bella J, Hindle KL, McEwan PA, Lovell SC. The leucine-rich repeat structure. <i>Cell Mol Life Sci.</i> 2008;65(15):2307-33.
23	Berardi, M.J., Shih, W.M., Harrison, S.C., Chou, J.J. Mitochondrial uncoupling protein 2 structure determined by NMR molecular fragment searching. <i>Nature.</i> 2011;476, 109–113.

24	Bertram, J. MATra - Magnet Assisted Transfection: combining nanotechnology and magnetic forces to improve intracellular delivery of nucleic acids. <i>Current Pharmaceutical Biotechnology</i> . 2006;7, 277-28.
25	Betticher DC, Thatcher N, Altermatt HJ, Hoban P, Ryder WD, Heighway J. Alternate splicing produces a novel cyclin D1 transcript. <i>Oncogene</i> . 1995;11(5):1005-11.
26	Bezwoda, W et al. The importance of gastric hydrochloric acid in the absorption of nonhaem food iron. <i>J. Lab. Clin. Med.</i> 1978;92: 108–117.
27	Bothwell, T.H. et al. Nutritional requirement and food iron absorption. <i>J. Int. Med.</i> 1989;226: 357–365.
28	Bourdon E <sup>1</sup> , Kang DK, Ghosh MC, Drake SK, Wey J, Levine RL, Rouault TA. The role of endogenous heme synthesis and degradation domain cysteines in cellular iron-dependent degradation of IRP2. <i>Blood Cells Mol Dis</i> . 2003 Sep-Oct;31(2):247-55.
29	Brasse-Lagnel C, Karim Z, Letteron P, Bekri S, Bado A, Beaumont C. Intestinal DMT1 cotransporter is down-regulated by hepcidin via proteasome internalization and degradation. <i>Gastroenterol</i> . 2011;140:1261–1271.
30	Braun, V. Regulation of iron uptake minimizes iron mediated oxidative stress. <i>J. Biosci</i> . 1998;483–489.
31	Breuer, W., and Cabantchik, Z.I. The importance of non-transferrin bound iron in disorders of iron metabolism. <i>Transf. Sci</i> . 2000;23:185-1.
32	Bridle KR, Frazer DM, Wilkins SJ, Dixon JL, Purdie DM, Crawford DH, Subramaniam VN, Powell LW, Anderson GJ, and Ram GA. Disrupted hepcidin regulation in HFE-associated haemochromatosis and the liver as a regulator of body iron homeostasis. <i>Lancet</i> . 2003;361: 669-673.
33	Brissot, P., T.L. Wright, W.L. Ma, and R.A. Weisinger. Efficient clearance of non-transferrin-bound iron by rat liver in implications for hepatic iron loading in iron overload states. <i>J. Clin. Invest</i> . 1985;76:1463–1470.
34	Brown MA, Stenberg LM, Mauk AG. Identification of catalytically important amino acids in human ceruloplasmin by site-directed mutagenesis. <i>FEBS Lett</i> . 2002;520:8–12.

35	Buyss SS <sup>1</sup> , Martin CB, Eldridge M, Kushner JP, Kaplan J. Iron absorption in hypotransferrinemic mice. <i>Blood</i> . 1991 Dec 15;78(12):3288-90.
36	Cargill M, Altshuler D, Ireland J, Sklar P, Ardlie K, Patil N, Shaw N, Lane CR, Lim EP, Kalyanaraman N, Nemesh J, Ziaugra L, Friedland L, Rolfe A, Warrington J, Lipshutz R, Daley GQ, Lander ES. Characterization of single-nucleotide polymorphisms in coding regions of human genes. <i>Nat Genet</i> . 1999;22(3):231-8.
37	Carpenter, C.E. and Mahoney, A.W. Contributions of haem and nonhaem iron to human nutrition, <i>Crit. Rev. Food Sci. Nutr</i> . 1992;31: 333–367.
38	Casanovas, G., Mleczko-Sanecka, K., Altamura, S., Hentze, M.W., and Muckenthaler, M.U. Bone morphogenetic protein (BMP)-responsive elements located in the proximal and distal hepcidin promoter are critical for its response to HJV/BMP/SMAD. <i>J. Mol. Med</i> . 2009;87, 471–480.
39	Casey, J.L. et al. Iron-responsive elements: regulatory RNA sequences that control mRNA levels and translation. <i>Science</i> . 1988;240: 924–928.
40	Cavill, I. Internal regulation of iron absorption. <i>Nature</i> . 1975;256: 328–330.
41	Cazzola M, et al Mitochondrial ferritin expression in erythroid cells from patients with sideroblastic anaemia. <i>Blood</i> 2003;101:1996–2000.
42	Chant A, C.M. Kraemer-Pecore, R. Watkin, G.G. Kneale. Attachment of a histidine tag to the minimal zinc Wnger protein of the <i>Aspergillus nidulans</i> gene regulatory protein AreA causes a conformational change at the DNA-binding site, <i>Protein Expr. Purif</i> . 2005;152–159.
43	Chaput N, Botton SD, Obeid M, Apetoh L, Ghiringhelli F, Panaretakis T, et al. Molecular determinants of immunogenic cell death: surface exposure of calreticulin makes the difference. <i>J Mol Med</i> . 2007;85:1069–76.
44	Charlton, R.W. and Bothwell, T.H. Iron absorption, <i>Annu. Rev. Med</i> . 1983;34: 55–75.
45	Chen H, Attieh ZK, Su T, Syed BA, Gao H, Alaeddine RM, Fox TC, Usta J, Naylor CE, Evans RW, McKie AT, Anderson GJ, Vulpe CD. 2004. Hephaestin is a

	ferroxidase that maintains partial activity in sex-linked anaemia mice. <i>Blood</i> 103:3933–3939.
46	Cherukuri S, Potla R, Sarkar J, Nurko S, Harris ZL, Fox PL. Unexpected role of ceruloplasmin in intestinal iron absorption. <i>Cell Metab.</i> 2005;2:309–319.
47	Chisari, L. and Izak, G. The effect of acute hemorrhage and acute haemolysis on intestinal iron absorption in the rat, <i>Brit. J. Haematol.</i> 1966;12: 611–622.
48	Chao, M.P. et al. Calreticulin is the dominant pro-phagocytic signal on multiple human cancers and is counterbalanced by CD47. <i>Sci. Transl. Med.</i> 2010;2(63).
49	Chen, H., Attieh, Z. K., Su, T., Syed, B. A., Gao, H., Alaeddine, R. M., et al. Hephaestin is a ferroxidase that maintains partial activity in sex-linked anaemia mice. <i>Blood.</i> 2004;103, 3933–3939.
50	Chen H, Z. Xu, N. Xu, P. Cen. Efficient production of a soluble fusion protein containing human beta-defensin-2 in E. coli cell-free system, <i>J. Biotechnol.</i> 2005;307–315.
51	Chen W, Paradkar PN, Li L, Pierce EL, Langer NB, Takahashi-Makise N, Hyde BB, Shirihai OS, Ward DM, Kaplan J, Paw BH. Abcb10 physically interacts with mitoferrin-1 (Slc25a37) to enhance its stability and function in the erythroid mitochondria. <i>Proc Natl Acad Sci U S A.</i> 2009;106(38):16263-8.
52	Chen W, Dailey HA, Paw BH. Ferrochelatase forms an oligomeric complex with mitoferrin-1 and Abcb10 for erythroid haem biosynthesis. <i>Blood.</i> 2010;116(4):628-30.
53	Chouquet, A. et al. X-ray structure of the human calreticulin globular domain reveals a peptide-binding area and suggests a multimolecular mechanism. <i>PLoS ONE.</i> 2011;6, e17886.
54	Conrad, M.E., Weintraub, L.R., and Crosby, W.H. The role of intestine in iron kinetics, <i>J. Clin. Invest.</i> 1964;43: 963–973.
55	Conrad, M.E. and Schade, S.G. Ascorbic acid chelate in iron absorption: a role for hydrochloric acid and bile. <i>Gastroenterology.</i> 1968;55: 35–45. Conrad ME, Barton JC. Factors affecting iron balance. <i>Am J Hematol.</i> 1981;10(2):199-225.
56	Conrad, M.E., Parmley, R.T., and Osterloh, K. Small intestinal regulation of iron absorption in the rat, <i>J. Lab. Clin. Med.</i> 1987;110: 418–426.

57	Conrad, M.E., J.N. Umbreit, E.G. Moore, R.D.A. Peterson, and M.B. Jones. A newly identified iron binding protein in duodenal mucosa of rats. Purification and characterization of mobilferrin. <i>J. Biol. Chem.</i> 1990;265:5273–5279.
58	Conrad, M.E., Umbreit, J.N., and Moore, E.G. A role for mucin in the absorption of inorganic iron and other metal cations, <i>Gastroenterology.</i> 1991;100: 129–136.
59	Conrad, M.E., J.N. Umbreit, R.D.A. Peterson, E.G. Moore, and K.P. Harper. Function of integrin in duodenal mucosal uptake of iron. <i>Blood.</i> 1993;81:517–521.
60	Conrad, M.E., J.N. Umbreit, E.G. Moore, C. Uzel, and M.R. Berry. Alternative iron transport pathway: Mobilferrin and integrin in K562 cells. <i>J. Biol. Chem.</i> 1994;269:7169–7173.
61	Conrad ME and Umbreit JN. Pathways of iron absorption. <i>Blood Cells Mol Dis.</i> 2002 Nov-Dec;29(3):336-55.
62	Constantine CC, Gurrin LC, McLaren CE, Bahlo M, Anderson GJ, Vulpe CD, Forrest SM, Allen KJ, Gertig DM; HealthIron Investigators. SNP selection for genes of iron metabolism in a study of genetic modifiers of hemochromatosis. <i>BMC Med Genet.</i> 2008;9:18.
63	Cook, J.D. Adaptation in iron metabolism, <i>Am. J. Nutr.</i> 1990;51: 301–319.
64	Corbett, E. F., Oikawa, K., Francois, P., Tessier, D. C., Kay, C., Bergeron, J. J. M., Thomas, D. Y., Krause, K.-H., and Michalak, M. Ca <sup>2+</sup> regulation of interactions between endoplasmic reticulum chaperones. <i>J. Biol. Chem.</i> 1999;274, 6203-6211.
65	Corradini E, Rozier M, Meynard D, Odhiambo A, Lin HY, Feng Q, Migas MC, Britton RS, Babitt JL, Fleming RE. Iron regulation of hepcidin despite attenuated Smad1,5,8 signaling in mice without transferrin receptor 2 or Hfe. <i>Gastroenterol.</i> 2011; 141:1907–1914.
66	Crosby WH. Mucosal block. An evaluation of concepts relating to control of iron absorption. <i>Semin Hematol.</i> 1966;3(4):299-313.
67	Dancourt, J. and Barlowe, C. Protein sorting receptors in the early secretory pathway. <i>Annu. Rev. Biochem.</i> 2010;79, 777–802.
68	David M. Hudson, Michael J. Krisinger, Tanya A.M. Griffiths, and Ross T.A. MacGillivray. Neither Human Hephaestin Nor Ceruloplasmin Forms a Stable

	Complex With Transferrin. <i>Journal of Cellular Biochemistry</i> . 2008;103:1849–1855.
69	Davis, P.S., Luke, C.G., and Deller, D.J. Reduction of gastric iron-binding protein in haemochromatosis. <i>Lancet</i> . 1966;2, 1431–1433.
70	Davis, P.S., Luke, C.G., and Deller, D.J. Gastric iron-binding protein in iron chelation by gastric juice. <i>Nature</i> . 1967;214: 1126–1128.
71	De Domenico I <sup>1</sup> , Ward DM, di Patti MC, Jeong SY, David S, Musci G, Kaplan J. Ferroxidase activity is required for the stability of cell surface ferroportin in cells expressing GPI-ceruloplasmin. <i>EMBO J</i> . 2007a Jun 20;26(12):2823-31.
72	De Domenico I, Ward DM, Langelier C, Vaughn MB, Nemeth E, Sundquist WI, Ganz T, Musci G, Kaplan J. The molecular mechanism of hepcidin-mediated ferroportin down-regulation. <i>Mol Biol Cell</i> . 2007b;18:2569–2578.
73	De Las Rivas J, Fontanillo C. Protein-protein interactions essentials: key concepts to building and analyzing interactome networks. <i>PLoS Comput Biol</i> . 2010;6(6).
74	Del Cid, N. et al. Modes of calreticulin recruitment to the major histocompatibility complex class I assembly pathway. <i>J. Biol. Chem</i> . 2010;285, 4520–4535.
75	De Silva DM, Askwith CC, Eide D, Kaplan J. The FET3 gene product required for high affinity iron transport in yeast is a cell surface ferroxidase. <i>J Biol Chem</i> . 1995;270:1098–1101.
76	de Sousa Abreu R, Penalva LO, Marcotte E, Vogel C. Global signatures of protein and mRNA expression levels. <i>Mol Biosyst</i> . 2009; 5:1512–1526.
77	de Vries, M.N. de Hooge, J.A. Gietema, S. de Jong, C.G. Ferreira et al., Apoptosis: Target of Cancer Therapy. <i>Clin. Cancer Res</i> . 2003;9:12.
78	Dollman, P.R. Iron deficiency in infancy and childhood. <i>Am. J. Clin. Nutr</i> . 1980;33: 86–95.
79	Donovan A, Brownlie A, Zhou Y, Shepard J, Pratt SJ, Moynihan J, Paw BH, Drejer A, Barut B, Zapata A, Law TC, Brugnara C, Lux SE, Pinkus GS, Pinkus JL, Kingsley PD, Palis J, Fleming MD, Andrews NC, Zon LI. Positional cloning of zebrafish ferroportin1 identifies a conserved vertebrate iron exporter. <i>Nature</i> . 2000;403:776–781.

80	Donovan A, Andrews NC. The molecular regulation of iron metabolism. <i>Hematol J.</i> 2004;5:373–380.
81	Donovan A, Lima CA, Pinkus JL, Pinkus GS, Zon LI, Robine S, and Andrews NC. The iron exporter ferroportin (Slc40a1) is essential for iron homeostasis. <i>Cell Metabolism.</i> 2005;1: 191-200.
82	Donovan A, Roy CN, Andrews NC. The ins and outs of iron homeostasis. <i>Physiology (Bethesda).</i> 2006;21:115-23.
83	Drysdale J, Arosio P, Invernizzi R, Cazzola M, Volz A, Corsi B, Biasiotto G, Levi S. Mitochondrial ferritin: a new player in iron metabolism. <i>Blood Cells Mol Dis.</i> 2002;29(3):376-83.
84	Duan J, Wainwright MS, Comeron JM, Saitou N, Sanders AR, Gelernter J, Gejman PV. Synonymous mutations in the human dopamine receptor D2 (DRD2) affect mRNA stability and synthesis of the receptor. <i>Hum Mol Genet.</i> 2003;12(3):205-16.
85	Duus, K. et al. Interaction of the chaperone calreticulin with proteins and peptides of different structural classes. <i>Protein Pept. Lett.</i> 2009;16, 1414–1423.
86	Edwards JA and Bannerman RM. Hereditary defect of intestinal iron transport in mice with sex-linked anaemia. <i>J Clin Invest.</i> 1970;49: 1869–1871.
87	Edwards, J.A., Hoke, J.E., Mattioli, M. & Reichlin, M. Ferritin distribution and synthesis in sex-linked anaemia. <i>J. Lab. Clin. Med.</i> 1977;90,68–76.
88	Eggleton P, Reid KB, Kishore U, Sontheimer RD. Clinical relevance of calreticulin in systemic lupus erythematosus. <i>Lupus.</i> 1997;6(7):564-71.
89	Eggleton P, Llewellyn DH. Pathophysiological roles of calreticulin in autoimmune disease. <i>Scand J Immunol.</i> 1999 May;49(5):466-73.
90	Ellgaard, L. et al. NMR structure of the calreticulin P domain. <i>Proc. Natl. Acad. Sci. U.S.A.</i> 2001;98, 3133–3138.
91	Ellgaard, L., Riek, R., Braun, D., Hermann, T., Helenius, A., and Wuthrich, K. Three-dimensional structure topology of the calreticulin P-domain based on NMR assignment. <i>FEBS Lett.</i> 2001;488, 69-73.
92	Ellgaard L, Helenius A. Quality control in the endoplasmic reticulum. <i>Nat Rev Mol Cell Biol.</i> 2003 Mar;4(3):181-91.

93	Eisenstein RS. Iron regulatory proteins and the molecular control of mammalian iron metabolism. <i>Annu Rev Nutr.</i> 2000;20:627-62.
94	Espósito, B.P., Epsztejn, S. Breuer, W. Cabantchik, Z.I. A review of fluorescence methods for assessing labile iron in cells and biological fluids. <i>Anal. Biochem.</i> 2002;1;304(1):1-18.
95	Fairweather-Tait SJ, Harvey L, Heath AL, Roe M. Effect of SNPs on iron metabolism. <i>Genes Nutr.</i> 2007;2(1):15-9.
96	Feder JN, Gnirke A, Thomas W, et al. A novel MHC class I-like gene is mutated in patients with hereditary haemochromatosis. <i>Nat. Genet.</i> 1996;13:399–408.
97	Feder JN, Penny DM, Irrinki A, et al. The hemochromatosis gene product complexes with the transferrin receptor and lowers its affinity for ligand binding. <i>Proc. Natl. Acad. Sci. USA.</i> 1998;95:1472–77.
98	Feig A L and Lippard S J. Reactions of non-heme iron(II) centers with dioxygen in biology and chemistry. <i>Chem. Rev.</i> 1994;94(3), pp 759–805.
99	Felgner PL et al. Lipofection: a highly efficient, lipid-mediated DNA-transfection procedure. <i>Proc Natl Acad Sci U S A.</i> 1987;84: 7413-7417.
100	Fiermonte, G., Dolce, V., Arrigoni, R., Runswick, M.J., Walker, J.E., Palmieri, F., 1999. Organization and sequence of the gene for the human mitochondrial dicarboxylate carrier: evolution of the carrier family. <i>Biochem. J.</i> 1999;344, 953–960.
101	Finberg KE, Heeney MM, Campagna DR, Aydinok Y, Pearson HA, Hartman KR, et al. Mutations in <i>Tmprss6</i> cause iron-refractory iron deficiency anaemia (IRIDA). <i>Nat Genet</i> 2008;40:569-71.
102	Finberg, K.E., Whittlesey, R.L., Fleming, M.D., and Andrews, N.C. Downregulation of Bmp/Smad signaling by <i>Tmprss6</i> is required for maintenance of systemic iron homeostasis. <i>Blood.</i> 2010;15, 3817–3826.
103	Finch, C.A. Erythropoiesis, erythropoietin, and iron. <i>Blood.</i> 1982;60: 1241–1246.
104	Flanaghan, P.R. Mechanisms and regulation of intestinal uptake and transfer of iron. <i>Acta Pediatr. Scand.</i> , suppl. 1989;361: 21–31.
105	Fleming MD, Trenor CC, 3rd Su MA, Foernzler D, Beier DR, Dietrich WF, and Andrews NC. Microcytic anaemia mice have a mutation in <i>Nramp2</i> , a candidate iron transporter gene. <i>Nat Genet.</i> 1997;16: 383-386.

106	Fleming, R.E. Hecpidin activation during inflammation: make it STAT. <i>Gastroenterology</i> . 2007;132, 447–449.
107	Fliegel, L., Burns, K., MacLennan, D. H., Reithmeier, R. A. F., and Michalak, M. Molecular cloning of the high affinity calcium-binding protein (calreticulin) of skeletal muscle sarcoplasmic reticulum. <i>J. Biol. Chem.</i> 1989;264, 21522-21528.
108	Fonda, M. Kenig, V. Gaberc-Porekar, P. Pristovaek, V. Menart. Attachment of histidine tags to recombinant tumor necrosis factoralpha drastically changes its properties, <i>Sci. World J.</i> 2002;1312–1325.
109	Foury F and Roganti T. Deletion of the mitochondrial carrier genes MRS3 and MRS4 suppresses mitochondrial iron accumulation in a yeast frataxin-deficient strain. <i>J Biol Chem.</i> 2002;277:24475–24483.
110	Frazer DM, Vulpe CD, McKie AT, Wilkins SJ, Trinder D, Cleghorn GJ, Anderson GJ. Cloning and gastrointestinal expression of rat hephaestin: relationship to other iron transport proteins. <i>Am J Physiol Gastrointest Liver Physiol.</i> 2001;281(4):G931-9.
111	Frazer DM, Wilkins SJ, Becker EM, Murphy TL, Vulpe CD, McKie AT, Anderson GJ. A rapid decrease in the expression of DMT1 and Dcytb but not Ireg1 or hephaestin explains the mucosal block phenomenon of iron absorption. <i>Gut.</i> 2003;52(3):340-6.
112	Frazer DM, Anderson GJ. Iron imports. I. Intestinal iron absorption and its regulation. <i>Am J Physiol Gastrointest Liver Physiol.</i> 2005;289(4):G631-5.
113	Frieden E and Hsieh HS. The biological role of ceruloplasmin and its oxidase activity. <i>Adv Exp Med Biol.</i> 1976;74:505-29.
114	Galy B, Ferring-Appel D, Kaden S, Gröne HJ, Hentze MW. Iron regulatory proteins are essential for intestinal function and control key iron absorption molecules in the duodenum. <i>Cell Metab.</i> 2008;7(1):79-85.
115	Gambling L, Danzeisen R, Gair S, et al. Effect of iron deficiency on placental transfer of iron and expression of iron transport proteins in vivo and in vitro. <i>Biochem J.</i> 2001;356: 883–889.
116	Ganz, T. Hecpidin, a key regulator of iron metabolism and mediator of anaemia of inflammation. <i>Blood.</i> 2003;783–788.

117	Gao, B. et al. Assembly and antigen-presenting function of MHC class I molecules in cells lacking the ER chaperone calreticulin. <i>Immunity</i> . 2002; 16, 99–109.
118	Gardai, S.J. et al. Cell-surface calreticulin initiates clearance of viable or apoptotic cells through trans-activation of LRP on the phagocyte. <i>Cell</i> . 2005;123, 321–334.
119	Giot L, Bader JS, Brouwer C, Chaudhuri A, Kuang B, Li Y, Rothberg JM et al. A protein interaction map of <i>Drosophila melanogaster</i> . <i>Science</i> . 2003;302(5651):1727-36.
120	Girelli D, Corrocher R, Bisceglia L, et al. Hereditary hyperferritinemia-cataract syndrome caused by a 29-base pair deletion in the iron responsive element of ferritin L-subunit gene. <i>Blood</i> . 1997;90:2084–88.
121	Gitlin D and Cruchoad A. On the kinetics of iron absorption in mice. <i>J Clin Invest</i> . 1962;41: 344-350.
122	Glahn, R.P. and Van Campen, D.R. Iron uptake is enhanced in Caco-2 cell monolayers by cysteine and reduced cysteinyl glycine. <i>J. Nutr</i> . 1997;127: 642–647.
123	Gleeson F, Ryan E, Barrett S, Russell J, Kelleher B, Crowe J. Duodenal Dcytb and hephaestin mRNA expression are not significantly modulated by variations in body iron homeostasis. <i>Blood Cells Mol Dis</i> . 2005;35(3):303-8.
124	Glickstein, H, Ben El , R., Shvartsman M. and and Z. loav Cabantchik. Intracellular labile iron pools as direct targets of iron chelators. A fluorescence study of chelator action in living cells. <i>Blood</i> . 2005;106: 3242-3250.
125	Goddard, W.P. et al. Iron uptake by isolated human enterocyte suspensions in vitro is dependent on body iron stores and inhibited by other metal cations, <i>J. Nutr.</i> . 1997;127: 177–183.
126	Goel A, D. Colcher, J.S. Koo, B.J. Booth, G. Pavlinkova, S.K. Batra. Relative position of the hexahistidine tag eVects binding properties of a tumor-associated single-chain Fv construct, <i>Biochim. Biophys. Acta</i> . 2000;13–20.
127	Gold LI, Eggleton P, Sweetwyne MT, Van Duyn LB, Greives MR, Naylor SM, et al. Calreticulin: non-endoplasmic reticulum functions in physiology and disease. <i>FASEB J</i> . 2010;24:665–83.

128	Granick, S. Iron metabolism. Bull. N.Y. Acad. Med. 1954;30: 81–101.
129	Green, R., Charlton, R., and Seftel, H. Body iron excretion in man. A collaborative study, Am. J. Med. 1968;45: 336–353.
130	Grewal MD. A sex-linked anaemia in the mouse. Genet Res. 1962;3: 238–247.
131	Griffiths TA, Mauk AG and MacGillivray RTA. Recombinant expression and functional characterization of human hephaestin: A multicopper oxidase with ferroxidase activity. Biochemistry. 2005;44:14725–14731.
132	Gruenheid S, Cellier M, Vidal S, and Gros P. Identification and characterization of a second mouse Nramp gene. Genomics. 1995;25: 514-525.
133	Gunshin H, Mackenzie B, Berger UV, Gunshin Y, Romero MF, Boron WF, Nussberger S, Gollan JL, and Hediger MA. Cloning and characterization of a mammalian proton-coupled metal-ion transporter. Nature. 1997;388: 482-488.
134	Gunshin H, Allerson CR, Polycarpou-Schwarz M, Rofts A, Rogers JT, Kishi F, Hentze MW, Rouault TA, Andrews NC, Hediger MA. Iron-dependent regulation of the divalent metal ion transporter. FEBS Lett. 2001 Dec 7;509(2):309-16.
135	Gunshin H, Starr CN, Drenzo C, Fleming MD, Jin J, Greer EL, Sellers VM, Galica SM, and Andrews NC. Cybrd1 (duodenal cytochrome b) is not necessary for dietary iron absorption in mice. Blood. 2005;106: 2879-2883.
136	Guo, B. et al. Characterization and expression of iron regulatory protein 2 (IRP2), J. Biol. Chem. 1995;270: 16529–16535.
137	Guo B <sup>1</sup> , Yu Y, Leibold EA. Iron regulates cytoplasmic levels of a novel iron-responsive element-binding protein without aconitase activity. J Biol Chem. 1994 Sep 30;269(39):24252-60.
138	Guo, L. et al. Cardiac-specific expression of calcineurin reverses embryonic lethality in calreticulin-deficient mouse. J. Biol. Chem. 2002;277, 50776–50779.
139	Hahn, P.F. Radioactive iron and its metabolism in anaemia. J. Exp. Med. 1941;74: 197–209.
140	Hahn, P.E. et al. Iron metabolism in early pregnancy as studied with radioactive isotope <sup>59</sup> Fe, Am. J. Obstet. Gynecol. 1951;61: 477–486.
141	Haile, D.J. et al. Regulation of interaction of the iron-responsive element binding protein with iron-responsive elements, Mol. Cell. Biol. 1989;9: 5055–5061.

142	Haile, D.J, T.A. Rouault, J.B. Harford, M.C. Kennedy, G.A. Blondin, H. Beinert, R.D. Klausner, Cellular regulation of the iron-responsive element binding protein: disassembly of the cubane iron–sulfur cluster results in high-affinity RNA binding, <i>Proc. Natl. Acad. Sci. U. S. A.</i> 1992;11735–11739.
143	Hallberg, L. et al. Menstrual blood loss: a population study. Variation at different ages and attempts to define normality. <i>Acta Obstet. Gynecol. Scand.</i> 1966;45: 320–351.
144	Hallberg, L., Bioavailability of dietary iron in man. <i>Annu. Rev. Nutr.</i> 1981;1: 123–161.
145	Hallberg, L. and Rossander-Hulten, L. Iron requirements in menstruating women. <i>Am. J. Clin. Nutr.</i> 1991;54: 1047–1058.
146	Han, O. et al. Reduction of Fe (III) is required for uptake of nonhaem iron by Caco-2 cells. <i>J. Nutr.</i> 1995;125: 1291–1299.
147	Han O, Kim E-Y. Colocalization of ferroportin-1 with hephaestin on the basolateral membrane of human intestinal absorptive cells. <i>J Cell Biochem.</i> 2007;101:1000–1010.
148	Hanson ES <sup>1</sup> , Rawlins ML, Leibold EA. Oxygen and iron regulation of iron regulatory protein 2. <i>J Biol Chem.</i> 2003 Oct 10;278(41):40337-42.
149	Harris ZL, Takahashi Y, Miyajima H, et al. Aceruloplasminemia: molecular characterization of this disorder of iron metabolism. <i>Proc. Natl. Acad. Sci.USA.</i> 1995;92:2539–43.
150	Harris ZL, Durley AP, Man TK, Gitlin JD. Targeted gene disruption reveals an essential role for ceruloplasmin in cellular iron efflux. <i>Proc. Natl. Acad. Sci.</i> 1999;96: 10812–10817.
151	Hazell, T., Ledwaed, D.A., and Neale, R.J. Iron binding from meat. <i>Brit. J. Nutr.</i> 1978;39: 631–640.
152	Helms C, Cao L, Krueger JG, Wijsman EM, Chamian F, Gordon D, Heffernan M, Daw JA, Robarge J, Ott J, Kwok PY, Menter A, Bowcock AM. A putative RUNX1 binding site variant between SLC9A3R1 and NAT9 is associated with susceptibility to psoriasis. <i>Nat Genet.</i> 2003;35(4):349-56.

153	Hendrickson SL, Hutcheson HB, Ruiz-Pesini E, Poole JC, Lautenberger J, et al. Mitochondrial DNA haplogroups influence AIDS progression. <i>AIDS</i> . 2008;22: 2429–2439.
154	Hentze, M.W. and Argos, P. Homology between IRE-BP, a regulatory RNA-binding protein, aconitase and isopropylmalate isomerase. <i>Nucleic Acid Res</i> . 1991;19: 1739–1740.
155	Hentze MW, Muckenthaler MU, Galy B, Camaschella C. Two to tango: regulation of Mammalian iron metabolism. <i>Cell</i> . 2010; 142:24–38.
156	Howe, C. et al. Calreticulin-dependent recycling in the early secretory pathway mediates optimal peptide loading of MHC class I molecules. <i>EMBO J</i> . 2009;28, 3730–3744.
157	Huang FW, Rubio-Aliaga I, Kushner JP, Andrews NC, and Fleming MD. Identification of a novel mutation (C321X) in HJV. <i>Blood</i> . 2004;104: 2176-2177.
158	Huang FW, Pinkus JL, Pinkus GS, Fleming MD, and Andrews NC. A mouse model of juvenile hemochromatosis. <i>J Clin Invest</i> . 2005;115: 2187-2191.
159	Huang, H., Constante, M., Layoun, A., and Santos, M.M. Contribution of STAT3 and SMAD4 pathways to the regulation of hepcidin by opposing stimuli. <i>Blood</i> . 2009a;113, 3593–3599.
160	Hughson EJ <sup>1</sup> and Hopkins CR. Endocytic pathways in polarized Caco-2 cells: identification of an endosomal compartment accessible from both apical and basolateral surfaces. <i>J Cell Biol</i> . 1990 Feb;110(2):337-48.
161	Ihara Y, Kageyama K, Kondo T. Overexpression of calreticulin sensitizes SERCA2a to oxidative stress. <i>Biochem Biophys Res Commun</i> . 2005;329(4):1343-9.
162	Ihara Y, Urata Y, Goto S, Kondo T. Role of calreticulin in the sensitivity of myocardial H9c2 cells to oxidative stress caused by hydrogen peroxide. <i>Am J Physiol Cell Physiol</i> . 2006;290(1):C208-21.
163	International Nutritional Anaemia Consultative Group. Iron Deficiency in Women, Washington, Nutrition Foundation. 1981;1–68.
164	International HapMap Consortium. The International HapMap Project. <i>Nature</i> . 2003 Dec 18;426(6968):789-96.

165	Iolascon A, Camaschella C, Pospisilova D, Piscopo C, Tchernia G, Beaumont C. Natural history of recessive inheritance of DMT1 mutations. <i>J Pediatr.</i> 2008;152:136-9.
166	Isobe K, Isobe Y, Sakurami T. Cytochemical demonstration of transferrin in the mitochondria of immature human erythroid cells. <i>Acta Haematol.</i> 1981;65:2–9.
167	Jacob L, Roznowski AB, Houen G et al. Evidence for human calreticulin (CRT) as an autoantigen specifically recognized by peripheral blood T cells of non-immunosuppressed patients with rheumatoid arthritis (RA) and other arthritic diseases. <i>Arthritis Rheum.</i> 1997;40:S197.
168	Jeffery, E. et al. The polypeptide binding conformation of calreticulin facilitates its cell surface expression under conditions of ER stress. <i>J. Biol. Chem.</i> 2011;286, 2402–2415.
169	Jenkins ZA, Hagar W, Bowlus CL, Johansson HE, Harmatz P, Vichinsky EP, Theil EC. Iron homeostasis during transfusional iron overload in beta-thalassemia and sickle cell disease: changes in iron regulatory protein, hepcidin, and ferritin expression. <i>Pediatr Hematol Oncol.</i> 2007;24(4):237-43.
170	Jeong SY, David S. GPI-anchored ceruloplasmin is required for iron efflux from cells in the central nervous system. <i>J Biol Chem.</i> 2003;278,27144–27148.
171	Johnson, G., Jacobs, P., and Purves, L.R. Iron-binding proteins of iron-absorbing rat intestinal mucosa. <i>J. Clin. Invest.</i> 1983;71: 1467–1476.
172	Johnson GC, Esposito L, Barratt BJ, Smith AN, Heward J, Di Genova G, Ueda H, Cordell HJ, Eaves IA, Dudbridge F, Twells RC, Payne F, Hughes W, Nutland S, Stevens H, Carr P, Tuomilehto-Wolf E, Tuomilehto J, Gough SC, Clayton DG, Todd JA. Haplotype tagging for the identification of common disease genes. <i>Nat Genet.</i> 2001;29(2):233-7.
173	Kageyama K, Ihara Y, Goto S, Urata Y, Toda G, Yano K, Kondo T. Overexpression of calreticulin modulates protein kinase B/Akt signaling to promote apoptosis during cardiac differentiation of cardiomyoblast H9c2 cells. <i>J. Biol. Chem.</i> 2002;277(22):19255-64.
174	Kaplan, J., I. Jordan, and A. Sturrock. Regulation of the transferrin-independent iron transport system in cultured cells. <i>J. Biol. Chem.</i> 1991;266:2997–3004.
175	Kawabata H, Fleming RE, Gui D, Moon SY, Saitoh T, O’Kelly J, Umehara Y, Wano Y, Said JW, and Koeffler HP. Expression of hepcidin is down-regulated in

	TfR2 mutant mice manifesting a phenotype of hereditary hemochromatosis. <i>Blood</i> . 2005;105:376-381.
176	Keskin O, Gursoy A, Ma B, Nussinov R. Principles of protein-protein interactions: what are the preferred ways for proteins to interact? <i>Chem Rev</i> . 2008;108(4):1225-44.
177	Kelleher SL, Lönnerdal B. Zinc supplementation reduces iron absorption through age-dependent changes in small intestine iron transporter expression in suckling rat pups. <i>J Nutr</i> . 2006;136: 1185–1191.
178	Kepp, O. et al. Molecular determinants of immunogenic cell death elicited by anticancer chemotherapy. <i>Cancer Metastasis Rev</i> . 2011;30, 61–69.
179	Khanna, N. C., Tokuda, M., and Waisman, D. M. Conformational changes induced by binding of divalent cations to calregulin. <i>J. Biol. Chem</i> . 1986;261, 8883-8887.
180	Khanna, N. C., Tokuda, M., and Waisman, D. M. Comparison of calregulins from vertebrate livers. <i>Biochem. J</i> . 1987;242, 245-251.
181	Klerkx AH, Tanck MW, Kastelein JJ, Molhuizen HO, Jukema JW, Zwinderman AH, Kuivenhoven JA. Haplotype analysis of the CETP gene: not TaqIB, but the closely linked -629C-->A polymorphism and a novel promoter variant are independently associated with CETP concentration. <i>Hum Mol Genet</i> . 2003;12(2):111-23.
182	Kou G, Shi S, Wang H, Tan M, Xue J, Zhang D, Hou S, Qian W, Wang S, Dai J, Li B, Guo Y. Preparation and characterization of recombinant protein ScFv(CD11c)-TRP2 for tumor therapy from inclusion bodies in <i>Escherichia coli</i> . <i>Protein Expr Purif</i> . 2007;52(1):131-8.
183	Kovar J, Neubauerova J, Cimburova M, Truksa J, Balusikova K, Horak J. Stimulation of non-transferrin iron uptake by iron deprivation in K562 cells. <i>Blood Cells Mol Dis</i> . 2006;37(2):95-9.
184	Kozlov, G. et al. Structural basis of carbohydrate recognition by calreticulin. <i>J. Biol. Chem</i> . 2010;285, 38612–38620.
185	Krause A, Neitz S, Magert HJ, Schulz A, Forssmann WG, Schulz-Knappe P, and Adermann K. LEAP-1, a novel highly disulfide-bonded human peptide, exhibits antimicrobial activity. <i>FEBS Lett</i> . 2000;480: 147-150.

186	Kruglyak L, Nickerson DA. Variation is the spice of life. <i>Nat Genet.</i> 2001;27(3):234-6.
187	Kuo YM, Su T, Chen H, Attieh Z, Syed BA, McKie AT, Anderson GJ, Gitschier J, Vulpe CD. Mislocalisation of hephaestin, a multicopper ferroxidase involved in basolateral intestinal iron transport, in the sex linked anaemia mouse. <i>Gut.</i> 2004;53:201–206.
188	Kurtz DM Jr. Oxygen-carrying proteins: three solutions to a common problem. <i>Essays Biochem.</i> 1999;34:85-100.
189	Laitinen OH, Hytönen VP, Nordlund HR, Kulomaa MS. Genetically engineered avidins and streptavidins. <i>Cell Mol Life Sci.</i> 2006;63(24):2992-3017.
190	Lange H, Kispal G, Lill R. Mechanism of iron transport to the site of haem synthesis inside yeast mitochondria. <i>J Biol Chem.</i> 1999 Jul 2;274(27):18989-96.
191	LaVaute T <sup>1</sup> , Smith S, Cooperman S, Iwai K, Land W, Meyron-Holtz E, Drake SK, Miller G, Abu-Asab M, Switzer R 3rd, Grinberg A, Love P, Tresser N, Rouault TA. Targeted deletion of the gene encoding iron regulatory protein-2 causes misregulation of iron metabolism and neurodegenerative disease in mice. <i>Nat Genet.</i> 2001 Feb;27(2):209-14.
192	Lawen A and Lane DJ. Mammalian iron homeostasis in health and disease: uptake, storage, transport, and molecular mechanisms of action. <i>Antioxid Redox Signal.</i> 2013;18(18):2473-507.
193	Layer G, Jahn D and Jahn M. Haem biosynthesis. In: <i>Handbook of Porphyrin Science with Applications to Chemistry, Physics, Material Science, Engineering, Biology and Medicine.</i> 2011;Vol 15,pp. 159-215.
194	Lee GR, Cartwright GE, Wintrobe MM. Heme biosynthesis in copper deficient swine. <i>Proc Soc Exp Biol Med.</i> 1968 Apr;127(4):977-81.
195	Lee, D.G., Lee, J.H., Choi, B.K., Kim, M.J., Kim, S.M., Kim, K.S., Chang, K., Park, S.H., Bae, Y.S., Kwon, B.S. H(+)-Myo-Inositol Transporter SLC2A13 as a Potential Marker for Cancer Stem Cells in an Oral Squamous Cell Carcinoma. <i>Curr. Cancer Drug Targets.</i> 2011.

196	Leibold, E.A, H.N. Munro, Cytoplasmic protein binds in vitro to a conserved sequence in the 5' untranslated region of ferritin H- and L-chain mRNAs, Proc. Natl. Acad. Sci. 1988; 2171–2175.
197	Levi S, et al. A human mitochondrial ferritin encoded by an intronless gene. J Biol Chem. 2001;276:24437–24440.
198	Li, L., Vulpe, C. D., and Kaplan, J. Functional studies of hephaestin in yeast: Evidence for multicopper oxidase activity in the endocytic pathway. Biochemical Journal. 2003;375, 793–798.
199	Lill R, Mühlenhoff U. Maturation of iron-sulfur proteins in eukaryotes: Mechanisms, connected processes, and diseases. Annu Rev Biochem. 2008;77:669–700.
200	Lindley PF, Card G, Zaitseva I, Zaitsev V, Reinhammar B, Selin-Lindgren E, Yoshida K. An X-ray structural study of human ceruloplasmin in relation to ferroxidase activity. J Biol Inorg Chem. 1997;2:454–463.
201	Lin L, Goldberg YP, and Ganz T. Competitive regulation of hepcidin mRNA by soluble and cell-associated hemojuvelin. Blood 2005;106: 2884-2889.
202	Liu, H., Takano, T., Abernathy, J., Wang, S., Sha, Z., Jiang, Y., Terhune, J., Kucuktas, H., Peatman, E., Liu, Z. Structure and expression of transferrin gene of channel catfish, <i>Ictalurus punctatus</i> . Fish Shellfish Immunol. 2010a;28(1), 159–166.
203	Liu H, Peatman E, Wang W, Abernathy J, Liu S, Kucuktas H, Lu J, Xu DH, Klesius P, Waldbieser G, Liu Z. Molecular responses of calreticulin genes to iron overload and bacterial challenge in channel catfish ( <i>Ictalurus punctatus</i> ). Dev Comp Immunol. 2011;35(3):267-72.
204	Livak KJ <sup>1</sup> and Schmittgen TD. Analysis of relative gene expression data using real-time quantitative PCR and the 2(-Delta Delta C(T)) Method. Methods. 2001;25(4):402-8.
205	Lynch JM, Chilibeck K, Qui Y, Michalak M. Assembling pieces of the cardiac puzzle; calreticulin and calcium-dependent pathways in cardiac development, health, and disease. Trends Cardiovasc Med. 2006;16(3):65-9.
206	Mackenzie B, Garrick MD. Iron Imports. II. Iron uptake at the apical membrane in the intestine. Am J Physiol Gastrointest Liver Physiol. 2005;289:G981–G986.

207	Manis, J.G. and Schachter, D. Active transport of iron by intestine: features of twostep mechanism. <i>Am. J. Physiol.</i> 1962;203: 73–80.
208	Manis, J. Active transport of iron by intestine: selective genetic defect in the mouse. <i>Nature.</i> 1970;227,385–386.
209	Maier T, Guell M, Serrano L. Correlation of mRNA and protein in complex biological samples. <i>FEBS Lett.</i> 2009; 583:3966–3973.
210	Meyer LA <sup>1</sup> , Durley AP, Prohaska JR, Harris ZL. Copper transport and metabolism are normal in aceruloplasminemic mice. <i>J Biol Chem.</i> 2001 Sep 28;276(39):36857-61.
211	Mayer A, S.K. Sharma, B. Tolner, N.P. Minton, D. Purdy, P. Amlot, G. Tharakan, R.H.J. Begent, K.A. Chester. Modifying an immunogenic epitope on a therapeutic protein: a step towards an improved system for antibody-directed enzyme prodrug therapy (ADEPT), <i>Br.J. Cancer.</i> 2004;2402–2410.
212	Mariani R, Trombini P, Pozzi M, Piperno A. Iron metabolism in thalassemia and sickle cell disease. <i>Mediterr J Hematol Infect Dis.</i> 2009;1(1).
213	McArdle HJ, Andersen HS, Jones H, Gambling L. Copper and iron transport across the placenta: regulation and interactions. <i>J Neuroendocrinol.</i> 2008; 20: 427–431.
214	McCauliffe, D. P., Lux, F. A., Lieu, T.-S., Sanz, I., Hanke, J., Newkirk, M. M., Bachinski, L. L., Itoh, Y., Siciliano, M. J., Reichlin, M., Sontheimer, R. D., and Capra, J. D. Molecular cloning, expression, and chromosome 19 localization of a human Ro/SS-A autoantigen. <i>J.Clin. Invest.</i> 1990;85, 1379-1391.
215	McKie AT, Marciani P, Rolfs A, Brennan K, Wehr K, Barrow D, Miret S, Bomford A, Peters TJ, Farzaneh F, Hediger MA, Hentze MW, Simpson RJ. A novel duodenal iron-regulated transporter, IREG1, implicated in the basolateral transfer of iron to the circulation. <i>Mol Cell.</i> 2000;5:299–309.
216	Menotti, E., Henderson, B.R., and Kuhn, L.C. Translational regulation of mRNAs with distinct IRE sequences by iron regulatory proteins 1 and 2. <i>J. Biol. Chem.</i> 1998;273:1821–1824.

217	Mesaeli N, Nakamura K, Zvaritch E, Dickie P, Dziak E, Krause KH, Opas M, MacLennan DH, Michalak M. Calreticulin is essential for cardiac development. <i>J Cell Biol.</i> 1999 Mar 8;144(5):857-68.
218	Michalak, M., Milner, R.E., Burns, K., and Opas, M. Calreticulin. <i>Biochem. J.</i> 1992;285, 681–692.
219	Michalak, M. Calreticulin. R. G. Landes Co., Austin. 1996.
220	Michalak M, Robert Parker JM, Opas M. Ca <sup>2+</sup> signaling and calcium binding chaperones of the endoplasmic reticulum. <i>Cell Calcium.</i> 2002 Nov-Dec;32(5-6):269-78.
221	Mitsuhashi N, et al. MTABC3, a novel mitochondrial ATP-binding cassette protein involved in iron homeostasis. <i>J Biol Chem.</i> 2000;275:17536–17540.
222	Muckenthaler M, Roy CN, Custodio AO, Minana B, deGraaf J, Montross LK, Andrews NC, and Hentze MW. Regulatory defects in liver and intestine implicate abnormal hepcidin and Cybrd1 expression in mouse hemochromatosis. <i>Nat Genet.</i> 2003;34: 102-107.
223	Muir, W.A., U. Hopfer, and M. King. Iron transport across brushborder membranes from normal and iron-deficient mouse upper small intestine. <i>J. Biol. Chem.</i> 1984;259:4846–4903.
224	Mullner, E.W., Neupert, B., and Kuhn, L.C. A specific mRNA binding factor regulates the iron-dependent stability of cytoplasmic transferrin receptor mRNA. <i>Cell.</i> 1989;58:373–382.
225	Multani, J.S. et al. Biochemical characterization of gastroferrin, <i>Biochemistry.</i> 1970;9: 3970–3976.
226	Nakamura K, Bossy-Wetzel E, Burns K, Fadel MP, Lozyk M, Goping IS, Opas M, Bleackley RC, Green DR, Michalak M. Changes in endoplasmic reticulum luminal environment affect cell sensitivity to apoptosis. <i>J Cell Biol.</i> 2000;150(4):731-40.
227	Nakamura K, Zuppini A, Arnaudeau S, Lynch J, Ahsan I, Krause R, Papp S, De Smedt H, Parys JB, Muller-Esterl W, Lew DP, Krause KH, Demaurex N, Opas M, Michalak M. Functional specialization of calreticulin domains. <i>J Cell Biol.</i> 2001a;154(5):961-72.
228	Nakamura K, Zuppini A, Arnaudeau S, Lynch J, Ahsan I, Krause R, Papp S, De Smedt H, Parys JB, Muller-Esterl W, Lew DP, Krause KH, Demaurex N, Opas

	M, Michalak M. Functional specialization of calreticulin domains. <i>J Cell Biol.</i> 2001b;154(5):961-72.
229	Nancy C. Andrews. Iron metabolism and absorption. <i>Reviews in Clinical and Experimental Hematology.</i> 2000;Volume 4, Issue 4, pages 283–301.
230	Nanney LB, Woodrell CD, Greives MR, Cardwell NL, Pollins AC, Bancroft TA, et al. Calreticulin enhances porcine wound repair by diverse biological effects. <i>Am J Pathol.</i> 2008;173:610–30.
231	Napier I, Ponka P, Richardson DR. Iron trafficking in the mitochondrion: Novel pathways revealed by disease. <i>Blood.</i> 2005;105:1867–1874.
232	Nemeth E, Tuttle MS, Powelson J, Vaughn MB, Donovan A, Ward DM, Ganz T, and Kaplan J. Heparin regulates cellular iron efflux by binding to ferroportin and inducing its internalization. <i>Science.</i> 2004;306: 2090-2093.
233	Nemeth E, Tuttle MS, Powelson J, Vaughn MB, Donovan A, Ward DM, Ganz T, and Kaplan J. Heparin regulates cellular iron efflux by binding to ferroportin and inducing its internalization. <i>Science.</i> 2004;306: 2090-2093.
234	Nemeth E, Roetto A, Garozzo G, Ganz T, and Camaschella C. Heparin is decreased in TFR2 hemochromatosis. <i>Blood.</i> 2005;105: 1803-1806.
235	Nicolas G, Bennoun M, Devaux I, Beaumont C, Grandchamp B, Kahn A, and Vaulont S. Lack of hepcidin gene expression and severe tissue iron overload in upstream stimulatory factor 2 (USF2) knockout mice. <i>Proc Natl Acad Sci.</i> 2001;98: 8780-8785.
236	Nicolas G, Chauvet C, Viatte L, Danan JL, Bigard X, Devaux I, Beaumont C, Kahn A, and Vaulont S. The gene encoding the iron regulatory peptide hepcidin is regulated by anaemia, hypoxia, and inflammation. <i>J Clin Invest.</i> 2002;110: 1037-1044.
237	Nie G, Sheftel AD, Kim SF, Ponka P. Overexpression of mitochondrial ferritin causes cytosolic iron depletion and changes cellular iron homeostasis. <i>Blood.</i> 2005;105:2161–2167.

238	Niederkofler V, Salie R, and Arber S. Hemojuvelin is essential for dietary iron sensing, and its mutation leads to severe iron overload. <i>J Clin Invest.</i> 2005;115: 2180-2186.
239	Nunez, M.T., Osorio, A., Tapia, V., Vergara, A., Mura, C.V. Iron-induced oxidative stress up-regulates calreticulin levels in intestinal epithelial (Caco-2) cells. <i>J. Cell Biochem.</i> 2001;82 (4), 660–665.
240	Obeid M, Tesniere A, Ghiringhelli F, Fimia GM, Apetoh L, Perfettini JL, et al. Calreticulin exposure dictates the immunogenicity of cancer cell death. <i>Nat Med.</i> 2007;13:54–62.
241	Oliveira, S.J., Pinto, J.P., Picarote, G., Costa, V.M., Carvalho, F., Rangel, M., de Sousa, M., and de Almeida, S.F. ER stress-inducible factor CHOP affects the expression of hepcidin by modulating C/EBPalpha activity. <i>PLoS ONE.</i> 2009;4, e6618.
242	Osaki S, Johnson DA, Frieden E. The mobilization of iron from the perfused mammalian liver by a serum copper enzyme, ferroxidase I. <i>J Biol Chem.</i> 1971;246:3018–3023.
243	Ostwald, T. J., and MacLennan, D. H. Isolation of a high affinity calcium-binding protein from sarcoplasmic reticulum. <i>J. Biol. Chem.</i> 1974;249, 974-979.
244	Ostwald, T. J., MacLennan, D. H., and Dorrington, K. J. Effects of cation binding on the conformation of calsequestrin and the high affinity calcium-binding protein of sarcoplasmic reticulum. <i>J. Biol. Chem.</i> 1974;249, 5867-5871.
245	Owen, D. and Kuhn, L.C. Non-coding sequences of the transferrin receptor gene are required for mRNA regulation by iron. <i>EMBO J.</i> 1987;6: 1287–1293.
246	Pak, M., Lopez, M.A., Gabayan, V., Ganz, T., and Rivera, S. (2006). Suppression of hepcidin during anaemia requires erythropoietic activity. <i>Blood.</i> 2006;108, 3730–3735.
247	Palmieri, F., Pierri, C.L., De Grassi, A., Nunes-Nesi, A., Fernie, A.R., 2011. Evolution, structure and function of mitochondrial carriers: a review with new insights. <i>Plant J.</i> 2011;66, 161–181.

248	Palmieri F. The mitochondrial transporter family SLC25: identification, properties and physiopathology. <i>Mol Aspects Med.</i> 2013;34(2-3):465-84.
249	Pantopoulos K, Porwal SK, Tartakoff A, Devireddy L. Mechanisms of mammalian iron homeostasis. <i>Biochemistry.</i> 2012;24;51(29):5705-24.
250	Papanikolaou G, Samuels ME, Ludwig EH, MacDonald ML, Franchini PL, Dube MP, Andres L, MacFarlane J, Sakellaropoulos N, Politou M, Nemeth E, Thompson J, Risler JK, Zaborowska C, Babakaiff R, Radomski CC, Pape TD, Davidas O, Christakis J, Brissot P, Lockitch G, Ganz T, Hayden MR, and Goldberg YP. Mutations in HFE2 cause iron overload in chromosome 1q-linked juvenile hemochromatosis. <i>Nat Genet.</i> 2004;36: 77-82.
251	Parmley, L.T. et al. Ferrocyanide staining of transferrin and ferritin-conjugated antibody to transferrin. <i>J. Histochem. Cytochem.</i> 1979;27: 681–685.
252	Parmley, R.T., J.C. Barton, and M.E. Conrad. Ultrastructural localization of transferrin, transferrin receptor and iron binding sites on human placental and duodenal microvilli. <i>Br. J. Haematol.</i> 1985;60:81–87.
253	Park CH, Valore EV, Waring AJ, and Ganz T. Hepcidin, a urinary antimicrobial peptide synthesized in the liver. <i>J Biol Chem.</i> 2001;276: 7806-7810.
254	Paz Y, Katz A, Pick U. A multicopper ferroxidase involved in iron binding to transferrins in <i>Dunaliella salina</i> plasma membranes. <i>J Biol Chem.</i> 2007;282:8658–8666.
255	Pebay-Peyroula, E., Dahout-Gonzalez, C., Kahn, R., Trézéguet, V., Lauquin, G., Brandolin, G., 2003. Structure of mitochondrial ADP/ATP carrier in complex with carboxyatractyloside. <i>Nature.</i> 2003;426, 39–44.
256	Pekarikova A, Sanchez D, Palova-Jelinkova L, Simsova M, Benes Z, Hoffmanova I, et al. Calreticulin is a B cell molecular target in some gastrointestinal malignancies. <i>J Trans Immunol.</i> 2009;160:215–22.
257	Peters LR, Raghavan M. Endoplasmic reticulum calcium depletion impacts chaperone secretion, innate immunity, and phagocytic uptake of cells. <i>J Immunol.</i> 2011;187:919–31.
258	Peterson, J. R., and Helenius, A. In vitro reconstitution of calreticulin-substrate interactions. <i>J. Cell Sci.</i> 1999;112, 2775-2784.
259	Petrak J, Vyoral D. Hephaestin--a ferroxidase of cellular iron export. <i>Int J Biochem Cell Biol.</i> 2005;37(6):1173-8.

260	Peyssonnaud, C., Zinkernagel, A.S., Schuepbach, R.A., Rankin, E., Vaulont, S., Haase, V.H., Nizet, V., and Johnson, R.S. Regulation of iron homeostasis by the hypoxia-inducible transcription factors (HIFs). <i>J. Clin. Invest.</i> 2007;117, 1926–1932.
261	Pietrangelo A, Dierssen U, Valli L, Garuti C, Rump A, Corradini E, Ernst M, Klein C, Trautwein C. STAT3 is required for IL-6-gp130-dependent activation of hepcidin in vivo. <i>Gastroenterology.</i> 2007;132(1):294-300.
262	Pfaffl MW. A new mathematical model for relative quantification in real-time RT-PCR. <i>Nucleic Acids Res.</i> 2001;29(9):e45.
263	Pigeon C, Ilyin G, Courselaud B, Leroyer P, Turlin B, Brissot P, and Loreal O. A new mouse liver-specific gene, encoding a protein homologous to human antimicrobial peptide hepcidin, is overexpressed during iron overload. <i>J Biol Chem.</i> 2001;276:7811-7819.
264	Pinkerton PH. 1968. Histological evidence of disordered iron transport in the x-linked hypochromic anaemia of mice. <i>J Pathol Bacteriol</i> 95:155–165.
265	Pocanschi, C.L. et al. Structural and functional relationships between the lectin and arm domains of calreticulin. <i>J. Biol. Chem.</i> 2011;286, 27266–27277.
266	Pootrakul, P., Breuer, W., Sametband, M., Sirankapracha P., Hershko, C. and Cabantchik, Z.I. Labile plasma iron (LPI) as an indicator of chelatable plasma redox activity in iron overloaded beta-thalassaemia/HbE patients treated with an oral chelator. <i>Blood.</i> 2004;104: 1504 – 1510.
267	Ponka P, Neuwirt J, Borova J, Fuchs O. Control of iron delivery to haemoglobin in erythroid cells. <i>Ciba Foundation Symposium 51 - Iron Metabolism</i> , eds Porter R, Fitzsimons DW (Elsevier/Excerpta Medica/North-Holland, Amsterdam), 1976;pp 167–200.
268	Ponka P, Borová J, Neuwirt J, Fuchs O. Mobilization of iron from reticulocytes. Identification of pyridoxal isonicotinoyl hydrazone as a new iron chelating agent. <i>FEBS Lett.</i> 1979;97:317–321.
269	Ponka P. Tissue-specific regulation of iron metabolism and haem synthesis: Distinct control mechanisms in erythroid cells. <i>Blood.</i> 1997;89:1–25.
270	Pulina MO, Zakharova ET, Sokolov AV, Shavlovski MM, Bass MG, Solovyov KV, Kokryakov VN, Vasilyev VB. Studies of the ceruloplasmin-lactoferrin complex. <i>Biochem Cell Biol.</i> 2002;80:35–39.

271	Quintanar L, Gebhard M, Wang TP, Kosman DJ, Solomon EI. Ferrous binding to the multicopper oxidases <i>Saccharomyces cerevisiae</i> Fet3p and human ceruloplasmin: contributions to ferroxidase activity. <i>J Am Chem Soc.</i> 2004;126:6579–6589.
272	Raffin SB, Woo CH, Roost KT, Price DC, and Schmid R. Intestinal absorption of haemoglobin iron-haem cleavage by mucosal haem oxygenase. <i>J Clin Invest.</i> 1974;54: 1344-1352.
273	Raghavan M <sup>1</sup> , Wijeyesakere SJ, Peters LR, Del Cid N. Calreticulin in the immune system: ins and outs. <i>Trends Immunol.</i> 2013 Jan;34(1):13-21.
274	Rajan S.S, H. Lackland, S. Stein, D.T. Denhardt. Presence of an Nterminal polyhistidine tag facilitates stable expression of an otherwise unstable N-terminal domain of mouse tissue inhibitor of metalloproteinase-1 in <i>Escherichia coli</i> , <i>Protein Expr. Purif.</i> 1998;67–72.
275	Ramos E, Kautz L, Rodriguez R, Hansen M, Gabayan V, Ginzburg Y, Roth MP, Nemeth E, Ganz T. Evidence for distinct pathways of hepcidin regulation by acute and chronic iron loading in mice. <i>Hepatology.</i> 2011; 53:1333–1341.
276	Reeves PG, DeMars LCS, Johnson WT, Lukaski HC. Dietary copper deficiency reduces iron absorption and duodenal enterocyte hephaestin protein in male and female rats. <i>J Nutr.</i> 2005;135: 92–98.
277	Reich DE, Cargill M, Bolk S, Ireland J, Sabeti PC, Richter DJ, Lavery T, Kouyoumjian R, Farhadian SF, Ward R, Lander ES. Linkage disequilibrium in the human genome. <i>Nature.</i> 2001;411(6834):199-204.
278	Reid D.W, G. J. Anderson , I. L. Lamont. Role of lung iron in determining the bacterial and host struggle in cystic fibrosis. <i>Am J of Physiology - Lung Cellular and Molecular Physiology.</i> 2009;Vol. 297.
279	Richardson DR, Ponka P, Vyoral D. Distribution of iron in reticulocytes after inhibition of haem synthesis with succinylacetone: Examination of the intermediates involved in iron metabolism. <i>Blood.</i> 1996;87:3477–3488.
280	Richardson DR and Ponka P. The molecular mechanisms of the metabolism and transport of iron in normal and neoplastic cells. <i>Biochim Biophys Acta.</i> 1997;1331:1–40.

281	Richardson DR, Milnes K. The potential of iron chelators of the pyridoxal isonicotinoyl hydrazone class as effective antiproliferative agents II: The mechanism of action of ligands derived from salicylaldehyde benzoyl hydrazone and 2-hydroxy-1-naphthylaldehyde benzoyl hydrazone. <i>Blood</i> . 1997;89:3025–3038.
282	Richardson DR, Lane DJ, Becker EM, Huang ML, Whitnall M, Suryo Rahmanto Y, Sheftel AD, Ponka P. Mitochondrial iron trafficking and the integration of iron metabolism between the mitochondrion and cytosol. <i>Proc Natl Acad Sci U S A</i> . 2010;107(24):10775-82.
283	Rigaut et al. A generic protein purification method for protein complex characterization and proteome exploration. <i>Nature Biotechnology</i> . 1999;17:1030-32.
284	Roetto A, Papanikolaou G, Politou M, Alberti F, Girelli D, Christakis J, Loukopoulos D, and Camaschella C. Mutant antimicrobial peptide hepcidin is associated with severe juvenile hemochromatosis. <i>Nat Genet</i> . 2003;33: 21-22.
285	Rouault, T.A, M.W. Hentze, S.W. Caughman, J.B. Harford, R.D. Klausner, Binding of a cytosolic protein to the iron-responsive element of human ferritin messenger RNA, <i>Science</i> . 1988;241,1207–1210.
286	Rouault, T.A. et al. Cloning of the cDNA encoding an RNA regulatory protein — the human iron-responsive element-binding protein, <i>Proc. Natl. Acad. Sci. U.S.A</i> . 1990;87: 7958–7962.
287	Rouault, T.A, C.D. Stout, S. Kaptain, J.B. Harford, R.D. Klausner, Structural relationship between an iron-regulated RNA-binding protein (IRE-BP) and aconitase: functional implications. <i>Cell</i> . 1991;64, 881–883.
288	Rouault TA. The role of iron regulatory proteins in mammalian iron homeostasis and disease. <i>Nat Chem Biol</i> . 2006;2(8):406-14.
289	Rouault TA. <i>Cell biology</i> . An ancient gauge for iron. <i>Science</i> . 2009;326(5953):676-7.
290	Routsias JG, Tzioufas AG, Sakarellos-Daitsiotis M, Sakarellos C, Moutsopoulos HM. Calreticulin synthetic peptide analogues: anti-peptide antibodies in autoimmune rheumatic diseases. <i>Clin Exp Immunol</i> . 1993;91(3):437-41.
291	Roy, A. et al. I-TASSER: a unified platform for automated protein structure and function prediction. <i>Nat. Protoc</i> . 2010;5, 725–738.

292	Roy CN. An update on iron homeostasis: make new friends, but keep the old. <i>Am J Med Sci.</i> 2013;346(5):413-9.
293	Ruston D, Hoare J, Henderson L, Gregory J, Bates C J, Prentice A, Birch M, Swan G, Farron M. The National Diet & Nutrition Survey: adults aged 19 to 64 years. Volume4;2003.
294	Rutkevich, L.A. and Williams, D.B. Participation of lectin chaperones and thiol oxidoreductases in protein folding within the endoplasmic reticulum. <i>Curr. Opin. Cell Biol.</i> 2011;23, 157–166.
295	Salahudeen AA, Thompson JW, Ruiz JC, Ma HW, Kinch LN, Li Q, Grishin NV, Bruick RK. An E3 ligase possessing an iron-responsive haemerythrin domain is a regulator of iron homeostasis. <i>Science.</i> 2009;326(5953):722-6.
296	Sanchez, M., Galy, B., Schwanhaeusser, B., Blake, J., Banerjee, T., Benes, V., Selbach, M., Muckenthaler, M.U., and Hentze, M.W. Iron regulatory protein-1 and -2: transcriptome-wide definition of binding mRNAs and shaping of the cellular proteome by iron regulatory proteins. <i>Blood.</i> 2011;118, e168–e179.
297	Santambrogio P, et al. Mitochondrial ferritin expression in adult mouse tissues. <i>J Histochem Cytochem.</i> 2007;55:1129–1137.
298	Schmidt TG and Skerra A. One-step affinity purification of bacterially produced proteins by means of the "Strep tag" and immobilized recombinant core streptavidin. <i>J Chromatogr A.</i> 1994;676(2):337-45.
299	Schmittgen TD <sup>1</sup> , Livak KJ. Analyzing real-time PCR data by the comparative C(T) method. <i>Nat Protoc.</i> 2008;3(6):1101-8.
300	Schrag, J.D. et al. The structure of calnexin, an ER chaperone involved in quality control of protein folding. <i>Mol. Cell.</i> 2001;8, 633–644.
301	Selezneva AI <sup>1</sup> , Cavigiolio G, Theil EC, Walden WE, Volz K. Crystallization and preliminary X-ray diffraction analysis of iron regulatory protein 1 in complex with ferritin IRE RNA. <i>Acta Crystallogr Sect F Struct Biol Cryst Commun.</i> 2006 Mar 1;62(Pt 3):249-52.
302	Shaw GC, Cope JJ, Li L, Corson K, Hersey C, Ackermann GE, Gwynn B, Lambert AJ, Wingert RA, Traver D, Trede NS, Barut BA, Zhou Y, Minet E, Donovan A, Brownlie A, Balzan R, Weiss MJ, Peters LL, Kaplan J, Zon LI, Paw

	BH. Mitoferrin is essential for erythroid iron assimilation. <i>Nature</i> . 2006;440(7080):96-100.
303	Shayeghi M, Latunde-Dada GO, Oakhill JS, Laftah AH, Takeuchi K, Halliday N, Khan Y, Warley A, McCann FE, Hider RC, Frazer DM, Anderson GJ, Vulpe CD, Simpson RJ, and McKie AT. Identification of an intestinal haem transporter. <i>Cell</i> . 2005;122: 789-801.
304	Sheftel AD, Zhang AS, Brown C, Shirihai OS, Ponka P. Direct interorganellar transfer of iron from endosome to mitochondrion. <i>Blood</i> . 2007;110(1):125-32.
305	Shoemaker BA, Panchenko AR. Deciphering protein-protein interactions. Part II. Computational methods to predict protein and domain interaction partners. <i>PLoS Comput Biol</i> . 2007;3(4):e43.
306	Shvartsman M, Kikkeri R, Shanzler A, Cabantchik ZI. Non-transferrin-bound iron reaches mitochondria by a chelator-inaccessible mechanism: biological and clinical implications. <i>Am J Physiol Cell Physiol</i> . 2007;293(4):C1383-94.
307	Silvestri, L., Pagani, A., Nai, A., De Domenico, I., Kaplan, J., and Camaschella, C. The serine protease matriptase-2 (TMPRSS6) inhibits hepcidin activation by cleaving membrane hemojuvelin. <i>Cell Metab</i> . 2008a;8, 502–511.
308	Singh A, Severance S, Kaur N, Wiltsie W, Kosman DJ. Assembly, activation, and trafficking of the Fet3p.Ftr1p high affinity iron permease complex in <i>Saccharomyces cerevisiae</i> . <i>J Biol Chem</i> . 2006;281:13355–13364.
309	Skaar JR, Pagan JK, Pagano M. SnapShot: F box proteins I. <i>Cell</i> . 2009;137(6):1160-1160.
310	Sklar P, Gabriel SB, McInnis MG, Bennett P, Lim Y, Tsan G, Schaffner S, Kirov G, Jones I, Owen M, Craddock N, DePaulo JR, Lander ES. Family-based association study of 76 candidate genes in bipolar disorder: BDNF is a potential risk locus. Brain derived neurotrophic factor. <i>Mol Psychiatry</i> . 2002;7(6):579-93.
311	Smyth D R, M.K. Mrozkiewicz, W.J. McGrath, P. Listwan, B. Kobe. Crystal structures of fusion proteins with large-αYnity tags, <i>Protein Sci</i> . 2003;1313–1322.
312	Sokolov AV, Pulina MO, Zakharova ET, Susorova AS, Runova OL, Kolodkin NI, Vasilyev VB. Identification and isolation from breast milk of ceruloplasminlactoferrin complex. <i>Biochemistry (Mosc)</i> . 2006;71:160–166.

313	Sonnichsen, B. et al. Retention and retrieval: both mechanisms cooperate to maintain calreticulin in the endoplasmic reticulum. <i>J. Cell Sci.</i> 1994;107, 2705–2717.
314	Smith, M. J., and Koch, G. L. E. Multiple zones in the sequence of calreticulin (CRP55, calregulin, HACBP), a major calcium binding ER/SR protein. <i>EMBO J.</i> 1989;8, 3581-3586.
315	Smith SR, Ghosh MC, Ollivierre-Wilson H, Hang Tong W, Rouault TA. Complete loss of iron regulatory proteins 1 and 2 prevents viability of murine zygotes beyond the blastocyst stage of embryonic development. <i>Blood Cells Mol Dis.</i> 2006;36(2):283-7.
316	Skerra A and Schmidt TG. Use of the Strep-Tag and streptavidin for detection and purification of recombinant proteins. <i>Methods Enzymol.</i> 2000;326:271-304.
317	Stearman R, Yuan DS, Yamaguchi-Iwai Y, Klausner RD, Dancis A. 1996. A permease-oxidase complex involved in high-affinity iron uptake in yeast. <i>Science</i> 271:1552–1557.
318	Stenkamp, R.E. Dioxygen and Haemrythrin. <i>Chemical Reviews.</i> 1994;94, 715-726.
319	Stofko-Hahn RE, Carr DW, Scott JD. A single step purification for recombinant proteins. Characterization of a microtubule associated protein (MAP 2) fragment which associates with the type II cAMP-dependent protein kinase. <i>FEBS Lett.</i> 1992;302(3):274-8.
320	Svenberg, B. Iron absorption in early pregnancy. A study of the absorption of nonhaem iron and ferric iron in early pregnancy, <i>Acta Obstet. Gynecol. Scand.</i> , 48, Suppl. 69–86, 1975.
321	Syed BA, Beaumont NJ, Patel A, Naylor CE, Bayele HK, Joannou CL, Rowe PS, Evans RW, Srai SK. Analysis of the human hephaestin gene and protein: Comparative modelling of the N-terminus ecto-domain based upon ceruloplasmin. <i>Protein Eng.</i> 2002;15:205–214.
322	Syed BA <sup>1</sup> , Sargent PJ, Farnaud S, Evans RW. An overview of molecular aspects of iron metabolism. <i>Hemoglobin.</i> 2006;30(1):69-80.
323	Tabachnick, G. G., and Fidell, L. S. <i>Experimental Designs Using ANOVA.</i> 2007.

324	Taketani S, et al. Molecular characterization of a newly identified haem-binding protein induced during differentiation of urine erythroleukemia cells. <i>J Biol Chem.</i> 1998;273:31388–31394.
325	Tang W, Z.Y. Sun, R. Pannell, V. Gurewich, J.N. Liu. An efficient system for production of recombinant urokinase-type plasminogen activator, <i>Protein Expr. Purif.</i> 1997;279–283.
326	Tanno, T., Bhanu, N.V., Oneal, P.A., Goh, S.H., Staker, P., Lee, Y.T., Moroney, J.W., Reed, C.H., Luban, N.L., Wang, R.H., et al. High levels of GDF15 in thalassemia suppress expression of the iron regulatory protein hepcidin. <i>Nat. Med.</i> 2007;13, 1096–1101.
327	Tanno, T., Porayette, P., Sripichai, O., Noh, S.J., Byrnes, C., Bhupatiraju, A., Lee, Y.T., Goodnough, J.B., Harandi, O., Ganz, T., et al. Identification of TWSG1 as a second novel erythroid regulator of hepcidin expression in murine and human cells. <i>Blood.</i> 2009;114, 181–186.
328	Tavill AS and Bacon BR. Hemochromatosis: how much iron is too much? <i>Hepatology.</i> 1986 Jan-Feb;6(1):142-5.
329	Taylor, P.G. et al. The effect of cysteine-containing peptides released during meat digestion on iron absorption in humans. <i>Am. J. Clin. Nutr.</i> 1986;43: 68–71.
330	Teichmann, R. and Stremmel, W. Iron uptake by human upper small intestine microvillous membrane vesicles, <i>J. Clin. Invest.</i> 1990;86: 2145–2153.
331	Testa U. Recent developments in the understanding of iron metabolism. <i>Hematol J.</i> 2002;3(2):63-89.
332	Tokuhiro S, Yamada R, Nakamura Y, Yamamoto K. An intronic SNP in a RUNX1 binding site of SLC22A4, encoding an organic cation transporter, is associated with rheumatoid arthritis. <i>Nat Genet.</i> 2003;35(4):341-8.
333	Torti FM and Torti SV. Regulation of ferritin genes and protein. <i>Blood.</i> 2002;99: 3505-3516.
334	Toyokuni, S. Iron and carcinogenesis: from Fenton reaction to target genes. <i>Redox. Rep.</i> 2002;189–197.
335	Treves, S., DeMattei, M., Lanfredi, M., Villa, A., Green, N. M., MacLennan, D. H., Meldolesi, J., and Pozzan, T. Calreticulin is a candidate for a calsequestrin-like function in Ca <sup>2+</sup> -storage compartments (calciosomes) of liver and brain. <i>Biochem. J.</i> 1990;271, 473-480.

336	Truksa, J., Gelbart, T., Peng, H., Beutler, E., Beutler, B., and Lee, P. Suppression of the hepcidin-encoding gene <i>Hamp</i> permits iron overloading mice lacking both hemojuvelin and matriptase-2/TMPRSS6. <i>Br. J. Haematol.</i> 2009;147, 571–581.
337	Tufi R, Panaretakis T, Bianchi K, Criollo A, Fazi B, Di Sano F, et al. Reduction of endoplasmic reticulum Ca <sup>2+</sup> levels favors plasma membrane surface exposure of calreticulin. <i>Cell Death Differ</i> 2008;15:274–82.
338	Uhlén M1, Björling E, Agaton C, Szigyarto CA, Amini B, Andersen E, Andersson AC, Angelidou P, Pontén F et al. A human protein atlas for normal and cancer tissues based on antibody proteomics. <i>Mol Cell Proteomics.</i> 2005;4(12):1920-32.
339	Ulrich E. Schaible & Stefan H. E. Kaufmann. Iron and microbial infection. <i>Nature Reviews Microbiology.</i> 2004;2, 946-953.
340	Umbreit JN1, Conrad ME, Berry MA, Moore EG, Latour LF, Tolliver BA, El Khalifa MY. The alternate iron transport pathway: mobilferrin and integrin in reticulocytes. <i>Br J Haematol.</i> 1997;96(3):521-9.
341	Van Nguyen, P., Peter, F., and Soling, H.D. Four intracisternal calcium-binding glycoproteins from rat liver microsomes with high affinity for calcium. No indication for calsequestrin-like proteins in inositol 1,4,5-trisphosphate-sensitive calcium sequestering rat liver vesicles. <i>J. Biol. Chem.</i> 1989;264, 17494-17501.
342	Vashchenko G, Macgillivray RT. Functional role of the putative iron ligands in the ferroxidase activity of recombinant human hephaestin. <i>J Biol Inorg Chem.</i> 2012;17(8):1187-95.
343	Vashisht AA, Zumbrennen KB, Huang X, Powers DN, Durazo A, Sun D, Bhaskaran N, Persson A, Uhlen M, Sangfelt O, Spruck C, Leibold EA, Wohlschlegel JA. Control of iron homeostasis by an iron-regulated ubiquitin ligase. <i>Science.</i> 2009;326(5953):718-21.
344	Vassilakos, A., Michalak, M., Lehrman, M. A., and Williams, D. B. Oligosaccharide binding characteristics of the molecular chaperones calnexin and calreticulin. <i>Biochemistry.</i> 1998;37, 3480-3490.
345	Vecchi, C., Montosi, G., Zhang, K., Lamberti, I., Duncan, S.A., Kaufman, R.J., and Pietrangelo, A. ER stress controls iron metabolism through induction of hepcidin. <i>Science.</i> 2009;325, 877–880.
346	Venter JC, et al. The sequence of the human genome. <i>Science.</i> 2001;291(5507):1304-51.

347	Verreck FA, Elferink D, Vermeulen CJ et al. DR4Dw4/DR53 molecules contain a peptide from the autoantigen calreticulin. <i>Tissue Antigens</i> . 1995;45:270–5.
348	Vulpe CD, Kuo YM, Murphy TL, Cowley L, Askwith C, Libina N, Gitschier J, Anderson GJ. Hephaestin, a ceruloplasmin homologue implicated in intestinal iron transport, is defective in the sla mouse. <i>Nat Genet</i> . 1999;21(2):195-9.
349	Wang J <sup>1</sup> , Chen G, Muckenthaler M, Galy B, Hentze MW, Pantopoulos K. Iron-mediated degradation of IRP2, an unexpected pathway involving a 2-oxoglutarate-dependent oxygenase activity. <i>Mol Cell Biol</i> . 2004 Feb;24(3):954-65.
350	Wang, R.H., Li, C., Xu, X., Zheng, Y., Xiao, C., Zervas, P., Cooperman, S., Eckhaus, M., Rouault, T., Mishra, L., and Deng, C.X. A role of SMAD4 in iron metabolism through the positive regulation of hepcidin expression. <i>Cell Metab</i> . 2005;2, 399–409.
351	Waser M, Mesaeli N, Spencer C, Michalak M. Regulation of calreticulin gene expression by calcium. <i>J Cell Biol</i> . 1997 Aug 11;138(3):547-57.
352	Weiss G. Iron metabolism in the anaemia of chronic disease. <i>Biochim Biophys Acta</i> . 2009;1790:682–693.
353	Weizer-Stern, O., Adamsky, K., Margalit, O., Ashur-Fabian, O., Givol, D., Amariglio, N., and Rechavi, G. Hepcidin, a key regulator of iron metabolism, is transcriptionally activated by p53. <i>Br. J. Haematol</i> . 2007;138, 253–262.
354	Westermarck J, Ivaska J, Corthals GL. Identification of protein interactions involved in cellular signaling. <i>Mol Cell Proteomics</i> . 2013;12(7):1752-63.
355	Wessling-Resnick M. Iron transport. <i>Annu Rev Nutr</i> . 2000;20:129-51.
356	Wheby MS, Suttle GE, Ford KT 3rd. Intestinal absorption of hemoglobin iron. <i>Gastroenterology</i> . 1970 May;58(5):647-54.
357	Whittaker, P.G., Lind, T., and Williams, J.C. Iron absorption during normal human pregnancy: a study with stable isotopes. <i>Brit. J. Nutr</i> . 1991;65: 457–463.
358	Wijeyesakere, S.J. et al. Calreticulin is a thermostable protein with distinct structural responses to different divalent cation environments. <i>J. Biol. Chem</i> . 2011;286, 8771–8785.
359	Winter, C.V.A. and Williams, R. Iron-binding properties of gastric juice in idiopathic haemochromatosis. <i>Lancet</i> . 1968; 2, 534–537.

360	Wheby, M.S., Suttle, G.E., and Ford, K.T. Intestinal absorption of haemoglobin iron, <i>Gastroenterology</i> 1970;58: 647–658.
361	Yamanaka K <sup>1</sup> , Ishikawa H, Ishimori K, Iwai K. Identification of the ubiquitin-protein ligase that recognizes oxidized IRP2. <i>Nat Cell Biol.</i> 2003 Apr;5(4):336-40.
362	Ye H and Rouault TA. Human iron-sulfur cluster assembly, cellular iron homeostasis, and disease. <i>Biochemistry.</i> 2010;49(24):4945-56.
363	Yeh KY, Yeh M, Mims L, Glass J. Iron feeding induces IREG1 and hephaestin migration and interaction in rat duodenal epithelium. <i>Am J Physiol Gastrointest Liver Physiol.</i> 2009;296(1):G55-65.
364	Yeh KY, Yeh M, Glass J. Interactions between IREG1 and Heph in rat enterocytes are reduced after iron ingestion. <i>Gastroenterology.</i> 2011 Jul;141(1):292-9, 299.
365	Zhang AS, Sheftel AD, Ponka P. Intracellular kinetics of iron in reticulocytes: Evidence for endosome involvement in iron targeting to mitochondria. <i>Blood.</i> 2005;105:368–375.
366	Zitvogel, L. et al. Decoding cell death signals in inflammation and immunity. <i>Cell.</i> 2010;140, 798–804.
367	Zoller H et al. Duodenal cytochrome b and hephaestin expression in patients with iron deficiency and hemochromatosis. <i>Gastroenterology.</i> 2003;12(3):746-54.